



FORMATION AND CONTROL OF NITROGEN-CONTAINING AIR POLLUTANTS

**Environmental Quality Laboratory
CALIFORNIA INSTITUTE OF TECHNOLOGY
Pasadena, California 91125**



FORMATION AND CONTROL OF
NITROGEN-CONTAINING AIR POLLUTANTS

edited by

Armistead G. Russell and Glen R. Cass

EQL Report 24

Environmental Quality Laboratory
California Institute of Technology
Pasadena, California 91125

May, 1987

ARB Research Contract No. A2-150-32

Final report prepared for
California Air Resources Board

in

completion of research under
ARB contract no. A2-150-32

"Control of Atmospheric Aerosol Nitrate
and Nitric Acid Concentrations"

by

Environmental Quality Laboratory
California Institute of Technology
Pasadena, California 91125

May, 1987

Disclaimer

The statements and conclusions in this report are those of the Contractor and not necessarily those of the State Air Resources Board. The mention of commercial products, their source or their use in connection with material reported herein is not to be construed as either an actual or an implied endorsement of such products.

ACKNOWLEDGMENTS

This research project represents a sustained effort over a period of years by a large number of investigators at Caltech. Dr. Gregory J. McRae, now at Carnegie-Mellon University, was a major contributor to the early phases of the air quality modeling work reported in this study. Many of the modeling techniques employed here are an outgrowth of his Ph.D. thesis research. Lynn Hildemann co-authored the report section dealing with comparison of ambient NH_3 and HNO_3 levels to the predictions of models based on thermodynamic equilibrium between the aerosol and gas phases. Dr. Kenneth McCue participated in the execution of the many CPU-months of computer-based modeling calculations reported in Chapters 7 and 8. The ammonia emissions inventory procedures used in parts of this report were developed by Shohreh Gharib, Mary (Peterson) Ligocki, and Dr. James Tilden. Dr. John Seinfeld contributed to the air quality modeling study reproduced as Appendix B to this report. The participation of each of these co-authors is acknowledged at the start of the chapters to which they contributed.

This work was conducted at the Environmental Quality Laboratory (EQL) of Caltech, and the support of its director, Dr. Norman H. Brooks is appreciated greatly. The manuscript was typed by Pat Houseworth, Christina Conti and Dixie Termin. Theresa Fall, Phil Dubé, and Nancy Tomer helped in preparing many of the illustrations that are to follow.

The list of people crucial to the project does not end there. Over twenty Caltech students and staff gave up two or more days of their time to help conduct the experiments described in this study. The South Coast Air Quality Management District (SCAQMD) provided much of the required air quality, meteorological and emissions data, and allowed the use of SCAQMD air monitoring sites for our experiments. We are grateful to the SCAQMD's staff members who helped in these matters, especially Bill Bope, Julian Foon, John Grissinger, Eric Lemke, and Chung Liu.

The California Air Resources Board provided not only emissions data, and use of one of their monitoring sites, but, under Agreement A2-150-32, also provided most of the monetary support required to conduct this project. Paul Allen, Andrew Ranzieri, Charles Unger, and Kit Wagner helped provide emissions data and had helpful comments on the development of the modeling work. Doug Lawson, Jack Suder and Chuck Unger were the contract monitors at different times during this project.

ABSTRACT

This work focuses on the formation, transport and control of nitrogen-containing air pollutants. Particular attention is paid to the problem of understanding how to control atmospheric aerosol nitrate and nitric acid concentrations. In the course of this study, additional insights are gained into the effects of emission controls on other co-pollutants, including NO_2 , O_3 , PAN and ammonia.

Computer-based theoretical models are employed that relate emissions of reactive organic gases, oxides of nitrogen and ammonia to downwind pollutant concentrations. Both trajectory models that follow the path of a single air parcel and grid models that examine an entire air basin are used. The trajectory version of the atmospheric model is used extensively to test the new features of the chemical mechanism that is built into these models. Nighttime atmospheric chemical reactions that can lead to nitric acid formation are examined, and are found to produce significant amounts of HNO_3 . The hypothesis that atmospheric HNO_3 and NH_3 are in equilibrium with the aerosol phase is tested, and found to be a useful basis for predicting the ambient HNO_3 and NH_3 levels.

Ambient measurements on O_3 and NO_2 concentrations are routinely available from governmental air monitoring stations, but short-term average data on the concentrations of HNO_3 , NH_3 , PAN and aerosol nitrate needed to test the performance of our models are lacking. Therefore, a major field experiment is conducted as part of this study during August, 1982, to acquire such a model verification data set in the South Coast Air Basin that surrounds Los Angeles. The product of the measured nitric acid and ammonia concentrations ranges from less than 1 ppbv² to greater than 300 ppbv² during the experiment, providing a wide range of conditions over which comparisons can be drawn between chemical equilibrium calculations and experimental results. The ionic material in the aerosol phase is found to be chemically more complex than is assumed by present theoretical models for the

equilibrium between NH_3 , HNO_3 and the aerosol phase, and includes significant amounts of Na^+ , Ca^{2+} , Mg^{2+} , K^+ and Cl^- in addition to NH_4^+ , SO_4^{2-} and NO_3^- . Results of the experiment show that aerosol nitrate levels in excess of $20 \mu\text{gm}^{-3}$ accumulate in near-coastal locations on the morning of 31 August, followed by subsequent transport across the air basin. Trajectory analysis shows that the afternoon aerosol nitrate peak observed inland at Rubidoux near Riverside on August 31 is associated with the same air mass that contains the high morning nitrate levels near the coast, indicating that description of both transport and atmospheric chemical reactions is important in understanding regional nitrate dynamics.

The performance of both the trajectory- and grid-based versions of the photochemical models used here is evaluated by comparison to the August 1982 field experiments. The trajectory model produces excellent agreement between observations and predictions, especially along the transport path from Long Beach to Riverside where all of the model's input data requirements can be satisfied by actual measured values. The predictions of the grid-based model for O_3 and PAN are in good agreement with observations. The absolute value of the total inorganic nitrate, NH_3 and HNO_3 predictions on average are within a few ppb of the observations. Lacking an inventory of ionic and alkaline aerosol emissions, accurate apportionment of total inorganic nitrate between the aerosol and gas phases is not possible at coastal locations. At mid-basin sites like Anaheim, where NH_4NO_3 is the dominant nitrate aerosol species present, the aerosol nitrate levels predicted by the model are in good agreement with observed values.

The completed grid-based airshed model then is used to study the effect of specific emission control measures on ambient NO_2 , total inorganic nitrate ($\text{TN} = \text{HNO}_3 + \text{aerosol nitrate}$), HNO_3 , aerosol nitrate, PAN, NH_3 and ozone concentrations in the Los Angeles area. NO_x and reactive hydrocarbon (RHC) emission reductions of up to 61% and 37%, respectively, are examined. NO_2 and TN concentration

reductions in excess of 50% averaged over 20 monitoring sites are achieved at the highest level of emission control studied. The distribution of TN air quality improvements between HNO_3 and aerosol nitrate is affected by the NH_3 emission rate of the NO_x control technologies employed. Peak 1-hr O_3 concentrations at many sites in the eastern portion of the air basin studied decline by more than 25% at the highest NO_x and RHC control levels studied, with the final increment of NO_x control alone capable of producing O_3 concentration improvements at locations with the highest O_3 concentrations.

TABLE OF CONTENTS

	Page
ACKNOWLEDGEMENTS	iii
ABSTRACT	v
LIST OF FIGURES	xi
LIST OF TABLES	xviii
 CHAPTER 1 INTRODUCTION	 1
1.1 Objective	1
1.2 The Importance of Nitrate Aerosol and Nitric Acid in the Atmosphere	 1
1.3 Approach and Methods	3
1.4 References	6
 CHAPTER 2 MATHEMATICAL MODELING OF THE FORMATION AND TRANSPORT OF AMMONIUM NITRATE AEROSOL	 8
 CHAPTER 3 THE DYNAMICS OF NITRIC ACID PRODUCTION AND THE FATE OF NITROGEN OXIDES	 25
 CHAPTER 4 ACQUISITION OF REGIONAL AIR QUALITY MODEL VALIDATION DATA FOR NITRATE, SULFATE, AMMONIUM ION AND THEIR PRECURSORS	 37
 CHAPTER 5 AMMONIA AND NITRIC ACID CONCENTRATIONS IN EQUILIBRIUM WITH ATMOSPHERIC AEROSOLS: EXPERIMENT VS. THEORY	 51
 CHAPTER 6 VERIFICATION OF A MATHEMATICAL MODEL FOR AEROSOL NITRATE AND NITRIC ACID FORMATION, AND ITS USE FOR CONTROL MEASURE EVALUATION	 66
6.1 Introduction	67
6.2 Model Description	67
6.3 Model Evaluation Data Base	68
6.4 Model Evaluation for 30-31 August 1982	72

TABLE OF CONTENTS

	Page
6.5 Evaluation of Control Strategies for HNO_3 and Aerosol Nitrate Abatement	78
6.6 Conclusions	80
6.7 References	81
 CHAPTER 7 MATHEMATICAL MODELING OF THE FORMATION OF NITROGEN-CONTAINING AIR POLLUTANTS—I. EVALUATION OF AN EULERIAN PHOTOCHEMICAL MODEL	 82
7.1 Introduction	84
7.2 Model Description	84
7.3 Modeling Region	89
7.4 Meteorological Fields	89
7.5 Pollutant Emissions	91
7.6 Initial and Boundary Conditions	91
7.7 Model Application on 30-31 August 1982	95
7.8 Statistical Evaluation of Model Results	104
7.9 Conclusions	111
References	112
 CHAPTER 8 MATHEMATICAL MODELING OF THE FORMATION OF NITROGEN-CONTAINING AIR POLLUTANTS—II. EVALUATION OF THE EFFECT OF EMISSION CONTROLS	 114
8.1 Introduction	116
8.2 Emission Control Opportunities	116
8.3 The Effect of Emission Controls	123
8.4 Summary and Conclusions	142
References	144

TABLE OF CONTENTS

	Page
APPENDIX A AMMONIA EMISSIONS IN THE SOUTH COAST AIR BASIN	A1
APPENDIX B ON SOME ASPECTS OF NIGHTTIME ATMOSPHERIC CHEMISTRY	B1

LIST OF FIGURES

Figure		Page
2.1	Schematic representation of (a) vertically resolved Lagrangian trajectory model and (b) the computational grid cell convention.	10
2.2	(a) NH_4NO_3 equilibrium dissociation constant as a function of temperature (r.h. 50%) and (b) NH_4NO_3 equilibrium dissociation constant as a function of r.h. (temperature, 25°C).	11
2.3	Flow diagram of NH_4NO_3 formation mechanism illustrating three basic steps in calculation procedure.	12
2.4	Predicted NH_4NO_3 concentration surfaces at 15, 25 and 35°C and 45, 65 and 85% r.h. for total NH_3 and total HNO_3 concentrations up to 20 and 40 ppb, respectively.	14
2.5	Gridded map of the South Coast Air Basin used for constructing NH_3 emissions inventory. Superimposed on the map is the trajectory path that reaches El Monte at 3 p.m. (PDT) on 28 June 1974.	14
2.6	Spatial representation of daily emissions of NH_3 , NO_x reactive hydrocarbons (RHC) and CO in the South Coast Air Basin (inventory period June 1974).	17
2.7	Concentration profiles at El Monte on 28 June 1974. (a) Predicted NH_4NO_3 , measured NH_4^+ and measured NO_3^- , (b) Predicted total ammonia ($\text{NH}_3 + \text{NH}_4^+$) and measured total ammonia, (c) Predicted and measured O_3 concentrations and (d) Sensitivity of NH_4NO_3 formation to a $\pm 2^\circ\text{C}$ change in the temperature field.	18
2.8	Predicted concentrations and observed meteorological variables for the air parcel reaching El Monte at 2 p.m. (PDT) 28 June 1974. (a) NH_4NO_3 , NH_3 , HNO_3 , and PAN profiles, (b) Total ammonia and total nitrate profiles, (c) NO, NO_2 , and O_3 profiles and (d) Meteorological parameters: mixing depth, temperature, and relative humidity.	21
2.9	Evolution of vertical concentration profiles of NO_3^- (---), HNO_3 (— —) and NH_4NO_3 (—) in the air parcel that reaches El Monte at 2 p.m. (PDT) 2 June 1974. Results shown are for 4 a.m., 8 a.m., and 12 noon, and the location is given for the air parcel at those times.	22
3.1	Trajectory path used in analyzing the nitrogen oxides in the Los Angeles basin, 28 June 1974.	28

LIST OF FIGURES

Figure		Page
3.2	Schematic representation of the net flux between nitrogen oxides species, including reaction paths for aerosol nitrate (NIT) formation. The width of these arrows indicates the magnitude of the net flux during the base case 24-hour trajectory simulation.	28
3.3	Nitrogen balance on the air column illustrating the relative contributions, $F(n)$, from initial conditions, emissions and removal by dry deposition.	28
3.4	Cumulative dry deposition of oxidized nitrogen air pollutants along a 24-hour trajectory in the Los Angeles area, in mg N per m ² of surface area at the bottom of the moving air column.	30
3.5	Diurnal variation in the contribution of different reaction pathways to the formation of gas phase nitric acid. The two reactions (53 and 54) between NO ₃ and organics have been added together for display purposes.	30
3.6	Predicted and measured NO ₃ concentrations at Riverside, 12 September 1979. (—) Predicted and (+) Measured (Platt et al. 1980).	33
3.7	Predicted and measured O ₃ and NO ₂ concentrations at Riverside, 12 September 1979. (—) Predicted, (x) Measured NO ₂ (Platt et al. 1980) and (o) Measured O ₃ (Platt et al. 1980).	33
3.8	Predicted vertical NO ₃ concentration profile at 1900 (PDT) on 12 September 1979. Air parcel is located at Riverside.	34
3.9	Predicted NO ₃ concentrations at Riverside, 12 September 1979 for the base case and for several perturbations from the base case.	35
4.1	Locations of nitrate monitoring sites in the South Coast Air Basin.	39
4.2	Schematic of the sampling apparatus used at nine of the ten sites. The tenth station used only the two 10 lpm lines with dual filters.	39

LIST OF FIGURES

Figure		Page
4.3	(a) Nitrate concentrations observed at Rubidoux, 30-31 August 1982. (b) Trajectory of the air mass passing over the Long Beach area at 1100 hours on 31 August and over the Rubidoux Area at 1800 hours on 31 August 1982. (c) Nitrate concentrations at Long Beach, 30-31 August 1982.	41
4.4	Ionic species concentration at Long Beach (a) Cations and (a) Anions.	42
4.5	Ionic species concentration at Rubidoux (a) Cations and (a) Anions.	43
4.6	Particulate nitrate and gaseous nitric acid concentrations ($\mu\text{g m}^{-3}$ as NO_3^-) (a) Long Beach and (b) Lennox.	44
4.7	Particulate ammonium and gaseous ammonia concentrations ($\mu\text{g m}^{-3}$ as NH_4^+) (a) Long Beach and (b) Lennox.	45
4.8	(a) Particulate nitrate and gaseous nitric acid concentrations at Anaheim ($\mu\text{g m}^{-3}$ as NO_3^-) (b) Particulate ammonium and gaseous ammonia concentrations at Anaheim ($\mu\text{g m}^{-3}$ as NH_4^+).	46
4.9	(a) Particulate nitrate and gaseous nitric acid at Rubidoux ($\mu\text{g m}^{-3}$ as NO_3^-) (b) Particulate ammonium and gaseous ammonia concentrations at Rubidoux ($\mu\text{g m}^{-3}$ as NH_4^+).	47
4.10	Partial pressure concentration product of ammonia and nitric acid at Rubidoux.	48
4.11	Measured NO , NO_2 , HNO_3 , PAN and Nitrate (in $\mu\text{g m}^{-3}$ stated as equivalent NO_3^-) (a) Pasadena and (b) Rubidoux.	49
5.1	Air monitoring sites in the South Coast Air Basin that surrounds Los Angeles.	53
5.2	Partial pressure product of ammonia and nitric acid in equilibrium with a sulfate, nitrate and ammonium containing aerosol as a function of relative humidity and ammonium nitrate ionic strength fraction at 25°C .	54
5.3	Observed $[\text{HNO}_3][\text{NH}_3]$ concentration product and calculated dissociation constant of pure ammonium nitrate at Anaheim, California.	56

LIST OF FIGURES

Figure		Page
5.4	Observed and calculated pollutant concentrations at Anaheim—external mixture with all aerosol nitrate available to form ammonium nitrate. (a) Nitric acid gas, (b) ammonia gas, (c) nitrate aerosol and (d) ammonium aerosol.	57
5.5	Observed $[\text{HNO}_3][\text{NH}_3]$ concentration product and calculated dissociation constant of pure ammonium nitrate at Rubidoux, California.	58
5.6	Observed and calculated pollutant concentrations at Rubidoux—external mixture with all aerosol nitrate available to form ammonium nitrate. (a) Nitric acid gas, (b) ammonia gas, (c) nitrate aerosol and (d) ammonium aerosol.	58
5.7	Observed $[\text{HNO}_3][\text{NH}_3]$ concentration product and calculated dissociation constant of pure ammonium nitrate at Long Beach, California.	59
5.8	Observed and calculated pollutant concentrations at Long Beach—external mixture with all aerosol nitrate available to form ammonium nitrate. (a) Nitric Acid Gas, (b) Ammonia Gas, (c) Nitrate Aerosol and (d) Ammonium Aerosol.	60
5.9	Observed and calculated pollutant concentrations at Long Beach—external mixture with only FREE NITRATE available to form NH_4NO_3 , (a) HNO_3 , (b) NH_3 and (c) FREE NITRATE.	61
5.10	Comparison of observed and calculated gas phase concentrations at all monitoring stations under two alternative external mixture hypothesis (180 observations). Case (1), all aerosol nitrate available to form NH_4NO_3 . Case (2), only the FREE NITRATE available to form NH_4NO_3 . (a) ammonia (Case 1), (b) nitric acid (Case 1), (c) ammonia (Case 2) and (d) nitric acid (Case 2).	62
5.11	Observed and calculated $[\text{HNO}_3][\text{NH}_3]$ concentration product at Upland—comparison of external mixture and size segregated internal mixture hypothesis. (a) external mixture and (b) size segregated internal mixture.	63

LIST OF FIGURES

Figure		Page
6.1	Gridded map of California's South Coast Air Basin (SoCAB) used for constructing concentration fields, meteorological fields, and emissions inventories. Symbols (●) indicate the locations of aerosol measurement stations used in this work. The solid line marks the boundary of the SoCAB.	68
6.2	Spatial distribution of the 1982 estimated daily emissions of NH_3 , NO_x , THC and CO in the South Coast Air Basin.	70
6.3	Observed and predicted O_3 at Rubidoux, CA, 31 August 1982.	75
6.4	Observed and predicted NO_2 at Rubidoux, CA, 31 August 1982.	75
6.5	Observed and predicted Total Nitrate ($\text{TN} = \text{AN} + \text{HNO}_3$) at Rubidoux, CA, 31 August 1982.	76
6.6	Observed and predicted $\text{HNO}_3(\text{g})$ at Rubidoux, CA, 31 August 1982.	76
6.7	Observed and predicted NO_3^- at Rubidoux, CA, 31 August 1982.	76
6.8	Observed and predicted NH_3 at Rubidoux, CA, 31 August 1982.	76
6.9	Observed and predicted NO_3^- at Rubidoux, CA, 31 August 1982 when the partition of computed TN between $\text{HNO}_3(\text{g})$ and aerosol nitrate is based on ambient temperatures and ammonia concentrations measured at the Rubidoux monitoring site.	77
6.10	Predicted Total Nitrate ($\text{TN} = \text{HNO}_3(\text{g}) + \text{NH}_4\text{NO}_3 + \text{BAN}$), Aerosol Nitrate ($\text{AN} = \text{NH}_4\text{NO}_3 + \text{BAN}$) and aerosol nitrate formed by reaction 58 (BAN, see text) at Rubidoux, CA, 31 August 1982.	77

LIST OF FIGURES

Figure		Page
7.1	The South Coast Air Basin of California, plus Ventura and Coastal Santa Barbara Counties. Emissions and meteorological data fields are developed over the 150 km x 400 km gridded area. Air monitoring sites at which HNO_3 , NH_3 , and aerosol nitrate data are available from reference (2) and are shown by (•). Air quality modeling calculations are performed within the region bounded by the heavy solid line in the center of the map.	90
7.2	The spatial distribution of NH_3 , NO_x , total hydrocarbons, and CO emissions within the grid system for the summer of 1982.	92
7.3	The spatial distribution of predicted concentrations of O_3 , NO_2 , HNO_3 , aerosol nitrate, and NH_3 at 0800, 1100, 1400, and 1700 hrs PST 31 August 1982.	97
7.4	Comparison of predicted and observed ozone concentrations in the South Coast Air Basin, 30-31 August 1982.	98
7.5	Comparison of predicted and observed concentrations of NO_2 , TN, HNO_3 , aerosol nitrate, and NH_3 at Central Los Angeles on 30-31 August 1982.	99
7.6	Comparison of predicted and observed concentrations of NO_2 , TN, HNO_3 , aerosol nitrate, and NH_3 at Anaheim on 30-31 August 1982.	100
7.7	Comparison of predicted and observed concentrations of NO_2 , TN, HNO_3 , aerosol nitrate, and NH_3 at Rubidoux on 30-31 August 1982.	101
7.8	Comparison of predicted and observed PAN concentrations at Pasadena on 30-31 August 1982.	105
7.9	Histogram of concentration residuals (predicted minus observed) determined over all times and locations of the two day period, 30-31 August 1982: (a) O_3 , (b) NO_2 , (c) total inorganic nitrate, (d) nitric acid, (e) aerosol nitrate, and (f) ammonia.	109
8.1	The South Coast Air Basin, showing 20 sites at which the effect of emission controls will be evaluated. Air quality modeling calculations are performed within the region bounded by the heavy solid line in the center of the map.	129

LIST OF FIGURES

Figure		Page
8.2	The spatial distribution of pollutant concentrations predicted in the presence of the maximum degree of NO_x and RHC control studied (case in lower right corner of Table 2).	132
8.3	The spatial distribution of pollutant concentration changes predicted in the presence of the maximum degree of NO_x and RHC control studied (difference between the case in lower right corner of Table 2 vs. the Base Case).	133
8.4	NO_2 and total inorganic nitrate (TN) concentrations at Los Angeles, Anaheim and Rubidoux under Base Case conditions and in the presence of the maximum degree of NO_x and RHC control studied.	134
8.5	Nitric acid, ammonia and aerosol nitrate concentrations at Los Angeles and at Rubidoux under Base Case conditions and in the presence of the maximum degree of NO_x and RHC control studied.	135
8.6	Ozone concentrations under Base Case conditions and in the presence of the maximum degree of NO_x and RHC control studied.	136
8.7	24-hour average NO_2 , inorganic nitrate, nitric acid, aerosol nitrate, O_3 and PAN concentrations in the presence of the maximum degree of NO_x and RHC control studied, expressed as a percentage of Base Case concentrations.	137

LIST OF TABLES

Table		Page
2.1	Sensitivity of ammonium nitrate formation model to input parameters	13
2.2	Summary of ammonia emissions by source category in the South Coast Air Basin 1974	15
3.1	Major reactions in the $\text{NO}_3\text{-N}_2\text{O}_5$ System at night	30
3.2	Species concentrations used in analysis	31
3.3	Percent of total nitric acid produced by each reaction along a 24-hour trajectory	32
4.1	Measurement uncertainties	40
5.1	Comparison of measurements at Long Beach to predictions given by the pure external mixture hypothesis based on FREE NITRATE (case 1) and by the size segregated internal mixture hypothesis (case 2)	64
6.1	1982 Estimated emissions in the South Coast Air Basin	69
6.2	Summary of ammonia emissions by source category in the South Coast Air Basin 1982	71
6.3	Splitting factors for converting total measured hydrocarbons (ppmC) into hydrocarbon classes for use as initial conditions	72
6.4	Predicted and measured concentrations along the trajectory beginning at Long Beach, California, at 1100 (PDT) 31 August 1982	74
6.5	Predicted inorganic nitrate concentrations at Rubidoux, California, resulting from decreases in emissions	78
6.6	Predicted peak one-hour ozone concentrations (ppb) at Rubidoux, California, as a function of emissions reductions	79
6.7	Predicted pollutant concentrations at Rubidoux, California, when emissions of SINK aerosol are included	80
7.1	Definition of chemical species symbols used in the chemical mechanism of Table 2	86

LIST OF TABLES

Table		Page
7.2	Kinetic mechanism (References 4,7,8,9)	87
7.3	Hydrocarbon splitting factors	94
7.4	Statistical evaluation of model performance for O ₃ and NO ₂	107
7.5	Statistical evaluation of model performance for total inorganic nitrate, ammonia, aerosol nitrate, and nitric acid	108
8.1	Specific emission control measures and their effect if applied to 1982 emissions in the South Coast Air Basin	118
8.2	Combinations of mobile and stationary source controls that will be examined for their effect on air quality in the South Coast Air Basin. Control measures refer to the control measures numbered in Table 1. Labels on columns and rows of this table are indicative of the maximum degree of NO _x control required	122
8.3	Effect of emission controls on basin-wide peak 1-hr average pollutant concentrations in the South Coast Air Basin, August 31, 1982. The combinations of emission control technologies considered in each cell of this matrix are defined in Tables 1 and 2. Values shown are the peak 1-hr average concentrations in the presence of the emission controls, followed by the % change relative to the Base Case (in parentheses)	125
8.4	Effect of emission controls on peak 1-hr average pollutant concentrations observed at the 20 sites shown in Figure 1. Values shown are averages over the 20 sites, followed by the range of the values observed among the 20 sites (in parentheses)	126

1. INTRODUCTION

1.1. Objective

The objective of this research has been to create a better understanding of the processes that govern the atmospheric formation of nitric acid (HNO_3) and nitrate aerosol. The knowledge gained is used to formulate mathematical models that simulate the relationship between emission sources and the ambient concentrations of those pollutants. These models then are employed to evaluate the effectiveness of alternative mobile and stationary source emission control strategies that could be used to abate presently observed aerosol nitrate and nitric acid concentrations. While exploring rational emission control strategies that will reduce the formation of nitric acid and ammonium nitrate, the effect of emission controls on coexisting pollutants, such as nitrogen dioxide (NO_2), peroxyacetyl nitrate (PAN), ammonia (NH_3), and ozone (O_3), also are investigated. The concepts developed are tested against experimental data obtained on particular days in the Los Angeles Basin during the years 1974 and 1982, but the methods developed are generally applicable to other urban areas and to other years given data representative of those times and places.

1.2. The Importance of Nitrate Aerosol and Nitric Acid in the Atmosphere

A substantial portion of the aerosol nitrate in the atmosphere is found to reside in the fine particle size fraction with particle diameter less than about $2\text{ }\mu\text{m}$ (Appel et al., 1978; Hobbs and Hegg, 1982; Grosjean, 1983). These fine particles, especially those with diameters of the same order as the wavelength of visible light, scatter light very effectively and can lead to pronounced visibility degradation (Friedlander, 1977; van de Hulst, 1957). Aerosol nitrate is estimated to account for up to 40% of the severe visibility problem experienced in the eastern portion of the Los Angeles Basin (White and Roberts, 1977). Groblicki et al. (1982) estimate that

about 17% of the decreased visibility in Denver is due to fine particulate nitrates. These small particles also are easily respirable (National Research Council, 1979), with possible accompanying health implications.

Nitric acid is of concern for a variety of reasons, not the least of which is that it is a precursor to the formation of aerosol nitrate (Duce, 1969; Stelson and Seinfeld, 1982; Russell and Cass, 1984). The presence of nitric acid in the atmosphere leads to the acidification of rain and fog and to acidic dry deposition (Liljestrand and Morgan, 1978; Waldman et al., 1982; Huebert, 1983). Nitric acid has been cited as a contributor to the formation of mutagenic, nitrated organic compounds in the atmosphere (Grosjean et al., 1983) and itself is probably not healthful if inhaled in conjunction with ozone and NO_2 (Mantz et al., 1985). Aerosol nitrates and nitric acid also are two of the major end products of nitrogen oxides (NO_x) emissions. Thus an understanding of how HNO_3 and aerosol nitrates are produced in the atmosphere forms an integral part of an improved understanding of the ultimate fate of NO_x emissions and the production of other photochemical pollutants (Seinfeld, 1975; Russell et al., 1985; Grosjean, 1983).

Problems associated with aerosol nitrate and nitric acid are not restricted to urban areas with large emissions of nitrogen oxides. Rural areas of the eastern United States and Canada experience acidification of the rain and lakes due to sulfates and nitrates that are being advected from more the populated areas (Galloway and Likens, 1981). Henderson, Nevada, near Las Vegas, experiences markedly decreased visibility from nitrate-containing aerosols (Clark County Health District, 1982), and it is the semi-rural areas near Riverside, CA, 60 KM downwind of Los Angeles, that experience the greatest decrease in visibility due to aerosol nitrates produced in the atmosphere of California's South Coast Air Basin.

1.3. Approach and Methods

One major route for fine particle nitrate production is suspected to proceed by the reaction between gaseous ammonia and nitric acid to form ammonium nitrate (NH_4NO_3) particles. Nitric acid, in turn, is produced by a series of photochemical and thermal reactions involving primary NO_x , reactive hydrocarbon (RHC) emissions, and their products. Thus, to describe correctly the dynamics of atmospheric ammonium nitrate aerosol and nitric acid, one must describe the complete system which has become known as photochemical air pollution, or smog. Chapter 2 reports on the development and testing of the trajectory formulation of a photochemical air pollution model that describes the emissions of NO_x , RHC, and NH_3 from their sources and the subsequent transport and reaction of these emissions to form O_3 , NO_2 , HNO_3 , and ammonium nitrate aerosol in equilibrium with atmospheric ammonia and nitric acid.

Chapter 3 and Appendix B use the trajectory model to investigate the relative importance of the competing chemical reactions that determine nitric acid concentrations in the atmosphere, as well as the fate of NO_x emissions and the deposition of nitrogenous pollutants. The research reveals that a significant amount of nitric acid can be formed at night as a product of nitrate radical (NO_3) and dinitrogen pentoxide (N_2O_5) reactions. This study confirms that the chemical mechanism and the description of the transport, deposition, and emissions used can accurately reproduce the observed behavior of NO_3 concentrations in the atmosphere. Also in Chapter 3 the role that scavenging of NO_3 and N_2O_5 by aerosols may play in the production of nitric acid and aerosol nitrates is discussed.

A major barrier encountered when studying the dynamics of atmospheric nitric acid and aerosol nitrate is the lack of high quality observations on the concentrations of these pollutants and their co-pollutants collected in a form that can be used to verify theoretical air quality modeling calculations. To advance this

research project, it was necessary to acquire a set of atmospheric pollutant concentration data that could be used to elucidate the important processes affecting basin-wide nitrate concentrations, to further test both an advanced trajectory model, and a full, grid-based, airshed model describing the dynamics of the pollutants. A major experiment was conducted in the Los Angeles Basin on 30-31 August 1982 during which ionic aerosol constituents, nitric acid, ammonia and other gaseous precursor concentrations were measured for 48 consecutive hours at ten sites. Results and conclusions derived from the field experiment are described in Chapter 4. The results of this experiment are incorporated into the model evaluation efforts described in Chapters 6 and 7.

The field experiment provided a very large set of data that can be used to test a key hypothesis in the air quality model: that nitric acid and ammonia are in equilibrium with the aerosol phase. A number of calculation procedures have been proposed to predict the equilibrium distribution of the species. Chapter 5 compares the field experimental findings to results obtained using alternative theoretical hypotheses about the chemical composition of the aerosol species present in the atmosphere. The likely importance of aerosol nitrates formed by routes other than the reaction of HNO_3 with NH_3 , such as chloride displacement from sea salt by HNO_3 to form NaNO_3 , is investigated.

Chapter 6 describes an evaluation of the accuracy of an advanced photochemical, trajectory air quality model that describes aerosol nitrate and nitric acid formation. Model calculations are compared with results of the 30-31 August 1982 field experiment. Within this chapter the effects of alternative control programs directed at reducing NO_x , NH_3 , and RHC emissions are depicted, and the implications of alternative control strategies are discussed further. Perturbing the emissions pattern in the air basin also illustrates the complex synergisms between photochemically generated air pollutants and shows that a given reduction in precursor emissions need

not result in a proportional reduction in the resulting pollutant concentrations.

Trajectory models have the disadvantage that only one location in a large airshed is examined at any single time. In order to predict pollutant concentrations simultaneously throughout an entire air basin, a grid-based Eulerian version of the nitric acid and aerosol nitrate air quality model is developed. In Chapter 7, that grid-based air quality model is tested against the pollutant concentrations and meteorological conditions observed during the August 30-31, 1982 field experiments in the South Coast Air Basin. Having evaluated the grid-based model's ability to reproduce historically observed air quality, it is possible to calculate the effects that can be expected if additional mobile and stationary source emission control measures had been in effect during the 1982 summer period examined here. In Chapter 8, a matrix of different combinations of increasingly stringent mobile source and stationary source controls is constructed. Stationary source controls include the reactive hydrocarbon and NO_x reductions expected as part of the 1982 Air Quality Management Plan for the South Coast Air Basin, plus additional NO_x controls based on catalytic and non-catalytic NH_3 injection techniques applied to electric utility, refinery, and industrial combustion sources. Mobile source emission controls examined include a vehicle inspection and maintenance program, NO_x controls on heavy-duty vehicles, plus the eventual attainment of 0.7 g/mi or 0.4 g/mi NO_x emission rates by the light-duty vehicle fleet. The air quality model is used to determine the effect that each combination of control measures would have on achieving reduced levels of NO_2 , PAN, HNO_3 , aerosol NH_4NO_3 , NH_3 and O_3 in the South Coast Air Basin.

1.4. References

- Appel, B.R., Kothny, E.L., Hoffer, E.M., Hidy, G.M., and Wesolowski, J.J. (1978) "Sulfate and Nitrate Data from the California Aerosol Characterization Experiment (ACHEX)," *Envir. Sci. Technol.*, **12**, 418-425.
- Clark County Health District (1982) "Air Quality in the Las Vegas Valley, Annual Report," Las Vegas, Nevada.
- Duce, R.A. (1969) "On the Source of Gaseous Chlorine in the Marine Atmosphere," *J. Geophys. Res.*, **70**, 1775-1779.
- Friedlander S.K. (1977) *Smoke Dust and Haze*, Wiley, New York.
- Galloway, J.N. and Likens, G.E. (1981) "Acid Precipitation: The Importance of Nitric Acid," *Atmospheric Environment*, **15**, 1081-1085.
- Groblicki, P.J., Wolff, G.T. and Countess, R.J. (1981) "Visibility Reducing Species in the Denver "Brown Cloud", Part I. Relationships Between Extinction and Chemical Composition," *Atmospheric Environment*, **15**, 2473-2484.
- Grosjean, D. (1983) "Distribution of Atmospheric Nitrogenous Pollutants at a Los Angeles Area Smog Receptor Site," *Envir. Sci. Technol.*, **17**, 13-19.
- Grosjean, D., Fung, K. and Harrison, J. (1983) "Interactions of Polycyclic Aromatic Hydrocarbons With Atmospheric Pollutants," *Envir. Sci. Technol.*, **17**, 673-679.
- Hobbs, P.V. and Hegg, D.A. (1982) "Sulfate and Nitrate Size Distributions in the Near Field of Some Coal Fired Power Plants," *Atmospheric Environment*, **16**, 2657-2662.
- Huebert, B.J. (1983) "Measurements of the Dry Deposition Flux of Nitric Acid Vapor to Grasslands and Forest," in *Precipitation Scavenging, Dry Deposition, and Resuspension*. Pruppacher, H.R., Semonin, R.G. and Slinn, W.G.N., coordinators, Elsevier, New York.
- Liljestrand, H.M. and Morgan, J.J. (1978) "Chemical Composition of Acid Precipitation in Pasadena, California," *Envir. Sci. Technol.*, **12**, 1271-1273.
- Mantz, W.J., Kleinman, M.T., McClure, T.R., and Phalen, R.F. (1985) "Synergistic Effects of Inhaled Ozone and Nitrogen Dioxide on Lung Damage in Rats," *Federation Proceedings*, **44**, 1272.
- National Research Council (1979) *Airborne Particles* University Park Press, Baltimore.
- Russell, A.G. and Cass, G.R. (1984) "Acquisition of Regional Air Quality Model Validation Data for Nitrate, Sulfate, Ammonium Ion and Their Precursors," *Atmospheric Environment*, **18**, 1815-1827.

- Russell, A.G., McRae, G.J. and Cass, G.R. (1983) "Mathematical Modeling of the Formation and Transport of Ammonium Nitrate Aerosol," *Atmospheric Environment*, 17, 949-964.
- Russell, A.G., McRae, G.J. and Cass, G.R. (1985) "The Dynamics of Nitric Acid Production and the Fate of Nitrogen Oxides," *Atmospheric Environment* (in press).
- Seinfeld, J.H. (1975) *Air Pollution, Physical and Chemical Fundamentals*, McGraw Hill, New York.
- Stelson, A.W. and Seinfeld, J.H. (1982) "Relative Humidity and Temperature Dependence of the Ammonium Nitrate Dissociation Constant," *Atmospheric Environment*, 16, 983-992.
- van de Hulst, H.C. (1957) *Light Scattering by Small Particles*, Wiley, New York.
- Waldman, J.M., Munger, J.W., Jacob, D.J., Flagan, R.C., Morgan, J.J. and Hoffmann, M.R. (1982) "Chemical Composition of Acid Fog," *Science*, 218, 677-680.
- White, W. H. and Roberts, P.T. (1977) "On the Nature and Origins of Visibility Reducing Species in the Los Angeles Basin," *Atmospheric Environment*, 11, 803-812.

CHAPTER 2
MATHEMATICAL MODELING OF THE FORMATION AND
TRANSPORT OF AMMONIUM NITRATE AEROSOL

(Reprinted from *Atmospheric Environment*, 17, 949-964)

MATHEMATICAL MODELING OF THE FORMATION AND TRANSPORT OF AMMONIUM NITRATE AEROSOL

ARMISTEAD G. RUSSELL,* GREGORY J. McRAE† and GLEN R. CASS‡

*Department of Mechanical Engineering, †Environmental Quality Laboratory, ‡Environmental Engineering Science Department, California Institute of Technology, Pasadena, CA 91125, U.S.A.

(First received 19 April 1982; and in revised form 11 August 1982)

Abstract—A mathematical model describing the transport and formation of aerosol NH_4NO_3 is presented. Based on a vertically resolved Lagrangian trajectory formulation incorporating gas phase kinetics, NH_4NO_3 concentrations are computed at thermodynamic equilibrium with precursor HNO_3 vapor and NH_3 concentrations. Sensitivity analysis shows that NH_4NO_3 concentration predictions are strongly influenced by ambient temperature and NH_3 levels. A brief description of the NH_3 emissions inventory used in this study is included to indicate the important sources. The model was tested by comparison to ambient NH_3 , NH_4^+ and NO_3^- concentrations measured at El Monte, California during June 1974. Model results compare favorably with the ambient measurements and are used to explain trends in those measurements. An early morning nitrate peak develops as HNO_3 produced soon after sunrise reacts with NH_3 accumulated overnight. A second peak in nitrate concentration is predicted and observed at El Monte later in the day. Potential applications of this model to control strategy decisions and to study the fate of NO_x are discussed.

INTRODUCTION

Aerosol nitrates are important contributors to visibility reduction in cities with photochemical air pollution problems. White and Roberts (1977) estimate that during the ACHEX study, aerosol nitrates were responsible for about 40% of the light scattering observed at Riverside in the eastern Los Angeles Basin. Groblicki *et al.* (1981) report that 17% of the visibility problem in Denver is attributable to aerosol nitrates. Control strategies for urban visibility improvement in such cities will need to address aerosol nitrate abatement alternatives. Before this can be done, a reliable means is needed for predicting the relationship between pollutant emission sources and resulting nitrate concentrations.

Ammonium nitrate is a secondary pollutant formed from reactions between NH_3 and HNO_3 vapor. From thermodynamic considerations Stelson *et al.* (1979) and Stelson and Seinfeld (1982a, b) have shown that atmospheric NH_4NO_3 should be in equilibrium with precursor HNO_3 and NH_3 concentrations. The validity of this assumption has been tested in field experiments by Doyle *et al.* (1979), where it was found that the NH_4NO_3 equilibrium constant derived from published thermochemical data is consistent with atmospheric observations.

In this paper a mathematical model relating pollutant emissions to NH_4NO_3 concentrations is proposed and tested. Based on a Lagrangian trajectory formulation, the model includes transport, gas phase kinetics and aerosol production. A sensitivity analysis is performed on the NH_4NO_3 formation mechanism used in the trajectory model to indicate which parameters are most important to formation of atmospheric NH_4NO_3 . A summary of the emissions inventory used in this modeling study details the important

sources of NH_3 and their spatial distribution (Cass *et al.*, 1982). Model results will be evaluated against NH_3 , NH_4^+ and NO_3^- concentrations observed at El Monte, California on 28 June 1974. Potential use of this model for studying acid deposition and the fate of nitrogen containing pollutants is discussed.

MODEL DESCRIPTION

Ammonium nitrate aerosol is classified as a secondary pollutant because it is formed in the atmosphere from reactions involving gas phase precursors. To predict NH_4NO_3 formation, this paper utilizes a photochemical trajectory model coupled with an equilibrium treatment of aerosol production. Concentrations of the gas phase precursors of NH_4NO_3 as well as other pollutant concentrations are calculated using a vertically resolved, Lagrangian trajectory form of the atmospheric diffusion equation presented in McRae *et al.* (1982a). The equation governing the concentration of species i , $c_i(z, t)$, is

$$\frac{\partial c_i}{\partial t} = \frac{\partial}{\partial z} \left(K_{zz} \frac{\partial c_i}{\partial z} \right) + R_i(c_1, c_2, \dots, c_n, T) - \frac{\partial v_s c_i}{\partial z}; \quad i = 1, 2, \dots, n \quad (1)$$

with initial conditions

$$c_i(z, 0) = c_i^0(z) \quad t = 0 \quad (2)$$

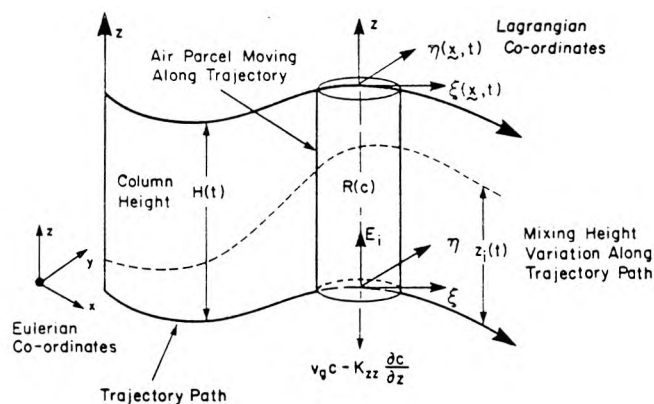
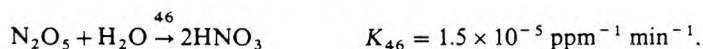
and boundary conditions

$$\left(K_{zz} \frac{\partial c_i}{\partial z} \right) = 0 \quad z = H \quad (3a)$$

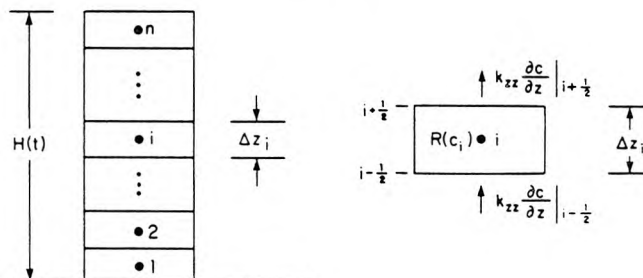
$$\left[v_s c_i - K_{zz} \frac{\partial c_i}{\partial z} \right] = E_i \quad z = 0, \quad (3b)$$

Ground level ($z = 0$) boundary conditions are a statement of mass continuity, accounting for surface deposition, diffusive transport and emissions. Since the top of the region ($z = H$) is well above the mixing depth, turbulent transport through the top of the air column is negligible. Deposition velocities are used to describe the interaction and reaction of gases and aerosols with surfaces. In general, v_g^i is dependent on meteorological conditions and on the reactivity of species i with the underlying surface. Limits on the aerosol deposition rates can be found using the same modeling techniques as those for gaseous pollutants. The vertically resolved trajectory model and computational cells are shown schematically in Fig. 1.

The chemical kinetics associated with the term $R_i(c_1, \dots, c_n, T)$ in (1) are described using the photochemical reaction mechanism of Falls and Seinfeld (1978), Falls *et al.* (1979), McRae *et al.* (1982a) and McRae and Seinfeld (1983). Only those homogeneous gas phase pathways producing HNO_3 and their corresponding rate constants, at 25°C, will be given here. These pathways are:



(a)



(b)

Fig. 1. Schematic representation of (a) vertically resolved Lagrangian trajectory model and (b) the computational grid cell convention.

Other than direct emissions, the only source of HNO_3 is assumed to be the photochemical production through the above reactions. Reaction 18 is the dominant route producing HNO_3 for typical daytime atmospheric conditions. Photolytic loss of HNO_3 is ignored since it is small.

Equilibrium concentrations of gaseous NH_3 and HNO_3 , and the resulting concentration of solid or aqueous NH_4NO_3 can be calculated from fundamental thermodynamic principles using the method presented by Stelson and Seinfeld (1982a). The procedure is composed of several steps, requiring as input the ambient temperature and relative humidity (r.h.). First, the equilibrium state of NH_4NO_3 is defined. If the ambient relative humidity is less than the relative humidity of deliquescence, (r.h.d.), given by

$$\ln(\text{r.h.d.}) = 723.7/T + 1.7037, \quad (4)$$

then the equilibrium state of NH_4NO_3 is modeled as a solid. Supersaturated solutions also are possible. Formation of solid NH_4NO_3 , from the gas phase precursors, is described by the equilibrium system

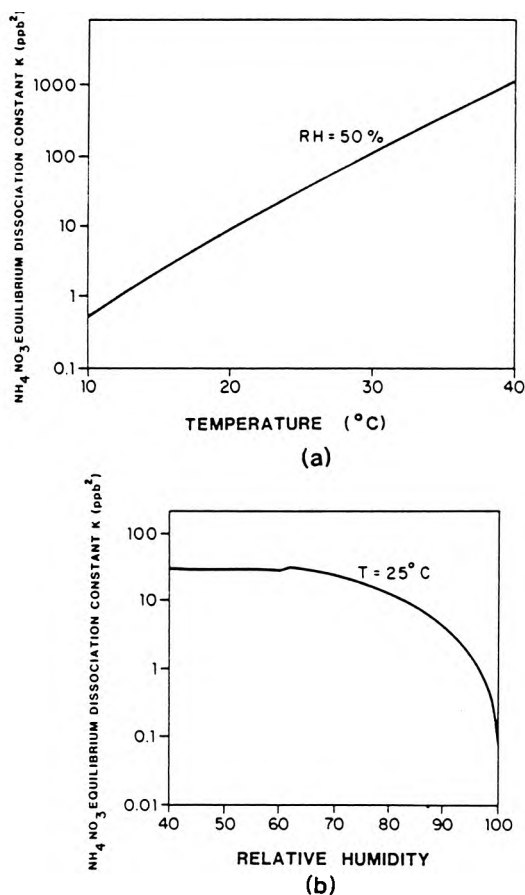
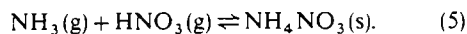


Fig. 2. (a) NH_4NO_3 equilibrium dissociation constant as a function of temperature (r.h. 50%). (b) NH_4NO_3 equilibrium dissociation constant as a function of r.h. (temperature, 25°C).

The dissociation constant is given by $K = P_{\text{NH}_3} P_{\text{HNO}_3}$, where P_{NH_3} and P_{HNO_3} are the partial pressures of NH_3 and HNO_3 , respectively. K can be estimated by integrating the van't Hoff equation. The resulting equation for K , in units of ppb^2 (assuming 1 atm of total pressure) is

$$\ln K = 84.6 - 24220/T - 6.1 \ln(T/298). \quad (6)$$

At relative humidities above that of deliquescence, NH_4NO_3 will be found in the aqueous state. A dissociation constant for the comparable reaction involving aqueous NH_4NO_3 can be found and is a function of both temperature and relative humidity. Temperature dependent equilibrium relative humidities above ionic solutions (r.h.t.) can be calculated from

$$\text{r.h.t.} = 100 \exp\left(\frac{-vmM\phi_T}{1000}\right), \quad (7)$$

where v is the number of moles of ions formed by ionization of one mole of solute. M the molecular weight of water, m the molality of the solution and ϕ_T is the osmotic coefficient given by

$$\phi_T = 1 + \frac{1}{m} \int_0^m m d(\ln \gamma^\pm)_T, \quad (8)$$

where γ^\pm is the mean molal activity of NH_4NO_3 in the solution at temperature T . The activity coefficient depends on temperature and molality. An iterative scheme is used to match the relative humidity calculated from (7) to the ambient relative humidity. This calculation gives the equilibrium solution molality and activity that are needed to evaluate K , the equilibrium dissociation constant, from the expression

$$\ln(K/(\gamma^\pm m)^2) = 54.18 - 15860/T + 11.206 \ln(T/298). \quad (9)$$

If the ambient relative humidity is between that of deliquescence and the value given by (7) for a saturated solution at $m = 25.954$, linear interpolation is used between the corresponding dissociation constants.

Figures 2(a) and (b) depict the dependence of K on T and r.h. For typical atmospheric conditions, the mechanism predicts an equilibrium dissociation constant between $0.04 (\text{ppb})^2$ at 5°C and 90% r.h. and $1400 (\text{ppb})^2$ at 40°C and a r.h. of 30% . Figure 2(b) indicates that extrapolation of the calculation scheme used for aqueous solutions to that for supersaturated solutions would give results slightly different than those found using (6) for solid NH_4NO_3 . In the case of a saturated solution surrounding solid NH_4NO_3 , equating the chemical potentials across interfaces shows that the appropriate dissociation constant is the same as that for the solid. This model assumes that the time required for the gaseous precursors, and water, to come to equilibrium is short compared to the characteristic time for the production of HNO_3 . This may not be true if the concentrations of the precursors differ by orders of magnitude, though this is seldom the case in

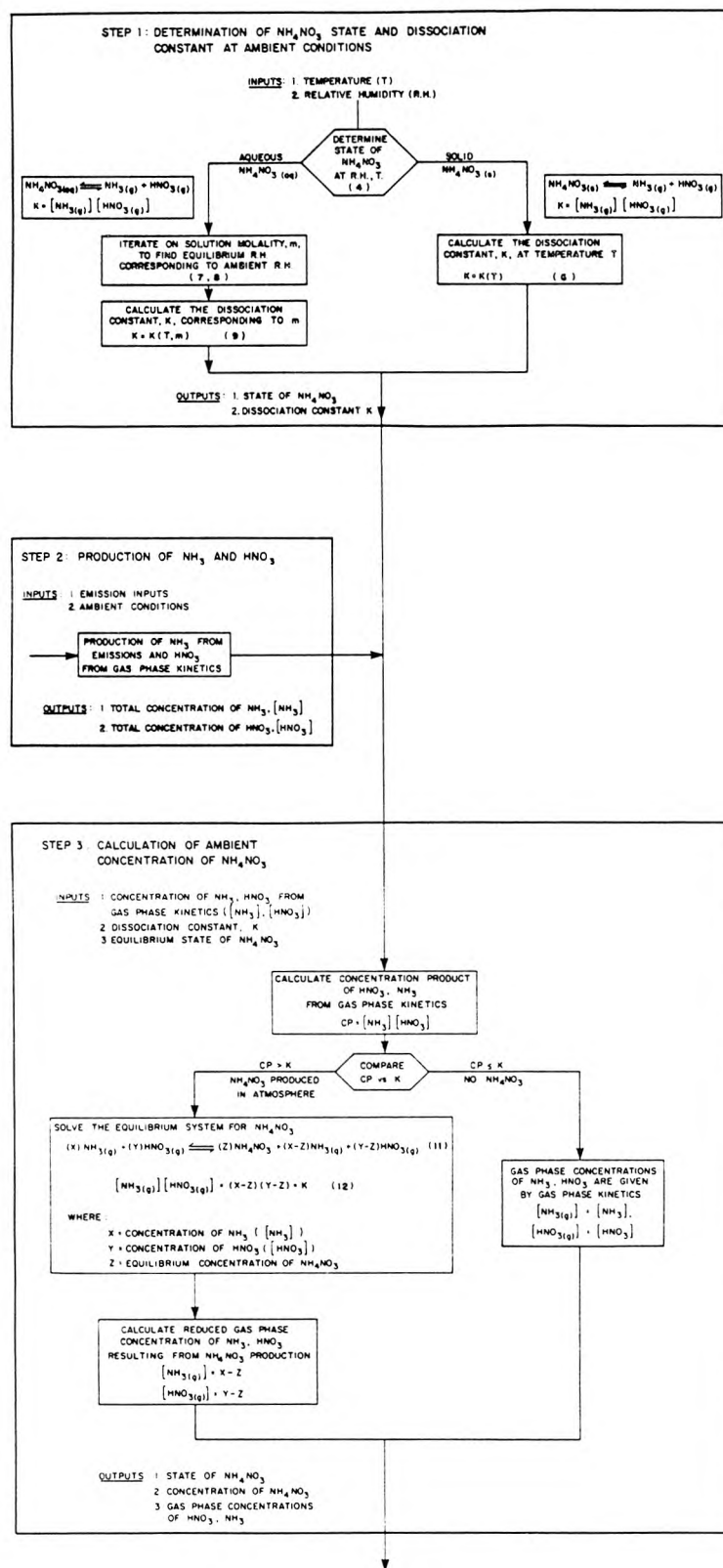
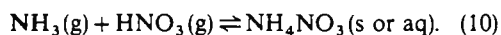


Fig. 3. Flow diagram of NH_4NO_3 formation mechanism illustrating three basic steps in calculation procedure.

urban basins. Nitric acid and NH_3 losses to other aerosol species are neglected at this point, and thus mixed aerosols are not considered. These effects can be incorporated once sufficient, appropriate field data become available to verify a more complex model.

Gas phase concentrations of NH_3 and HNO_3 and the concentration of NH_4NO_3 are then calculated from precursor concentrations and the equilibrium system



Concentrations of the different species can be determined mathematically by solving the following system of equations.

$$\begin{aligned} (x)\text{NH}_3(\text{g}) + (y)\text{HNO}_3(\text{g}) &\rightleftharpoons (a)\text{NH}_4\text{NO}_3 \\ &+ (x-a)\text{NH}_3(\text{g}) \\ &+ (y-a)\text{HNO}_3(\text{g}) \end{aligned} \quad (11)$$

and

$$[\text{NH}_3(\text{g})][\text{HNO}_3(\text{g})] = (x-a)(y-a) = K, \quad (12)$$

where x is the total concentration of NH_3 plus NH_4^+ , y is the total concentration of HNO_3 plus nitrate, a is the resulting concentration of NH_4NO_3 aerosol, and $(x-a)$, $(y-a)$ are the equilibrium gas phase concentrations of NH_3 and HNO_3 , respectively.

If the product of the concentrations of NH_3 and HNO_3 is smaller than the dissociation constant,

$$[\text{NH}_3(\text{g})][\text{HNO}_3(\text{g})] = (x)(y) < K \quad (13)$$

no NH_4NO_3 should be present. In this case the gas phase concentrations are as given by the gas phase kinetics. The steps involved in predicting the nitrate concentrations are shown schematically in Fig. 3.

SENSITIVITY STUDY

A Fourier amplitude sensitivity test (FAST) (Koda *et al.*, 1979; McRae *et al.*, 1982b) was performed on the NH_4NO_3 calculation scheme to assess which parameters contribute most to the formation of NH_4NO_3 in the atmosphere. The ranges of species concentrations used in the analysis are representative of those observed by Tuazon *et al.* (1981) for Claremont, California and were measured by Fourier transform infrared (FTIR) spectroscopy. In these experiments the FTIR sampling cell temperature was often considerably higher than ambient, which could volatilize some of the NH_4NO_3 , so the measurements may give $\text{NH}_3(\text{g})$ and $\text{HNO}_3(\text{g})$ levels higher than ambient. The results of the FAST analysis are shown in Table 1, where it can be seen that NH_4NO_3 formation is most sensitive to variations in temperature. The reason for this is the strong dependence of the dissociation constant on T . Two insights can be gained from FAST analysis, the first being that it is critically important to specify the temperature field accurately. Secondly, since nitrate formation is sensitive to NH_3 over the range encountered, control of upwind NH_3 emissions

Table 1. Sensitivity of ammonium nitrate formation model to input parameters

Parameter	Range	Sensitivity* (%)
Temperature	10–40°C	41
Ammonia	4–23 ppb†	39
Nitric acid	6–49 ppb†	17
Relative humidity	20–90%	3

* Partial variance, normalized to 100%, indicates the relative importance of variation of model inputs on NH_4NO_3 formation.

† Values representative of those found in Tuazon *et al.* (1981) for Claremont, California.

should prove to be beneficial in limiting NH_4NO_3 concentrations at Claremont and that an accurate description of the NH_3 emissions is required for modeling purposes.

To show how the concentrations of NH_4NO_3 change with ambient meteorological conditions, representative levels of total NH_3 (i.e. $\text{NH}_3(\text{g}) + \text{NH}_4^+$) and total HNO_3 (i.e. $\text{HNO}_3(\text{g}) + \text{NO}_3^-$) were used to calculate NH_4NO_3 concentrations over a range of atmospheric conditions. Predicted concentrations of NH_4NO_3 ranged from 0 to $67.6 \mu\text{g m}^{-3}$, with typical values of about $10 \mu\text{g m}^{-3}$ corresponding to 25°C, 65% r.h., 8 ppb of total NH_3 and 16 ppb of total HNO_3 . Concentration plots in Fig. 4 again show that NH_4NO_3 formation is sensitive to temperature, decreasing rapidly as temperature increases. An interesting aspect of the temperature dependence is the flat area indicating that no NH_4NO_3 is present. Above 35°C little NH_4NO_3 would be present except at high ambient levels of the gas phase precursors, while at 15°C some NH_4NO_3 would be present at most precursor concentrations. Figure 4 also shows that there is little change in NH_4NO_3 formation as the r.h. changes, although the effect is to create slightly more NH_4NO_3 as r.h. increases.

EMISSIONS DATA REQUIRED FOR MODEL EVALUATION

Once the model has been formulated the next step is to evaluate its ability to predict ambient levels of NH_4NO_3 . The data required for such tests include; pollutant emissions, observed air quality and the prevailing meteorology. In the Los Angeles Basin accurate emission inventories exist only for the period between 26 and 28 June 1974, limiting model evaluation to those three days. Descriptions of the emission inventories for NO_x and reactive hydrocarbons together with the local meteorological conditions for this period are available in McRae and Seinfeld (1983). As indicated by the sensitivity analysis, there is a need for an accurate description of the NH_3 emissions. Cass *et al.* (1982) have recently completed such a study for the year 1974, and the principal results are summarized here. A grid system composed of $5 \times 5 \text{ km}$ cells was

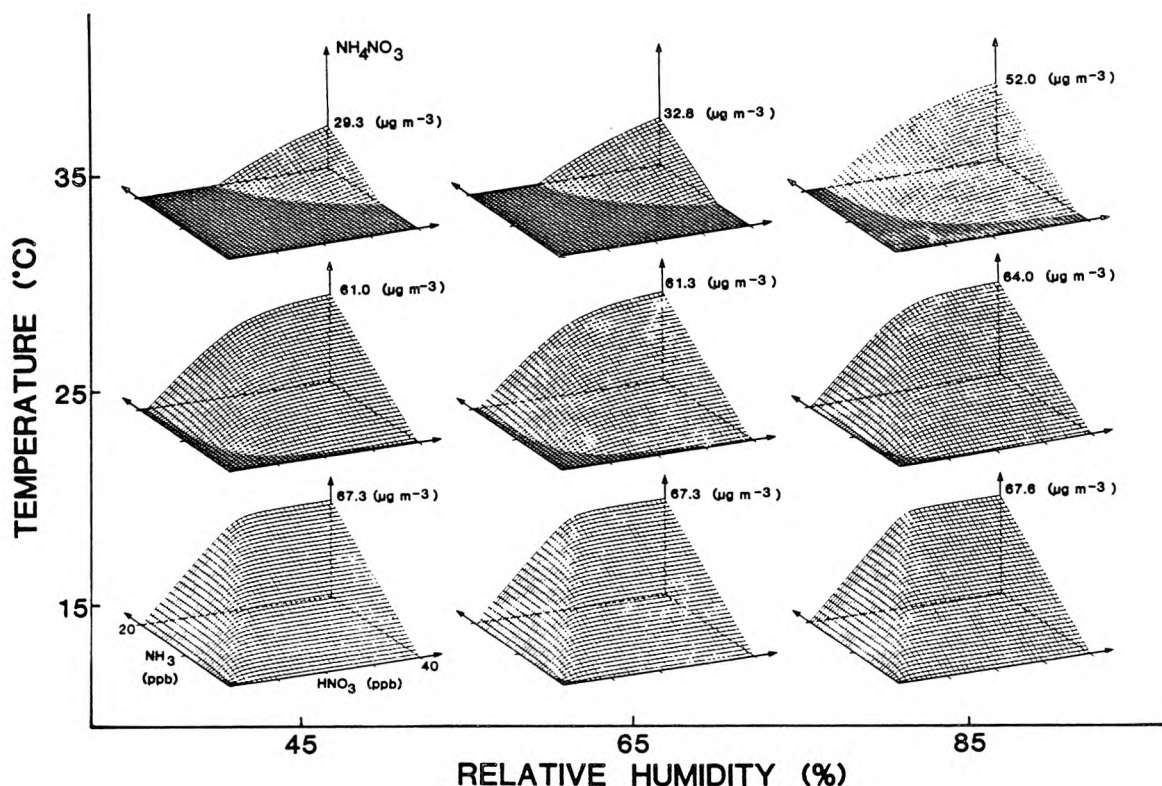


Fig. 4. Predicted NH_4NO_3 concentration surfaces at 15, 25 and 35°C and 45, 65 and 85% r.h. for total NH_3 and total HNO_3 concentrations up to 20 and 40 ppb, respectively.

superimposed on the South Coast Air Basin map (Fig. 5). Ammonia emissions were estimated within each grid cell for the 53 classes of mobile and stationary source types listed in Table 2.

Source tests show that trace amounts of NH_3 are present in the exhaust of both mobile and stationary

combustion sources (Cadle and Mulawa, 1980; Gentel *et al.*, 1973; Harkins and Nicksic, 1967; Henein, 1975; Hovey *et al.*, 1966; Hunter, 1971; Muzio and Arand, 1976; Wohlers and Bell, 1956). Emission factors for NH_3 release obtained from these and other references were combined with fuel use data reported by Cass

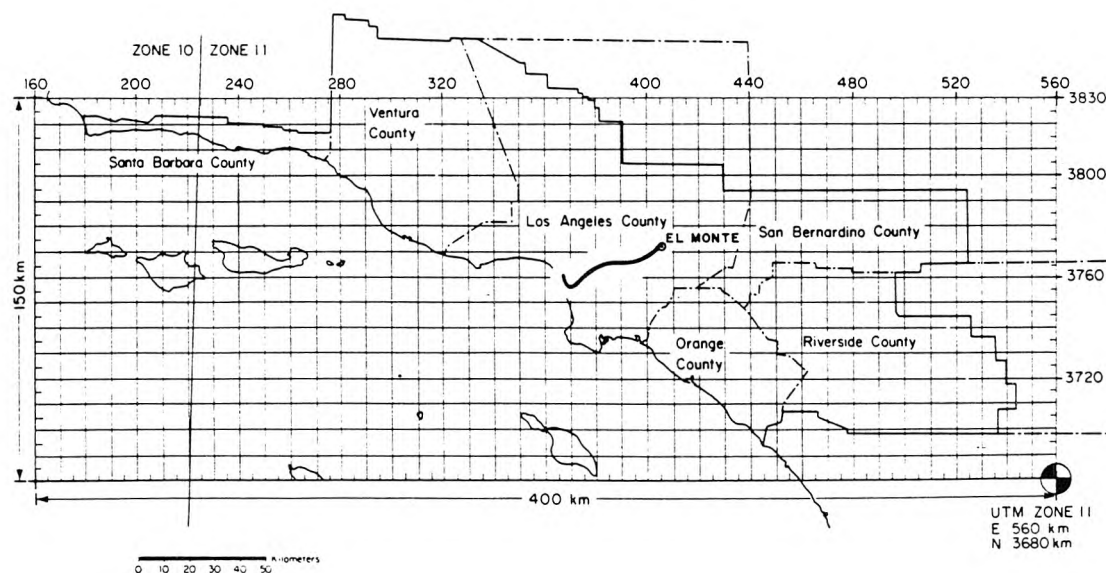


Fig. 5. Gridded map of the South Coast Air Basin used for constructing NH_3 emissions inventory. Superimposed on the map is the trajectory path that reaches El Monte at 3 p.m. (PDT) on 28 June 1974.

Table 2. Summary of ammonia emissions by source category in the South Coast Air Basin 1974

Source category	Total emissions (kg day ⁻¹)
Stationary fuel combustion	
Electric utility	
Natural gas	590.0
Residual oil	2000.0
Digester gas	0.5
Refinery fuel burning	
Natural gas	160.0
Residual oil	99.0
Refinery gas	420.0
Industrial fuel burning	
Natural gas	610.0
Liquified petroleum gas (LPG)	4.0
Residual oil	150.0
Distillate oil	140.0
Digester gas	9.0
Coke oven gas	15.0
Residential/commercial fuel burning	
Natural gas	270.0
Liquified petroleum gas (LPG)	4.0
Residual oil	62.0
Distillate oil	73.0
Coal	20.0
Sub totals	4626.5 (3.09 %)
Mobile source fuel combustion	
Automotive	
Non-catalyst autos and light trucks	3309.0
Medium and heavy duty trucks	449.9
Diesel vehicles	370.0
LPG for carburetion	10.0
Civilian aircraft	
Jet	150.0
Piston	2.9
Shipping	
Residual oil boilers	70.0
Diesel ships	50.0
Railroad-diesel oil	90.0
Military	
Gasoline	10.0
Diesel	60.0
Jet fuel	50.0
Residual oil	0.8
Off highway vehicles	120.0
Sub totals	4742.6 (3.17 %)
Industrial point sources	2070.0 (1.38 %)
Soil surface	23790.0 (15.9 %)
Fertilizer	
Farm crop	2870.0
Orchards	2390.0
Handling	380.0
Non-farm	7420.0
Sub totals	13060.0 (8.72 %)
Livestock	
Cattle	
Dairy	24390.0
Feedlot	6880.0
Range	12160.0
Horses	16220.0
Sheep	990.0
Hogs	250.0
Chickens	18200.0
Turkeys	1120.0
Sub totals	80210.0 (53.6 %)

Table 2. (contd).

Source category	Total emissions (kg day ⁻¹)
Domestic	
Dogs	10350.0
Cats	3230.0
Human respiration	46.0
Human perspiration	7000.0
Household ammonia use	600.0
Sub totals	21226.0 (14.2%)
Total	149725.1 (100.0)%

(1978) to give total NH_3 emissions from autos, trucks, railroads, shipping, plus industrial, residential and commercial fuel use. Within each fuel use category, the NH_3 emissions shown in Table 2 were distributed spatially in the same manner as NO_x emissions. A number of industrial processes are known to emit NH_3 (National Research Council, 1979; Miner, 1969), including refinery operations, NH_3 -based fertilizer manufacturing, NH_3 storage facilities, refrigeration plants, chemical plants and steel mill coke ovens. Estimates of NH_3 emissions from industrial facilities were derived from source test information and questionnaires sent to individual companies.

Biological decay processes also produce NH_3 and the release rates from a variety of soil surface types are available (Porter *et al.*, 1975; Elliot *et al.*, 1971; Denmead *et al.*, 1978; Denmead *et al.*, 1976; Miner, 1976). Using aerial photographs and maps available from the U.S. Geological Survey (1976) the land use within each grid square was summarized by type. Emissions from exposed land surfaces were estimated within each square by matching emission rate data to soil surface types.

Chemical fertilizers used in the air basin include NH_3 , urea, NH_4NO_3 and $(\text{NH}_4)_2\text{SO}_4$. Depending on fertilizer type and method of application, anywhere from a few percent to several tenths of the nitrogen content may be lost to the atmosphere as NH_3 (Baker *et al.*, 1959; Ernst and Massey, 1960; Gasser, 1964; McDowell and Smith, 1958; Stanley and Smith, 1955; Trickey and Smith, 1955; Wahhab *et al.*, 1957; Walkup and Nevins, 1966). The NH_3 loss characteristics of fertilizers were estimated by consultation with a local agricultural expert (Meyer, personal communication). Fertilizer use statistics were obtained from the California Department of Food and Agriculture (1974) and from the U.S. Bureau of the Census (1977). Chemical fertilizer consumption, subdivided into cropland, orchard and non-farm use, was combined with the NH_3 loss data to compute total NH_3 emissions.

Decomposition of livestock wastes is a major source of NH_3 emissions. Animal inventories by county were obtained from the U.S. Bureau of the Census (1977) and from state and county agricultural agents. Waste production rates, nitrogen content and NH_3 volatilization

rates were estimated for each major commercial animal type from previous studies (Adriano *et al.*, 1974; Fogg, 1971; Giddens and Rao, 1975; Lauer *et al.*, 1976; Luebs *et al.*, 1973a,b; Stewart, 1970; Taiganides and Hazen, 1966; Viets, 1971). Emissions from range animals were distributed spatially in proportion to pasture and herbaceous range land areas. U.S. Geological Survey (1976) maps were used to locate emissions from animals raised in confinement (e.g. dairy cattle, feedlot cattle). Ammonia losses from domestic animals (cats and dogs only) plus human respiration, perspiration and household cleaning chemicals were distributed in proportion to residential land use.

The overall spatial distribution of NH_3 , NO_x , reactive hydrocarbon and CO emissions in the South Coast Air Basin is shown in Fig. 6. The largest spike in the NH_3 diagram is centered over the town of Chino on the prevailing upwind side of the city of Riverside, and results from the intensity of livestock operations in that area.

AIR QUALITY DATA FOR MODEL EVALUATION

Within the three day time period for which emission data are available, aerosol nitrate measurements were sought that were taken over short sampling intervals (1–2 h) using methods that would minimize the possible interferences. Simultaneous concentration measurements of related aerosol species such as sulfate and ammonium were desired, as well as the concentration of relevant gas phase species, such as NH_3 , HNO_3 , NO_x and O_3 . The data set most nearly fulfilling the requirements was found for El Monte, California. The measurements were taken on 28 June 1974, and consist of 2-h averaged concentrations of aerosol nitrate and NH_4^+ , and gas phase NH_3 (Reynolds *et al.*, 1975). Aerosol nitrate and ammonium concentrations were obtained by using a low volume sampler with Gelman A glass fiber filters for collection followed by wet chemical analysis. Gaseous NH_3 concentrations were found using oxalic acid impregnated backup filters.

Ammonium nitrate data for other time periods in the Los Angeles area are available and are consistent with the results presented in Reynolds *et al.* (1975). These studies have found measured ambient nitrate

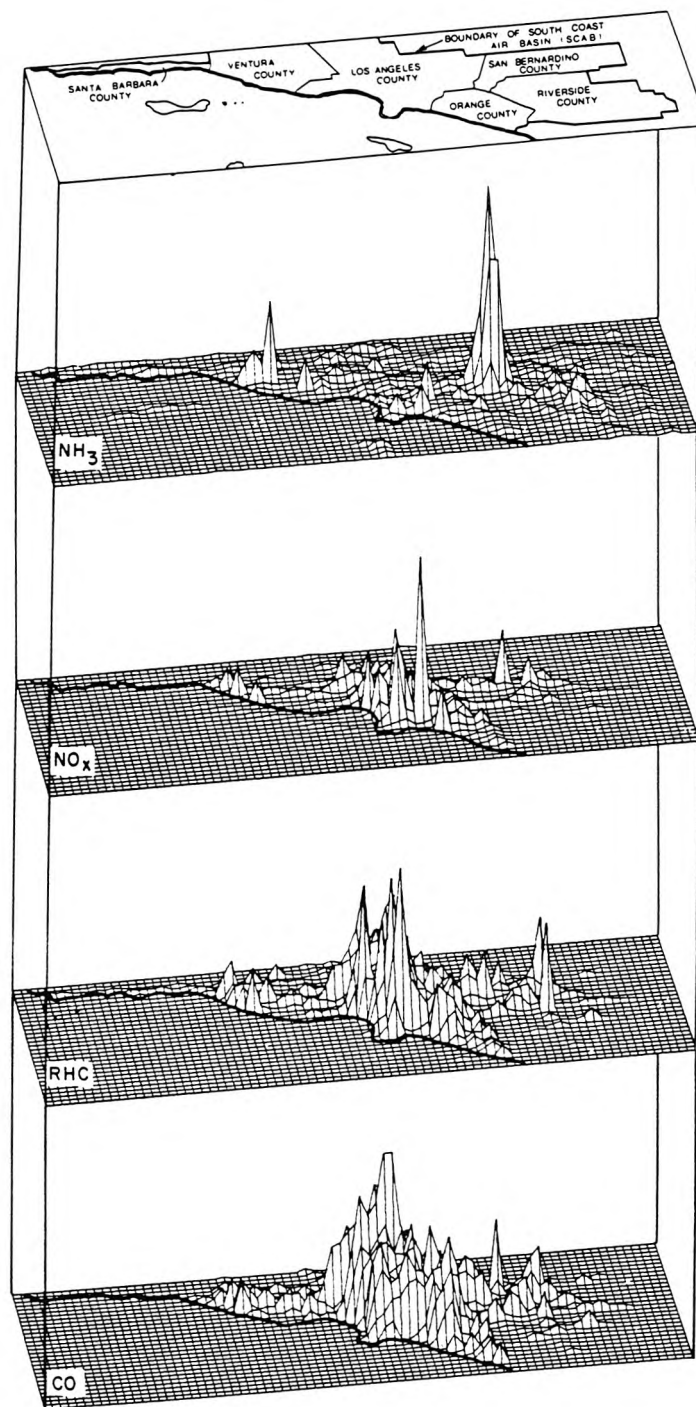


Fig. 6. Spatial representation of daily emissions of NH_3 , NO_x , reactive hydrocarbons (RHC) and CO in the South Coast Air Basin. (Inventory period June 1974.)

concentrations ranging up to $149 \mu\text{g m}^{-3}$, though values are generally lower (Lundgren, 1970; Hidy *et al.*, 1980; Appel *et al.*, 1978; Spicer, 1974; Appel *et al.*, 1981; Tuazon *et al.*, 1981). In Claremont, California, ambient levels of gaseous HNO_3 and NH_3 have been observed up to 49 and 23 ppb, respectively (Tuazon *et al.*, 1981). Concentrations of up to $86.4 \mu\text{g m}^{-3}$ of particulate

nitrate were also found at Claremont (Appel *et al.*, 1980). Nitrate levels were found to vary diurnally, peaking in the midmorning. Ozone and HNO_3 peaked later in the afternoon. Partial pressure products of NH_3 (g) and HNO_3 (g) from data taken at Claremont were compared against relative humidity and temperature. The product decreased with relative humidity and

increased with temperature, the same trend predicted from thermodynamic considerations.

When interpreting ambient measurements, it is important to be aware of the potential for artifact nitrate formation on filter substrates (Pierson *et al.*, 1980; Spicer and Schumacher, 1979; Appel *et al.*, 1979; Witz and McPhee, 1977). The physical nature of the nitrate artifact problem is that the gaseous HNO_3 may react with the filter substrate forming nitrate on the filter. This results in a positive error as more nitrate is measured on the filter than was deposited as an aerosol. A negative error can result from revolatilization of the NH_4NO_3 prior to sample analysis, or by reaction with other gaseous or particulate acids displacing the HNO_3 (Appel *et al.*, 1980). The observed revolatilization is in agreement with the equilibrium hypothesis employed in this paper. If the filter, after being loaded and before being analyzed, is exposed to a change in environment it would set up a new equilibrium between the aerosol and its environment, possibly altering the aerosol's measured composition. The new equilibrium could be due either to a change in temperature or to a change in the gaseous environment during or after sampling. To prevent this problem the NH_4NO_3 would have to be collected, stored and analyzed in a manner that prevents volatilization of the aerosol from the filter.

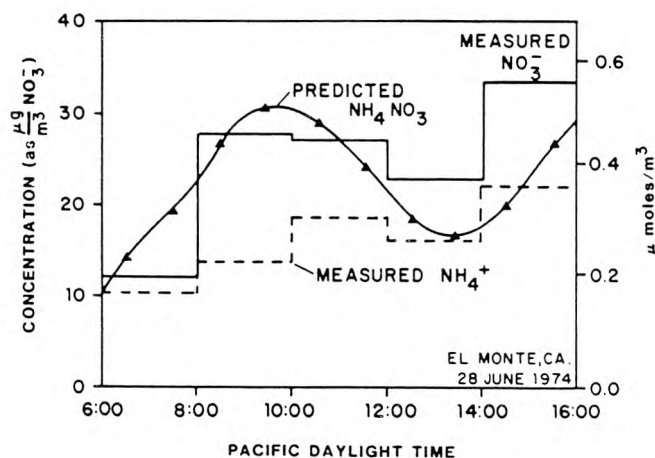
Steps have been taken to correct the filter artifact problem, the most direct being the use of a substrate that does not react with gaseous HNO_3 to form nitrate. Substrates that have been tested and show little reactivity with HNO_3 include polycarbonate, Teflon and quartz fiber (Spicer and Shumacher, 1979). Most glass fiber and nylon filters prove to be quite susceptible to artifact nitrate formation, although Gelman A filters are not as susceptible as many others (Appel *et al.*, 1979). Another method involves stripping the HNO_3 (g) from the sampling stream prior to filtration by passing the gas through a denuder, then measuring total nitrate downstream (Appel *et al.*, 1981).

MODEL EVALUATION AGAINST AMBIENT MEASUREMENTS

Usually ambient measurements are made at a fixed location. A Lagrangian model, however, predicts concentrations along a trajectory in a single air mass as it flows through the air basin. The path of a sample trajectory, the one starting at 1 a.m. and reaching E1 Monte at 3 p.m. Pacific Daylight Time (PDT) on 28 June 1974, is shown on a map of the Los Angeles basin (Fig. 5). Use of a trajectory model to predict concentrations at different times for a fixed geographical location then requires finding the path that each air mass takes to reach that location at the appropriate time. This is done for trajectories reaching E1 Monte throughout the day of 28 June 1974 using the method prescribed in Goodin *et al.* (1979).

By taking a series of trajectories reaching E1 Monte during the day, a time history of species concentrations can be constructed (Fig. 7). Each concentration prediction shown represents a weighted average of three trajectories arriving at E1 Monte at 1 h intervals, and are plotted on the half hour. In Fig. 7(a), the predicted ground level NH_4NO_3 concentration is plotted along with the measured nitrate and NH_4^+ concentration. Concentrations are given in $\mu\text{mol m}^{-3}$ for all species and NO_3^- concentrations are restated in $\mu\text{g m}^{-3}$. Gas phase concentrations are also shown in ppm or ppb. Use of a system based on molar concentrations is more convenient in the presence of chemical reactions, and clarifies the relationship between aerosols and their gas phase precursors. Considering the difficulty in obtaining ambient nitrate measurements, comparison between observed and predicted nitrate concentrations is quite good.

From Fig. 7(a), it can be seen that the measured molar concentrations of aerosol nitrate exceed that of NH_4^+ . The difference could arise if species other than NH_4NO_3 were present in the aerosol (e.g. NaNO_3), or as a result of the filter artifact problem. Filter artifact problems can lead to either a positive error due to



(a)

Fig. 7(a).

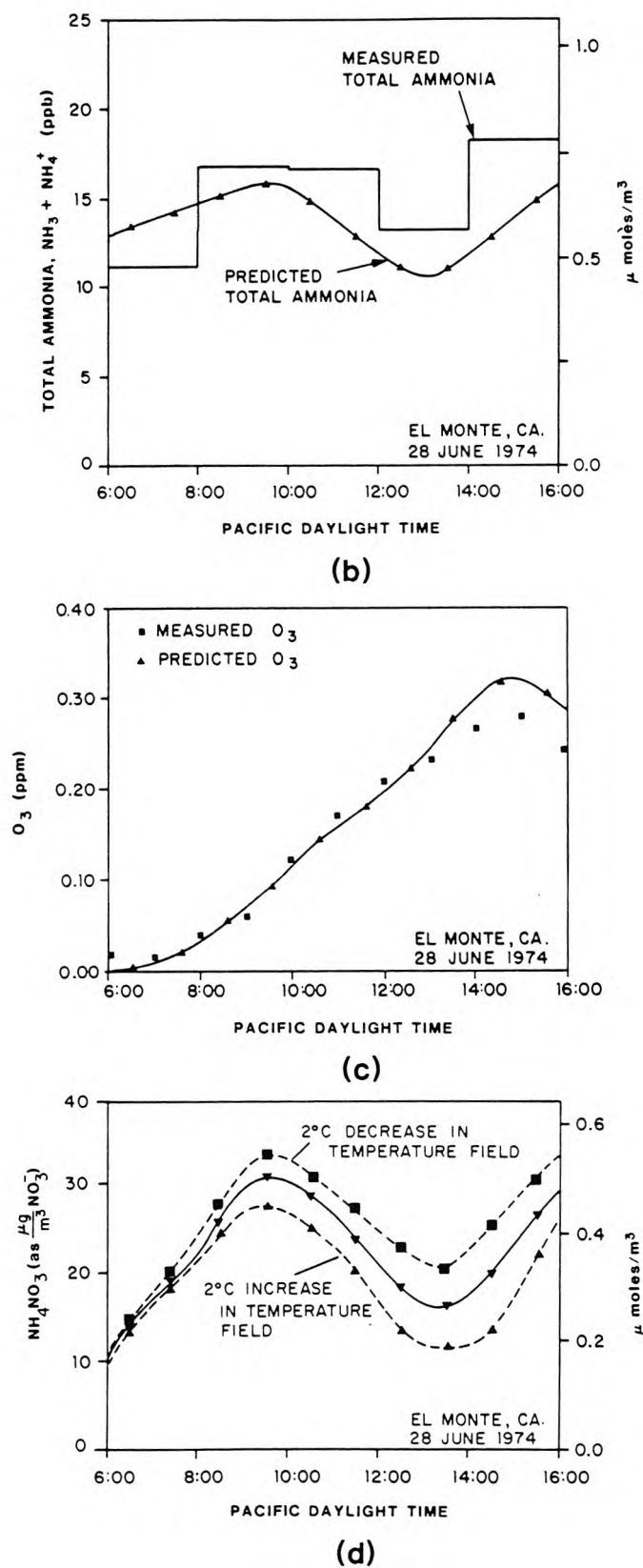


Fig. 7. Concentration profiles at El Monte on 28 June 1974. (a) Predicted NH_4NO_3 , measured NH_4^+ and measured NO_3^- . (b) Predicted total ammonia ($\text{NH}_3 + \text{NH}_4^+$) and measured total ammonia. (c) Predicted and measured O_3 concentrations. (d) Sensitivity of NH_4NO_3 formation to a $\pm 2^\circ\text{C}$ change in the temperature field.

HNO_3 reacting with the filter or a negative error from the volatilization of either ammonium or nitrate containing species. Twenty four hour averaged measurements for the day modeled showed only $5.1 \mu\text{g m}^{-3}$ of sulfate. Previous studies (e.g. Appel *et al.*, 1978) showed that most of the sulfate aerosol appears in the late afternoon. Thus, the interference from sulfate should be small for the period modeled. It is impossible to say how the predicted nitrate should compare to the measured nitrate concentrations without knowing the magnitude of the two types of possible sampling error.

Relatively little NH_4NO_3 is measured or predicted in the early morning. The concentration rises until about 10 a.m. (PDT) at which time it starts to decrease as the temperature increases. The same trend is found by other investigators (Appel *et al.*, 1980). Both the measurements and predictions for 28 June 1974, show an afternoon rise that is uncharacteristic of the usual decrease in NH_4NO_3 as the temperature increases. Figure 7(b), the plot of the predicted and measured total (gas plus aerosol phase) NH_3 concentrations, shows that the reason for the unexpected afternoon peak is that the air mass contains more NH_3 . Figure 7(b) also serves as a check on the NH_3 emissions inventory. Even in the presence of possible transfer of revolatilized NH_3 to the oxalic acid impregnated backup filter used to measure NH_3 , the sum of measured NH_3 and NH_4^+ should give total NH_3 . Predicted total NH_3 is about 10–20% low through most of the day, except in the early morning. Predictions follow the same diurnal trends as the measurements, indicating the spatial accuracy of the inventory over which the trajectory passed.

In view of the possible effects occurring from nitrate artifact formation, it is interesting to note that the predicted nitrate levels are high in the morning when the potential to form artifact nitrate is small. In the afternoon the increasing HNO_3 concentration raises the potential formation of artifact nitrate, and it is seen that the predicted nitrate concentrations begin to fall below the measured levels.

As an additional check on model performance, predicted O_3 concentrations at El Monte are compared to measurements in Fig. 7(c), and the two profiles compare well. Ozone measurements were not taken at El Monte, so the measured values being used are interpolated from surrounding monitoring sites.

A good measure of the sensitivity of nitrate formation to temperature variations is obtained from Fig. 7(d). Increase in the separation between the curves is due almost totally to the change in K from the temperature change, not from a change in the amount of total inorganic nitrate produced. This figure also illustrates the potential problems arising from either upsetting the equilibrium, or from errors in the temperature field specification.

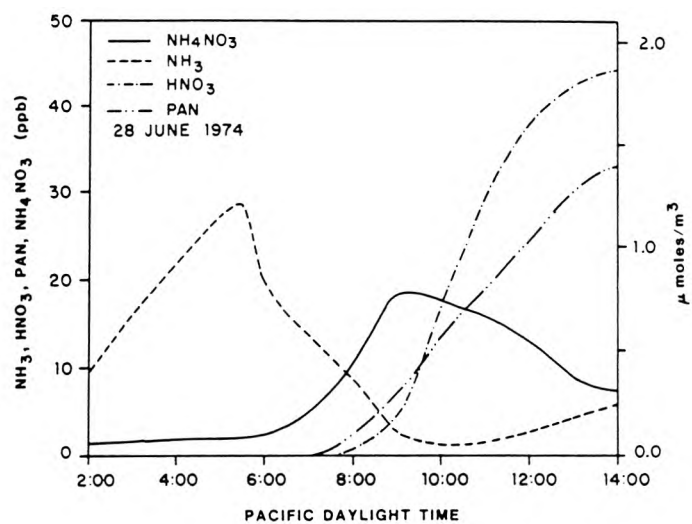
For model evaluation purposes it was necessary to compare predictions and observations at a fixed point; however, it is more illuminating to investigate dynamics of the nitrate aerosol production along a single

trajectory. In this manner the effects of the physical processes are more easily isolated. In the series of plots shown in Fig. 8, the evolution of pollutant concentrations is shown as the air mass traverses the basin. Early morning NH_3 emissions into the air parcel increase the NH_3 concentrations but have only a small effect on the aerosol levels because little HNO_3 has been produced by photochemical reactions (Fig. 8a). After sunrise, photochemical reactions start forming inorganic nitrate from the oxidation of NO_x emissions. Initially most of the nitrate formed is tied up in the aerosol phase increasing the NH_4NO_3 concentration and decreasing that of NH_3 . Nitric acid continues to be the limiting species for aerosol formation until 8 a.m. when the HNO_3 concentration begins to rise rapidly. Both NH_4NO_3 and HNO_3 levels continue to increase, and NH_3 to drop, until about 9 a.m. when a midmorning NH_4NO_3 peak occurs. After this time the NH_4NO_3 concentration decreases due to two effects, aerosol volatilization by the increasing temperature and dilution by the growing mixed layer. The profile for PAN, an organic nitrate, is shown in Fig. 8(a). PAN follows the same diurnal trend as HNO_3 , peaking at 33 ppb compared to 44 ppb for HNO_3 . The peak HNO_3 concentration was 13% that of O_3 . Tuazon *et al.* (1981) found a similar PAN to HNO_3 ratio and approximately the same maximum values. For example, the peak HNO_3 levels were 11% of the observed O_3 concentrations at Claremont, California in 1978.

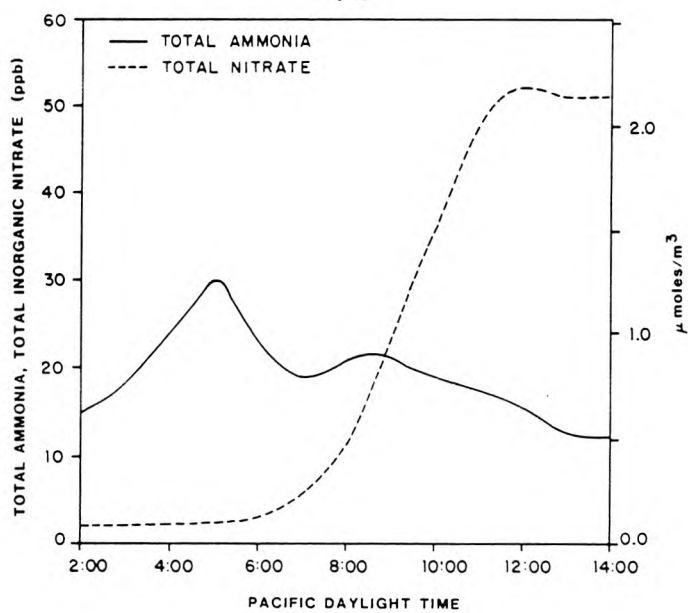
Figure 8(b) graphically illustrates the initial rise in NH_3 from emissions. Photochemical reaction of NO_x causes a rapid increase in the concentration of total inorganic nitrate shortly after sunrise at 5:45 a.m. Total nitrate increases until about noon when dilution and deposition of HNO_3 and NH_4NO_3 cause the total nitrate concentrations to stabilize. Profiles of three pollutants related to HNO_3 formation, O_3 , NO and NO_2 , are shown in Fig. 8(c) for comparison.

Vertically-resolved profiles of NH_4NO_3 and its precursors are plotted in Fig. 9 at three different times during the day. Early in the morning, the most marked profile is that of NH_3 showing that the emissions are being trapped within the mixed layer. Four hours later, at 8 a.m., the mixing depth has increased and so has the NH_4NO_3 , but the availability of HNO_3 is still limiting the formation. By noon, HNO_3 is the most abundant species below the temperature inversion and NH_3 availability now limits aerosol formation. Directly above the inversion base the change in the NH_3 profile is created by the decrease in HNO_3 allowing a higher equilibrium NH_3 concentration.

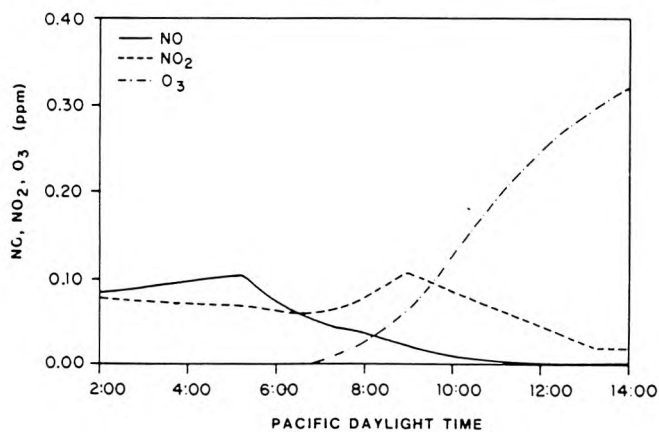
In this study, the currently available collection of simultaneous observations on emissions and air quality has been pursued as far as it can be taken, and it is apparent that additional model applications should be supported by a data set explicitly designed for nitrate air quality model verification. Such a data set should include simultaneous measurements on all species of interest including NH_3 and HNO_3 vapor, plus NH_4^+ and NO_3^- concentrations. Measurement



(a)



(b)



(c)

Figs 8(a)-(c).

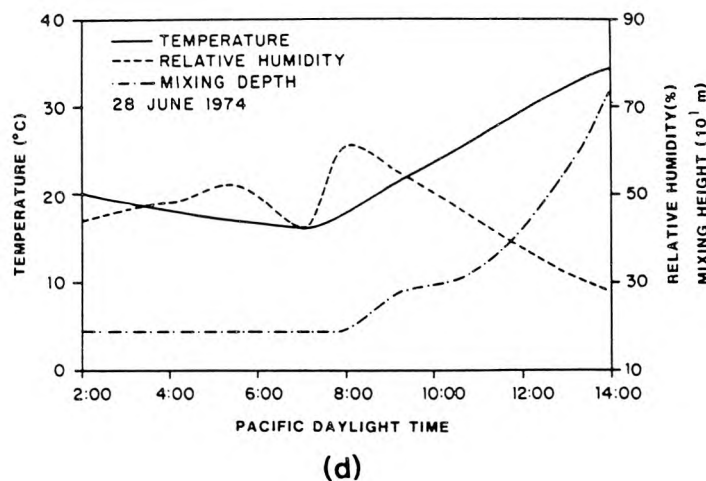


Fig. 8. Predicted concentrations and observed meteorological variables for the air parcel reaching El Monte at 2 p.m. (PDT) 28 June 1974. (a) NH_4NO_3 , NH_3 , HNO_3 and PAN profiles. (b) Total ammonia and total nitrate profiles (c) NO , NO_2 and O_3 profiles. (d) Meteorological parameters: mixing depth, temperature and relative humidity.

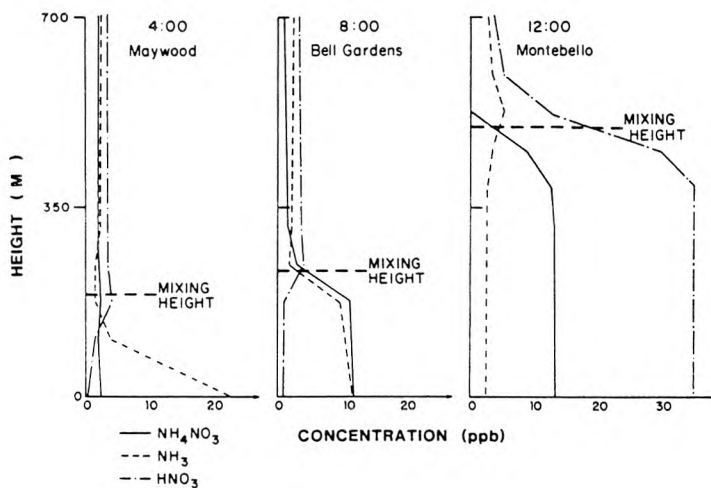


Fig. 9. Evolution of vertical concentration profiles of NH_3 (---), HNO_3 (— · —) and NH_4NO_3 (—) in the air parcel that reaches El Monte at 2 p.m. (PDT) 28 June 1974. Results shown are for 4 a.m., 8 a.m. and 12 noon and the location is given for the air parcel at those times.

methods should be selected that will minimize sampling artifact problems. The sensitivity analysis presented in this paper points to the need for highly accurate temperature data. Model structure dictates that temperature measurements must be available along the trajectory considered, not just at the end point of the trajectory.

FUTURE MODEL APPLICATIONS

Potential uses of this model include control strategy determination for visibility improvement and the

study of aerosol processes, acid deposition and the fate of nitrogen containing species. Results from this model as well as field measurements (Tuazon *et al.*, 1981) indicate that along most of the trajectories in the western portion of the Los Angeles Basin there is more HNO_3 than NH_3 , and that the main factors limiting the formation of aerosol are warm temperatures and lack of NH_3 . This result was also indicated by the sensitivity analysis performed on the formation mechanism alone. In the eastern part of the basin, downwind of the dairies, the situation may well be reversed, resulting in a HNO_3 deficiency.

Since both HNO_3 and NH_4NO_3 are products of NO_x reactions, the ability to model these two species can be valuable in studying the final fate of pollutant nitrogen. The model can give bounds on the amount of HNO_3 and aerosol nitrate deposition. Also by using the vertically resolved species concentrations, the mass of nitrogen containing species advected out of the basin can be approximated. Possible future uses of this work include studying acid deposition. An important part of that investigation would include the transport and production of NH_3 which would act to neutralize acid deposition of both the solid and aqueous phases.

CONCLUSIONS

The mathematical model for urban air pollution presented here solves the basic equations describing the transport and production of gaseous species, and the generation of NH_4NO_3 aerosol. This model is able to quantitatively predict an aerosol species concentration produced by gas phase reactions and condensation in an urban atmosphere directly from species emissions using a mechanistic description of atmospheric processes. Predictions of this model include vertically resolved species concentration profiles of gaseous pollutants and aerosol NH_4NO_3 .

Predictions from the proposed model agree well with the 1974 ambient measurements at El Monte, California, and show qualitatively the trends and concentrations found by more recent studies where measurement methods were used that suppress artifact nitrate problems. Future uses of the model include control strategy design for visibility improvement, the study of aerosol processes and the fate of NO_x emissions.

Acknowledgements—This work was supported by the California Air Resources Board under contract No. A7-169-30. The authors wish to acknowledge the assistance of Arthur Stelson and John Seinfeld in formulating the equilibrium model and William Goodin with help in supplying the necessary computational resources.

REFERENCES

- Adriano D. C., Chang A. C. and Sharpless R. (1974) Nitrogen loss from manure as influenced by moisture and temperature. *J. envir. Quality* **3**, 258–261.
- Appel B. R., Kothny E. L., Hoffer E. M., Hidy G. M. and Wesolowski J. J. (1978) Sulfate and nitrate data from the California aerosol characterization experiment (ACHEX). *Envir. Sci. Technol.* **12**, 418–425.
- Appel B. R., Wall S. M., Tokiwa Y. and Haik M. (1979) Interference effects in sampling particulate nitrate in ambient air. *Atmospheric Environment* **13**, 319–325.
- Appel B. R., Wall S. M., Tokiwa Y. and Haik M. (1980) Simultaneous nitric acid, particulate nitrate and acidity measurements in ambient air. *Atmospheric Environment* **14**, 549–554.
- Appel B. R., Tokiwa Y. and Haik M. (1981) Sampling of nitrates in ambient air. *Atmospheric Environment* **15**, 283–289.
- Baker J. H., Peech M. and Musgrave R. B. (1959) Determination of application losses of anhydrous ammonia. *Agron. J.* **51**, 361–362.
- Cadle S. H. and Mulawa P. A. (1980) Low molecular weight aliphatic amines in exhaust from catalyst-equipped cars. *Envir. Sci. Technol.* **14**, 718–723.
- California Department of Food and Agriculture (1974) Fertilizing materials—tonnage report, Oct–Nov–Dec 1974, California Department of Food and Agriculture, Sacramento, CA.
- Cass G. R. (1978) Methods for sulfate air quality management with applications to Los Angeles. Ph.D. thesis, California Institute of Technology, Pasadena, CA.
- Cass G. R., Gharib S., Peterson M. and Tilden J. W. (1982) The origin of ammonia emissions to the atmosphere in an urban area, Open File Report 82–6, Environmental Quality Laboratory, California Institute of Technology, Pasadena, CA.
- Denmead O. T., Freney J. R. and Simpson J. R. (1976) A closed ammonia cycle within a plant canopy. *Soil Biol. Biochem.* **8**, 161–164.
- Denmead O. T., Nulsen R. and Thurtell G. W. (1978) Ammonia exchange over a corn crop. *Soil Sci. Soc. Am. J.* **42**, 840–842.
- Doyle G. J., Tuazon E. C., Graham R. A., Mischke T. M., Winer A. M. and Pitts J. N., Jr. (1979) Simultaneous concentrations of ammonia and nitric acid in a polluted atmosphere and their equilibrium relationship to particulate ammonium nitrate. *Envir. Sci. Technol.* **13**, 1416–1419.
- Elliot L. F., Schuman G. E. and Viets F. G., Jr. (1971) Volatilization of nitrogen-containing compounds from beef cattle areas. *Soil Sci. Soc. Am. Proc.* **35**, 752–755.
- Ernst J. W. and Massey H. F. (1960) The effects of several factors on volatilization of ammonia formed from urea in the soil. *Soil Sci. Soc. Am. Proc.* **24**, 87–90.
- Falls A. H. and Seinfeld J. H. (1978) Continued development of a kinetic mechanism for photochemical smog. *Envir. Sci. Technol.* **12**, 1398–1406.
- Falls A. H., McRae G. J. and Seinfeld J. H. (1979) Sensitivity and uncertainty of reaction mechanisms for photochemical air pollution. *Int. J. chem. Kinetics* **11**, 1137–1162.
- Fogg C. E. (1971) Livestock waste management and the conservation plan. *Livestock Waste Management and Pollution Abatement—Proc. Int. Symp. Livestock Wastes*, American Society of Agricultural Engineers, St. Joseph, MI, pp. 34–35.
- Gasser J. K. R. (1964) Some factors affecting losses of ammonia from urea and ammonium sulphate applied to soils. *J. Soil Sci.* **15**, 258–272.
- Gentel J. E., Manary O. J. and Valenta J. C. (1973) Characterization of particulates and other non-regulated emissions from mobile sources and the effects of exhaust emissions control devices on these emissions. Dow Chemical Company, U.S. Environmental Protection Agency Document APTD-1567, Midland, MI.
- Giddens J. and Rao A. M. (1975) Effect of incubation and contact with soil on microbial and nitrogen changes in poultry manure. *J. envir. Quality* **4**, 275–278.
- Goodin W. R., McRae G. J. and Seinfeld J. H. (1979) An objective analysis technique for constructing three-dimensional, urban-scale wind fields. *J. appl. Met.* **19**, 98–108.
- Groblicki P. J., Wolff G. T. and Countess R. J. (1981) Visibility-reducing species in the Denver “brown cloud.” Part I. Relationships between extinction and chemical composition. *Atmospheric Environment* **15**, 2473–2484.
- Harkins J. H. and Nicksic S. W. (1967) Ammonia in auto exhaust. *Envir. Sci. Technol.* **1**, 751–752.
- Henein N. (1975) The diesel as an alternative automobile engine. Wayne State University, SAE Paper 750931.
- Hidy G. M., Mueller P. K., Grosjean D., Appel B. R. and Wesolowski J. J., editors (1980) *The Character and Origins of Smog Aerosols*. John Wiley, New York. 776 pp.
- Hovey H. H., Risman A. and Cunnann J. F. (1966) The

- development of air contaminant emission tables for non-process emissions. *J. Air Pollut. Control Ass.* **16**, 362-366.
- Hunter J. E., Jr. (1971) Effect of catalytic converters on automotive ammonia emissions, General Motors Research Laboratories, Research Publication GMR-1061, Warren, MI.
- Koda M., McRae G. J. and Seinfeld J. H. (1979) Automatic sensitivity analysis of kinetic mechanisms. *Int. J. chem. Kinetics* **11**, 427-444.
- Lauer D. A., Bouldin D. R. and Klausner S. D. (1976) Ammonia volatilization from dairy manure spread on the soil surface. *J. envir. Quality* **5**, 134-141.
- Liu M.-K. and Seinfeld J. H. (1975) On the validity of grid and trajectory models of urban air pollution. *Atmospheric Environment* **9**, 555-574.
- Luebs R. E., Davis K. R. and Laag A. E. (1973a) Enrichment of the atmosphere with nitrogen compounds volatilized from a large dairy area. *J. envir. Quality* **2**, 137-141.
- Luebs R. E., Laag A. E. and Davis K. R. (1973b) Ammonia and related gases emanating from a large dairy area. *Calif. Agric.* February pp. 10-12.
- Lundgren D. A. (1970) Atmospheric aerosol composition and concentration as a function of particle size and of time. *J. Air Pollut. Control Ass.* **20**, 603-608.
- McDowell L. L. and Smith G. E. (1958) The retention and reactions of anhydrous ammonia on different soil types. *Soil Sci. Soc. Am. Proc.* **22**, 38-42.
- McRae G. J. and Seinfeld J. H. (1983) Development of a second generation mathematical model for urban air pollution, II. Performance evaluation. *Atmospheric Environment* **17**, 501-523.
- McRae G. J., Goodin W. R. and Seinfeld J. H. (1982a) Development of a second generation mathematical model for urban air pollution, I. Model formulation. *Atmospheric Environment* **16**, 679-696.
- McRae G. J., Tilden J. W. and Seinfeld J. H. (1982b) Global sensitivity analysis—A computational implementation of the fourier amplitude sensitivity test (FAST). *Computers chem. Engng* **6**, 15-25.
- Miner J. R. (1976) Production and Transport of Gaseous NH_3 and H_2S Associated With Livestock Production. U.S. Environmental Protection Agency Document EPA-600/2-76-239, Ada, OK.
- Miner S. (1969) Air pollution aspects of ammonia, Litton Systems Inc., National Air Pollution Control Administration Document APTD 69-25, Bethesda, MD.
- Muzio L. J. and Arand J. K. (1976) Homogeneous gas phase decomposition of oxides of nitrogen. KVB Incorporated, Electric Power Research Institute Report FP-253, Project 461-1, Tustin, CA.
- National Research Council (1979) Ammonia. A report by the Subcommittee on Ammonia, Committee on Medical and Biologic Effects of Environmental Pollutants, National Research Council, University Park Press, Baltimore, MD.
- Pierson W. R., Brachaczek W. W., Korniski T. J., Truex T. J. and Butler J. W. (1980) Artifact formation of sulfate, nitrate and hydrogen ion on backup filters: Allegheny Mountain experiment. *J. Air Pollut. Control Ass.* **30**, 30-34.
- Porter L. K., Viets F. G., Jr., McCalla T. M. *et al.* (1975) Pollution Abatement from Cattle Feedlots in Northeastern Colorado and Nebraska, U.S. Environmental Protection Agency Report No. EPA-660/2-75-015, Corvallis, OR.
- Reynolds R., Tsou G. and Holmes J. (1975) The influence of gas phase ammonia on formation of aerosol. California Air Resources Board report, El Monte, CA.
- Spicer C. W. (1974) The fate of nitrogen oxides in the atmosphere. In *Advances in Environmental Science and Technology*, Vol. 7 (Edited by Pitts J. N. and Metcalf R. L.), Wiley, New York, pp. 163-261.
- Spicer C. W. and Schumacher P. M. (1979) Particulate nitrate: laboratory and field studies of major sampling interferences. *Atmospheric Environment* **13**, 543-552.
- Stanley F. A. and Smith G. E. (1955) Proper application improves value of NH_3 . *Agricultural Ammonia News*, April-June.
- Stelson A. W., Friedlander S. K. and Seinfeld J. H. (1979) A note on the equilibrium relationship between ammonia and nitric acid and particulate ammonium nitrate. *Atmospheric Environment* **13**, 369-371.
- Stelson A. W. and Seinfeld J. H. (1982a) Relative humidity and temperature dependence of the ammonium nitrate dissociation constant. *Atmospheric Environment* **16**, 983-992.
- Stelson A. W. and Seinfeld J. H. (1982b) Relative humidity and pH dependence of the vapor pressure of ammonium nitrate-nitric acid solutions at 25°C. *Atmospheric Environment* **16**, 993-1000.
- Stewart B. A. (1970) Volatilization and nitrification of nitrogen from urine under simulated cattle feedlot conditions. *Envir. Sci. Technol.* **4**, 579-582.
- Taiganides E. P. and Hazen T. E. (1966) Properties of farm animal excreta. *Trans. Am. Soc. agric. Engrs* **9**, 374-376.
- Trickey N. G. and Smith G. E. (1955) Losses of nitrogen from solution materials. *Soil Sci. Soc. Am. Proc.* **19**, 222-224.
- Tuazon E. C., Winer A. M. and Pitts J. N. (1981) Trace pollutant concentrations in a multiday smog episode in the California South Coast Air Basin by long pathlength FT-IR spectroscopy. *Envir. Sci. Technol.* **15**, 1232-1237.
- U.S. Bureau of the Census (1977) 1974 Census of Agriculture, Vol. 1, Part 5, California State and County Data, U.S. Department of Commerce, Washington, DC.
- U.S. Geological Survey (1976) Land Use and Land Cover 1972-1975, Santa Ana, CA (1971-1974, San Bernardino, CA; 1971-1974, Santa Maria, CA; 1972-1975, Long Beach, CA; 1973-1975, Los Angeles, CA) U.S. Department of the Interior, Geological Survey, Open File Maps No. 76-114-1 (76-115-1; 76-117-1; 76-118-1; 76-119-1), Land Use Series.
- Viets F. G., Jr. (1971) Cattle feedlot pollution. Animal Waste Management. *Proc. Nat. Symp. Animal Waste Management*, Washington, DC, Council of State Governments, pp. 97-106. Also published in *Agric. Sci. Rev.* **9**, 1-8.
- Wahhab A., Randhawa M. S. and Alam S. Q. (1957) Loss of ammonia from ammonium sulphate under different conditions when applied to soils. *Soil Sci.* **84**, 249-255.
- Walkup H. G. and Nevins J. L. (1966) The cost of doing business in agricultural ammonia for direct application. *Agric. Ammonia News* **16**, 96-100.
- White W. H. and Roberts P. T. (1977) On the nature and origins of visibility reducing species in the Los Angeles Basin. *Atmospheric Environment* **11**, 803-812.
- Witz S. and McPhee R. D. (1977) Effect of different types of glass filters on total suspended particulates and their chemical composition. *J. Air Pollut. Control Ass.* **27**, 239-241.
- Wohlens H. C. and Bell G. B. (1956) Literature Review of Metropolitan Air Pollutant Concentrations—Preparation, Sampling, and Assay of Synthetic Atmospheres. Stanford Research Institute, final report on Project No. SU1816, Menlo Park, CA.

CHAPTER 3

THE DYNAMICS OF NITRIC ACID PRODUCTION AND THE FATE OF NITROGEN OXIDES

(Reprinted from *Atmospheric Environment*, 19, 893-903)

THE DYNAMICS OF NITRIC ACID PRODUCTION AND THE FATE OF NITROGEN OXIDES

ARMISTEAD G. RUSSELL*, GREGORY J. McRAE† and GLEN R. CASS‡

Environmental Quality Laboratory, California Institute of Technology, Pasadena, CA 91125, U.S.A.

(First received 20 June 1984 and in final form 26 October 1984)

Abstract—A mathematical model is used to study the fate of nitrogen oxides (NO_x) emissions and the reactions responsible for the formation of nitric acid (HNO_3). Model results indicate that the majority of the NO_x inserted into an air parcel in the Los Angeles basin is removed by dry deposition at the ground during the first 24 h of travel, and that HNO_3 is the largest single contributor to this deposition flux. A significant amount of the nitric acid is produced at night by N_2O_5 hydrolysis. Perturbation of the N_2O_5 hydrolysis rate constant within the chemical mechanism results in redistribution of the pathway by which HNO_3 is formed, but does not greatly affect the total amount of HNO_3 produced. Inclusion of NO_3 -aerosol and N_2O_5 -aerosol reactions does not affect the system greatly at collision efficiencies, α , of 0.001, but at $\alpha = 0.1$ or $\alpha = 1.0$, a great deal of nitric acid could be produced by heterogeneous chemical processes.

Ability to account for the observed nitrate radical (NO_3) concentrations in the atmosphere provides a key test of the air quality modeling procedure. Predicted NO_3 concentrations compare well with those measured by Platt *et al.* (*Geophys. Res. Lett.* 7, 89–92, 1980). Analysis shows that transport, deposition and emissions, as well as chemistry, are important in explaining the behavior of NO_3 in the atmosphere.

Key word index: Dry deposition, dinitrogen pentoxide (N_2O_5), NO_3 , nitrate aerosol, nitric acid, nitrogen oxides, photochemical modeling, peroxyacetyl nitrate.

1. INTRODUCTION

Nitric acid is a major end product of nitrogen oxides emissions. Its presence in the atmosphere can lead to the acidification of rain and fog (Galloway and Likens, 1981; Waldman *et al.*, 1982; Levine and Schwartz, 1982; Liljestrand and Morgan, 1978; Adewuyi and Carmichael, 1982) and to dry deposition (Russell *et al.*, 1984; Liljestrand, 1980; Huebert, 1983). Aerosol nitrates, formed by reaction between nitric acid and either ammonia or pre-existing aerosol, are key contributors to the visibility problems observed in cities like Los Angeles and Denver (White and Roberts, 1977; Groblicki *et al.*, 1981). As a result, there is considerable interest in better understanding the mechanisms by which nitric acid is formed in and removed from the atmosphere.

Recent studies of the deposition of nitrogen-containing species and the formation of aerosol nitrates (McRae and Russell, 1984; Russell *et al.*, 1983, 1984; Russell and Cass, 1984) show that an understanding of the fate of nitrogen oxides (NO_x) emissions depends on several poorly understood steps in the nitric acid production cycle. Calculations are sensitive to the treatment of dinitrogen pentoxide (N_2O_5) hydrolysis, dry deposition rates, aerosol scavenging processes, and temporary storage of NO_x in the form

of aerosol nitrates and peroxyacetyl nitrate (PAN). The purpose of the present paper is to estimate the relative importance of these key processes to the formation and fate of nitric acid and other major nitrogen-containing pollutants.

A number of different methods may be employed to investigate nitric acid production, notably: smog chamber studies, mathematical models and atmospheric measurements. Each of these approaches has its individual strengths and weaknesses. Smog chamber studies do not take into account fresh emissions, diffusion, transport and deposition to natural surfaces, although they do allow accurate characterization of the pollutant evolution within a confined air mass. Studies based on atmospheric measurements have the advantage that the air being sampled has been exposed to all of the actual processes affecting pollutant formation. In practice, however, it is hard to follow individual air parcels in the field. In addition, field data usually are taken at ground level, with little or no attention being given to the chemistry and transport processes taking place aloft. Likewise, it is very difficult to separate the effects of transport, chemistry, and emissions from one another given most sets of field experimental data.

Mathematical models, in their many forms, can retain most of the strengths of the two previous methods. All theoretical formulations embody some degree of approximation, and a variety of assumptions must be used. However, if a model can be formulated that performs well when compared to smog chamber and field observations, its use has many advantages as a

* Department of Mechanical Engineering.

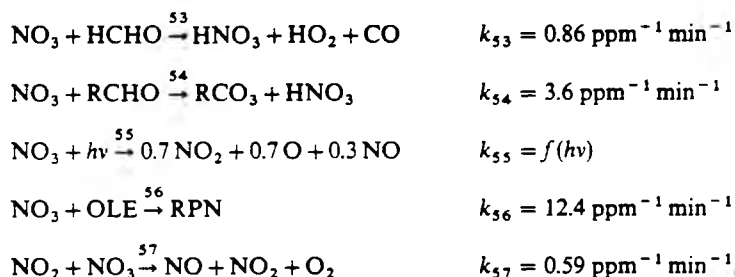
† Department of Chemical Engineering, Carnegie-Mellon University, Pittsburgh, PA 15213, U.S.A.

‡ Environmental Engineering Science Department.

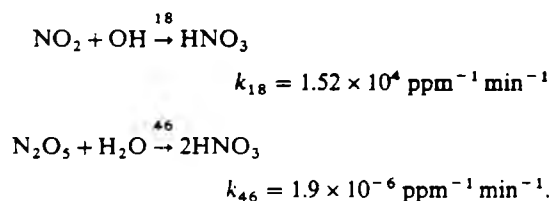
diagnostic tool for exploring atmospheric processes. These models incorporate descriptions of vertical diffusion, deposition, pollutant emissions and advective transport. By suppressing each of these processes in turn, one can investigate the extent to which particular physical or chemical mechanisms are responsible for the time rate of change of pollutant concentrations observed at ground-based air monitoring sites. In the present study, a photochemical trajectory model will be used to explore the mechanisms that determine nitric acid concentrations in the atmosphere.

2. TRAJECTORY MODEL DESCRIPTION

The trajectory model adopted for use in this study is described by Russell *et al.* (1983), and includes the effects of gas phase chemistry, the formation of nitrate aerosol, emissions, deposition and vertical diffusion. The photochemical mechanism based on McRae *et al.* (1982) has been augmented with the aerosol nitrate chemistry of Russell *et al.* (1983). Five additional reactions involving NO_3 have been added



Rate constants for the nitrate radical attack on aldehydes and olefins, (OLE), are from Atkinson *et al.* (1984). The NO_3 photolysis rate used is from Graham and Johnston (1978). The ultimate products of reaction 56 are reported to be nitroxypoxyalkyl nitrates and dinitrates, abbreviated RPN (Bandow *et al.*, 1980). Tests performed on the model show that inclusion of reactions 53–57 has little effect on the predictions of ozone, NO or NO_2 , but is important to the dynamics of NO_3 and the production of nitric acid. Two other nitric acid-producing reactions are



The reaction numbers correspond to McRae *et al.* (1982). Rate constants have been updated to reflect the recommendations of Atkinson and Lloyd (1984) and Baulch *et al.* (1982).

An evaluation of the chemical mechanism's ability to

describe the atmospheric chemistry was accomplished by comparing predictions against a set of smog chamber experiments (Falls and Seinfeld, 1978; McRae, 1981). That comparison showed good agreement between measurements and predictions for both ozone and the measured nitrogen-containing species. Evaluation of the complete trajectory model indicated that it adequately predicts the concentrations of gas phase pollutants, like ozone, and also the production of ammonium nitrate aerosol (see Russell *et al.*, 1983).

3. NITROGEN FLUXES AND THE FATE OF NITROGEN OXIDES EMISSIONS

The air quality model was applied to follow the fate of NO_x emissions along a 24-h trajectory across the Los Angeles basin. The air parcel trajectory used in this analysis is shown in Fig. 1, and passed over the Claremont, California, area at 1600 (PST) on 28 June 1974, the same day for which the initial model verification was accomplished. The air parcel was modeled as a column 1000 m high, divided into 10 cells.

The cell thicknesses, starting with the ground level cell, were 30, 50, 70, five at 100 m thick, 150 and 200 m. The day was marked by warm temperatures with an elevated inversion and high photochemical activity. Emissions into the air parcel were derived from a spatially resolved emissions inventory of the Los Angeles area. This trajectory was chosen because the Claremont area experiences high ozone levels, and because comparison will be made to NO_3 measurements taken in the same location by Platt *et al.* (1980).

Results of that model application are shown in Fig. 2. The widths of the arrows in Fig. 2 represent the magnitude of the integrated net fluxes of nitrogen species between the start of the trajectory and the end of that 24-h period. These calculations represent net fluxes in the following manner

$$F_{i \rightarrow j}(t) = \sum_m \int_0^t R_m^{i \rightarrow j} dt - \sum_n \int_0^t R_n^{j \rightarrow i} dt, \quad (1)$$

where $F_{i \rightarrow j}(t)$ is the net flux of nitrogen from species i directly to species j from the beginning of the trajectory to time t , $R_m^{i \rightarrow j}$ is the instantaneous flux of nitrogen from species i to j by reaction m and $R_n^{j \rightarrow i}$ is similarly

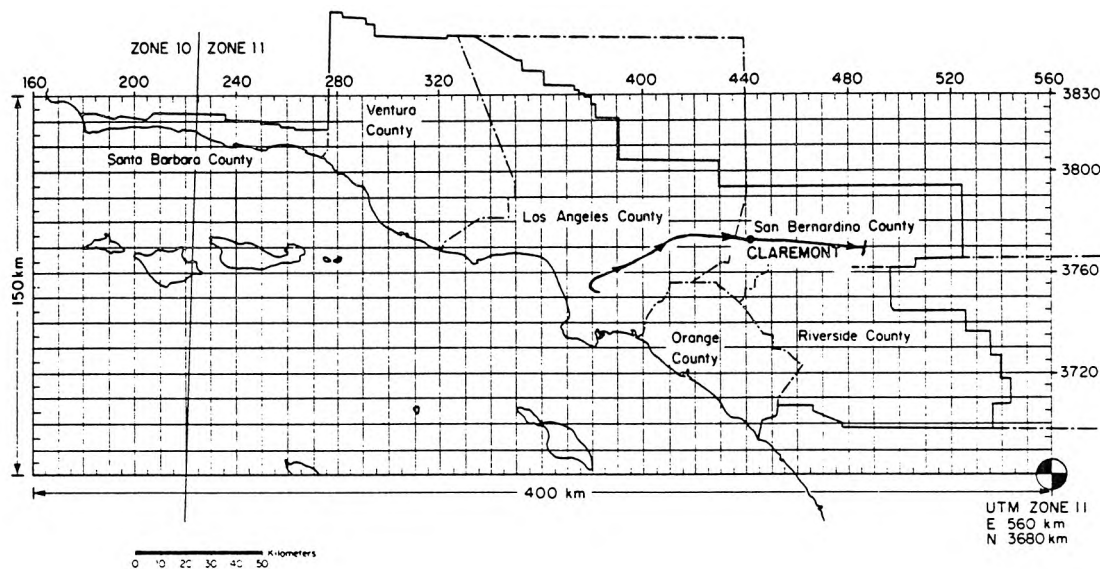


Fig. 1. Trajectory path used in analyzing the nitrogen oxides in the Los Angeles basin, 28 June 1974.

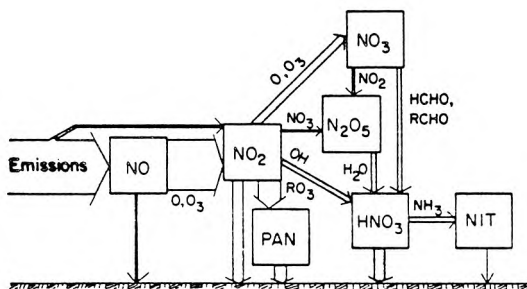


Fig. 2. Schematic representation of the net flux between nitrogen oxides species, including reaction paths for aerosol nitrate (NIT) formation. The width of these arrows indicates the magnitude of the net flux during the base case 24-h trajectory simulation.

the flux from species j to i by reaction n . The summation is taken over all pertinent reactions. These results, of course, depend on the trajectory chosen and on the meteorology of the particular day studied, but they do indicate the general magnitude of each pathway. From Fig. 2 it is seen that emissions of NO comprise about 97% of the flux of NO_x into the system, the remaining 3% being NO_2 . The NO is quickly oxidized to NO_2 (the net flux between species is shown), with very little nitrogen deposited out as NO. NO_2 then reacts to form a variety of products: 13% is converted directly to HNO_3 , 47% forms PAN, 13% NO_3 , 4% N_2O_5 , and 20% is removed by dry deposition at the earth's surface. Three percent of the NO_2 remains in the air parcel at the end of 24 h. About 25% of the net NO_3 formed combines with NO_2 to form N_2O_5 , which hydrolyzes to form HNO_3 . Most of the NO_3 reacts with the organics to form HNO_3 . Dry deposition removes 43% of the PAN in the first 24 h, leaving the rest to deposit out in subsequent days or to

thermally decompose into NO_2 and the peroxyacetyl radical. Thus PAN can act as a reservoir for NO_2 . Since nitric acid is very reactive with most surfaces, it deposits out quickly. Almost 73% of the nitric acid formed is lost by dry deposition. Nitric acid and PAN are found to be the major end products of nitrogen oxides emissions at the end of 24 h. Additional HNO_3 will be produced the next day from the remaining NO_2 and PAN.

A balance on the nitrogen in the air column, Fig. 3, indicates the importance of dry deposition. Fifty-eight per cent of the NO_x initially present in the air parcel or emitted along the trajectory has deposited out before reaching the end of the 24-h trajectory. The high HNO_3 formation rates present in photochemical smog

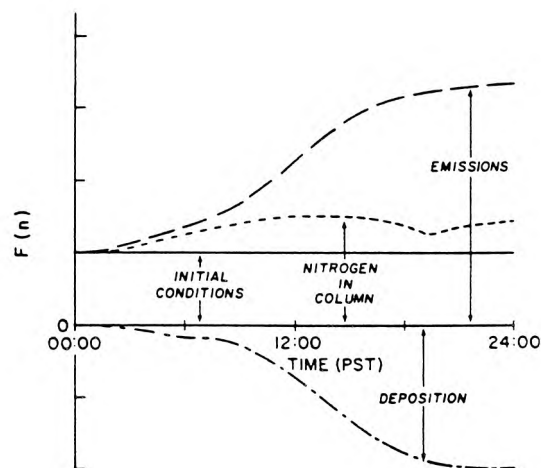


Fig. 3. Nitrogen balance on the air column illustrating the relative contributions, $F(n)$, from initial conditions, emissions and removal by dry deposition.

promote rapid nitrogen oxides removal at the ground because the deposition velocity of HNO_3 is higher than for many other NO_x species (Huebert, 1983). In addition, the smog condition studied here is caused in part by low mixing depths that increase pollutant concentrations adjacent to the ground, accelerating dry deposition processes. A plot of the cumulative deposition along the trajectory shows that 39% of the oxides of nitrogen deposited as HNO_3 (Fig. 4). PAN and NO_2 contribute 33 and 24%, respectively, to the dry deposition flux, while particulate ammonium nitrate accounts for only 1%.

4. NITRIC ACID PRODUCTION AT NIGHT

A comparison of the rates of the four reactions (18, 46, 53, 54) leading to HNO_3 formation is shown in Fig. 5. As expected, most of the daytime production of nitric acid occurs due to the reaction of NO_2 with OH. During daylight hours the NO_3 and N_2O_5 levels are very low because of NO_3 photolysis and NO_3 scavenging by NO (Stockwell and Calvert, 1983). At night a considerable amount of nitric acid may be produced by N_2O_5 hydrolysis and NO_3 reactions with organics. During the 24-h period studied, OH attack on NO_2 and N_2O_5 hydrolysis, respectively, account for 44 and 24% of the total nitric acid produced. The two NO_3 reactions (53, 54), in total, account for 32% of the nitric acid generated, mostly by reaction (54).

Clearly the relative importance of various nitric acid formation pathways is dependant on the accuracy of measured rate data. The rate constant for N_2O_5 hydrolysis, k_{46} , adopted in Table 1 is the value recently measured by Tuazon *et al.* (1983). Earlier research by Morris and Niki (1973) placed an upper limit on k_{46} that is a factor of 8 higher than used in the present

study, and the actual rate could still be smaller than used here. Measurement of that rate constant is plagued by rapid heterogeneous reactions with the surfaces of smog chambers used to study that reaction. Two approaches will be taken to estimate the magnitude of the effect that this uncertainty can have on the production of nitric acid. First, the chemical mechanism itself will be dissected to indicate the approximate functional dependence of overall nitric acid production on each of the key rate constants. Then the trajectory model will be used to conduct a study of the effect of perturbed rate constants on predicted HNO_3 formation routes.

The dynamics of the night-time NO_3 - N_2O_5 system is described by the set of 11 reactions shown in Table 1 and can be studied in spite of the possible uncertainty in the rate constant for reaction (46). Excluding the aerosol reactions, the rate expressions for NO_3 and N_2O_5 using the system in Table 1 become

$$\frac{d[\text{NO}_3]}{dt} = k_7[\text{NO}_2][\text{O}_3] - k_8[\text{NO}_3][\text{NO}] - k_{44}[\text{NO}_2][\text{NO}_3] + k_{45}[\text{N}_2\text{O}_5] - k_{\text{org}}[\text{ORG}][\text{NO}_3] - k_{57}[\text{NO}_2][\text{NO}_3] \quad (2)$$

and

$$\frac{d[\text{N}_2\text{O}_5]}{dt} = k_{44}[\text{NO}_2][\text{NO}_3] - k_{45}[\text{N}_2\text{O}_5] - k_{46}[\text{N}_2\text{O}_5][\text{H}_2\text{O}] \quad (3)$$

where

$$k_{\text{org}}[\text{ORG}] = k_{53}[\text{HCHO}] + k_{54}[\text{RCHO}] + k_{56}[\text{OLE}] \quad (4)$$

accounts for the reaction of the organics with NO_3 . Both NO_3 and N_2O_5 have short characteristic reaction times, and the pseudo-steady state approximation can be made

$$[\text{NO}_3] = \frac{k_7[\text{O}_3][\text{NO}_2](k_{45} + k_{46}[\text{H}_2\text{O}])}{\{k_8[\text{NO}] + k_{\text{org}}[\text{ORG}] + k_{57}[\text{NO}_2]\} \{k_{45} + k_{46}[\text{H}_2\text{O}]\} + k_{46}k_{44}[\text{NO}_2][\text{H}_2\text{O}]} \quad (5)$$

and

$$[\text{N}_2\text{O}_5] = \frac{k_{44}k_7[\text{NO}_2]^2[\text{O}_3]}{\{k_8[\text{NO}] + k_{\text{org}}[\text{ORG}] + k_{57}[\text{NO}_2]\} \{k_{45} + k_{46}[\text{H}_2\text{O}]\} + k_{44}k_{46}[\text{NO}_2][\text{H}_2\text{O}]} \quad (6)$$

or

$$[\text{N}_2\text{O}_5] = \frac{k_{44}[\text{NO}_2]}{k_{45} + k_{46}[\text{H}_2\text{O}]} [\text{NO}_3] \quad (7)$$

Further simplification is possible in (5) by noting that $k_{45} \gg k_{46}[\text{H}_2\text{O}]$

$$[\text{NO}_3] = \frac{k_7k_{45}[\text{O}_3][\text{NO}_2]}{k_8k_{45}[\text{NO}] + k_{45}k_{\text{org}}[\text{ORG}] + k_{57}k_{45}[\text{NO}_2] + k_{46}k_{44}[\text{NO}_2][\text{H}_2\text{O}]} \quad (8)$$

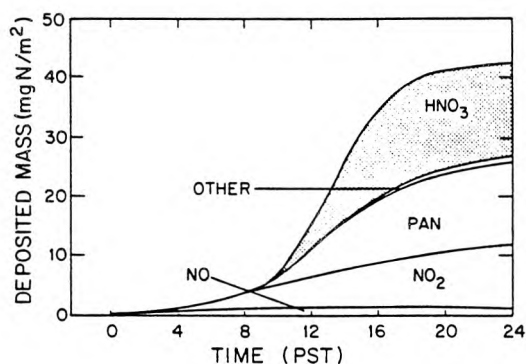


Fig. 4. Cumulative dry deposition of oxidized nitrogen air pollutants along a 24-h trajectory in the Los Angeles area, in mg N m^{-2} of surface area at the bottom of the moving air column.

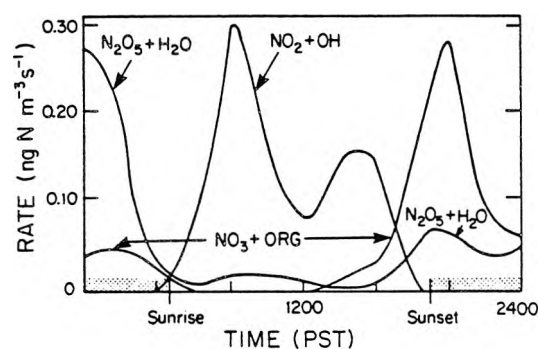


Fig. 5. Diurnal variation in the contribution of different reaction pathways to the formation of gas phase nitric acid. The two reactions [(53) and (54)] between NO_3 and organics have been added together for display purposes.

The formation of N_2O_5 depends on the availability of NO_2 , and the NO_2 concentrations at the beginning of the trajectory in west-central Los Angeles County are higher than at the end of the trajectory in San Bernardino County. For that reason, HNO_3 production via the $\text{N}_2\text{O}_5 + \text{H}_2\text{O}$ reaction is higher at the start than at the end of the calculation.

Table 1. Major reactions in the NO_3 - N_2O_5 system at night

Reaction	Rate constant (ppm min units)	298 K	Reference
$\text{NO}_2 + \text{O}_3 \xrightarrow{7} \text{NO}_3$	$k_7 = 0.05$		1
$\text{NO} + \text{NO}_3 \xrightarrow{8} 2\text{NO}_2$	$k_8 = 29560$		1
$\text{NO}_2 + \text{NO}_3 \xrightarrow{44} \text{N}_2\text{O}_5$	$k_{44} = 2510$		2
$\text{N}_2\text{O}_5 \xrightarrow{45} \text{NO}_2 + \text{NO}_3$	$k_{45} = 2.9$		1, 3
$\text{N}_2\text{O}_5 + \text{H}_2\text{O} \xrightarrow{46} 2\text{HNO}_3$	$k_{46} = 1.9 \times 10^{-6}$		4
$\text{NO}_3 + \text{HCHO} \xrightarrow{53} \text{HNO}_3 + \text{HO}_2 + \text{CO}$	$k_{53} = 0.86$		5
$\text{NO}_3 + \text{RCHO} \xrightarrow{54} \text{RCO}_3 + \text{HNO}_3$	$k_{54} = 3.6$		5, 6
$\text{NO}_3 + \text{OLE} \xrightarrow{56} \text{RPN}^8$	$k_{56} = 12.4$		5, 7, 9
$\text{NO}_2 + \text{NO}_3 \xrightarrow{57} \text{NO} + \text{NO}_2 + \text{O}_2$	$k_{57} = 0.59$		10
$\text{N}_2\text{O}_5 + \text{aerosol} \rightarrow 2\text{HNO}_3$	$k_{\text{N}_2\text{O}_5}^*$		11
$\text{NO}_3 + \text{aerosol} \rightarrow \text{aerosol}$	$k_{\text{NO}_3}^*$		11

(1) Baulch *et al.* (1982).

(2) Tuazon *et al.* (1984).

(3) Malko and Troe (1982).

(4) Tuazon *et al.* (1983).

(5) Atkinson *et al.* (1984).

(6) The rate constant used for the NO_3 reaction with higher aldehydes is that measured for acetaldehyde.

(7) The value used for the rate constant of the NO_3 reaction with olefins is that measured for the NO_3 reaction with propene.

(8) The ultimate products of reaction (56) are reported to be nitroxypoxyalkyl nitrates and dinitrates (Bandow *et al.*, 1980).

(9) Bandow *et al.* (1980).

(10) Atkinson and Lloyd (1984).

(11) See text.

The denominator in expression (8) is made up from the four sinks in the N_2O_5 - NO_3 system. The first term is due to NO_3 scavenging by NO, the second to the NO_3 reaction with organics, the third to the reaction with NO_2 to form NO, and the last corresponds to nitric acid production by N_2O_5 hydrolysis.

These steady state expressions can be used to perform an uncomplicated check on the NO_3 concentration values reported by Platt *et al.* (1980) at Claremont, California. Using the NO_2 (0.05 ppm) and olefins plus aldehydes (0.04 ppm) values representative of night-time conditions during Platt *et al.*'s (1980) experiments, given in Table 2, the magnitudes of the last three terms in the denominator of Equation (8) are about 0.3, 0.09 and 5 min^{-2} , respectively. Compared to NO, the NO_2 and olefins plus aldehydes concentrations should be relatively constant with height. NO concentrations at ground level are needed if the first term in the denominator of (8) is to be evaluated. Platt *et al.* (1980) were unable to measure NO, and Tuazon *et al.* (1981) report NO concentrations at sunset below the detection limit of 1 ppb at Claremont, California. If 1 ppb is taken as an upper limit on the NO concentration at ground level, the first term in the denominator of (8) is of the order 86 min^{-2} , or much greater than the other terms combined. At that ground level NO concentration, the corresponding NO_3 concentration is 12 ppt. At the other extreme, if the ground

level NO concentration is negligible, then the corresponding NO_3 concentration is 211 ppt. That range of NO_3 values brackets the peak NO_3 concentrations measured at ground level by Platt *et al.* (1980) at Claremont.

Equation (8) next can be used to examine the likely situation at night several hundred meters above the ground. Ozone scavenges the NO aloft, and the stability of the atmosphere at night does not allow surface NO emissions to diffuse upward rapidly. Under those conditions, the NO concentration several hundred meters above the ground should be very low (the trajectory model predicts less than 1×10^{-6} ppm aloft just after sunset). With NO levels very low, the uncertainty in NO concentration present at ground level is removed, and NO_3 values aloft approaching the NO negligible case of 211 ppt should be present. These predictions derived quickly from a steady state analysis of an approximate night-time chemical mechanism will be compared to the results of the full trajectory model shortly.

The expressions derived for NO_3 and N_2O_5 can be used to compute the nitric acid production rates at night and also to test the sensitivity of nitric acid production to the uncertainty in the N_2O_5 hydrolysis rate. Nitric acid is produced at night by N_2O_5 hydrolysis (reaction 46) and by two reactions between the organics and NO_3 (reactions 53, 54). Rates for these reactions are, respectively

$$\frac{d[\text{HNO}_3]}{dt} = \frac{2k_{46}k_{44}k_7[\text{H}_2\text{O}][\text{O}_3][\text{NO}_2]^2}{k_{46}k_{44}[\text{NO}_2][\text{H}_2\text{O}] + k_{45}k_8[\text{NO}] + k_{45}k_{\text{org}}[\text{ORG}] + k_{45}k_{57}[\text{NO}_2]} \quad (9)$$

and

$$\frac{d[\text{HNO}_3]}{dt} = \frac{k_{45}k_7[\text{O}_3][\text{NO}_2](k_{53}[\text{HCHO}] + k_{54}[\text{RCHO}])}{k_{46}k_{44}[\text{NO}_2][\text{H}_2\text{O}] + k_{45}k_8[\text{NO}] + k_{45}k_{\text{org}}[\text{ORG}] + k_{45}k_{57}[\text{NO}_2]} \quad (10)$$

Table 2. Species concentration used in analysis

Species	Concentration (ppm)
NO (average)	$1 \times 10^{-4*}$
NO_2	0.05†
O_3	0.15†
H_2O	$2 \times 10^4†$
HCHO	0.020‡
RCHO	0.020§
OLE	0.001*
NO (ground level)	$1 \times 10^{-3}‡$
NO (above inversion)	$1 \times 10^{-6*}$

* Value taken from trajectory model calculations used in this study at 19:00 PST.

† Value representative of those measured by Platt *et al.* (1980).

‡ Value representative of those measured by Tuazon *et al.* (1981).

§ Concentration of higher aldehydes set equal to that of formaldehyde.

It is instructive to look at the magnitude of equations (9) and (10) in two regimes: if the NO is about 1 ppb and if the NO is negligible.

Using the species concentrations given in Table 2, with NO concentration at 1 ppb, and $k_{46} = 1.9 \times 10^{-6} \text{ ppm}^{-1} \text{ min}^{-1}$, the dominant route for nitric acid production is reaction (46), producing $4 \times 10^{-5} \text{ ppm min}^{-1}$ of HNO_3 [Equation (9)] compared to $1 \times 10^{-6} \text{ ppm min}^{-1}$ by the set of NO_3 -organics reactions [Equation (10)].

At high altitudes the NO concentration is very small, decreasing NO_3 scavenging and increasing HNO_3 production. If the NO concentration is negligible, then the nitric acid production rates by reaction (46) and by the organics- NO_3 reactions [reactions (53) and (54)] are increased to 7×10^{-4} and $1.9 \times 10^{-5} \text{ ppm min}^{-1}$, respectively. Note that in the absence of NO, decreasing k_{46} has much less effect on HNO_3 production by N_2O_5 hydrolysis. This is because if $[\text{NO}] < 10^{-6} \text{ ppm}$ and $k_{46}k_{44}[\text{NO}_2][\text{H}_2\text{O}] \gg k_{45}k_{\text{org}}[\text{ORG}]$, then (9)

simplifies to

$$\frac{d[\text{HNO}_3]}{dt} = 2k_7[\text{O}_3][\text{NO}_2] \quad (11)$$

with no dependence on k_{46} .

An estimate of the importance of the N_2O_5 hydrolysis to the total rate of nitric acid production can be found by comparing the previous calculations to the rate of the NO_2 -OH radical reaction at noon. Assuming an NO_2 concentration of 0.100 ppm (Tuazon *et al.*, 1981) and an OH radical level of 2×10^{-7} ppm (Chameides and Davis, 1982), daytime nitric acid production is about 3×10^{-4} ppm min $^{-1}$, less than the production of HNO_3 by reaction (46) after sunset at locations where the NO concentration is negligible (e.g. above the surface layer affected by fresh NO emissions).

Next the complete photochemical trajectory model was used to test the sensitivity of nitric acid production to variations in a number of key parameters. A comparison of the amount of nitric acid produced by the various reactions in six different cases is shown in Table 3. The base case reflects the calculations previously described in part 3 of this paper. Rate constants shown in Table 1 were used, and no scavenging of NO_3 and N_2O_5 by aerosols was assumed to take place. In this case, night-time reactions [reactions (46), (53) and (54)] account for 56% of the HNO_3 formed during the 24-h trajectory, 41% of that by the homogeneous hydrolysis of N_2O_5 .

There is some possibility that the value of k_{46} given in Table 1 may be too high. A second set of calculations was executed with k_{46} decreased by an order of magnitude below the value in Table 1. In this case only 6% of the nitric acid is produced by reaction (46). However, reducing k_{46} increases the predicted NO_3 concentrations and thus increases the production of HNO_3 by the reactions involving organics. Still, 47% of the nitric acid is produced by night-time reactions, and the total nitric acid produced is reduced by only 3% (see Table 3).

Morris and Niki (1973) placed an upper limit on the value of k_{46} equal to 1.5×10^{-5} ppm $^{-1}$ min $^{-1}$. If this value is used, 44% of the nitric acid is produced by

homogeneous hydrolysis of N_2O_5 and 36% by the OH- NO_2 daytime reaction. At the other extreme, if k_{46} is set equal to zero, the total nitric acid produced decreases by only 7%, and the nitrate radical reactions with organics now account for 44% of that produced. The final three columns of Table 3 indicate the possible effect that heterogeneous reactions could have on the production of nitric acid. These reactions will be discussed further in following paragraphs.

The results shown here indicate that the homogeneous hydrolysis of N_2O_5 probably is an important mechanism in the formation of nitric acid in the atmosphere. Reducing the rate constant used from that of Morris and Niki (1973) to that of Tuazon *et al.* (1983), a factor of eight decrease lowered the amount of HNO_3 produced via reaction (46) by only 55%. Further reduction of k_{46} by an order of magnitude decreased total nitric acid produced at night by only 18%. In all cases the nitric acid produced at night is a significant fraction of the total. NO_3 -organic reactions also are shown to be an important source of nitric acid in this analysis. Perturbing k_{46} results in a redistribution of the amount of nitric acid produced by each reaction, but the total nitric formed is not as greatly affected (see bottom of Table 3).

5. PREDICTION OF NO_3 CONCENTRATIONS

As indicated earlier, two key species in explaining the production of HNO_3 are N_2O_5 and NO_3 . Unfortunately, there are no ground level measurements of N_2O_5 available and only one set of ambient measurements of NO_3 , NO_2 and O_3 (Platt *et al.*, 1980). However, the rapid conversion of NO_3 to N_2O_5 , and subsequent rapid decomposition of N_2O_5 should cause NO_2 , NO_3 and N_2O_5 to reach equilibrium at night, such that

$$\frac{[\text{NO}_3][\text{NO}_2]}{[\text{N}_2\text{O}_5]} = K$$

where $K = 1.2 \times 10^{-3}$ ppm (Tuazon *et al.*, 1984). Other reactions of NO_3 and N_2O_5 would perturb this equilibrium state only slightly because the timescales for the other competitive reactions are significantly

Table 3. Percentage of total nitric acid produced by each reaction along a 24-h trajectory

Reaction step producing HNO_3		Base case (%)	k_{46} decreased by 10x (%)	k_{46} of Morris and Niki (%)	Aerosol scavenging			
					$k_{46} = 0$ (%)	$(\alpha = 0.001)$ (%)	$(\alpha = 0.1)$ (%)	$(\alpha = 1.0)$ (%)
$\text{NO}_2 + \text{OH}$	(18)	44	53	36	56	44	37	29
$\text{N}_2\text{O}_5 + \text{H}_2\text{O(g)}$	(46)	24	6	44	0	22	5	tr*
$\text{NO}_3 + \text{HCHO}$	(53)	4	7	2	7	4	1	tr
$\text{NO}_3 + \text{RCHO}$	(54)	28	34	18	37	28	11	4
$\text{N}_2\text{O}_5 + \text{Aerosol}$						2	46	67
Percentage of base case nitric acid produced		100%	97	117	93	101	114	124

* tr, trace amount, less than 1%.

longer than those that establish the equilibrium condition. Hence, an ability to correctly predict NO_3 concentrations at night would suggest that N_2O_5 concentrations also have been predicted correctly. A key test of night-time nitric acid formation calculations at present thus involves comparison of observed and predicted NO_3 concentrations.

The trajectory model employed earlier can be used to estimate the NO_3 concentrations observed at Riverside on 12 September 1979 by Platt *et al.* (1980). The initial conditions used were the NO_2 (0.08 ppm), H_2O (23200 ppm), O_3 (0.23 ppm) and NO_3 (0.0 ppm) concentrations measured by Platt *et al.* (1980) at Riverside at 1800 Pacific Daylight Time (PDT). Emissions, again, were derived from a spatially resolved 1974 inventory of the area. Air mass motion at night on this occasion was small, and the nominal motion of the air parcel between 1800 and 2400 h PDT would have been only 5.6 km. Since the emission inventory and the air parcel characteristics are defined over 5×5 km grids, a horizontal transport distance of only 5.6 km implies that Platt *et al.*'s (1980) measurements at a fixed site in Riverside can be compared to a short Lagrangian trajectory calculation passing over that site. A comparison of the measured and predicted ground level NO_3 concentrations is shown in Fig. 6. The measured peak was 288 ppt and the predicted peak was about 255 ppt, both profiles showing the dramatic rise in NO_3 just after sunset, and then a rapid decline. The predicted concentrations peak about one half hour before the measured concentrations, possibly due to dissociation rates of NO_2 and NO_3 after sunset that are greater than that modeled, or due to transport on a sub-grid scale. The latter is unlikely as the wind velocities during the experiment were not very great, and the measured ozone and nitrogen dioxide concentrations did not change markedly. O_3 and NO_2 predictions and measurements are shown in Fig. 7. Predicted and observed ozone concentrations compare quite well. The NO_2 predictions are lower than observed, but the NO_2 trends over time track one another.

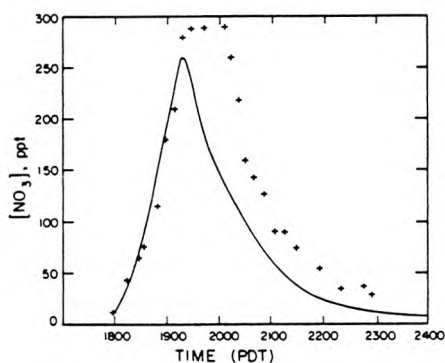


Fig. 6. Predicted and measured NO_3 concentrations at Riverside, 12 September 1979: —, predicted; +, measured (Platt *et al.*, 1980).

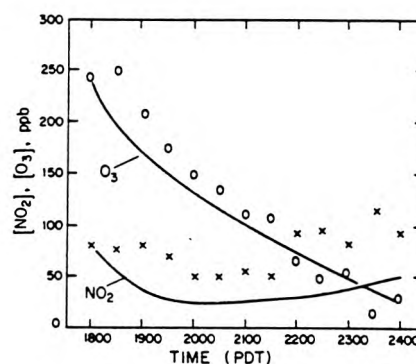


Fig. 7. Predicted and measured O_3 and NO_2 concentrations at Riverside, 12 September 1979: —, predicted; x, measured NO_2 (Platt *et al.*, 1980); o, measured O_3 (Platt *et al.*, 1980).

In order to account for the rapid decrease in ground level NO_3 concentrations observed after the peak at 1930 h as shown in Fig. 6, the O_3 concentration must decrease and the NO concentration increase. Stockwell and Calvert (1983) used a box model, lacking vertical resolution and vertical diffusion, and achieved this result by greatly increasing NO emissions into their model. However, NO emissions in Los Angeles, in fact are decreasing at that time of day. There are several key reasons why the trajectory model used here can reproduce the observed NO_3 peak without an NO emissions increase. Emissions into the vertically resolved trajectory model are treated as ground level sources. As night falls the atmosphere stabilizes, which decreases mixing, causing an increase in the ground level NO concentrations. However, the effect of this lowered mixing rate in the trajectory model is more widespread than its effect on increasing NO concentrations alone and is not equivalent to injecting more NO into a box model. The lowered mixing rate also affects the NO_2 and O_3 loss rate at the ground and slows the downward flux of O_3 from elevations above the ground level cell in the model. Emissions used in this study are derived from a spatially resolved emissions inventory for the Los Angeles basin, from which the emissions density in the Riverside area can be determined. In the trajectory model, deposition fluxes are computed based on the concentration in the bottom cell only. Use of ground level emissions and deposition, coupled with a stably stratified atmosphere at night, leads to a very pronounced NO_3 concentration profile with elevation in the atmosphere, as shown in Fig. 8. Figure 8 also indicates the potential importance of nitric acid production aloft, where the NO_3 and N_2O_5 concentrations are predicted to be much greater than those observed at ground level.

The trajectory model can be used to elucidate the important processes affecting the NO_3 concentration at ground level over time. This will be done by systematically removing physical processes, such as mixing, deposition, chemical reaction and emissions of NO , from the trajectory model run that was initiated

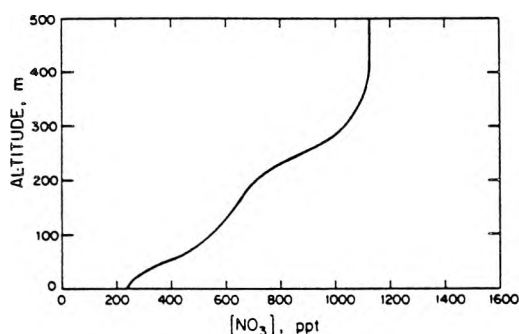


Fig. 8. Predicted vertical NO_3 concentration profile at 1900 (PDT) on 12 September 1979. Air parcel is located at Riverside.

using the O_3 and NO_2 values that were measured by Platt *et al.* (1980) at 1800 PDT on 12 September 1979 at Riverside. The results of this analysis are shown in Fig. 9. Removing NO emissions increases the NO_3 peak, to about 575 ppt, because NO is a very efficient NO_3 scavenger. Decreasing the N_2O_5 hydrolysis rate constant, k_{46} , by an order of magnitude, again increases the peak NO_3 concentration to about 830 ppt. Further decreasing k_{46} to zero only increases the NO_3 concentration peak to 1000 ppt. Reduction of the value of k_{46} in the two preceding cases causes a delay in the occurrence of the NO_3 peak because the removal of nitrogen oxides from the system is delayed. Deleting deposition of all species changes the NO_3 profile greatly, increasing the peak NO_3 concentration by about fifty percent relative to the base case.

Vertical mixing has a major effect on the NO_3 concentrations. Trapping the emissions in the bottom cell of the model almost removes the peak, whereas the base case calculation of the atmospheric mixing after sunset increases the peak NO_3 value and pushes the peak to a later time. Reduced vertical mixing in effect traps more NO emissions in the bottom cell of the model, giving an effect that is opposite to that discussed previously for the case where emissions are suppressed.

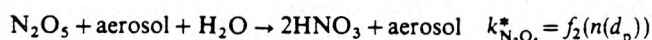
This brief analysis shows that chemistry alone cannot explain the behavior of NO_3 in the atmosphere. A complete analysis requires including the effects of transport, deposition and emissions. Given detailed data on emissions, meteorology, and O_3 and NO_2 concentrations, a similar analysis could be applied to the data of Noxon *et al.* (1980).

6. AEROSOL-RADICAL INTERACTIONS

Both NO_3 and N_2O_5 possibly could be scavenged by surface reactions with aerosols (Chameides and

Davis, 1982). Though the rates of these reactions are unknown, an upper bound can be found from kinetic theory. The trajectory model can be used to assess the maximum effect of aerosol scavenging.

Possible products of the nitrate radical interaction with aerosols include aerosol nitrate, a sink in the system, or decomposition of the NO_3 into NO_2 and O. N_2O_5 also might decompose into its precursors, react with the aerosol surface to form aerosol nitrate, or, if the N_2O_5 contacts water on the aerosol surface, it could undergo heterogeneous hydrolysis to produce nitric acid. In the following analysis, the aerosol surface reaction with NO_3 will be modeled as a sink for NO_3 , the products remaining in the aerosol phase; while N_2O_5 reaction with the aerosol will be assumed to produce nitric acid that could re-enter the gas phase. Thus, the two reactions added to the system are



where the two rate constants are calculated as functions of the aerosol size distribution function, $n(d_p)$, which determines the aerosol surface area as a function of particle diameter, d_p .

An upper bound for these rate constants can be derived from kinetic theory by calculating the collision rate of the gas molecules with the aerosol surface. Assuming that 100% of the collisions are effective in achieving reaction, these upper limit rate constants are given by (Dahneke, 1983)

$$k_i^* = \int_0^\infty 2\pi D_i \left[\frac{1 + Kn}{\frac{2Kn(1 + Kn)}{\alpha} + 1} \right] d_p n(d_p) d(d_p), \quad (12)$$

where D_i is the diffusion coefficient of species i , Kn is the Knudsen number based on aerosol size and the mean free path of gaseous species i , and α is the collision efficiency. An estimate of the heterogeneous reaction rate constants in the Los Angeles atmosphere can be found using the measured aerosol size distribution of Table 3 in Whitby *et al.* (1972). Upper bounds on these rate constants, using $\alpha = 1$, are calculated to be

$$k_{\text{NO}_3}^* (\alpha = 1) = 2.4 \text{ min}^{-1}$$

$$k_{\text{N}_2\text{O}_5}^* (\alpha = 1) = 1.5 \text{ min}^{-1}.$$

Collision efficiencies are both hard to measure and highly dependent on the aerosol surface characteristics. Baldwin and Golden (1979) measured the collision efficiency of N_2O_5 on a sulfuric acid surface to be greater than 3.8×10^{-5} . Chameides and Davis (1982) report measured efficiencies for OH radical-aerosol reactions from less than 10^{-4} to 0.25, the magnitude depending largely on the surface composition. In the present work, the assumed collision efficiency, α , for both N_2O_5 and NO_3 -surface reactions will be taken as

10^{-3} , which is between that measured for N_2O_5 on sulfuric acid and the OH interaction with $NaNO_3$ (Jech *et al.*, 1982). The actual rate will vary as the aerosol surface characteristics and size distribution change.

The importance of aerosol scavenging is dependent on the time scales associated with the different sinks in the NO_3 - N_2O_5 system. At night, given the species concentrations in Table 2, these sinks and their time scales (given as the NO_3 reaction rate per unit NO_3 concentration) are

NO Scavenging $0.03 < k_8[NO] < 30 \text{ min}^{-1}$

Organic reactions $k_{org}[ORG] \sim 0.10 \text{ min}^{-1}$

Aerosol interaction $k_{NO_3}^* (\alpha = 0.001) \sim 0.004 \text{ min}^{-1}$.

From these results, aerosol scavenging of NO_3 at night should be important only at very low NO concentrations or at collision efficiencies much higher than the $\alpha = 10^{-3}$ value assumed here. During daylight hours, the losses due to photolysis and NO scavenging are very much greater than the loss due to aerosols.

At night N_2O_5 -aerosol reactions can be examined by comparing the time scales for N_2O_5 loss:

Homogeneous hydrolysis $k_{46}[H_2O] < 0.04 \text{ min}^{-1}$

Aerosol interaction $k_{N_2O_5}^* (\alpha = 0.001) \sim 0.003 \text{ min}^{-1}$.

Considering the uncertainties, the time scales associated with the N_2O_5 sinks at night are close. The N_2O_5 homogeneous hydrolysis rate could easily be an order of magnitude lower and the aerosol interaction higher, the conclusion being that N_2O_5 -aerosol interactions are possibly important at night, lowering the concentrations of both NO_3 and N_2O_5 in the atmosphere.

The trajectory model again can be used to explore the effect of aerosols on the oxides of nitrogen system and on the production of nitric acid by adding the last two reactions shown in Table 1. Again the 24-h trajectory passing through Claremont was modeled, first with the collision efficiency equal to 0.001 and then with $\alpha = 0.1$ and 1.0. For $\alpha = 0.001$, little effect is seen on the nitric acid produced when compared to the base case as shown in Table 3. Likewise, with $\alpha = 0.001$ there is little effect on the NO_3 peak shown in Fig. 9. If $\alpha = 0.1$ or 1.0, the NO_3 peak almost disappears, but a great deal of nitric acid is produced heterogeneously, indicating the importance of aerosol interactions at high collision efficiencies.

CONCLUSIONS

The photochemical trajectory model used by Russell *et al.* (1983) was applied to calculations along a 24-h air parcel trajectory crossing the Los Angeles basin during a day that exhibits summertime high photochemical smog conditions. Ground level dry deposition calculations show that 58% of the nitrogen oxides inserted into the air parcel have deposited at the ground during that 24-h period. Nitrogen oxides removal is domi-

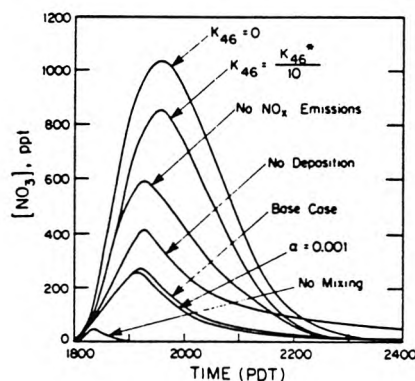


Fig. 9. Predicted NO_3 concentrations at Riverside, 12 September 1979 for the base case and for several perturbations from the base case.

nated by HNO_3 (39%), PAN (33%) and NO_2 (24%). Much of the nitrogen left in the air column at the end of the 24-h trajectory is predicted to be associated with NO_2 or PAN. During the following day, this PAN can either continue to deposit or thermally decompose releasing NO_2 .

Significant nitric acid production takes place both at night and during the daytime. For the most probable case studied here (the base case of Table 3), about 56% of the nitric acid produced during a 24-h urban trajectory traveling across the Los Angeles basin is generated at night by reactions involving NO_3 and N_2O_5 . Most of that HNO_3 production at night is due to the NO_3 reaction with higher aldehydes and hydrolysis of N_2O_5 . Both pseudo-steady state analysis of the night-time chemical mechanism and trajectory model results indicate that nitric acid production is slightly sensitive to an order of magnitude decrease in the N_2O_5 homogeneous hydrolysis rate constant, except at high NO levels or if aerosol scavenging is relatively efficient ($\alpha \gg 0.001$).

Aerosol interactions with NO_3 should perturb the system only slightly except at very low NO concentrations, or if the aerosol collision efficiency is high. N_2O_5 interactions with aerosols are more important than NO_3 -aerosol reactions at the same collision efficiency, an effect magnified by any decrease in the N_2O_5 homogeneous hydrolysis rate constant. Heterogeneous reactions on aerosols may be important both in the formation of nitric acid, and as a sink for N_2O_5 .

An analysis of the possible effects of uncertainties in the N_2O_5 homogeneous hydrolysis rate constant shows that the effect of this uncertainty is much different near the ground than at several hundred meters above the ground. Many of the perturbations used to estimate the effect of uncertainties within the trajectory model cause a redistribution of the mechanism by which nitric acid is formed but do not affect the total amount of nitric acid produced greatly during a 24-h period (see the bottom of Table 3).

The nitrate radical, NO_3 , is a key species in the mechanism producing HNO_3 by N_2O_5 hydrolysis.

The behavior of NO_3 predicted by the trajectory model used here compares well with field observations, and is consistent with known emission rates and atmospheric dynamics in the Los Angeles area. Results indicate that simultaneous calculation of dry deposition, emissions, chemistry, and vertical transport is needed to reproduce Platt *et al.*'s (1980) observations and that atmospheric measurements made at fixed ground level monitoring sites must be interpreted very carefully if one is to correctly capture the effect of transport processes on atmospheric chemical dynamics.

Acknowledgements—This work was supported, in part, by a grant from the Andrew W. Mellon Foundation and by gifts to the Environmental Quality Laboratory. The California Air Resources Board supported AGR and recent calculations under Agreement A2-150-32.

REFERENCES

- Adewuyi Y. G. and Carmichael G. R. (1982) A theoretical investigation of gaseous absorption by water droplets from SO_2 - HNO_3 - NH_3 - CO_2 - HCl mixtures. *Atmospheric Environment* **16**, 719-729.
- Atkinson R., Plum C. N., Carter W. P., Winer A. M. and Pitts J. N., Jr. (1984) Rate constants for the gas phase reactions of NO_3 radicals with a series of organics in air at 298 ± 1 K. *J. phys. Chem.* **88**, 1210-1215.
- Atkinson R. and Lloyd A. C. (1984) Evaluation of kinetic and mechanistic data for modeling of photochemical smog. *J. phys. Chem. Ref. Data* **13**, 315-444.
- Baldwin A. C. and Golden D. M. (1979) Heterogeneous atmospheric reactions: sulfuric acid aerosols as tropospheric sinks. *Science, Wash.* **206**, 562-563.
- Bandow H., Okuda M. and Akimoto H. (1980) Mechanism of the gas-phase reactions of C_3H_6 and NO_3 radicals. *J. phys. Chem.* **84**, 3604-3608.
- Baulch D. L., Cox R. A., Crutzen P. J., Hampson R. F., Kerr J. A., Troe J. and Watson R. T. (1982) Evaluated kinetic and photochemical data for atmospheric chemistry: supplement 1. *J. phys. Chem. Ref. Data* **11**, 327-496.
- Chameides W. L. and Davis D. D. (1982) The free radical chemistry of cloud droplets and its impact on the composition of rain. *J. geophys. Res.* **87**, 4863-4877.
- Dahneke, B. (1983) Simple kinetic theory of Brownian diffusion in vapors and aerosols. In *Theory of Dispersed Multiphase Flow* (edited by Meyer R.). Academic Press, New York.
- Falls A. H. and Seinfeld J. H. (1978) Continued development of a kinetic mechanism for photochemical smog. *Envir. Sci. Technol.* **12**, 1398-1406.
- Galloway J. N. and Likens G. E. (1981) Acid precipitation: the importance of nitric acid. *Atmospheric Environment* **15**, 1081-1085.
- Graham R. A. and Johnston H. S. (1978) The photochemistry of NO_3 and the kinetics of the N_2O_5 - O_3 system. *J. phys. Chem.* **82**, 254-268.
- Groblicki P. J., Wolff G. T. and Countess R. J. (1981) Visibility reducing species in the Denver "Brown Cloud"—I. Relationships between extinction and chemical composition. *Atmospheric Environment* **15**, 2473-2484.
- Huebert B. J. (1983) Measurements of the dry deposition flux of nitric acid vapor to grasslands and forest. In *Precipitation Scavenging, Dry Deposition, and Resuspension* (edited by Pruppacher H. R., Semonin R. G. and Slinn W. G. N.). Elsevier, New York.
- Jech D. D., Easley P. G. and Krieger B. B. (1982) Kinetics of reactions between free radicals and surfaces (aerosols) applicable to atmospheric chemistry. In *Heterogeneous Atmospheric Chemistry* (edited by Schryer D. R.), pp. 107-121. Am. Geophys. Un., Washington, D.C.
- Levine S. Z. and Schwartz S. E. (1982) In-cloud and below-cloud scavenging of nitric acid vapor. *Atmospheric Environment* **16**, 1725-1734.
- Liljestrand H. M. and Morgan J. J. (1978) Chemical composition of acid precipitation in Pasadena, California. *Envir. Sci. Technol.* **12**, 1271-1273.
- Liljestrand H. M. (1980) Atmospheric transport of acidity in southern California by wet and dry mechanisms. Ph.D. thesis, California Institute of Technology, Pasadena, California.
- Malco M. W. and Troe J. (1982) Analysis of the unimolecular reaction $\text{N}_2\text{O}_5 + \text{M} \rightarrow \text{NO}_2 + \text{NO}_3 + \text{M}$. *Int. J. Chem. Kinet.* **14**, 399-416.
- McRae G. J. (1981) Mathematical modeling of photochemical air pollution. Ph.D. thesis, California Institute of Technology, Pasadena, California.
- McRae G. J., Goodin W. R. and Seinfeld J. H. (1982) Development of a second generation mathematical model for urban air pollution—I. Model formulation. *Atmospheric Environment* **16**, 679-696.
- McRae G. J. and Russell A. G. (1984) Dry deposition of nitrogen-containing species. In *Deposition Both Wet and Dry* (edited by Hicks B. B.), pp. 153-193. Acid Precipitation Series, Volume 4. Butterworth, Boston.
- Morris E. D. and Niki H. (1973) Reaction of dinitrogen pentoxide with water. *J. phys. Chem.* **77**, 1929-1932.
- Noxon J. F., Norton R. B. and Marovich E. (1980) NO_3 in the troposphere. *Geophys. Res. Lett.* **7**, 125-128.
- Platt U., Perner D., Winer A. M., Harris G. W. and Pitts J. N. (1980) Detection of NO_3 in the polluted troposphere by differential optical absorption. *Geophys. Res. Lett.* **7**, 89-92.
- Russell A. G., McRae G. J. and Cass G. R. (1983) Mathematical modeling of the formation and transport of ammonium nitrate aerosol. *Atmospheric Environment* **17**, 949-964.
- Russell A. G. and Cass G. R. (1984) Acquisition of regional air quality model validation data for nitrate, sulfate, ammonium ion and their precursors. *Atmospheric Environment* **18**, 1815-1827.
- Russell A. G., McRae G. J. and Cass G. R. (1984) Acid deposition of photochemical oxidation products—a study using a Lagrangian trajectory model. In *Air Pollution Modeling and Its Application III* (edited by DeWispelaere C.). Plenum Publishing Corporation, New York.
- Stockwell W. R. and Calvert J. G. (1983) The mechanism of NO_3 and HONO formation in the night-time chemistry of the urban atmosphere. *J. geophys. Res.* **88**, 6673-6682.
- Tuazon E. C., Winer A. M. and Pitts J. N., Jr. (1981) Trace pollutant concentrations in a multiday smog episode in the California South Coast Air Basin by long path length Fourier-transform infrared spectroscopy. *Envir. Sci. Technol.* **15**, 1232-1237.
- Tuazon E. C., Atkinson R., Plum C. N., Winer A. M. and Pitts J. N., Jr. (1983) The reaction of gas phase N_2O_5 with water vapor. *Geophys. Res. Lett.* **10**, 953-956.
- Tuazon E. C., Sanhueza E., Atkinson R., Carter W. P. L., Winer A. M. and Pitts J. N., Jr. (1984) Direct determination of the equilibrium constant at 298 K for the $\text{NO}_2 + \text{NO}_3 \rightleftharpoons \text{N}_2\text{O}_5$ reactions. *J. Phys. Chem.* **88**, 3095-3098.
- Waldman J. M., Munger J. W., Jacob D. J., Flagan R. C., Morgan J. J. and Hoffmann M. R. (1982) Chemical composition of acid fog. *Science, Wash.* **218**, 677-680.
- Whitby K. T., Husar R. B. and Liu B. Y. H. (1972) The aerosol size distribution of Los Angeles Smog. *J. Colloid Interface Sci.* **39**, 177-204.
- White W. H. and Roberts P. T. (1977) On the nature and origins of visibility reducing species in the Los Angeles Basin. *Atmospheric Environment* **11**, 803-812.

CHAPTER 4

ACQUISITION OF REGIONAL AIR QUALITY MODEL
VALIDATION DATA FOR NITRATE, SULFATE, AMMONIUM
ION AND THEIR PRECURSORS

(Reprinted from *Atmospheric Environment*, 18, 1815-1827)

ACQUISITION OF REGIONAL AIR QUALITY MODEL VALIDATION DATA FOR NITRATE, SULFATE, AMMONIUM ION AND THEIR PRECURSORS

ARMISTEAD G. RUSSELL* and GLEN R. CASS†

*Mechanical Engineering Department and Environmental Quality Laboratory and †Environmental Engineering Science Department and Environmental Quality Laboratory, California Institute of Technology, Pasadena, CA 91125, U.S.A.

Abstract—An intensive field study was conducted throughout California's South Coast Air Basin to acquire air quality model validation data for use with aerosol nitrate formation models. Aerosol nitrate, sulfate, ammonium, other major ionic aerosol species, nitric acid gas and ammonia were measured concurrently at ten sites for forty-eight consecutive hours during the period 30–31 August 1982. Ozone, NO and NO_x were measured at all locations, and PAN was measured at Pasadena and Riverside, completing a nitrogen balance on the air masses studied.

The product of the measured nitric acid and ammonia concentrations ranged from less than 1 ppbv² to greater than 300 ppbv² during the experiment, providing a wide range of conditions over which comparisons can be drawn between chemical equilibrium calculations and experimental results. The ionic material in the aerosol phase was chemically more complex than is assumed by present theoretical models for the equilibrium between NH₃, HNO₃ and the aerosol phase, and included significant amounts of Na⁺, Ca²⁺, Mg²⁺, K⁺ and Cl[−] in addition to NH₄⁺, SO₄^{2−} and NO₃[−]. Results of the experiment showed that aerosol nitrate levels in excess of 20 μgm^{−3} accumulated in near-coastal locations in the morning of 31 August, followed by subsequent transport across the air basin. Trajectory analysis showed that the afternoon aerosol nitrate peak observed inland at Rubidoux near Riverside was associated with the same air mass that contained the high morning nitrate levels near the coast, indicating that description of both transport and atmospheric chemical reactions is important in understanding regional nitrate dynamics.

1. INTRODUCTION

Ammonia and nitric acid vapor react to form ammonium nitrate aerosol. This is important because ammonium nitrate containing aerosols account for a significant fraction of local and regional visibility problems, particularly in Los Angeles and Denver (White and Roberts, 1977; Cass, 1979; Groblicki *et al.*, 1981). Nitric acid concentrations also are important because of their contribution to wet and dry acid deposition processes. Since NH₄NO₃ formation acts as an important sink for nitric acid, the formation of NH₄NO₃ must be understood if nitric acid levels are to be controlled in a deliberate fashion. Reliable air quality models are needed if emission control strategy development is to proceed. But before air quality models that compute aerosol nitrate and nitric acid concentrations are used for emission control strategy testing, the accuracy of their predictions must be evaluated.

An air quality model for NH₄NO₃ formation and transport recently has been developed (Russell *et al.*, 1983). The Caltech photochemical airshed model developed by McRae and Seinfeld (1983) is used to compute gaseous HNO₃ concentrations from reactive hydrocarbon and oxides of nitrogen emissions. An inventory of ammonia emissions is introduced into the model. Then NH₄NO₃ concentrations are computed at thermodynamic equilibrium between gaseous

HNO₃ and NH₃ using the approach outlined by Stelson and Seinfeld (1982a,b).

To date, this model has been tested in its trajectory form against the time series of gaseous ammonia, particulate ammonium ion and particulate nitrate ion concentration measurements at El Monte, California on a summer day during 1974. Although the model appears to perform well, the ability to confirm this conclusion is limited by the absence of field data on gaseous nitric acid during that event, and by the potential for artifact nitrate formation during sample collection by the measurement methods used in 1974. Better model validation data are needed.

Ideally, an air quality model validation data set for aerosol nitrate formation should provide measurements of all relevant gaseous species: NO, NO₂, HNO₃, NH₃, PAN (and O₃ if photochemical oxidant concentrations are to be checked as well). In addition, the concentration of the aerosol species NO₃[−], SO₄^{2−}, NH₄⁺ should be measured along with all other ionic species that are present in the aerosol. Temperature and relative humidity data are needed to compute the equilibrium dissociation constant that relates gaseous HNO₃ and NH₃ to the aerosol phase. Simultaneous measurements at a number of widely spaced monitoring sites are desirable if an Eulerian grid-based version of the aerosol nitrate formation model is to be tested. Two or more consecutive days of observation are required in Los Angeles if air is to be tracked from the

marine environment all of the way to the eastern end of the air basin near Riverside. Low artifact measurement methods are desired.

The purpose of this paper is to report on the acquisition of such an aerosol nitrate air quality model verification data set in southern California.

2. EXPERIMENTAL

A field experiment was conducted in the South Coast Air Basin (SCAB) that surrounds Los Angeles during the period 30–31 August 1982. Moderate levels of photochemical smog were encountered during the two days studied. Both days were warm with scattered clouds. Peak temperatures reached 35 and 37°C on 30 and 31 August, respectively at the eastern end of the Los Angeles basin. During the afternoons, onshore winds transported pollutants inland, with typical wind speeds of about 5 m s^{-1} . This combination of high temperatures and inland transport resulted in a peak 1-h average ozone concentration of 0.18 ppm on August 30, increasing to a 1-h average peak ozone level of 0.26 ppm in the Riverside area on 31 August.

Ten monitoring sites were established at the locations shown in Fig. 1. The sampling network operated for 48 consecutive hours from midnight at the start of the first day to midnight at the end of 31 August. Two-hour average and 4-h average measurements of $\text{HNO}_3(\text{g})$, $\text{NH}_3(\text{g})$, NO_3^- , NH_4^+ , SO_4^{2-} and other major ionic species were obtained at each site. All sites except Riverside were co-located with a South Coast Air Quality Management District (SCAQMD) or California Air Resources Board (CARB) continuous air monitoring station, and 1-h average data on NO , NO_2 , O_3 and SO_2 were obtained by cooperation with these agencies. Site descriptions are given by the U.S. Environmental Protection Agency (1973, 1978 *et seq.*). PAN was measured by electron capture gas chromatography, and NO and NO_2 were measured by chemiluminescence by researchers at the University of California at Riverside (UCR). PAN also was measured by the same principle at Caltech in Pasadena.

The aerosol, nitric acid and ammonia sampling apparatus for this experiment is shown schematically in Fig. 2. Aerosol nitrate and nitric acid concentrations were measured both by dual filter methods and by the denuder difference method. Gaseous ammonia was measured by a dual filter method using oxalic acid impregnated filters as a sink for NH_3 . Filter holders were of open-faced design so that any large particle nitrates would be collected. The sampling apparatus was surrounded by a bug screen and shaded by a sun shield to prevent nitrate volatilization through over-heating. Nine of the ten sampling sites shown in Fig. 1 were equipped as indicated in Fig. 2, while the 10th site at Riverside (UCR)

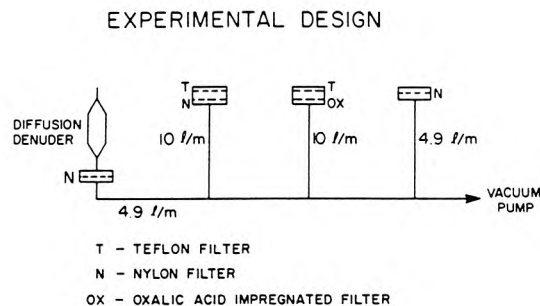


Fig. 2. Schematic of the sampling apparatus used at nine of the ten sites. The tenth station used only the two 10 l min^{-1} lines with dual filters.

consisted of only the two sampling lines that contained dual filter packs.

In the dual filter method for nitric acid determination, air was drawn at a rate of 10 l min^{-1} through a dual filter pack (Grosjean, 1983; Spicer *et al.*, 1982; Appel *et al.*, 1980). A Teflon prefilter (Membrana, Zeffluor, 47 mm diameter, $1 \mu\text{m}$ pore size) first removed the aerosol phase constituents. Gaseous nitric acid that passed through the inert Teflon prefilter was collected as nitrate on a nylon after-filter (Ghia Corp., Nylasorb, 47 mm dia, $1 \mu\text{m}$ pore size). Filters, after exposure, were sealed immediately in petri dishes and chilled until analysis to minimize volatilization from the samples.

Water soluble material was extracted from these filters by mechanical shaking in distilled-deionized-distilled water for 1 h or more. Measured extraction efficiencies typically were above 97%. The extract was divided for subsequent chemical analysis. The aerosol material extracted from the Teflon prefilters was analyzed for nitrate, sulfate, chloride, potassium and sodium ions using Dionex Model 10 and Model 2120 ion chromatographs (Mueller *et al.*, 1978). Divalent cations (calcium and magnesium) were measured using a Varian Techtron model AA-6 atomic absorption spectrophotometer (Varian, 1975). Ammonium ion on the Teflon filters was determined by the phenol—hypochlorite method (Salorzano, 1967). Nitric acid concentrations were determined by extracting the nitrate ion collected on the nylon after-filters, with chemical analysis by ion chromatography as described above. Analytical uncertainties were assessed by analysis of reagent grade standards prepared in the range 0–5 ppm (wt/vol aqueous solution). Five replicate analyses of each of three standard solutions that span the concentration range of interest for each species were used to estimate the uncertainty associated with the laboratory procedures. The relative uncertainty associated with these measurements is shown in the first data column of Table 1. A contribution due to the

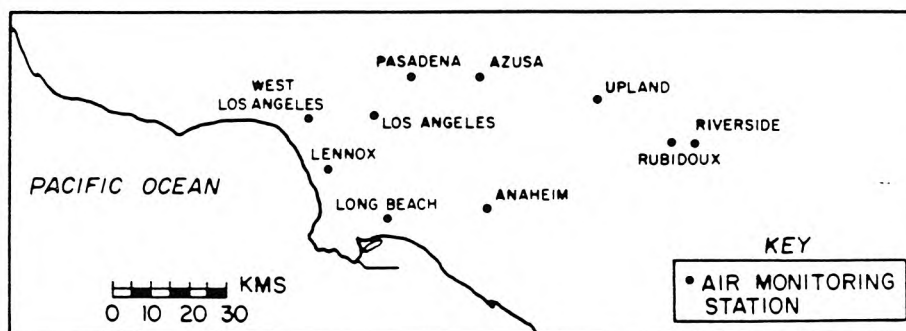


Fig. 1. Locations of nitrate monitoring sites in the South Coast Air Basin.

Table 1. Measurement uncertainties

Species	Uncertainty due to chemical analysis procedure* (%)	Uncertainty due to filter blank† ($\mu\text{g m}^{-3}$)
NO_3^-	15	1.0
SO_4^{2-}	15	1.6
Cl^-	22	0.6
NH_4^+	20	0.2
Ca^{2+}	18	1.4
Na^+	15	0.8
K^+	18	1.1
Mg^{2+}	18	0.5
HNO_3	15	0.8
NH_3	20	0.3

* One standard error, as % of nominally measured value.

† One standard error, stated in equivalent atmospheric concentration.

variability of the filter blanks was added to this analytical error. More than twenty blank filters of each type were taken into the field but not exposed. The average blank values from these filters were subtracted from the measured filter loadings. The contribution to the uncertainty in these measurements due to the variability of the filter blank also is shown in Table 1. This uncertainty in the filter blank governs the lowest quantifiable pollutant concentrations during this experiment. A complete listing of the data from this experiment and their associated uncertainties has been compiled (Russell and Cass, 1983).

The dual filter method for measuring aerosol nitrate and nitric acid has the advantage of simplicity, low cost, sensitivity and ability to produce both particulate and gaseous nitrate concentration data from the same air stream. Results from the nitric acid measurement method intercomparison (Spicer *et al.*, 1982) conducted in the SCAB showed that the dual filter measurements were highly correlated with the median value obtained by all competitive nitric acid measurement methods. One of the two groups of investigators that used a Teflon-nylon filter pair during the intercomparison study obtained results suggesting a small positive proportional bias, while a second group obtained results that suggest no significant bias when measuring nitric acid. Dual filter methods are susceptible to both positive and negative errors. Volatilization of ammonium nitrate would decrease measured nitrate aerosol (Appel *et al.*, 1980). Nitric acid may also react with collected aerosol increasing the measured nitrate aerosol (Appel *et al.*, 1980; Spicer and Schumacher, 1979).

The second method used for nitric acid determination during the present experiment was based on the diffusion denuder design described by Forrest *et al.* (1982), except that 10 sodium carbonate coated tubes 30 cm in length were contained within each denuder housing. At a total air flow rate of 4.9 l min^{-1} , laminar flow was achieved inside the denuder tubes at a nominal Reynolds number of 175 based on tube diameter. Air flowing through the denuder was stripped of nitric acid by reaction with the tube walls. Particulate nitrate (PN) penetrated the denuder and was collected on the nylon after-filter. A separate parallel sample line operating at 4.9 l min^{-1} contained a single nylon filter used to collect total inorganic nitrate (i.e. nitric acid plus aerosol nitrate). Nitric acid concentrations by the denuder difference method were obtained by subtracting the particulate nitrate concentration from the total inorganic nitrate concentration. Nitrate ion levels on these nylon filters were determined by water extraction and ion chromatography, with filter blank subtraction as described previously.

Nitrate measurements obtained by denuder also are susceptible to interferences. Large particle nitrate may be lost in the denuder by impaction. Laboratory experiments performed on the denuders used in this experiment show losses of about 30% for particles larger than $4 \mu\text{m}$ in diameter (Strand, 1983). Because of this measurable bias in the denuder system, nitric acid concentrations presented in this paper will be based on the dual filter method.

Gaseous ammonia concentrations were determined from the dual filter pack shown in Fig. 2 that contained an oxalic acid impregnated back-up filter. The aerosol phase containing ammonium ion first was removed by a Teflon prefilter (Membrana, Zefluor, 47 mm dia, $1.0 \mu\text{m}$ pore size). Ammonia gas remaining in the air stream was collected by reaction with an oxalic acid impregnated glass fiber filter (Gelman Type AE, 47 mm diameter) (Yoong, 1981; Appel *et al.*, 1980; Cadle *et al.*, 1980). After collection, filters were sealed and chilled as described previously. Ammonia concentrations were determined from the ammonium ion collected on the oxalic acid impregnated filters by a modified version of the phenol-hypochlorite method (Salorzano, 1967). The excess oxalate and acid on the glass fiber filters interfered significantly with the method of Salorzano (1967), so the method was modified, adding a phosphate buffer (Harwood and Kuhn, 1970) and additional hydroxide. The modified method is described by Russell (1983) and was found to give reproducible results with a correlation coefficient of $r = 0.99$. Standard deviations for recovery of NH_4^+ standards containing 1 and 0.5 ppm (N by wt) were 2.5 and 3.5%, respectively.

The calculated equilibrium dissociation constant for the $\text{HNO}_3\text{-NH}_3\text{-NH}_4\text{NO}_3$ system is highly dependent on ambient temperature and relative humidity. Temperature measurements to accompany each ambient sample were obtained from nearby weather monitoring stations, where possible, or from temperature measurements that were taken at the air monitoring site by the station operators using mercury thermometers. Instantaneous temperatures were taken each hour. Relative humidities were computed from measured dew point saturation temperatures that are monitored at a number of locations in the SCAB. Dew point temperatures were interpolated to the location of each monitoring site by the method of Goodin *et al.* (1979).

3. RESULTS

Based on previous descriptions of aerosol nitrate concentrations in the Los Angeles area (Appel *et al.*, 1978), high aerosol nitrate concentrations were expected in the Riverside area in the late afternoon due to production of nitric acid in the plume downwind of metropolitan Los Angeles. High aerosol nitrate levels (above $25 \mu\text{g m}^{-3}$) were observed at Rubidoux as expected, as is seen in Fig. 3(a). However, unexpectedly high nitrate levels also were observed at near-coastal sites like Lennox and Long Beach in the morning of 31 August, as seen in Fig. 3(c).

Hourly averaged data on surface wind speed and direction at 39 monitoring sites in Southern California were acquired from governmental agencies for the period 30–31 August 1982. A mass-consistent wind field defined over a $5 \text{ km} \times 5 \text{ km}$ grid system that covers the geographic area shown in Fig. 1 was developed for each hour by the method of Goodin *et al.* (1979). Air parcel trajectories were integrated over these gridded wind fields using 10 min time steps. Trajectory analysis shows that the peak nitrate concen-

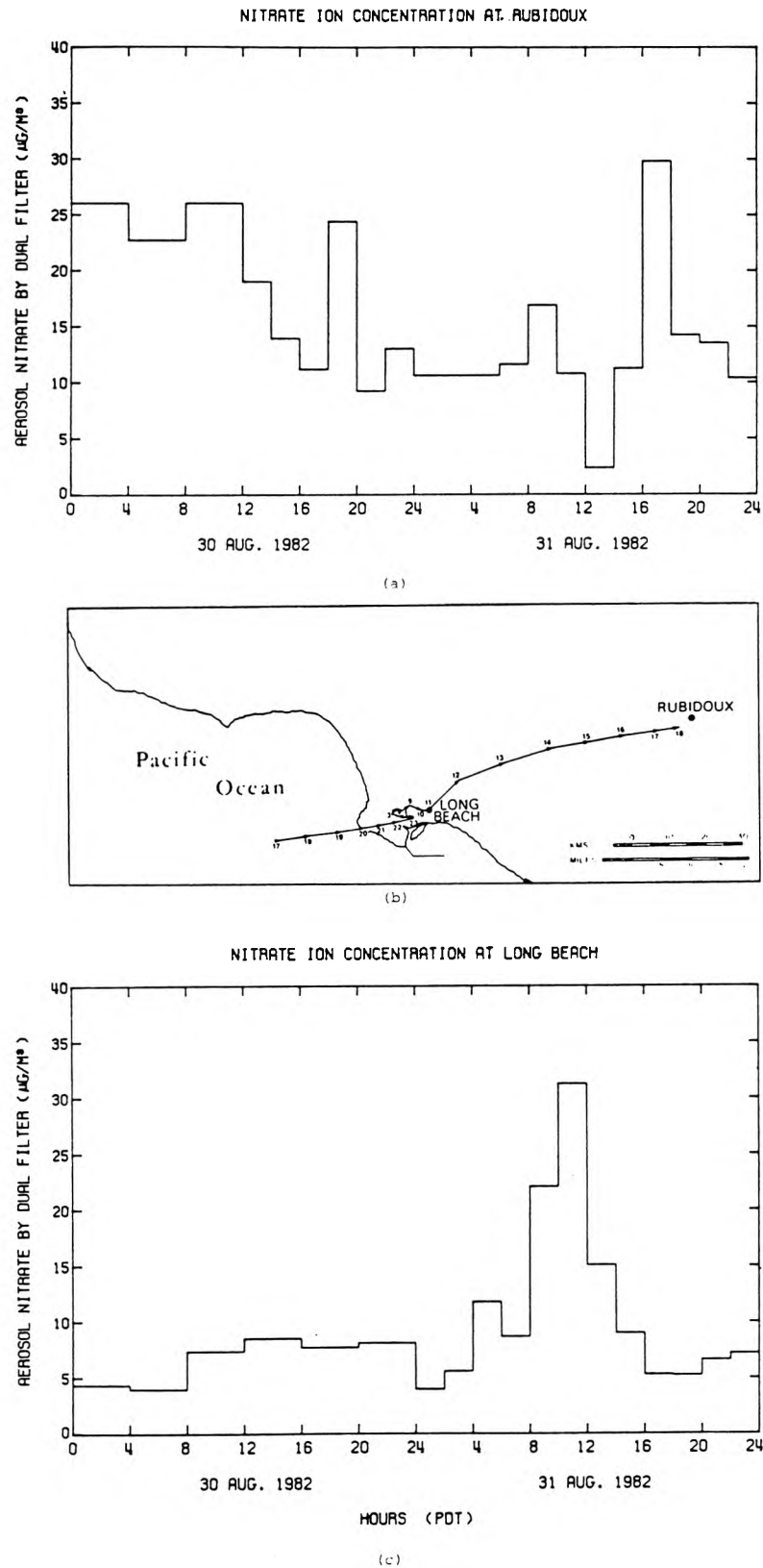


Fig. 3. (a) Nitrate concentration observed at Rubidoux, 30–31 August 1982. (b) Trajectory of the air mass passing over the Long Beach area at 1100 on 31 August and over the Rubidoux area at 1800 on 31 August 1982. (c) Nitrate concentrations at Long Beach, 30–31 August 1982.

tration at Rubidoux on the afternoon of 31 August is related to the coastal peak observed at Long Beach earlier that morning. A forward trajectory drawn from the nitrate peak in the Long Beach area at 1100 hours on the morning of 31 August passes within 3.5 km of Rubidoux between 1700 and 1800 hours in the late afternoon at the time of the nitrate peak in the eastern portion of the air basin [see Fig. 3(b)]. A backward trajectory drawn from Long Beach at 1100 hours on 31 August shows that that air mass first crossed the coastline during the sea breeze portion of the late afternoon of 30 August. At night, wind speeds dropped to less than 0.5 m s^{-1} with variable wind direction. The air mass stagnated overnight in Long Beach, an area of

high NO_x emissions (see Fig. 6 in Russell *et al.*, 1983). The high nitrate concentration observed at Long Beach in the morning of 31 August resulted from progressive aerosol accumulation within a largely stagnant and stable air mass. This nitrate-rich air parcel then was advected inland on the next day's sea breeze. It appears that transport may play as important a role as chemical reaction in accumulating high nitrate levels.

A balance on the ionic material in the samples taken at Long Beach is shown in Fig. 4. The major constituents are NH_4^+ , NO_3^- and SO_4^{2-} , but Na^+ and Ca^{2+} often account for about one third of the cations present, suggesting sea salt and soil dust contributions

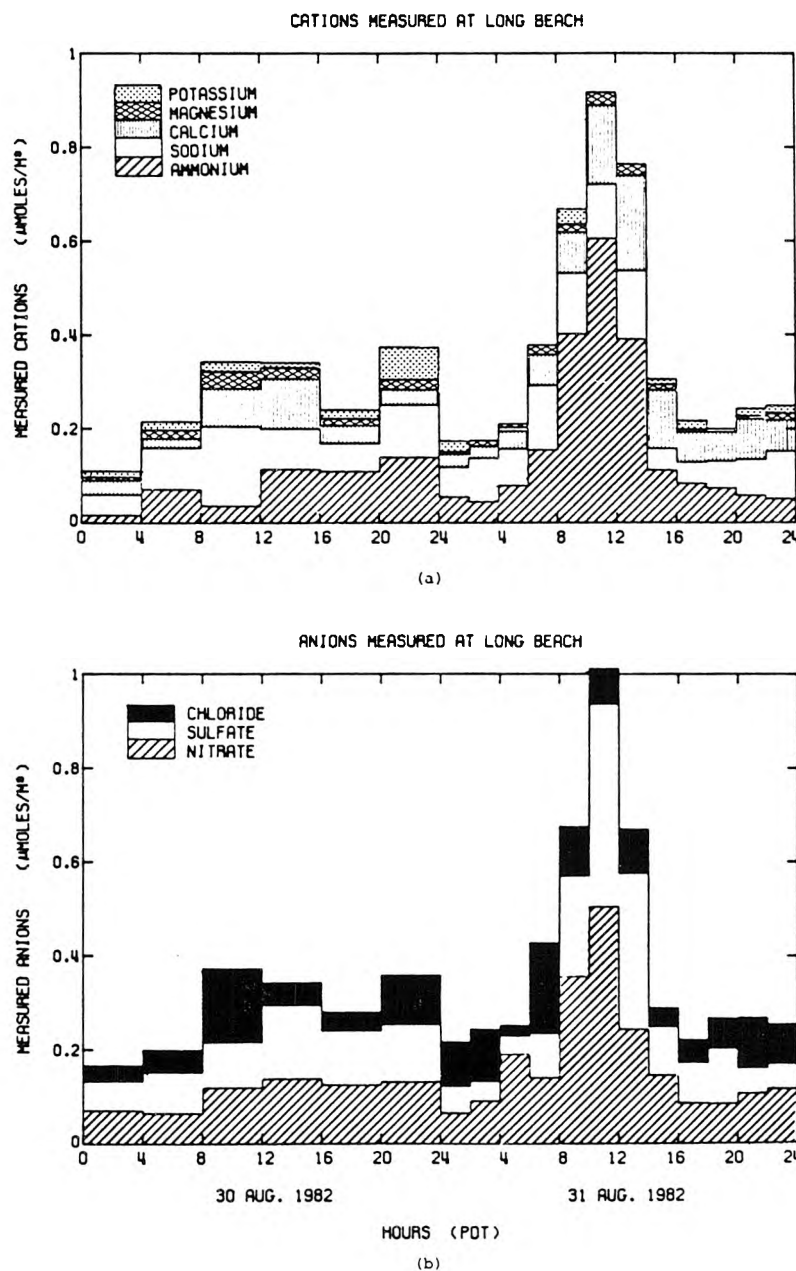


Fig. 4. Ionic species concentration at Long Beach. (a) Cations. (b) Anions.

to the aerosol samples. Na^+ usually is present in excess of Cl^- , suggesting that reaction with strong acids like H_2SO_4 or HNO_3 has displaced some of the chloride from the sea salt portion of the aerosol (Martens *et al.*, 1973; Duce, 1969; Robbins *et al.*, 1959; Hitchcock *et al.*, 1980). The ion balance is good in spite of the fact that CO_3^{2-} , OH^- and H^+ concentrations were not measured. Previous studies in the SCAB show the presence of very low carbonate carbon levels in the aerosol (Mueller *et al.*, 1972). Large amounts of hydrogen ion would not be expected because of the great excess of ammonia present during this experiment.

The composition of the aerosol observed inland at Riverside is shown in Fig. 5. The largest contributors to the ionic material are NH_4^+ and NO_3^- , but noticeable amounts of K^+ , Mg^{2+} , Ca^{2+} , Na^+ and Cl^- also are found. Note that Cl^- arrives with the aerosol between 1600 and 1800 hours on 31 August near the time of arrival of the trajectory from Long Beach discussed previously. The important point to note from these ion balances is that the ionic material in the actual aerosol is much more complex than the mixed sulfate, nitrate and ammonium salts that can be described by present theoretical models for the equilibrium between NH_3 , HNO_3 and the aerosol phase.

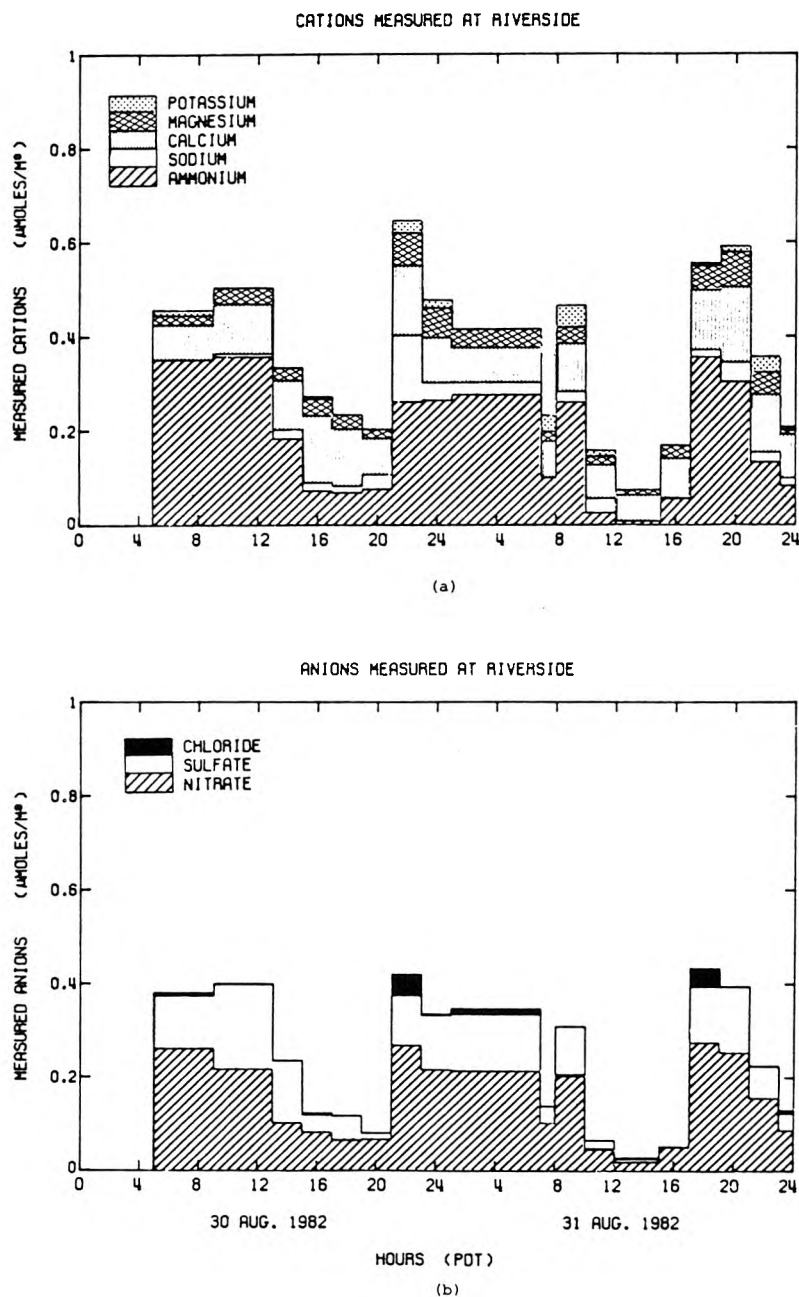


Fig. 5. Ionic species concentration at Riverside. (a) Cations. (b) Anions.

Gas phase HNO_3 concentrations are compared to aerosol NO_3^- at the polluted near-coastal sites at Long Beach and Lennox in Fig. 6. Nearly all of the inorganic nitrate is in the aerosol phase. In contrast, Fig. 7 shows that ammonia is partitioned about equally between $\text{NH}_3(\text{g})$ and aerosol NH_4^+ at Long Beach, while at Lennox ammonia gas concentrations often were quite elevated, suggesting an NH_3 source upwind of Lennox (possibly at a nearby refinery or at the nearby Hyperion sewage treatment plant).

Inland from the coast, gaseous nitric acid concentrations begin to increase in the late morning and early afternoon, due possibly to photochemical production

of HNO_3 or to volatilization of NH_4NO_3 . This can be seen in Fig. 8 at Anaheim (which is located between Long Beach and Riverside). By the time that the air parcel defined at Long Beach at 1100 hours on 31 August reaches Rubidoux between 1600 and 1800 hours, a tremendous increase in NH_3 in the air parcel has occurred [Fig. 9(b)], and most of the inorganic nitrate again is found in the aerosol phase [Fig. 9(a)]. This increase in NH_3 is consistent with estimates of the spatial distribution of NH_3 sources in the Los Angeles area given by Cass *et al.* (1982) and Russell *et al.* (1983), which shows that the largest source of NH_3 in the Los Angeles area arises from a large group of dairies and

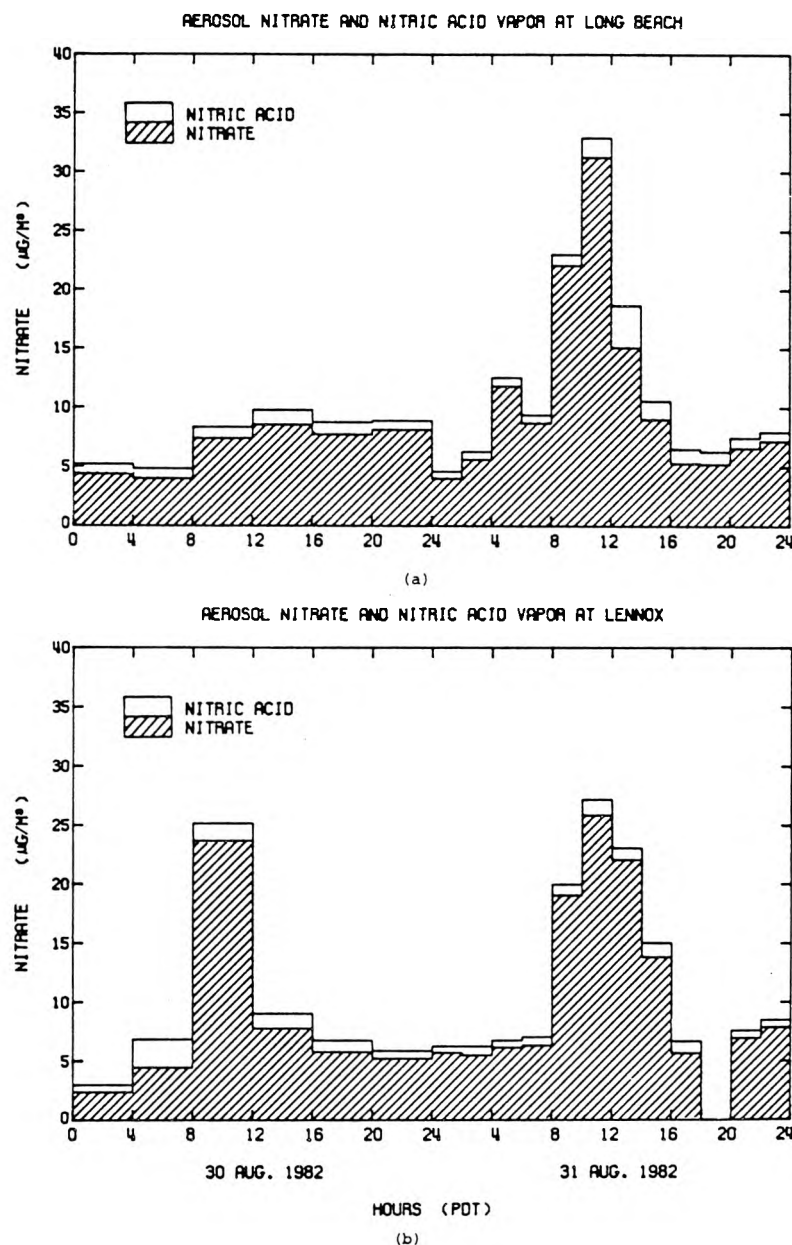


Fig. 6. Particulate nitrate and gaseous nitric acid concentrations ($\mu\text{g m}^{-3}$ as NO_3^-).
(a) Long Beach. (b) Lennox.

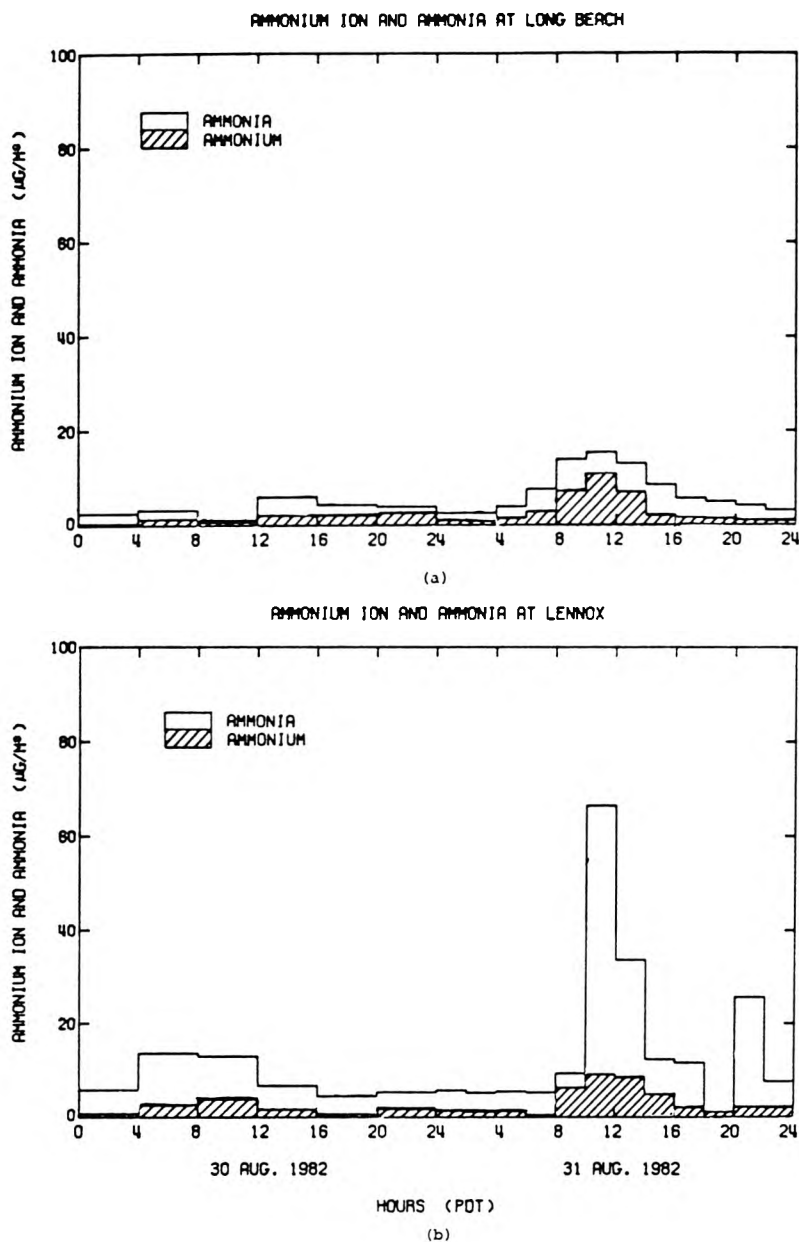


Fig. 7. Particulate ammonium and gaseous ammonia concentrations ($\mu\text{g m}^{-3}$ as NH_4^+).
(a) Long Beach. (b) Lennox.

animal husbandry operations in the Chino area just to the west of Riverside and Rubidoux.

The product of the measured concentrations of ammonia and nitric acid vapor is a key parameter that can be compared to the predictions of theoretical models for the ammonia and nitric acid concentrations expected at thermodynamic equilibrium with the aerosol phase. Nitric acid and ammonia concentration measurements were used to calculate their concentration product (CP) at each monitoring site. As seen in Fig. 10, the measured CP at Rubidoux varies from less than 20 to over 300 ppbv^2 , and measured CP's at some monitoring sites were observed below 1 ppbv^2 . A very

wide range of NH_3 and HNO_3 concentration product data thus have been acquired for use in verifying theoretical calculations. The hypothesis that aerosol nitrates were in equilibrium with gas phase nitric acid and ammonia during this experiment has been tested by Hildemann *et al.* (1984).

At two locations, Riverside and Pasadena, the major gaseous and aerosol species that evolve from NO_x emissions were measured. Fig. 11 shows that most of the pollutant oxides of nitrogen at these two sites were present as NO and NO_2 throughout this experiment. Only a small fractional conversion of NO emissions to HNO_3 and NH_4NO_3 is needed to explain the nitrate

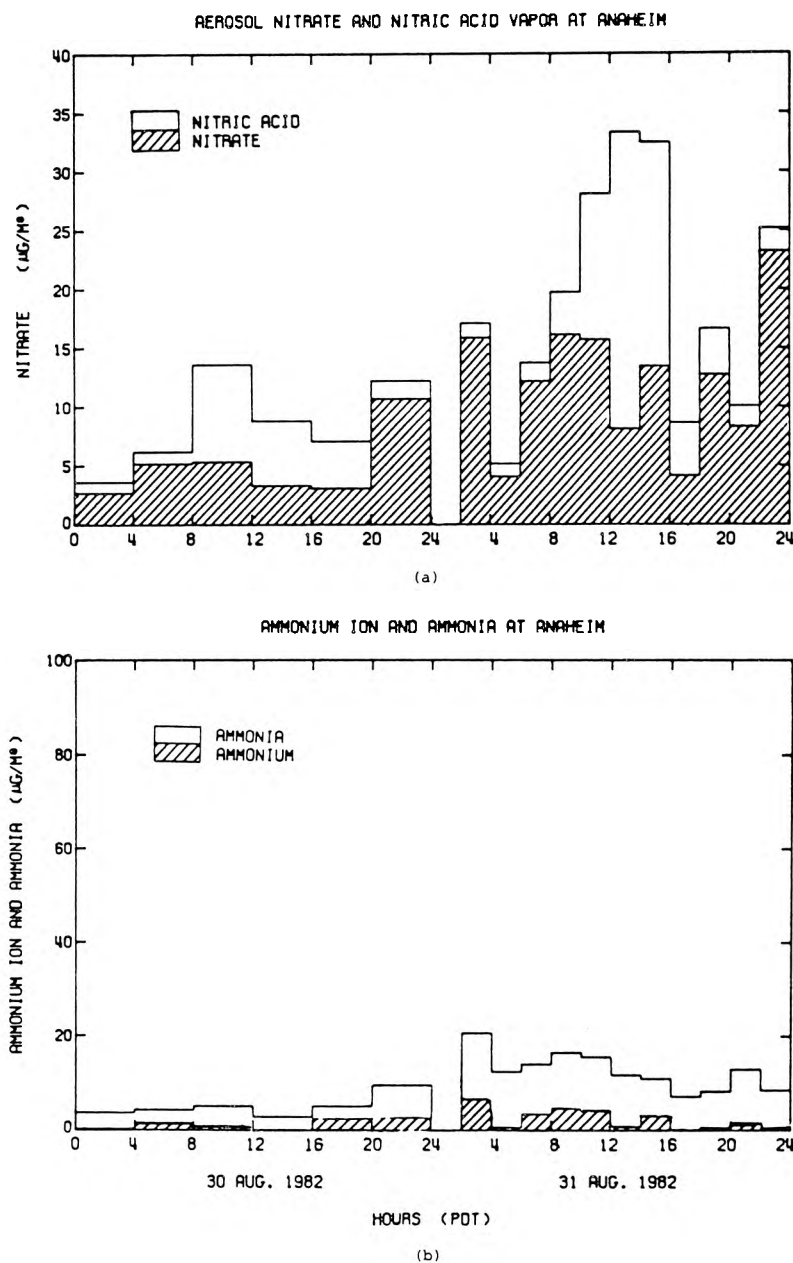


Fig. 8. (a) Particulate nitrate and gaseous nitric acid concentrations at Anaheim ($\mu\text{g m}^{-3}$ as NO_3^-). (b) Particulate ammonium and gaseous ammonia concentrations at Anaheim ($\mu\text{g m}^{-3}$ as NH_4^+).

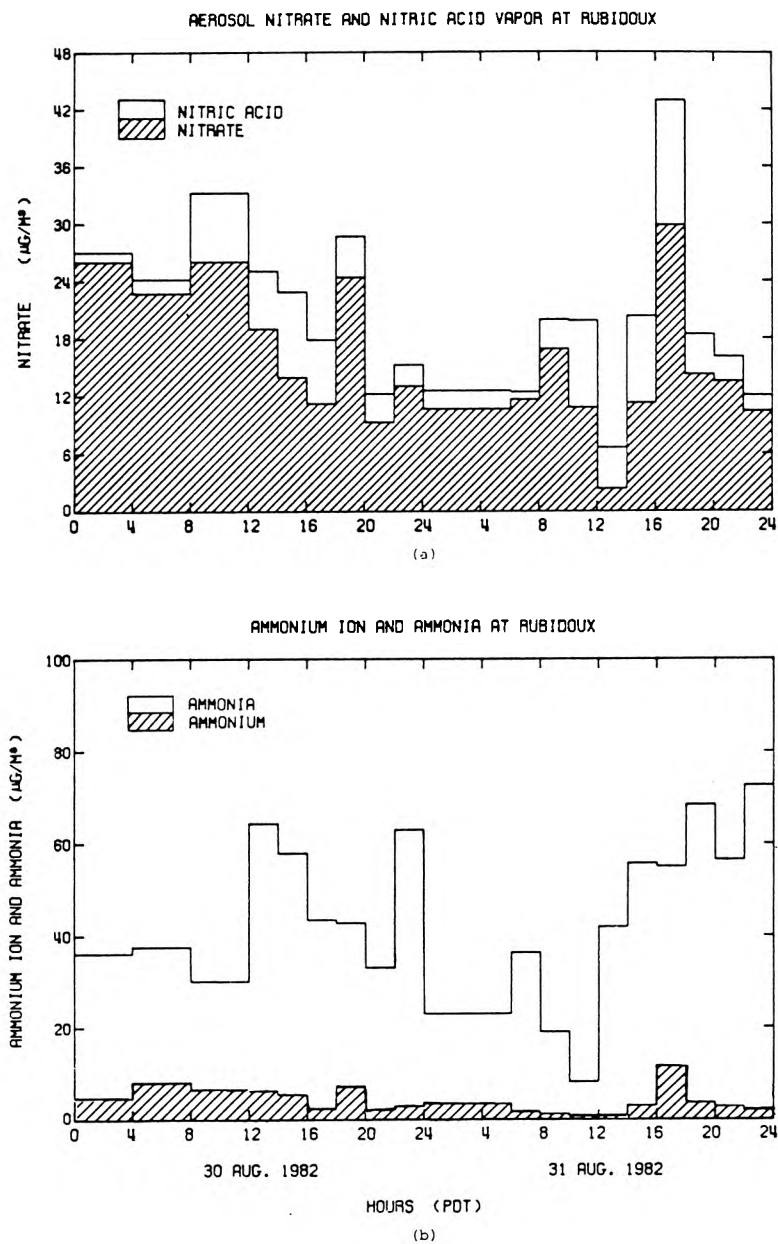


Fig. 9. (a) Particulate nitrate and gaseous nitric acid at Rubidoux ($\mu\text{g m}^{-3}$ as NO_3^-).
 (b) Particulate ammonium and gaseous ammonia concentrations at Rubidoux ($\mu\text{g m}^{-3}$ as NH_4^+).

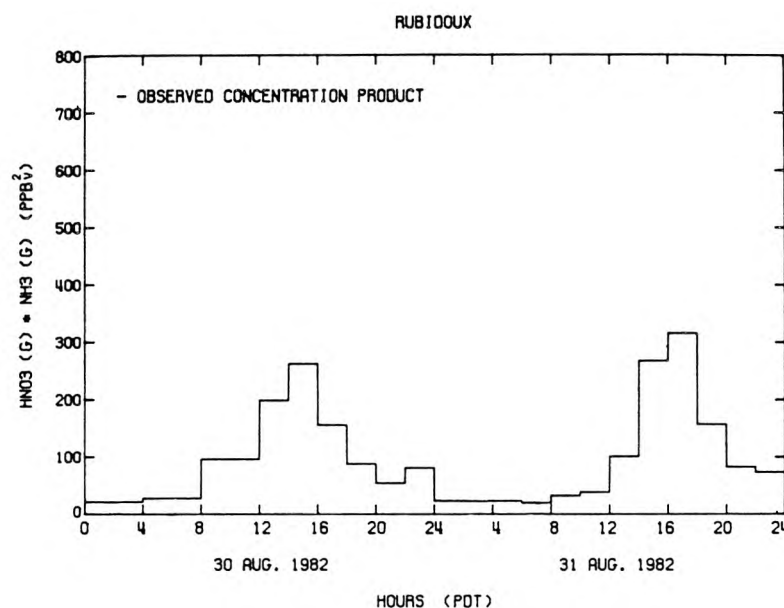


Fig. 10. Partial pressure concentration product of ammonia and nitric acid at Rubidoux.

concentrations observed. The fractional conversion of NO and NO_2 to nitrate species during this experiment is lower than observed during some other field measurement programs (Grosjean, 1983; Spicer, 1982) but this is consistent with the lower level of photochemical activity experienced during this 2-day experiment. On the days sampled, peak 1-h average O_3 concentrations exceeded 0.20 ppm at only a few monitoring sites, with the basin-wide 1-h O_3 peak within the region shown in Fig. 1 amounting to 0.26 ppm. In contrast, the O_3 concentration on the 1974 day modeled previously by Russell *et al.* (1983) exceeded 0.40 ppm with a correspondingly higher conversion of NO_x to HNO_3 and PAN.

4. CONCLUSIONS

Results from the field experiment show that the ionic material in the aerosol phase throughout the South Coast Air Basin is chemically complex. At most times, the bulk of the ionic aerosol is composed of nitrate, sulfate and ammonium ion. However there are significant amounts of Na^+ , Ca^{2+} , Mg^{2+} , K^+ , Cl^- and possibly CO_3^{2-} , OH^- or H^+ ions also present. The coastal nitrate-containing aerosol has a significant sea salt derived fraction, probably from the displacement of chloride by reaction with nitric acid. These multi-component aerosols are more complex than can be handled by present mathematical models for the equilibrium between HNO_3 , NH_3 and a mixed sulfate, nitrate and ammonium containing aerosol.

Trajectory analysis has been used to judge the importance of transport in determining aerosol nitrate concentrations. Large amounts of nitrate were shown to accumulate in an air mass that stagnated near the coast at night. Later, this nitrate laden air mass was transported inland by the sea breeze. The time of the nitrate peak inland near Riverside coincided with the time that that nitrate laden air mass reached that area. This indicates that a description of transport characteristics as well as atmospheric chemistry is important in understanding the dynamics that govern the high nitrate levels observed in the eastern portion of the Los Angeles basin.

A nitrogen balance constructed at two locations in the Los Angeles basin shows that conversion of only a small fraction of the NO_x emissions to HNO_3 and NH_4NO_3 is sufficient to explain the aerosol nitrate and nitric acid observed. The two days studied here were both considered to have moderate smog (fairly typical of a summer day), and a correspondingly lower oxidation of NO_x to HNO_3 and PAN than would occur during an extreme air pollution episode in Los Angeles.

The data set derived from this experiment can be used in verification tests of aerosol nitrate formation models, and will challenge the predictive capability of current air quality models. The days sampled during this experiment exhibited both interesting transport patterns and evidence of chemical transformations that can be used to test both the transport and gas-to-particle conversion descriptions built into regional scale air quality models.

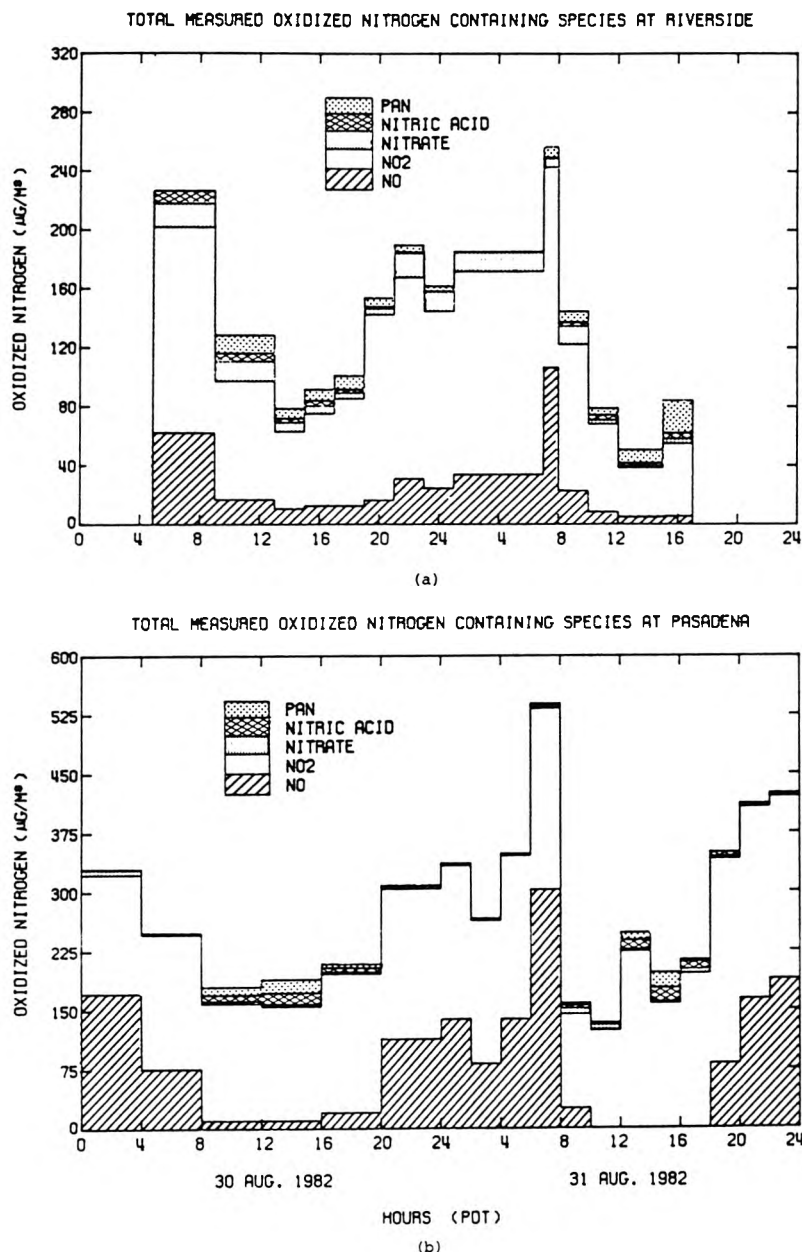


Fig. 11. Measured NO , NO_2 , HNO_3 , PAN and nitrate (in $\mu\text{g m}^{-3}$ stated as equivalent NO_3^-). (a) Pasadena. (b) Rubidoux.

Acknowledgements—This study was supported by the California Air Resources Board under Agreement No. A2-150-32 and by gifts to the Environmental Quality Laboratory. The South Coast Air Quality Management District and the California Air Resources Board cooperated by allowing access to their air monitoring sites, and provided meteorological and gaseous pollutant data. Special thanks also goes to Dennis Fitz and the Statewide Air Pollution Research Center at the University of California at Riverside whose services were greatly appreciated. We would also like to thank the Caltech students and staff who helped to operate each of the pollutant sampling sites.

REFERENCES

- Appel B. R., Kothny E. L., Hoffer E. M., Hidy G. M. and Wesolowski J. J. (1978) Sulfate and nitrate data from the California Aerosol Characterization Experiment (ACHEX). *Envir. Sci. Technol.* **12**, 418–425.
- Appel B. R., Wall S. M., Tokiwa Y. and Haik M. (1980) Simultaneous nitric acid, particulate nitrate and acidity measurements in ambient air. *Atmospheric Environment* **14**, 549–554.
- Cadle S. H., Countess R. J. and Kelly N. A. (1980) Nitric acid and ammonia concentrations in urban and rural locations.

- Atmospheric Environment* **16**, 2501–2506.
- Cass G. R. (1979) On the relationship between sulfate air quality and visibility with examples in Los Angeles. *Atmospheric Environment* **13**, 1069–1084.
- Cass G. R., Gharib S., Peterson M. and Tilden J. W. (1982) The origin of ammonia emissions to the atmosphere in an urban area. Open File Report 82-6, Environmental Quality Laboratory, California Institute of Technology, Pasadena, CA.
- Duce R. A. (1969) On the source of gaseous chlorine in the marine atmosphere. *J. geophys. Res.* **70**, 1775–1779.
- Forrest J., Spandau D. J., Tanner R. L. and Newman L. (1982) Determination of atmospheric nitrate and nitric acid employing a diffusion denuder with a filter pack. *Atmospheric Environment* **16**, 1473–1485.
- Goodin W. R., McRae G. J. and Seinfeld J. H. (1979) A comparison of interpolation methods for sparse data: application to wind and concentration fields. *J. appl. Met.* **18**, 761–771.
- Groblicki P. J., Wolff G. T. and Countess R. J. (1981) Visibility-reducing species in the Denver "Brown Cloud"—I. Relationships between extinction and chemical composition. *Atmospheric Environment* **15**, 2473–2484.
- Grosjean D. (1983) Distribution of atmospheric nitrogenous pollutants at a Los Angeles area receptor site. *Envir. Sci. Technol.* **17**, 13–19.
- Harwood J. E. and Kuhn A. L. (1970) A colorimetric method for ammonia in natural waters. *Water Res.* **4**, 805–811.
- Hildemann L. M., Russell A. G. and Cass G. R. (1984) Ammonia and nitric acid concentrations in equilibrium with atmospheric aerosols: experiment vs theory. *Atmospheric Environment* **18**, 1737–1750.
- Hitchcock D. R., Spiller L. L., and Wilson W. E. (1980) Sulfuric acid aerosols and HCl release in coastal atmospheres: evidence of rapid transformation of sulphuric acid particulates. *Atmospheric Environment* **14**, 165–182.
- Martens C. S., Wesolowski J. J., Harriss R. C. and Kaifer R. (1973) Chlorine Loss from Puerto Rican and San Francisco Bay Area Marine Aerosols. *J. geophys. Res.* **78**, 8778–8792.
- McRae G. J. and Seinfeld J. H. (1983) Development of a second generation mathematical model for urban air pollution—II. Performance evaluation. *Atmospheric Environment* **17**, 501–523.
- Mueller P. K., Mendoza B. V., Collins J. C. and Wilgus E. S. (1978) Application of ion chromatography to the analysis of anions extracted from airborne particulate matter. In *Ion Chromatographic Analysis of Environmental Pollutants* (edited by Sawicki E., Mulik J. D. and Wittgenstein E.). Ann Arbor Science, Ann Arbor, MI.
- Mueller P. K., Mosley R. W. and Pierce L. B. (1972) Chemical composition of Pasadena aerosol by particle size and time of day. *J. Colloid Interface Sci.* **39**, 235–239.
- Robbins R. C., Cadle R. D. and Eckhardt D. L. (1959) The conversion of sodium chloride to hydrogen chloride in the atmosphere. *J. Met.* **16**, 53–56.
- Russell A. G. (1983) Analysis of oxalic acid impregnated filters for ammonia determination. Open File Report 83-1, Environmental Quality Laboratory, California Institute of Technology, Pasadena, CA.
- Russell A. G. and Cass G. R. (1983) Nitric acid, ammonia and atmospheric particulate matter concentrations in the South Coast Air Basin, 30–31 August 1982. Open File Report 83-3, Environmental Quality Laboratory, California Institute of Technology, Pasadena, CA.
- Russell A. G., McRae G. J. and Cass G. R. (1983) Mathematical modeling of the formation and transport of ammonium nitrate aerosol. *Atmospheric Environment* **17**, 949–964.
- Salorzano L. (1967) Determination of ammonia in natural waters by the phenylhypochlorite method. *Limnol Oceanogr.* **14**, 799–801.
- Spicer C. W. (1982) The distribution of oxidized nitrogen in urban air. *Sci. Tot. Envir.* **24**, 183–192.
- Spicer C. W., Howes J. E., Bishop T. A., Arnold L. H. and Stevens R. K. (1982) Nitric acid measurement methods: an intercomparison. *Atmospheric Environment* **16**, 1407–1500.
- Spicer C. W. and Schumacher P. M. (1979) Particulate nitrate: laboratory and field studies of major sampling interferences. *Atmospheric Environment* **13**, 543–552.
- Stelson A. W. and Seinfeld J. H. (1982a) Relative humidity and temperature dependence of the ammonium nitrate dissociation constant. *Atmospheric Environment* **16**, 983–992.
- Stelson A. W. and Seinfeld J. H. (1982b) Relative humidity and pH dependence of the vapor pressure of ammonium nitrate–nitric acid solutions at 25°C. *Atmospheric Environment* **16**, 993–1000.
- Strand S. R. (1983) Aerosol losses in diffusion denuders. Laboratory report, California Institute of Technology, Pasadena, CA.
- U.S. Environmental Protection Agency (1973) Directory of Air Quality Monitoring Sites—1972. Document EPA-450/2-73-006, U.S. Environmental Protection Agency, Research Triangle Park, NC.
- U.S. Environmental Protection Agency (1978) Directory of Air Quality Monitoring Sites Active in 1977. Document EPA-450/2-78-048, U.S. Environmental Protection Agency, Research Triangle Park, NC.
- Varian (1975) Instruction Manual for Model AA-6 Atomic Absorption Spectrophotometer. Varian Techtron, Melbourne, Australia.
- White W. H. and Roberts P. T. (1977) On the nature and origins of visibility reducing species in the Los Angeles Basin. *Atmospheric Environment* **11**, 803–812.
- Yoong M. (1981) Measurement of ambient ammonia concentrations in southern California. Rockwell International, Newbury Park, CA. Final Report to the California Air Resources Board under Contract No. A7-188-30. To be available from NTIS.

CHAPTER 5
AMMONIA AND NITRIC ACID CONCENTRATIONS IN
EQUILIBRIUM WITH ATMOSPHERIC AEROSOLS:
EXPERIMENT VS THEORY

(Reprinted from *Atmospheric Environment*, 18, 1737-1750)

AMMONIA AND NITRIC ACID CONCENTRATIONS IN EQUILIBRIUM WITH ATMOSPHERIC AEROSOLS: EXPERIMENT VS THEORY

LYNN M. HILDEMAN*, ARMISTEAD G. RUSSELL† and GLEN R. CASS*

*Environmental Engineering Science Department and Environmental Quality Laboratory and †Mechanical Engineering Department and Environmental Quality Laboratory, California Institute of Technology, Pasadena, CA 91125, U.S.A.

Abstract—The equilibrium between gaseous ammonia, nitric acid, and aerosol nitrate is discussed on the basis of a recent field experiment in southern California. Comparison is drawn between theoretical equilibrium calculations and simultaneous measurements of nitric acid, ammonia, ammonium ion, nitrate ion, sulfate ion, other ionic species, temperature and dewpoint. Particulate and gaseous pollutant concentrations at some inland sampling sites are readily explained if the aerosol is assumed to exist as an external mixture with all particulate nitrate and ammonium available to form pure NH_4NO_3 . At other monitoring sites, especially near the coast, aerosol nitrate is found in the presence of NH_3 and HNO_3 concentrations that thermodynamic calculations show are too low to produce pure NH_4NO_3 . This can be explained when the amount of aerosol nitrate that can be derived from reaction of nitric acid with sea salt and soil dust is taken into account. A calculation approach that accounts for the presence of mixed sulfate and nitrate salts improves the agreement between predicted and observed pollutant concentrations in the majority of cases studied. Uncertainties in these calculations arise from a number of sources including the thermodynamic quantities, and the effect of these uncertainties on the comparison between theory and experiment is discussed.

INTRODUCTION

Theoretical calculations for the formation of atmospheric aerosol nitrate based on thermodynamic equilibrium between ammonia, nitric acid and aerosol constituents have been presented recently by several research groups (Stelson *et al.*, 1979; Stelson and Seinfeld, 1982 a,b,c; Tang, 1976, 1980; Saxena and Peterson, 1981; Saxena *et al.*, 1983; Bassett and Seinfeld, 1983). These chemical equilibrium calculations when embedded within a photochemical airshed model show promise of being able to predict the aerosol nitrate concentrations that will result from regional emissions of sulfurous, nitrogenous and hydrocarbon (HC) gaseous precursors (Russell *et al.*, 1983).

Very few complete sets of atmospheric measurements exist, however, against which these chemical equilibrium calculations have been tested. Stelson *et al.* (1979) and Doyle *et al.* (1979) have shown that measurements of gaseous nitric acid and ammonia often are consistent with the upper limit on those concentrations predicted if the gases were in equilibrium with pure solid NH_4NO_3 . In those studies, the aerosol phase was not characterized completely, and little insight is gained into the cause of those cases where the atmospheric concentration products of NH_3 and HNO_3 fall below the equilibrium dissociation constant for pure NH_4NO_3 . The hypothesis that NH_3 , HNO_3 , and NH_4NO_3 are in equilibrium also has been pursued in cool humid atmospheres (Harrison and Pio, 1983) and at the low concentrations present in rural atmospheres (Cadle *et al.*, 1982). Very little work has been published to date that examines

the agreement between equilibrium-based calculation schemes and field observations in cases where the ionic components in the aerosol are treated as being more complex than pure NH_4NO_3 . A step in this direction is provided by Tanner (1982), who compared the thermodynamics of aqueous mixed sulfate-nitrate solutions and solid ammonium nitrate to field experiments under conditions present on Long Island, New York.

In the present paper, the role of atmospheric nitric acid and ammonia in the formation of nitrate-containing aerosols is discussed on the basis of field experiments conducted in southern California. Comparison is drawn between theoretical equilibrium calculations and an extensive collection of simultaneous observations on HNO_3 , NH_3 , NH_4^+ , NO_3^- , SO_4^{2-} , other ionic species, temperature and dewpoint. Calculations for the chemical equilibrium within multi-component aerosols are contrasted to the results obtained if a pure NH_3 , HNO_3 , NH_4NO_3 system had been present. The case where non-volatile nitrates are present due to reaction between nitric acid and either sea salt or soil dust is considered. The effect of uncertainties in the thermochemical data required for these equilibrium calculations is discussed, as well as the implications that these uncertainties hold for verification studies of regional airshed models for aerosol nitrate formation.

EXPERIMENTAL

The measurements used in this comparison were taken on 30–31 August 1982, as part of a project designed to acquire an air quality model validation data set for use in testing models for aerosol nitrate formation and transport. Gaseous nitric

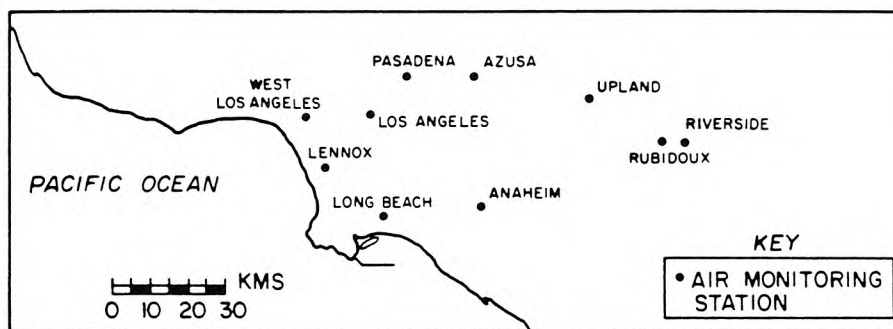


Fig. 1. Air monitoring sites in the South Coast Air Basin that surrounds Los Angeles.

acid and ammonia, and aerosol sulfate, nitrate, ammonium and other major ionic species were monitored at 10 locations in southern California (Fig. 1) over a 48-h period. The details of the experiment are described by Russell and Cass (1984), and only will be summarized here.

Gaseous nitric acid and ammonia and the major ionic aerosol species were measured over 2-h and 4-h intervals using filter-based techniques. Nitric acid measurements used in this study were obtained by the dual filter method, using a Teflon prefilter (Membrana Zeflur, 47 mm dia, 1 μ m pore size) for aerosol removal, followed by a nylon filter (Ghia Nylasorb, 47 mm dia, 1 μ m pore size) which quantitatively collects nitric acid as nitrate (Spicer and Schumacher, 1979; Appel *et al.*, 1980; Spicer *et al.*, 1982). Ammonia was collected as ammonium using an oxalic acid impregnated glass fiber filter (Gelman AE) preceded by a separate Teflon prefilter that removed aerosol NH_4^+ (Yoong, 1981; Appel *et al.*, 1980; Cadle *et al.*, 1982). Aerosol phase constituents were measured from material collected on the two Teflon prefilters. Ion chromatography was used to determine SO_4^{2-} , NO_3^- , Cl^- , Na^+ and K^+ concentrations. Divalent cations, Ca^{2+} and Mg^{2+} , were analyzed using atomic absorption spectroscopy (Varian Techtron Model AA6). Ammonium ion concentrations were measured by the phenol hypochlorite method (Salorzano, 1967; Harwood and Kuhn, 1970; Russell, 1983).

EQUILIBRIUM CALCULATIONS

Several alternative methods were used to calculate the partial pressures of ammonia and nitric acid vapor which in theory should be found in equilibrium with the aerosol phase. When the aerosol phase was assumed to consist of pure ammonium nitrate (s or aq) or an aqueous NH_4^+ , NO_3^- , SO_4^{2-} mixture, the calculations were based on the studies by Stelson and Seinfeld (1982a,c). Calculations involving dry, internally mixed NH_4^+ , NO_3^- , SO_4^{2-} aerosols can be viewed, from two perspectives. If the solid phase is assumed to exist as a solid solution, then calculations can be performed by the method of Saxena *et al.* (1983). If the solid phase exists as a heterogeneous mixture of various crystalline phases, then the vapor pressures could be as high as over solid NH_4NO_3 (Stelson and Seinfeld, 1982c). Each of these approaches is based on fundamental thermodynamic concepts, and provides a method for calculating the equilibrium partial pressure product of NH_3 and HNO_3 which should be found in the presence of a specified level of gaseous and aerosol constituents. The algorithm outlined by Russell *et al.*

(1983) was used to check the apportionment of measured total nitrate ($\text{HNO}_3(\text{g})$ plus NO_3^-) and total ammonia ($\text{NH}_3(\text{g})$ + NH_4^+) between the gaseous and aerosol phases.

Because it is important to an understanding of the data analysis which follows, the mechanics of the aerosol equilibrium model calculations will be described here in some detail, illustrated for the case of pure NH_4NO_3 formation. First, the equilibrium dissociation constant, K , for pure ammonium nitrate is calculated from the ambient temperature, (T), and relative humidity, (r.h.) (Stelson and Seinfeld, 1982a). Then the total nitrate, $[\text{TN}]$, and total ammonia, $[\text{TA}]$, available to form ammonium nitrate is calculated as

$$[\text{TN}] = [\text{HNO}_3(\text{g})]_m + [\text{NO}_3^-]_m \quad (1)$$

$$[\text{TA}] = [\text{NH}_3(\text{g})]_m + [\text{NH}_4^+]_m \quad (2)$$

where $[\text{HNO}_3(\text{g})]_m$ is the measured gaseous nitric acid concentration, $[\text{NH}_3(\text{g})]_m$ is the measured gaseous ammonia concentration, and $[\text{NO}_3^-]_m$ and $[\text{NH}_4^+]_m$ are the measured aerosol nitrate and ammonium concentrations, respectively, available or free to form NH_4NO_3 . Then the equilibrium constraint

$$[\text{NH}_3(\text{g})][\text{HNO}_3(\text{g})] \leq K$$

is imposed. If $[\text{TN}][\text{TA}] \leq K$, no ammonium nitrate is predicted to be present because there is not enough total nitrate and total ammonia to support aerosol NH_4NO_3 formation. If $[\text{TN}][\text{TA}] > K$ then aerosol ammonium nitrate is predicted to form from the gas phase precursors such that the product $[\text{NH}_3(\text{g})]_c [\text{HNO}_3(\text{g})]_c = K$. The subscript c indicates a theoretically computed pollutant concentration that may differ from measured values. Conservation of TA and TN gives the final expression for the ammonium nitrate formed as

$$[\text{NH}_4\text{NO}_3]_c = \frac{1}{2} \{ [\text{TA}] + [\text{TN}] - ([\text{TA}]^2 + [\text{TN}]^2 - 4([\text{TA}][\text{TN}] - K))^{1/2} \} \quad (3)$$

and the gas phase concentrations

$$[\text{NH}_3(\text{g})]_c = [\text{TA}] - [\text{NH}_4\text{NO}_3]_c \quad (4)$$

and

$$[\text{HNO}_3(\text{g})]_c = [\text{TN}] - [\text{NH}_4\text{NO}_3]_c \quad (5)$$

Thus the inputs to the model calculation are TA, TN, T

and r.h., and the outputs are the calculated aerosol and gas phase concentrations, and the dissociation constant, K . K and the calculated concentrations are very sensitive to T , and also to r.h. if the r.h. is high (Fig. 2).

Addition of ammonium sulfate to solutions containing aqueous ammonium nitrate would lower the vapor pressure product $[\text{NH}_3][\text{HNO}_3]$ in equilibrium with the aerosol phase (Fig. 2). In Fig. 2, Y is the ionic strength fraction of ammonium nitrate and is calculated as

$$Y = \frac{[\text{NH}_4\text{NO}_3]}{[\text{NH}_4\text{NO}_3] + 3[(\text{NH}_4)_2\text{SO}_4]} \quad (6)$$

Note that the concentration product of nitric acid times ammonia in equilibrium with a mixed sulfate/nitrate solution having a value of $Y = 0.5$ is about half as high as that in equilibrium with a pure ammonium nitrate solution. The temperature dependence of the partial pressure product for the aqueous mixed salt case should be similar to that of the pure salt. In the case of a dry internally mixed ammonium nitrate and sulfate solid solution, the vapor pressure product is given as

$$[\text{NH}_3][\text{HNO}_3] = zK, \quad (7)$$

where z is the mole fraction NH_4NO_3 in the aerosol phase and K is the dissociation constant for ammonium nitrate (Saxena *et al.*, 1983). If the dry mixed salt is viewed as a combination of the stable NH_4^+ , NO_3^- , SO_4^{2-} salts, such as NH_4NO_3 and $3(\text{NH}_4\text{NO}_3)(\text{NH}_4)_2\text{SO}_4$, then the concentration

product $[\text{NH}_3][\text{HNO}_3]$ at equilibrium with the solid phase could be as high as K calculated for pure NH_4NO_3 (Stelson and Seinfeld, 1982c).

UNCERTAINTY ANALYSIS

Uncertainties arise in this analysis from a number of sources and are important when comparing the theoretically computed pollutant concentrations to the field experimental results. For those cases where the gas phase is assumed to be in equilibrium with pure ammonium nitrate, a formal error analysis was conducted.

An estimate was provided for the standard error of each of the measured parameters required in the calculation: NH_3 , NH_4^+ , HNO_3 , NO_3^- , T and r.h. Uncertainties associated with the Gibbs free energies involved in calculations by the method of Stelson and Seinfeld (1982a) were taken from Parker *et al.* (1976).

The global sensitivity of the calculation scheme to uncertainties in the input variables is very non-linear, and analytical methods for calculating the standard error associated with the model outputs are difficult to execute. Instead, a stochastic simulation approach was used to propagate the error estimates for the measured quantities and Gibbs free energies through the equilibrium calculations. For each time interval at all air sampling sites, the modified Box-Mueller method (Jansson, 1966) was used to generate 200 random, normally distributed, perturbed values for the model input parameters, each set having a mean equal to the nominally measured parameter value and a standard deviation associated with the uncertainty in that value. Then 200 alternative values for K were calculated and 200 estimates of the partition of TN and TA between the gaseous and aerosol phase were generated using the perturbed data sets. In the figures that follow, error bounds shown represent one standard error about the nominally measured or computed value based on the error propagation study just described. In most cases, uncertainty in the ambient temperatures is the principal contributor to uncertainty in the computed value of the equilibrium dissociation constant, K .

Additional potential contributors to uncertainty in this analysis can be noted, but were not quantified. No attempt was made to include the contribution from uncertainties in thermodynamic properties other than the Gibbs free energies. The additional uncertainty due to the other thermodynamic properties involved in the calculations, such as the molal heat content, osmotic coefficient, ionic activity and specific heats, should be small. The equilibrium between nitric acid, ammonia, water vapor and the aerosol is assumed to prevail at a single instant in time, but calculations were actually based on concentrations and temperatures averaged over 2-h and 4-h intervals. It can be shown that if the ambient nitric acid and ammonia concentrations are positively correlated, then the product of the averaged concentrations is less than the averaged concentration

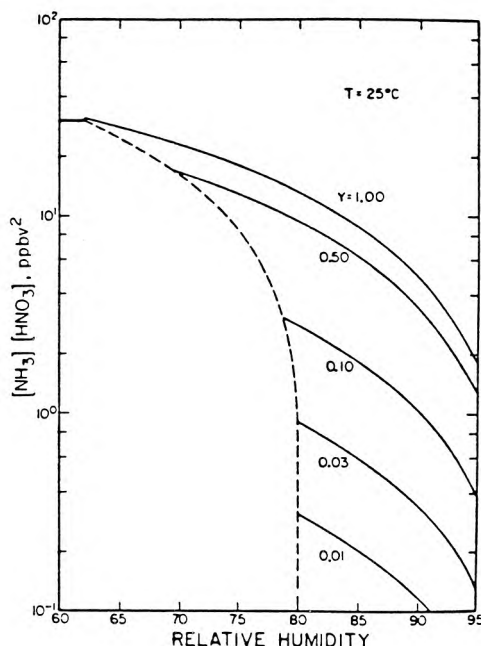


Fig. 2. Partial pressure product of ammonia and nitric acid in equilibrium with a sulfate, nitrate and ammonium containing aerosol as a function of relative humidity and ammonium nitrate ionic strength fraction at 25°C (from Stelson and Seinfeld, 1982c).

product,

$$\overline{P_{\text{HNO}_3}} \overline{P_{\text{NH}_3}} < \overline{P_{\text{HNO}_3 P_{\text{NH}_3}}} \quad (8)$$

for any finite time period. Since the extent of this bias is unknown, it was not included in the error analysis. The duration of the sampling interval may also affect the extent of artifact nitrate formation (Appel *et al.*, 1980; Spicer and Schumacher, 1979). It will be seen in the figures that follow that generally better agreement is obtained between theory and experiment when the shorter-term (2-h) samples are used rather than the longer-term (4-h) samples.

CASES EXAMINED

Models for ionic aerosol formation in equilibrium with gas phase precursors have been developed only for a limited range of aerosol chemical compositions. The most advanced treatments at present are for concentrated mixed salt solutions containing different combinations of nitrate, sulfate, ammonium, hydrogen and magnesium ions (Saxena *et al.*, 1983; Tang, 1980; Bassett and Seinfeld, 1983). The actual aerosol is much more complex than is assumed by current theoretical models. Results from the present experiment show that the ionic portion of the bulk aerosol contains all of the above, plus sodium, potassium, calcium and chloride ions (see Figs 4 and 5 of Russell and Cass, 1984). From the experimental data, it is impossible to tell how the individual aerosol particles are speciated. In other words, it is not known what fraction of the nitrate or ammonium, if any, is present as ammonium nitrate, and whether the ammonium nitrate is associated with ammonium sulfate (for example) within individual aerosol particles. As a result, three hypothetical distributions of aerosol constituents between particles will be discussed which span the likely range of aerosol composition: a purely external mixture, a purely internal mixture, and a size-segregated internal mixture.

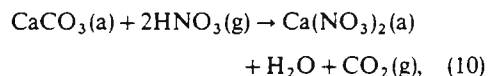
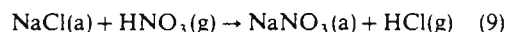
In an external mixture, each particle is composed of a single salt (possibly aqueous) such as pure NH_4NO_3 , $(\text{NH}_4)_2\text{SO}_4$ or NaCl , and the bulk aerosol composition (as seen in Figs 4 and 5 of Russell and Cass, 1984) is achieved by dispersing a variety of particles with different chemical compositions in the same air mass. At the other extreme, an internal mixture is achieved if each particle has the same chemical composition as the bulk aerosol, and hence consists of a complex mixture of many different anions and cations.

An interesting and intermediate case is that of a size-segregated internal mixture. In this case, the aerosol will be assumed to exist in two size classes, coarse (particle diameter, d_p , $> 2.5 \mu\text{m}$) and fine ($d_p \leq 2.5 \mu\text{m}$). Coarse aerosols usually are generated mechanically. Sea spray and soil dust aerosols would be prime examples. Gas-particle reactions may take place on the surface of coarse particles, altering the original composition of the aerosol, but the particle

size would not decrease significantly. Ionic species concentrated in the large particle fraction would include chiefly, Ca^{2+} , Mg^{2+} , K^+ , Na^+ and Cl^- , plus enough large particle NO_3^- to achieve a charge balance (obtained by reaction of nitric acid with sea salt or soil dust). The fine particle fraction will be assumed to have been formed by gas to particle conversion processes, and would contain all of the ammonium, all of the sulfate and that portion of the nitrate not attributed to the coarse particle mode. This framework for the size-segregated internal mixture hypothesis is consistent with observations that sulfate and ammonium are found chiefly in the small particle size ranges; Na^+ , Ca^{2+} and Cl^- are found in large particles, while NO_3^- is found in significant amounts in both the coarse and fine fractions (Appel *et al.*, 1978; Kadowaki, 1977).

EXTERNAL MIXTURE

In the case of an external mixture, pure salt particles, such as NH_4NO_3 , NaCl , or $(\text{NH}_4)_2\text{SO}_4$, are assumed to be present, and the gas phase concentrations of NH_3 and HNO_3 are governed by equilibrium with NH_4NO_3 . The key remaining question centers on the possibility that other nitrate containing aerosol species less volatile than NH_4NO_3 are present in separate particles (e.g. NaNO_3), and hence some of the aerosol nitrate is not available to interact with the precursor gases. Field experimental measurements do not give an absolute answer to this question, but two extreme possible cases can be studied. In the first case, all of the ammonia, nitric acid, and aerosol ammonium and nitrate are assumed to be available to form NH_4NO_3 . This provides an upper limit on the amount of pure NH_4NO_3 that can be formed. A second case provides the lower limit on the predicted pure ammonium nitrate concentration by assuming that the NO_3^- ion is bound preferentially as a relatively non-volatile salt of Ca^{2+} , Mg^{2+} , K^+ or Na^+ . A number of displacement reactions would bind nitrate in this manner, such as



where (a) indicates the aerosol phase. NaNO_3 has been identified in field measurements in the Los Angeles area (Mamane and Pueschel, 1980). In this study the term FREE NITRATE will be used to identify the fraction of the aerosol nitrate in excess of that which could be bound with the alkali metals or alkaline earths, given mathematically for this experiment as

$$[\text{FREE NITRATE}] = [\text{NO}_3^-] - \{2[\text{Ca}^{2+}] + 2[\text{Mg}^{2+}] + [\text{K}^+] + [\text{Na}^+] - [\text{Cl}^-]\} \quad (11)$$

where the brackets [] indicate the measured ionic aerosol concentration in $\mu\text{moles m}^{-3}$. The FREE NITRATE concentration was constrained to be

greater than or equal to zero. In constructing (11) it was assumed that the chloride ion present is found as sodium chloride. The HCl produced by reaction (9) might, in some cases, react with NH_3 to form NH_4Cl , and thus alternative forms of (11) could be hypothesized.

The choice between the two types of external mixtures just described has no effect on the calculated equilibrium dissociation constant of ammonium nitrate, as K is solely a function of T and r.h., but it does affect the calculated gas and aerosol phase pollutant concentrations. If pure ammonium nitrate is present and is at equilibrium with the gas phase, then the equilibrium dissociation constant should be equal to the observed partial pressure product of NH_3 times HNO_3 to within experimental and calculation uncertainties. If the FREE NITRATE concentration is zero, then ammonium nitrate may not be present, and the calculated dissociation constant has no bearing on the partial pressure of ammonia and nitric acid gas, except that it should act as an upper bound on the measured concentration product, CP .

Given the external mixture hypotheses, the theoretically predicted partition of measured total nitrate and total ammonia between the aerosol and gas phases was computed at each monitoring site shown in Fig. 1 over each sampling interval during the period 30–31 August 1982. Results at three locations in the basin will be discussed in detail: a near coastal site, Long Beach, a mid-basin site, Anaheim, and a far inland site, Rubidoux. Data on aerosol speciation at these sites are

presented elsewhere (Russell and Cass, 1984). The Long Beach sampling station, which is located about 6 km from the Pacific Ocean, experienced lower temperatures (down to 18°C) and higher relative humidities (1-h average above 90%) than the inland sites. This led to a minimum 2-h average calculated NH_4NO_3 dissociation constant of less than $0.75 (\text{ppbv})^2$. Rubidoux, located about 60 km inland, was typically hotter and dryer, with peak temperatures above 38°C , and a correspondingly high calculated dissociation constant that exceeded $650 (\text{ppbv})^2$ over one 2-h sampling interval. Comparison between theory and experiment thus will be discussed for dissociation constants varying over about three orders of magnitude.

The calculated NH_4NO_3 dissociation constant, K , and the product of the measured $\text{HNO}_3(\text{g})$ and $\text{NH}_3(\text{g})$ concentrations at Anaheim are shown in Fig. 3. One standard error about each calculated value of K is given by the vertical bars, while the standard error of the measured concentration product is indicated by the dashed horizontal lines. Agreement between the theoretical calculations and measurements generally is good, especially for the second day when shorter sampling intervals were used. Recall that the calculated dissociation constant should serve as an upper bound on the concentration product, CP .

In the first of the two external mixture cases considered, all of the aerosol nitrate is assumed to be present as ammonium nitrate. Given the time history of the computed dissociation constant, the measured

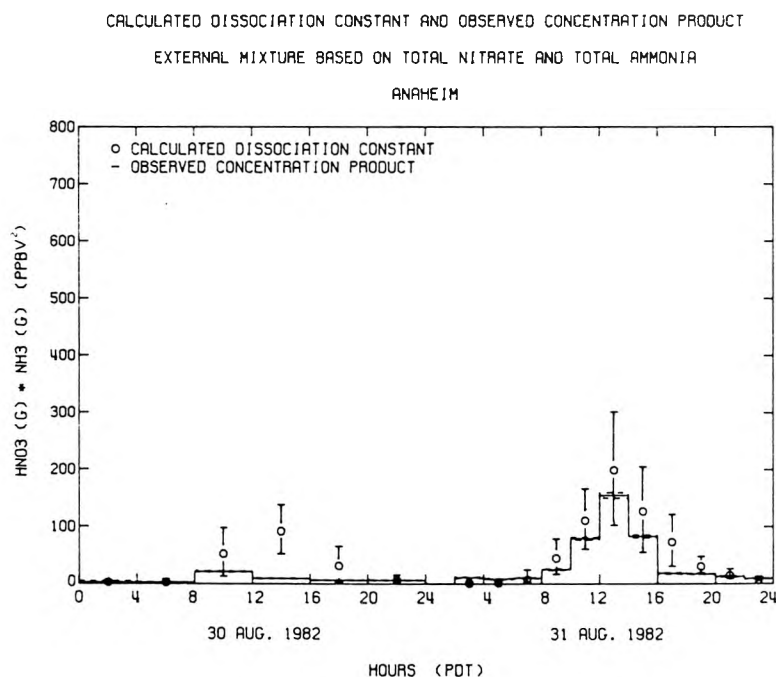


Fig. 3. Observed $[\text{HNO}_3][\text{NH}_3]$ concentration product and calculated dissociation constant of pure NH_4NO_3 at Anaheim, CA. No data between 0000 and 0200 on 31 August.

total inorganic nitrate and total ammonia concentrations at Anaheim were apportioned between the gaseous and the aerosol phase in accordance with the equilibrium calculations. As seen in Figs 4(a) and (b), the measured gas phase concentrations are somewhat below those predicted, but still are in good agreement given the results of the uncertainty analysis. The calculated and measured aerosol concentrations likewise are in good agreement at Anaheim [Figs 4(c) and (d)]. Note that at a number of times (e.g. between 0800 and 1200 hours on 30 August) no ammonium nitrate was predicted to be present. In this case there was not enough total ammonia and total nitrate to support the formation of pure ammonium nitrate at the prevailing ambient conditions.

Moving further inland to Rubidoux, the agreement between the calculated K and measured CP still is good, with the measured CP , again, usually at or below the theoretical value for K during the midday (Fig. 5). At night the measured concentration product often lies slightly above K , but there is very little nitric acid vapor present and thus the nitric acid measurement is prone

to larger than usual relative error. Rubidoux is downwind of a large collection of dairy farms, and experiences very high ammonia and ammonium ion concentrations [as seen in Figs 6(b) and (d)]. Agreement between measured and predicted NH_3 concentrations is quite good at all times. The remaining predicted pollutant concentrations match observations at most times, with the largest exceptions occurring between 1000 and 1200 hours and between 1400 and 1600 hours on 31 August (see Fig. 6).

At the near-coastal sites, like Long Beach and Lennox, the agreement between calculated dissociation constants and measured concentration products is very poor during the daytime (Fig. 7). The measured product of the concentrations of nitric acid vapor and ammonia falls significantly below that expected if the gas phase material were in equilibrium with pure NH_4NO_3 . In Fig. 8, it can be seen that the lower than expected concentration product measured in the atmosphere is due mainly to lower nitric acid concentrations than would be expected if aerosol ammonium and nitrate ion concentrations were governed solely by the

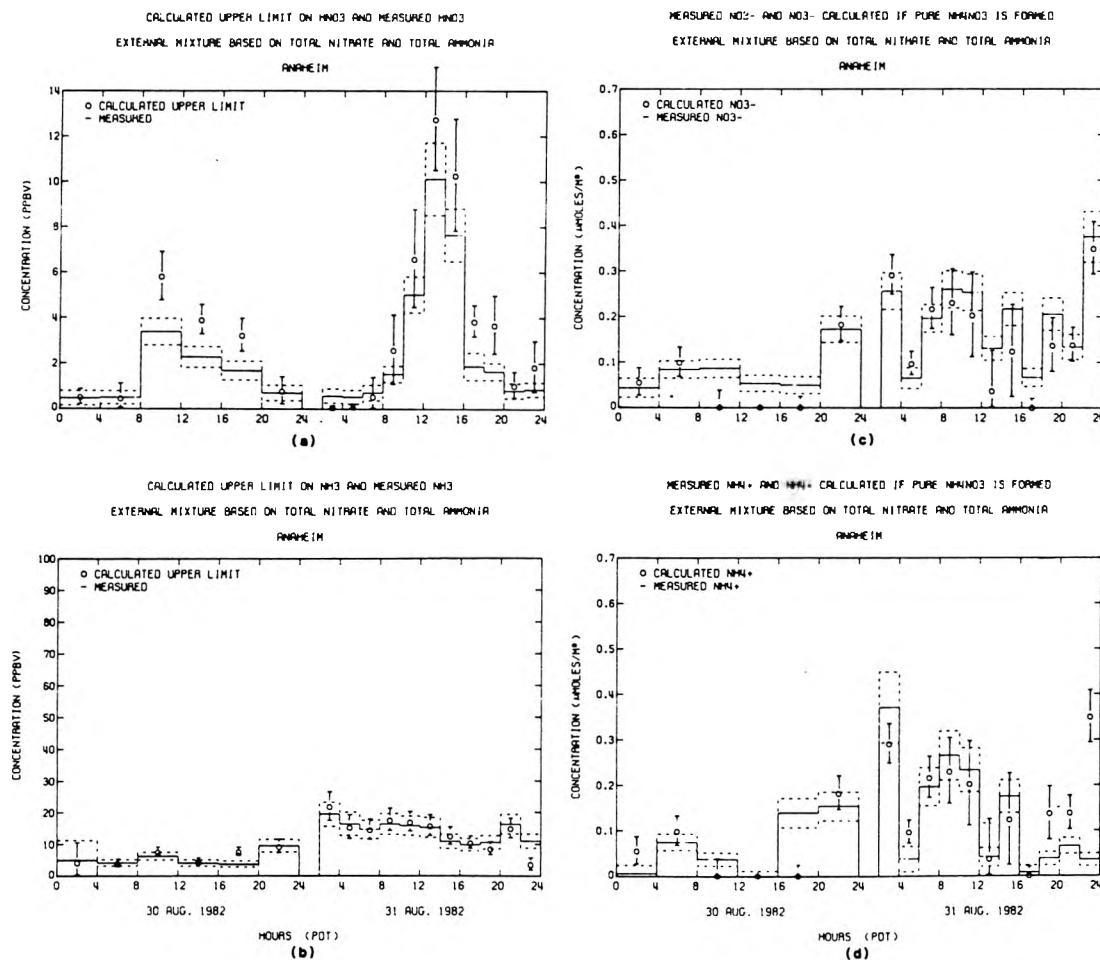


Fig. 4. Observed and calculated pollutant concentrations at Anaheim—external mixture with all aerosol nitrate available to form NH_4NO_3 . No data between 0000 and 0200 on 31 August. (a) HNO_3 , (b) NH_3 , (c) NO_3^- , (d) NH_4^+ .

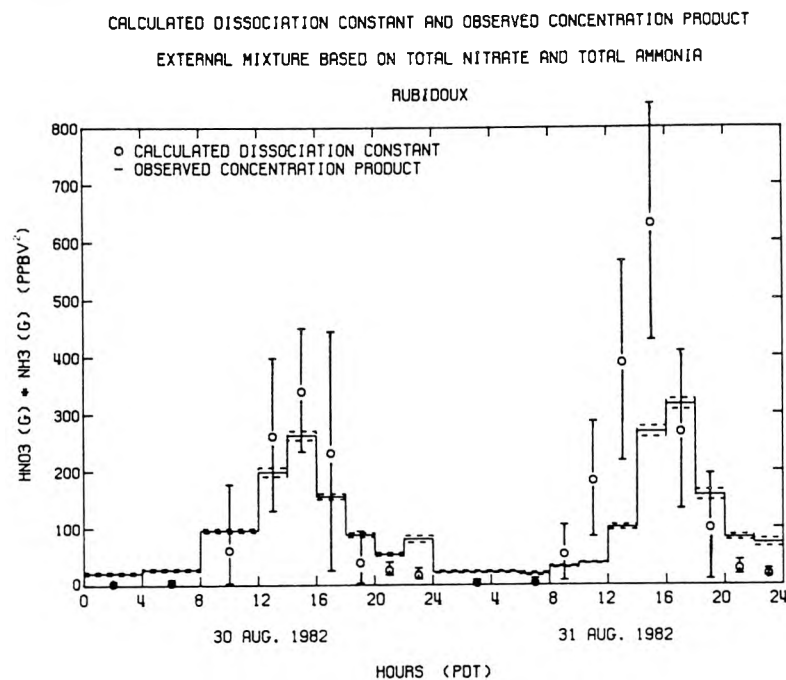


Fig. 5. Observed $[\text{HNO}_3][\text{NH}_3]$ concentration product and calculated dissociation constant of pure NH_4NO_3 at Rubidoux, CA.

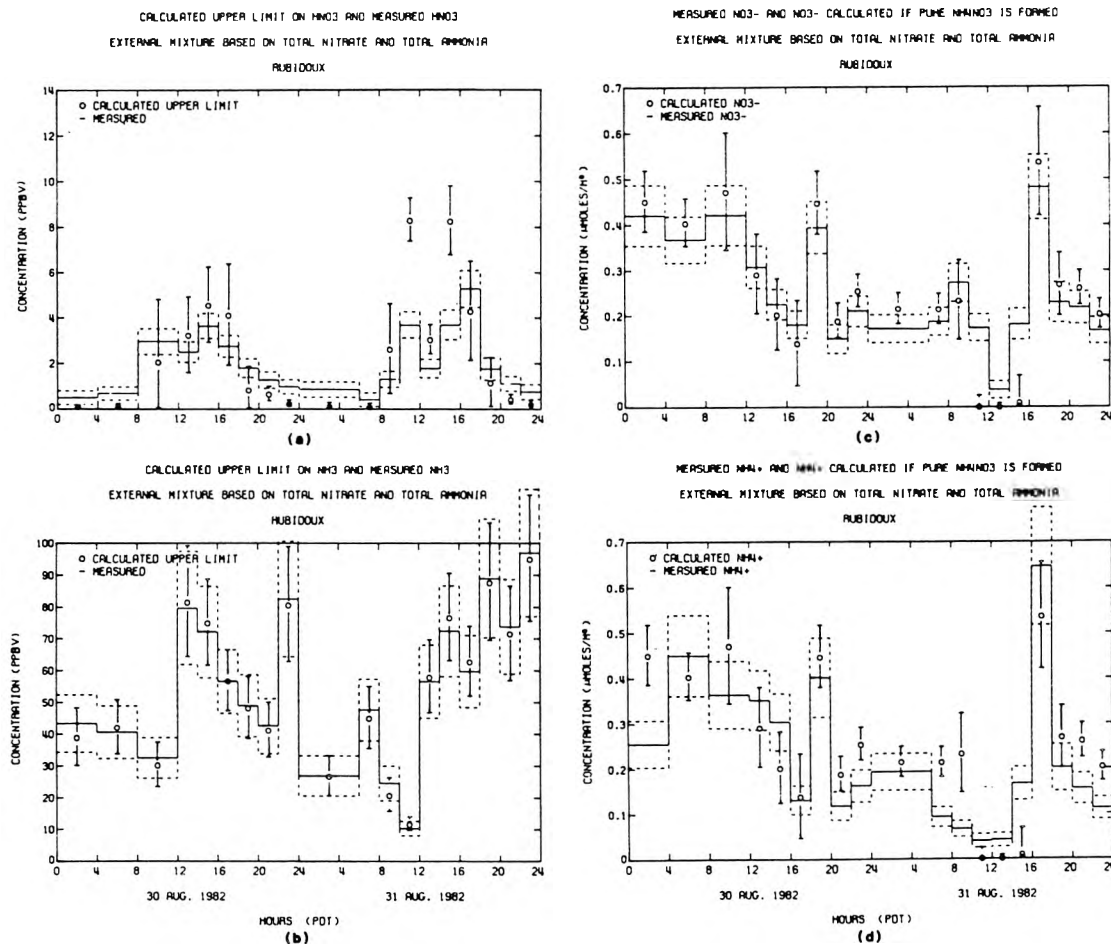


Fig. 6. Observed and calculated pollutant concentrations at Rubidoux—external mixture with all aerosol nitrate available to form NH_4NO_3 . (a) HNO_3 , (b) NH_3 , (c) NO_3^- , (d) NH_4^+ .

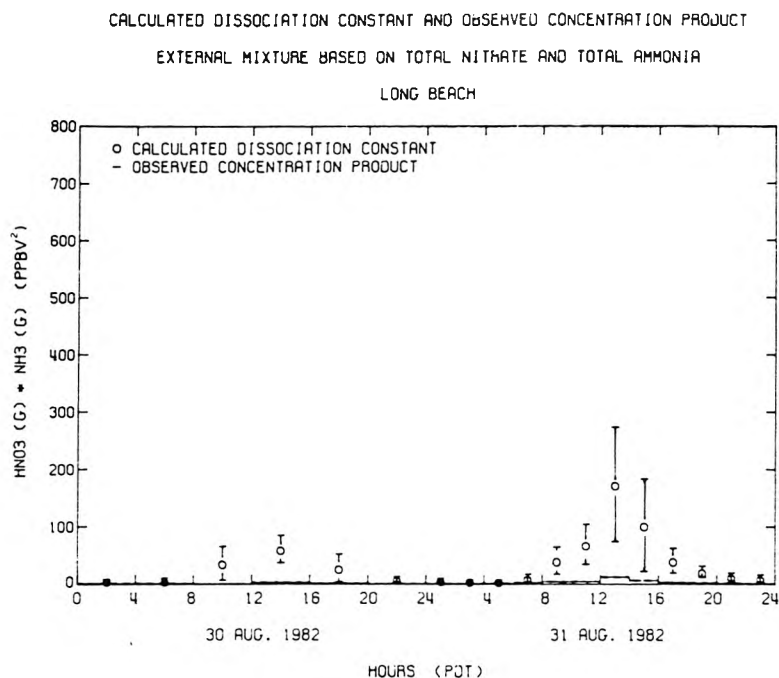


Fig. 7. Observed $[\text{HNO}_3][\text{NH}_3]$ concentration product and calculated dissociation constant of pure NH_4NO_3 at Long Beach, CA.

equilibrium between HNO_3 , NH_3 and NH_4NO_3 . At a number of times in the afternoon of both days sampled, the total nitrate and total ammonia concentrations fall below the level needed to form any ammonium nitrate aerosol, as seen in Figs 8(c) and (d). Nevertheless, measurable nitrate and ammonium ion concentrations were observed in the aerosol phase during both afternoons (Fig. 8). The likely explanation is that pure ammonium nitrate is not present, but that other nitrate and ammonium containing species are formed. In this case, the second external mixture hypothesis will be examined to determine whether part (if not all) of the nitrate could be bound as a relatively non-volatile salt.

The amount of nitrate ion present at each monitoring site in excess of that that could be bound with Na^+ , Ca^{2+} , Mg^{2+} and K^+ was determined. This excess NO_3^- ion, called FREE NITRATE, is defined in (11). The HNO_3 , NH_3 , NH_4NO_3 equilibrium calculations then were repeated assuming that only the FREE NITRATE plus an equal amount of ammonium ion was available to equilibrate with the gas phase. Results obtained under this hypothesis at Long Beach are shown in Fig. 9. In 15 of the 18 sampling periods, no NH_4NO_3 formation would be predicted and indeed no FREE NITRATE was present. At a sixteenth sampling interval NH_4NO_3 is predicted to be present, and the predicted NO_3^- level matches the observed FREE NITRATE almost exactly. Two of the 18 observations still show that FREE NITRATE was present at times when the $[\text{NH}_3][\text{HNO}_3]$ concentration product was too low to form pure NH_4NO_3 .

Results at the remaining monitoring sites are similar to those at Long Beach. The great majority of the occasions where nitrate aerosol is observed at NH_3 and HNO_3 concentrations too low to form pure NH_4NO_3 occur when the aerosol composition is consistent with the presence of nitrate species other than ammonium nitrate. This is illustrated in Fig. 10. Figures 10(a) and (b) show the NH_3 and HNO_3 concentrations predicted at all stations under the first external mixture hypothesis (that all aerosol nitrate is speciated as NH_4NO_3). A large number of the theoretically calculated HNO_3 concentrations exceed the field observations in that case, indicating that more inorganic nitrate should have been found in the gas phase. When the second external mixture hypothesis is imposed (e.g. some nitrate speciated as NaNO_3 , $\text{Ca}(\text{NO}_3)_2$ and other non-volatile salts) then the number of outlying data points is reduced to about 10% of the 180 total observations, as shown in Fig. 10(d). Agreement between observed and predicted NH_3 gaseous concentrations is fairly good at all times under both external mixture hypotheses, as seen in Figs 10(a) and (c). This is because gaseous NH_3 is present in such excess that transfer of NH_4^+ ion from the aerosol into the gas phase will not change gaseous NH_3 levels greatly.

INTERNAL MIXTURE

The aerosol observed at each sampling site could be idealized as a pure internal mixture. In this case each aerosol particle would contain a variety of anions and

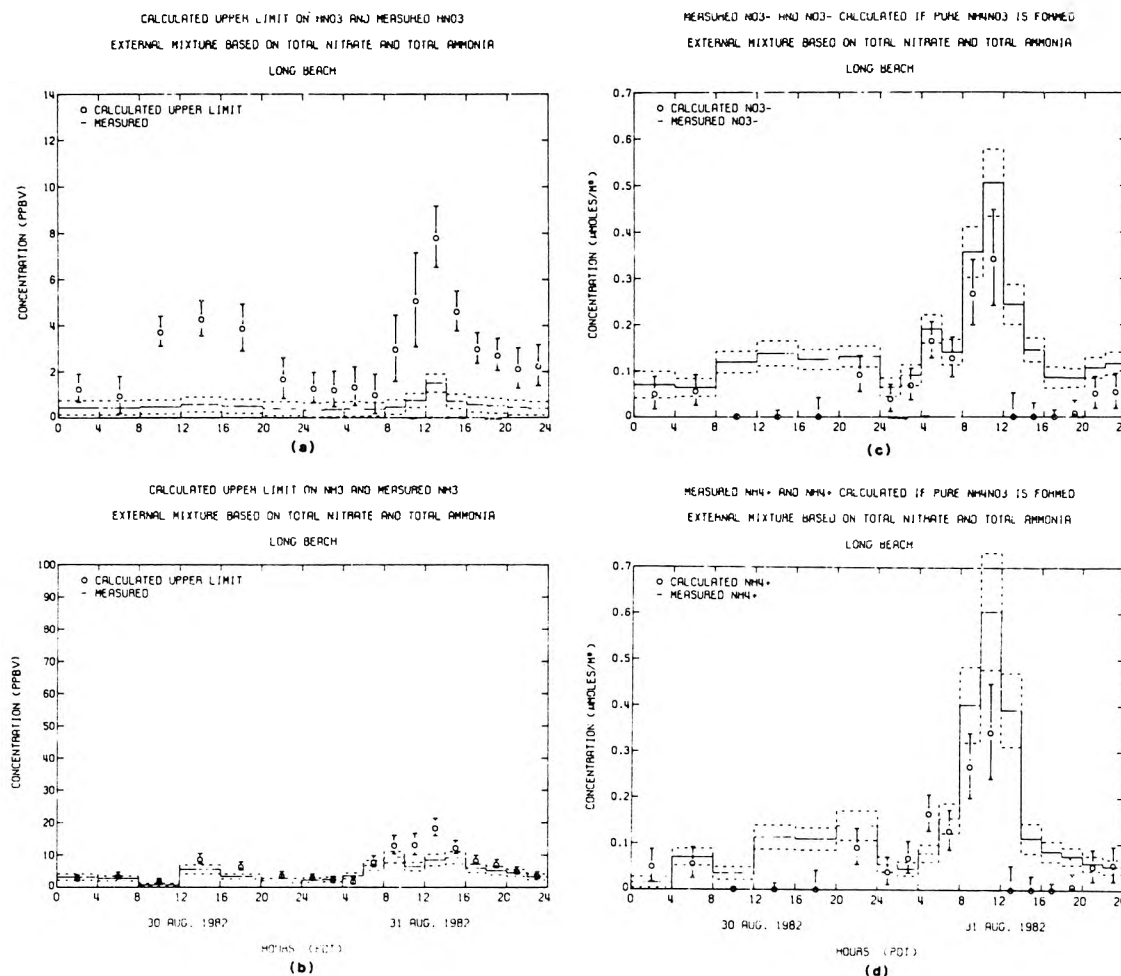


Fig. 8. Observed and calculated pollutant concentrations at Long Beach—external mixture with all aerosol nitrate available to form NH_4NO_3 . (a) HNO_3 , (b) NH_3 , (c) NO_3^- , (d) NH_4^+ .

cations in direct proportion to their ionic abundance in the bulk filter sample. For the conditions observed during this experiment, such an internally mixed aerosol would be much more complex than the mixed sulfate, nitrate and ammonium containing aerosols that can be handled by present theoretical models that describe the equilibrium between aerosol and gas phase constituents. If a complete set of thermodynamic data for the species possible in a highly concentrated mixed NH_4^+ , Na^+ , Ca^{2+} , Mg^{2+} , K^+ , NO_3^- , SO_4^{2-} , Cl^- system existed, which it does not, then a general purpose Gibbs free energy minimization technique could provide predictions. Such a technique has been used successfully for the sulfate/nitrate/ammonium system (Bassett and Seinfeld, 1983). Data from the present study can be used to test the predictions of such a complete model once the thermodynamic data for the full system become available. Lacking the thermodynamic data at present, no attempt will be made to model a purely internal mixture at this time.

SIZE-SEGREGATED INTERNAL MIXTURE

Chemically resolved size distribution measurements show that most of the atmospheric aerosol sulfate and ammonium, and much of the nitrate, is found in a fine particle accumulation mode ($d_p \leq 2.5 \mu\text{m}$), reflecting that they are formed by a gas to particle conversion process. Sea salt, soil dust and other mechanically generated aerosols typically are found in a coarse particle mode ($d_p > 2.5 \mu\text{m}$). Any nitrate aerosol formed by reaction of nitric acid with sea salt or soil dust likewise would be concentrated in the coarse particle mode. To capture these characteristics of the atmospheric aerosol, a size-segregated internal mixture hypothesis was tested. The aerosol was assumed to exist in two size fractions for computational purposes. The large particle fraction was taken to be composed of the sea salt and soil dust derived material (all Na^+ , Ca^{2+} , Mg^{2+} , K^+ , Cl^- and enough NO_3^- to achieve a charge balance) and the fine particle fraction was

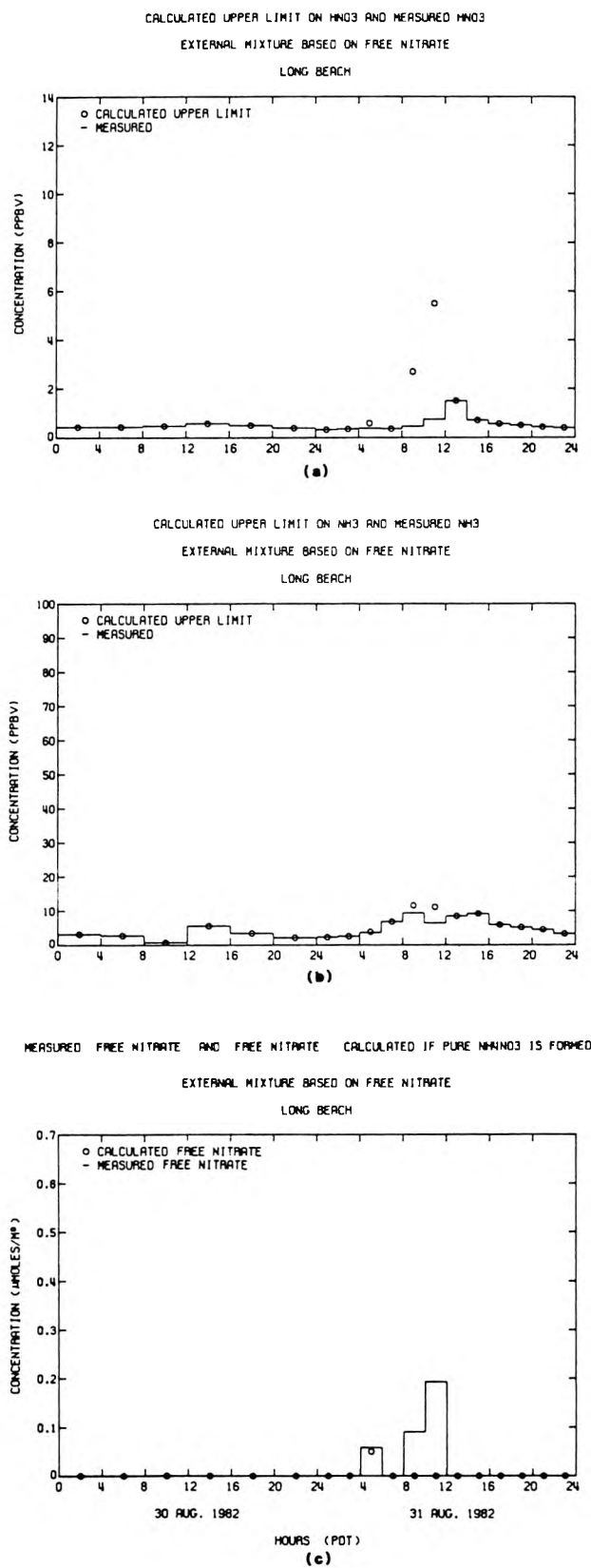


Fig. 9. Observed and calculated pollutant concentrations at Long Beach—external mixture with only the FREE NITRATE available to form NH_4NO_3 . (a) HNO_3 , (b) NH_3 , (c) FREE NITRATE.

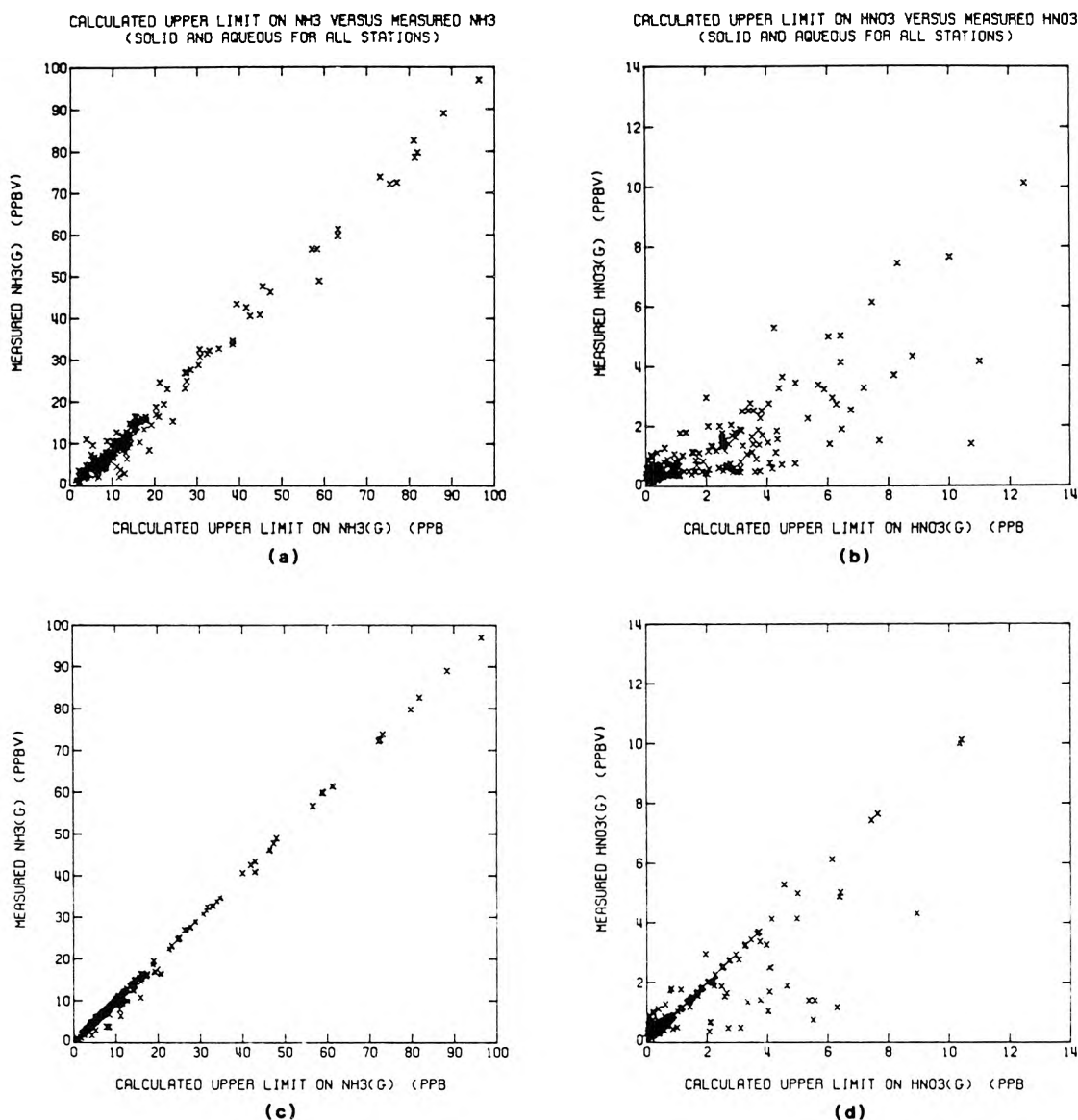


Fig. 10. Comparison of observed and calculated gas phase concentrations at all monitoring stations under two alternative external mixture hypotheses (180 observations). Case (1), all aerosol nitrate available to form NH_4NO_3 . Case (2), only the FREE NITRATE available to form NH_4NO_3 . (a) Ammonia (Case 1), (b) Nitric Acid (Case 1), (c) Ammonia (Case 2), (d) Nitric Acid (Case 2).

assumed to contain the sulfate, ammonium and FREE NITRATE in the form of an internally mixed aerosol. Again, the resulting aerosol may be aqueous or solid, for which the calculation methods of Stelson and Seinfeld (1982a, c) and Saxena *et al.* (1983) will be used, as described previously. Both Fig. 2 and Equation (7) indicate that addition of ammonium sulfate to the internal mixture lowers the resulting vapor pressures in equilibrium with the aerosol phase below the levels observed when pure NH_4NO_3 is present. Thus the size segregated internal mixture hypothesis acts in the direction needed to account for the few cases in Fig. 10(d) where HNO_3 concentrations are found to be

lower than would be expected in equilibrium with NH_4NO_3 alone.

A difficulty arises when considering the size-segregated internal mixture case if no FREE NITRATE is present. If no ammonium nitrate is mixed with the sulfate, the predicted CP goes to zero. At any time when this occurs in the presence of a significant concentration product of ammonia and nitric acid, it will be assumed that the size-segregated internal mixture idealization for the distribution of nitrates between fine and coarse particles is inappropriate. There must have been some nitrate aerosol not bound in a non-volatile form even though ion balance considerations

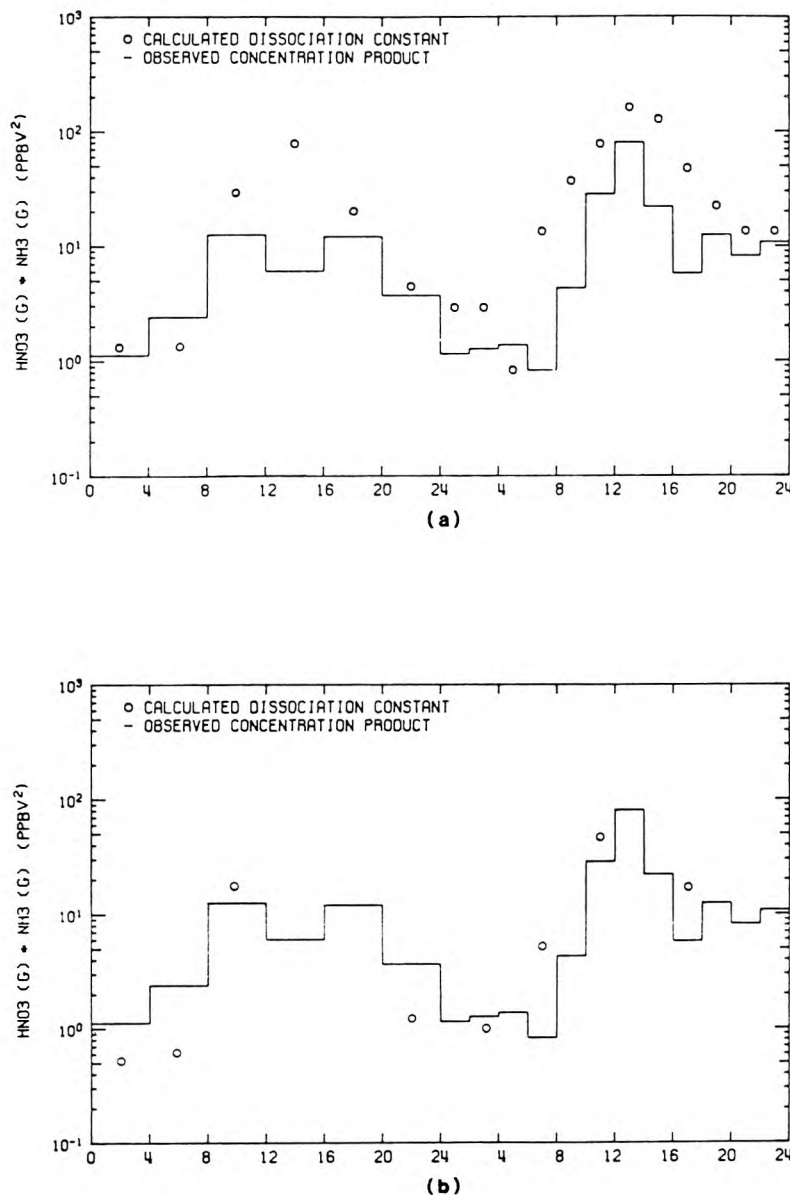


Fig. 11. Observed and calculated $[\text{HNO}_3][\text{NH}_3]$ concentration product at Upland—comparison of external mixture and size-segregated internal mixture hypotheses. (a) External mixture, (b) Size-segregated internal mixture.

show that all nitrates might have been speciated as non-volatile coarse particle material. No theoretical calculations will be attempted in those cases where the underlying assumption about particle composition is untenable.

The concentration product of HNO_3 and NH_3 calculated for the size-segregated internal mixture case is compared to ambient measurements at Upland in Fig. 11 and Long Beach in Table 1. Concentration products that would be predicted for the case of equilibrium with pure NH_4NO_3 also are shown. At Upland, the aerosol is predicted to be aqueous from 0000 to 0800 and from 2000 to 2400 on 30 August and

between 0000 and 0800 on 31 August. The remainder of the time, the aerosol was predicted to be in the solid phase. Results shown in Fig. 11(b), when the aerosol is solid, are those obtained by the method of Saxena *et al.* (1983). Alternatively, if the solid mixed salt consists of a heterogeneous mix of solid phases, such as NH_4NO_3 and $3\text{NH}_4\text{NO}_3 \cdot (\text{NH}_4)_2\text{SO}_4$, then the CP could be as high as for NH_4NO_3 shown in Fig. 11(a). At Upland the observed and computed concentration products shown in Fig. 11(b) are in better agreement with the size segregated internal mixture case than with the pure external mixture hypothesis in five of the cases, particularly those cases with the higher concentration products.

Table 1. Comparison of measurements at Long Beach to predictions given by the pure external mixture hypothesis based on FREE NITRATE (Case 1) and by the size-segregated internal mixture hypothesis (Case 2)

Time*	Phase†	CP (ppbv ²)			HNO ₃ (ppbv)			NH ₃ (ppbv)			FREE NITRATE (μg m ⁻³)		
		Case 1†	Case 2	Meas.	Case 1	Case 2	Meas.	Case 1	Case 2	Meas.	Case 1	Case 2	Meas.

4-6 aqueous(aq) 2.6 1.4 1.2 0.6 0.3 0.3 4.3 4.1 4.0 2.6 3.4 3.5
 8-10 solid(s) 39.0 9.6 4.5 2.7 1.0 0.5 11.7 9.9 9.5 0.0 4.4 5.9
 10-12 solid(s) 69.0 16.0 4.9 5.4 2.1 0.8 11.1 7.7 6.4 0.0 8.4 12.0

* At all other times Case 1, Case 2 and measurements match exactly because no FREE NITRATE is present. All times shown are on 31 August 1983.
 † When solid, Case 2 is computed by the method of Saxena *et al.* (1983). For solid particles containing a mixture of solid phases, such as NH₄NO₃ and 3NH₄NO₃·(NH₄)₂SO₄, CP could be as high as for pure NH₄NO₃ in the Case 1 column.
 ‡ Values shown are for equilibrium dissociation constant, K, for NH₄NO₃. This can exceed concentration product of [NH₃][HNO₃] if no FREE NITRATE is predicted to be present.

In the three cases where improvement is not noted, the absolute value of the discrepancy is only 1 or 2 (ppbv)². At Long Beach, the size-segregated internal mixture hypothesis brings the aqueous phase observation into almost complete agreement between computed and observed concentration products.

CONCLUSIONS

In theory, the equilibrium dissociation constant for NH₄NO₃ should place an upper limit on the product of the NH₃ and HNO₃ concentrations in the atmosphere. In most cases the [NH₃][HNO₃] concentration product measured during this experiment indeed is found to be less than or equal to the calculated dissociation constant of pure NH₄NO₃ at the prevailing conditions. At inland sites like Anaheim and Rubidoux, the assumption that NH₃ and HNO₃ are in equilibrium with pure NH₄NO₃ yields agreement between predicted and measured gas and aerosol phase pollutant concentrations that is qualitatively and, in most cases, quantitatively quite good. At other sites, particularly near the coast, the measured CP and HNO₃ concentrations fall well below those predicted if pure ammonium nitrate is present. A majority of those measurements can be explained by the hypothesis that some nitrate is bound in large particles by the reaction of nitric acid with sea salt or soil dust. If the aerosol is assumed to exist as a size-segregated internal mixture with nitrates distributed on the basis of ion balance considerations between non-volatile coarse particle material and fine particles containing NH₄⁺, SO₄²⁻ and NO₃⁻, then further improvement is obtained between observed and predicted [NH₃][HNO₃] concentration products.

The results of this study hold important implications for the construction and use of mathematical models for the formation and transport of nitrate-containing aerosols. First, in the vast majority of cases, measured pollutant concentrations are consistent with computations based on equilibrium between the gas phase and aerosol phase species, to within our present ability to supply the necessary data for the calculations. Given a model like that of Russell *et al.* (1983) which can compute HNO₃ and NH₃ concentrations from emissions plus gas phase kinetics, in principle it is possible to predict the amount of aerosol nitrate formed. The simplest treatment, that of pure NH₄NO₃ formation, will work well at some monitoring sites, but it is not universally applicable. A knowledge of the speciation of the co-existing non-nitrate ionic material in the aerosol phase is needed if accurate aerosol nitrate concentration predictions are to be made. A formidable problem is faced if that co-existing aerosol concentration and composition also must be computed from emissions data.

Acknowledgements—This work was supported by the California Air Resources Board under Agreement No. A2-

150-32, and by gifts to the Environmental Quality Laboratory.

REFERENCES

- Appel B. R., Kothny E. L., Hoffer E. M., Hidy G. M. and Wesolowski J. J. (1978) Sulfate and nitrate data from the California Aerosol Characterization Experiment (ACHEX). *Envir. Sci. Technol.* **12**, 418-425.
- Appel B. R., Wall S. M., Tokiwa Y. and Haik M. (1980). Simultaneous nitric acid, particulate nitrate and acidity measurements in ambient air. *Atmospheric Environment* **14**, 549-554.
- Bassett M. and Seinfeld J. H. (1983) Atmospheric equilibrium model of sulfate and nitrate aerosols. *Atmospheric Environment* **17**, 2237-2252.
- Cadle S. H., Countess R. J. and Kelly N. A. (1982) Nitric acid and ammonia concentrations in urban and rural locations. *Atmospheric Environment* **16**, 2501-2506.
- Doyle G. J., Tuazon E. C., Graham R. A., Mischke T. M., Winer A. M. and Pitts J. N., Jr. (1979) Simultaneous concentrations of ammonia and nitric acid in a polluted atmosphere and their equilibrium relationship to particulate ammonium nitrate. *Envir. Sci. Technol.* **13**, 1416-1419.
- Harrison R. M. and Pio C. A. (1983) An investigation of the atmospheric HNO_3 - NH_3 - NH_4NO_3 equilibrium relationship in a cool, humid climate. *Tellus* **35B**, 155-159.
- Harwood J. E. and Kuhn A. L. (1970) A colorimetric method for ammonia in natural waters. *Water Res.* **4**, 805-811.
- Jansson B. (1966) *Random Number Generator*, p. 177. Almquist and Wiksell, Stockholm.
- Kadowaki S. (1977) Size distribution and chemical composition of atmospheric particulate in the Nagoya area. *Atmospheric Environment* **11**, 671-675.
- Mamane Y. and Pueschel R. F. (1980) A method for the detection of individual nitrate particles. *Atmospheric Environment* **14**, 629-639.
- Parker V. B., Wagman D. D. and Garvin D. (1976) Selected thermochemical data compatible with the CODATA recommendations. NBSIR 75-968.
- Russell A. G. and Cass G. R. (1984) Acquisition of regional air quality model validation data for nitrate, sulfate, ammonium ion and their precursors. *Atmospheric Environment* **18**, 1815-1827.
- Russell A. G. (1983) Analysis of oxalic acid impregnated filters for ammonia determination. Open File Report 83-1; Environmental Quality Laboratory, California Institute of Technology, Pasadena, CA.
- Russell A. G., McRae G. J. and Cass G. R. (1983) Mathematical modeling of the formation and transport of ammonium nitrate aerosol. *Atmospheric Environment* **17**, 949-964.
- Salorzano L. (1967) Determination of ammonia in natural waters by the phenol hypochlorite method. *Limnol. Oceanogr.* **14**, 799-801.
- Saxena P. and Peterson T. W. (1981) Thermodynamics of multicomponent electrolytic aerosols. *J. Colloid. Interface Sci.* **79**, 496-510.
- Saxena P., Seigneur S. and Peterson T. W. (1983) Modeling of multiphase atmospheric aerosols. *Atmospheric Environment* **17**, 1315-1329.
- Spicer C. W., Howes J. E., Bishop T. A., Arnold L. H. and Stevens R. K. (1982) Nitric acid measurement methods: an intercomparison. *Atmospheric Environment* **16**, 1407-1500.
- Spicer C. W. and Schumacher P. M. (1979) Particulate nitrate: laboratory and field studies of major sampling interferences. *Atmospheric Environment* **13**, 543-552.
- Stelson A. W. and Seinfeld J. H. (1982a) Relative humidity and temperature dependence of the ammonium nitrate dissociation constant. *Atmospheric Environment* **16**, 983-992.
- Stelson A. W. and Seinfeld J. H. (1982b) Relative humidity and pH dependence of the vapor pressure of ammonium nitrate-nitric acid solutions at 25°C. *Atmospheric Environment* **16**, 993-1000.
- Stelson A. W. and Seinfeld J. H. (1982c) Thermodynamic prediction of the water activity, NH_4NO_3 dissociation constant, density and refractive index for the NH_4NO_3 -(NH_4)₂ SO_4 - H_2O system at 25°C. *Atmospheric Environment* **16**, 2507-2514.
- Stelson A. W., Friedlander S. K. and Seinfeld J. H. (1979) A note on the equilibrium relationship between ammonia and nitric acid and particulate ammonium nitrate. *Atmospheric Environment* **13**, 369-371.
- Tang I. N. (1976) Phase transformation and growth of mixed salts. *J. Aerosol Sci.* **7**, 361-371.
- Tang I. N. (1980) On the equilibrium partial pressures of nitric acid and ammonia in the atmosphere. *Atmospheric Environment* **14**, 819-828.
- Tanner R. L. (1982) An ambient experimental study of phase equilibrium in the atmospheric system: aerosol H^+ , NH_4^+ , SO_4^{2-} , NO_3^- , $\text{NH}_3(\text{g})$, $\text{HNO}_3(\text{g})$. *Atmospheric Environment* **16**, 2935-2942.
- Yoong M. (1981) Measurement of ambient ammonia concentrations in southern California. Rockwell International, Newbury Park, California, Final Report to the California Air Resources Board under Contract No. A7-188-30. Available from NTIS.

CHAPTER 6
VERIFICATION OF A MATHEMATICAL MODEL FOR AEROSOL
NITRATE AND NITRIC ACID FORMATION, AND ITS USE
FOR CONTROL MEASURE EVALUATION

(Reprinted from *Atmospheric Environment*, 20, 2011-2025)

VERIFICATION OF A MATHEMATICAL MODEL FOR AEROSOL NITRATE AND NITRIC ACID FORMATION AND ITS USE FOR CONTROL MEASURE EVALUATION

ARMISTEAD G. RUSSELL* and GLEN R. CASS†

Environmental Quality Laboratory 138-78, California Institute of Technology, Pasadena, California 91125,
 U.S.A.

(First received 14 March 1985 and received for publication 22 January 1986)

Abstract—A mathematical model for the formation of atmospheric nitric acid and aerosol nitrate has been developed and employed to study the effect of emission controls. Based on a Lagrangian formulation of the atmospheric diffusion equation, the model computes nitric acid concentrations from a description of daytime photochemical reactions and night-time reactions involving NO_3 and N_2O_5 . Ammonium nitrate formation is computed at a thermodynamic equilibrium between HNO_3 and NH_3 , and heterogeneous reactions between HNO_3 and preexisting aerosol are considered. The accuracy of the air quality model's predictions is verified by comparison to O_3 , NO_2 , HNO_3 , NH_3 , aerosol nitrate and PAN measurements made for this purpose in California's South Coast Air Basin during the period of 30–31 August 1982.

Examination of emission control alternatives shows that reduction in NO_x emissions yields a nearly proportional decrease in total inorganic nitrate levels (HNO_3 + aerosol nitrates). Reduction in NH_3 emissions suppresses aerosol nitrate formation, resulting in higher HNO_3 levels. Control of organic species emissions by the amounts expected in Los Angeles in future years causes a partial shift away from PAN formation toward greater production of HNO_3 . Emission control strategies can be formulated that include a combination of controls on NO_x , organic gases and NH_3 emissions that will achieve a greater reduction in HNO_3 , aerosol nitrate and O_3 levels than a strategy predicated on control of only a single precursor species.

Key word index: Ammonia, dinitrogen pentoxide (N_2O_5), hydrocarbons, nitrate aerosol, nitrate radical (NO_3), nitric acid, nitrogen dioxide, ozone, peroxyacetyl nitrate, photochemical modeling, emission control.

1. INTRODUCTION

Anthropogenic emissions of NO_x and reactive organic gases (ROG) are the recognized precursors for a number of pollutants found in the atmosphere including O_3 , NO_2 , HNO_3 and aerosol nitrate (AN). Emission control measures are being taken to reduce the formation of O_3 and NO_2 in areas with excessive concentrations. These control programs are expensive, and the most effective strategies to reduce O_3 and NO_2 concentrations (Pitts *et al.*, 1983; Chock *et al.*, 1981, 1983; Glasston, 1981, 1983) are still in question. A key problem faced when selecting between alternative control programs is that the decisions made will also affect the concentrations of a number of currently unregulated but potentially damaging co-pollutants, in particular HNO_3 and AN. HNO_3 production results in deposition of strong acids at the earth's surface. HNO_3 also reacts with NH_3 and preexisting particulate matter in the atmosphere to produce fine AN which is very effective in reducing visibility.

The purpose of the present study is to develop and test engineering methods for predicting the effect of ROG, NO_x and NH_3 control programs on atmospheric HNO_3 , O_3 and AN concentrations. A photochemical trajectory model that predicts O_3 , NO_2 , total

inorganic nitrate (TN), AN, HNO_3 , NH_3 and PAN concentrations from emissions data is tested for its ability to reproduce field experimental data. Following this evaluation, the air quality model is used to determine the effect that reducing the emissions of ROG, NO_x and NH_3 has on O_3 , PAN, HNO_3 , NH_3 and AN concentrations. Example calculations are presented for Rubidoux, near Riverside, CA, which experiences some of the most serious nitrate-induced fine particulate loading and visibility problems in the U.S.

2. MODEL DESCRIPTION

Results presented in this paper were obtained using a Lagrangian trajectory formulation of the atmospheric diffusion equation that describes atmospheric chemical reactions, turbulent vertical diffusion, horizontal advective transport, and ground level pollutant deposition. Within the chemical mechanism the concentration of ammonium nitrate aerosol is computed to be at thermodynamic equilibrium with NH_3 and HNO_3 vapor, and where noted, the heterogeneous formation of AN from the reaction of HNO_3 with preexisting aerosol is treated. Except for the following specific details, a complete description of the gas phase model appears elsewhere (Russell *et al.*, 1983, 1985), and it will not be described further here.

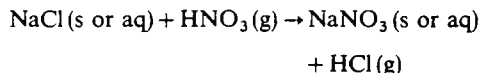
*Department of Mechanical Engineering.

†Environmental Engineering Science Department.

Reaction 58, describing the interaction between preexisting aerosol and HNO_3 , has been added to the previously described version of this model in order to simulate the stripping of atmospheric HNO_3 by certain aerosols, such as sea salt,



where SINK is that portion of the aerosol material available to react with HNO_3 and BAN is irreversibly Bound Aerosol Nitrate. This is a generalized reaction that includes a variety of specific chemical reactions, such as the displacement reaction



which is thermodynamically favorable, and is suggested by the excess of Na^+ ions in comparison to the Cl^- ions in many atmospheric aerosol samples (Russell and Cass, 1984; Duce, 1969; Martens *et al.*, 1973). The rate constant for this reaction is derived from kinetic theory for the bombardment of the aerosol surface by HNO_3 vapor. Aerosol surface area per unit mass is computed from the size distribution of Larson *et al.* (1984), which was obtained on a moderately smoggy August day in California's South Coast Air Basin (SoCAB). Collision efficiencies for the reactions between gases and atmospheric aerosol surfaces vary with aerosol surface characteristics and composition and are not known for all the relevant combinations of reactive gases and aerosols. Baldwin and Golden (1979) measured a value of 2.4×10^{-4} as the lower bound on the collision efficiency of HNO_3 with an H_2SO_4 surface. With this in mind, a collision efficiency of 0.001 was assumed for the reaction of HNO_3 vapor with the SINK aerosol surface.

In this study, the height of the air column modeled is 1000 m, divided into 10 cells with vertical dimensions of 30, 50, 70, five 100, 150 and 200 m. The emissions inventory, meteorological fields and terrain characteristics are developed on a grid system containing 5 km by 5 km cells, so the horizontal dimensions of the air parcels studied are set to the same size as a single grid cell.

3. MODEL EVALUATION DATA BASE

3.1. Pollutant concentrations

Model evaluation tests will be conducted using a number of air parcel trajectories that cross the SoCAB (Fig. 1) on 30–31 August 1982. During this 2-day period an experiment was conducted to acquire a set of data for use in verifying this type of photochemical air quality model (Russell and Cass, 1984). That set of experimental data includes observations on AN, sulfate, ammonium and other ionic species concentrations, as well as gas phase NH_3 , HNO_3 and PAN levels. Gas phase concentrations of total hydrocarbons (THC), CO, NO, NO_x and O_3 for this time period were obtained from South Coast Air Quality Management District (SCAQMD) and California Air Resources Board (CARB) monitoring stations that are colocated with the aerosol monitoring sites. PAN concentrations were measured at the University of California, Riverside (UCR) and at Caltech in Pasadena, CA.

3.2. Hourly meteorological data

Wind fields for the 2-day period of interest were obtained using measured wind velocities at 39 sites in the SoCAB. These wind data were interpolated over

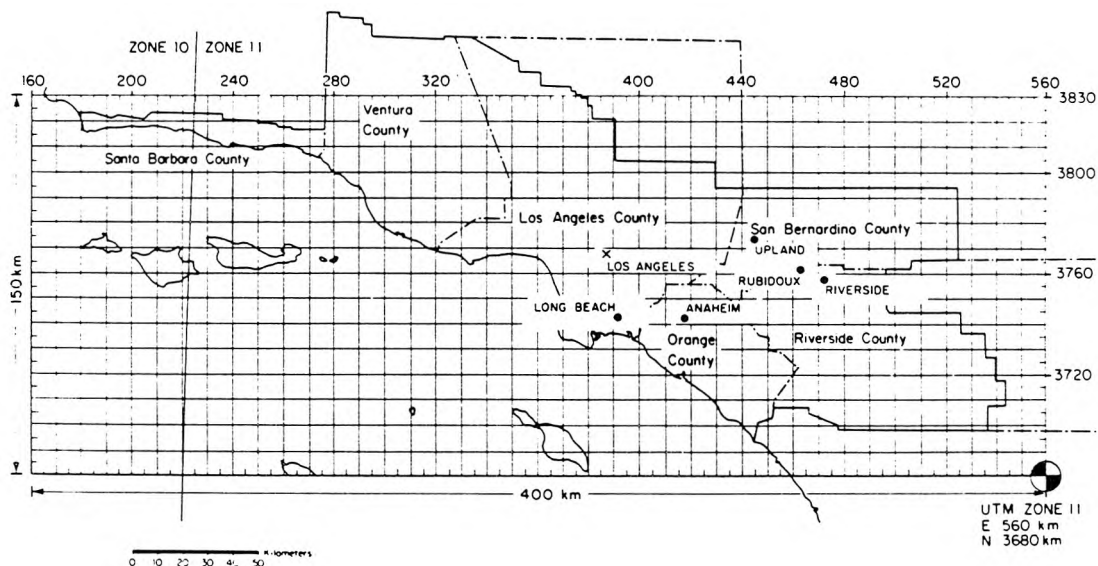


Fig. 1. Gridded map of California's South Coast Air Basin (SoCAB) used for constructing concentration fields, meteorological fields, and emissions inventories. Symbols (●) indicate the locations of aerosol measurement stations used in this work. The solid line marks the boundary of the SoCAB.

the 80×30 grid of 25 km^2 cells superimposed over the air basin using the r^{-2} weighting method detailed by Goodin *et al.* (1979). Air parcel trajectories were calculated from these wind fields using 10-min time steps. Hourly average temperature and relative humidity fields were obtained by interpolation between the 29 and 18 locations at which these parameters are measured, respectively. Hourly average mixing depth fields were obtained from the measured vertical atmospheric temperature profiles available at eight locations. Solar radiation levels measured at central Los Angeles, Pasadena, and Upland were used to set the photolysis rate constants within the chemical mechanism.

3.3. Emissions

NO_x , total hydrocarbon (THC) and CO emissions into the air parcels modeled are calculated from a 1982 forecast emission inventory for the SoCAB provided by the California Air Resources Board (Ranzieri, 1983, 1984). The inventory details the emissions, by species,

from over 2600 source categories distributed spatially and temporally over the basin. Hourly emission rates are given for over 200 organic species, NO, NO_2 and CO for each of the $5 \text{ km} \times 5 \text{ km}$ grid cells throughout the SoCAB. A summary of the daily totals of the emissions from mobile and stationary sources is given in Table 1. The spatial distributions of the THC, NO_x and CO emissions are shown in Fig. 2. Emission rates given for the individual organic gas species are lumped into the six organic classes compatible with the model used in this study.

The NH_3 emissions inventory for 1982 used in this study was developed by updating the 1974 emissions inventory previously described by Cass *et al.* (1982) and Russell *et al.* (1983). Total NH_3 emissions by source category are shown in Table 2, and the spatial distribution of NH_3 emissions is given in Fig. 2. Variables that affect NH_3 emissions from animal waste decomposition have been investigated by Muck and Steenhuis (1982) and Steenhuis *et al.* (1982). Based on their work, the diurnal variation of the NH_3 release

Table 1. 1982 estimated emissions within the modeling region shown in Fig. 1

Source type	THC tons/day	Emission rate NO_x tons/day	CO tons/day
<u>Stationary sources</u>			
Fuel combustion			
External combustion boilers			
Utilities	6.7	97.7	8.2
Industrial	3.0	41.0	7.1
Commercial and institutional	0.1	3.6	0.03
Internal combustion engines			
Utilities	4.5	8.4	3.0
Industrial	25.1	58.1	19.2
Petroleum refining and production	2.8	35.3	1.1
Other manufacturing	3.1	39.5	181.3
Residential, agricultural and other	16.9	53.3	127.1
Subtotal fuel combustion	62.2	336.9	347.0
Waste burning and incineration	0.09	0.4	0.3
Landfill	777.9	0.0	0.0
Solvent use			
Surface coating	195.4	1.9	0.4
Other	161.8	0.2	0.03
Petroleum processes, storage and transfer	99.9	11.3	13.6
Industrial processes	26.1	2.6	18.1
Miscellaneous	440.0	3.8	118.6
Subtotal stationary sources	1763.4	357.1	498.0
<u>Motor vehicle emissions</u>			
On-road vehicles	581.4	662.5	5001.9
Off-road vehicles	26.8	67.1	172.6
Railroads	3.8	15.3	5.8
Ships	22.2	16.0	88.6
Aircraft	18.1	16.3	84.5
Subtotal motor vehicle emissions	652.3	777.2	5353.4
Total	2415.7	1134.3	5851.4

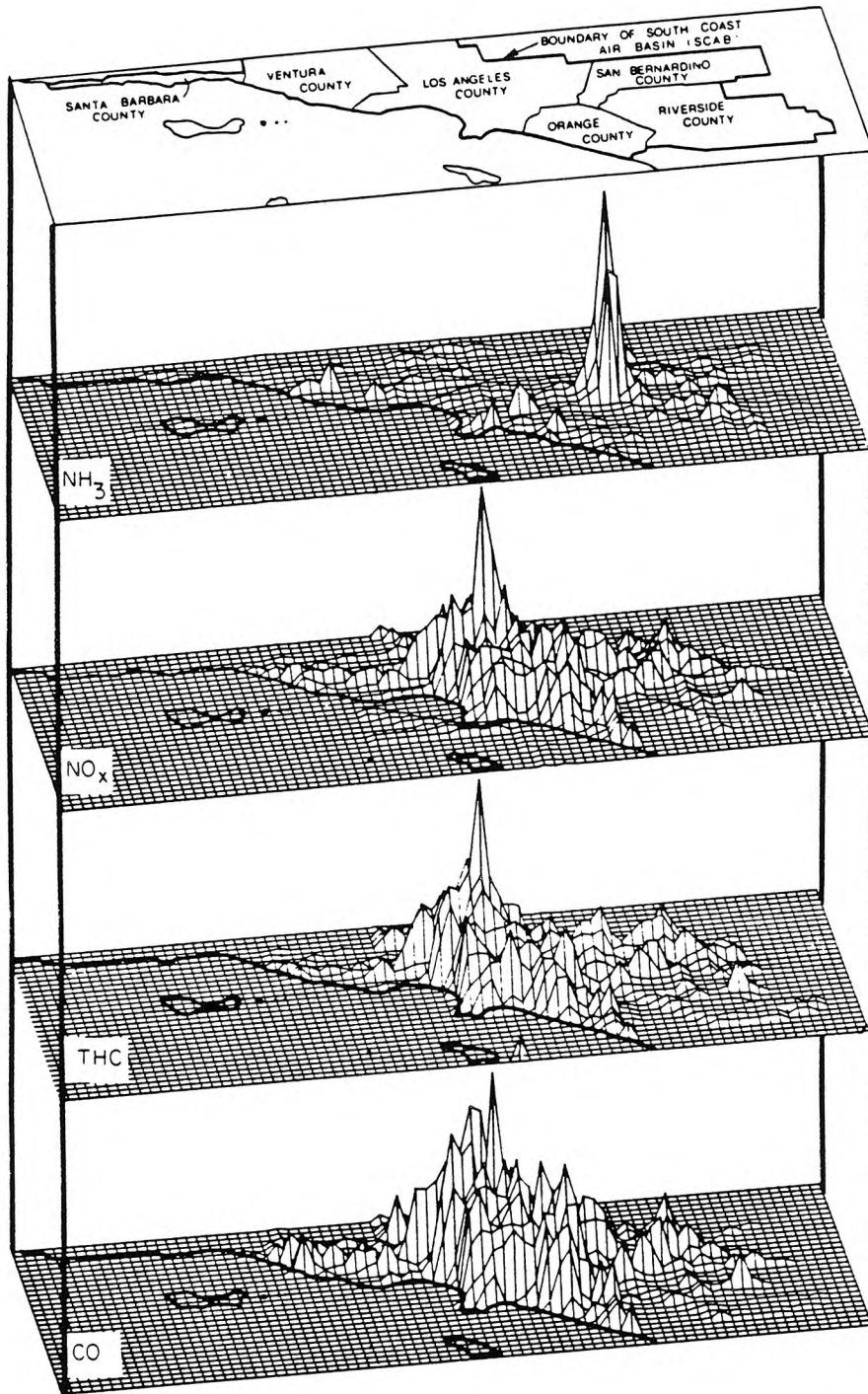


Fig. 2. Spatial distribution of the 1982 estimated daily emissions of NH_3 , NO_x , THC and CO in the South Coast Air Basin.

rate from animal waste decomposition is assumed to depend on temperature and wind velocity, such that:

$$E_i \propto 2.36 \left(\frac{T_i - 273}{10} \right) V_i^{0.8} A \quad (1)$$

$$A = \sum_{i=1}^{24} E_i \quad (2)$$

where E_i is the hourly emission rate in the grid cell at

hour i from animal waste decomposition, A is the daily total emission rate of NH_3 from animal waste in the grid cell, T_i is the absolute temperature in K, and V_i is the wind velocity in m s^{-1} at hour i . A minimum wind velocity of 0.1 m s^{-1} is assumed.

3.4. Initial conditions

Surface level initial conditions for trajectories ending at Rubidoux were based on the concentration fields constructed by spatial interpolation of the

Table 2. Summary of ammonia emissions by source category within the modeling region shown in Fig. 1

Source category	Total emissions (tons day ⁻¹)	
Stationary fuel combustion		
Electric utility		
Natural gas	1.2	
Residual oil	0.38	
Digester gas	0.00	
Refinery fuel burning		
Natural gas	0.12	
Residual oil	0.015	
Refinery gas	0.39	
Industrial fuel burning		
Natural gas	0.47	
Liquified petroleum gas (LPG)	0.008	
Residual oil	0.022	
Distillate oil	0.12	
Digester gas	0.026	
Coke oven gas	0.015	
Residential/commercial fuel burning		
Natural gas	0.21	
Liquid petroleum gas (LPG)	0.004	
Residual oil	0.085	
Distillate oil	0.079	
Coal	0.023	
Subtotals	3.2	(1.9 %)
Mobile source fuel combustion		
Automobiles		
Catalyst autos and light trucks	2.4	
Non-catalyst autos and light trucks	0.48	
Diesel autos and light trucks	0.004	
Catalyst medium vehicles	0.23	
Non-catalyst medium and heavy trucks	0.14	
Diesel trucks	0.023	
LPG for carburetion	0.007	
Civilian aircraft		
Jet	0.007	
Piston	0.002	
Shipping		
Residual oil boilers	0.068	
Diesel ships	0.002	
Railroad-diesel oil	0.004	
Military		
Gasoline	0.005	
Diesel	0.002	
Jet fuel	0.002	
Residual oil	0.001	
Off-highway vehicles	0.006	
Subtotals	3.4	(2.0 %)
Industrial point sources	2.4	(1.5 %)
Sewage treatment plants	14.6	(8.9 %)
Soil surface	23.8	(14.5 %)
Fertilizer		
Farm crop	2.0	
Orchards	1.6	
Handling	0.4	
Non-farm	4.8	
Subtotals	8.8	(5.4 %)

Table 2. (Contd.)

Source category	Total emissions (tons day ⁻¹)	
Livestock		
Cattle		
Dairy	29.8	
Feedlot	7.2	
Range	13.6	
Horses	16.2	
Sheep	0.86	
Hogs	0.26	
Chickens	16.4	
Turkeys	0.49	
Subtotals	84.8	(51.6%)
Domestic		
Dogs	11.6	
Cats	3.5	
Human respiration	0.046	
Human perspiration	7.6	
Household ammonia use	0.57	
Subtotals	23.3	(14.2%)
Total	164.3	(100%)

measured concentrations. Those concentration fields start with the Pacific Ocean background values (in ppb: O₃, 40; NO₂, 10; NO, 10; CO, 100; HNO₃, 1; NH₃, 1; THC, 1000) at the western edge of the grid and rise to match the on-land data at the near coastal monitoring sites established during the field experiment. Initial upper level pollutant concentrations over the ocean were set to (in ppb): O₃, 40; NO, 0.0; NO₂, 1.0; CO, 500; HNO₃, 1.0; NH₃, 1.0; and THC, 500. Initial NH₄NO₃ concentrations over the ocean were set to 3.25 µg m⁻³ (the NO₃⁻ equivalent of 1 ppb HNO₃).

Atmospheric THC measurements taken by the SCAQMD are reported on a ppm C atoms basis and are not speciated into the many different organic gases actually present. The initial conditions for each of the six hydrocarbon (HC) classes employed by the trajectory model are found by splitting the measured THC values into the six classes using the set of splitting factors given in Table 3. These factors were derived

from the measurements taken by Grosjean and Fung (1984) of the speciated HC composition of Los Angeles air, averaged over a number of sampling periods.

4. MODEL EVALUATION FOR 30-31 AUGUST 1982

The ability to accurately predict O₃ and NO₂ concentrations usually is the most stringent test used to evaluate a gas phase photochemical model. In this study, the ability to calculate total inorganic nitrate (TN), HNO₃, NH₃, AN and PAN will be tested in addition to O₃ and NO₂.

Progress towards model verification for a few of these co-pollutants was reported by Russell *et al.* (1983), when an earlier version of this model was tested using nitrate ion, ammonium ion and NH₃ gas concentration data available for a short period on 28 June 1974. Model verification data used during that study were limited, and because the AN samples were collected on glass fiber filters, questions of artifact nitrate formation cloud the assessment of data quality. In this section a much more extensive model evaluation effort is carried out for the 2-day period of 30-31 August 1982.

Two sets of trajectories are studied in this evaluation: a forward trajectory starting at Long Beach and ending near Rubidoux, and a set of trajectories ending at Rubidoux throughout 31 August 1982. Rubidoux is in the eastern portion of the SoCAB, downwind of the Los Angeles metropolitan area, and is affected by the reaction products formed in the atmosphere downwind of a major city. Long-term air quality data taken throughout the SoCAB during 1982 (Gray *et al.*, 1986) show that Rubidoux is the monitoring site with the highest AN levels, as has been the case historically. The Rubidoux-Riverside area also experienced the highest

Table 3. Splitting factors for converting total measured hydrocarbons (ppmC) into hydrocarbon classes for use as initial conditions

Class	Factor
HCHO	0.0037
RCHO	0.0033
OLE	0.0042
ALK	0.0675
ARO	0.0177
C2H4	0.0061

For example, the initial HCHO concentration equals 0.0037 × THC measured in ppmC. The splitting factors above incorporate the conversion from total hydrocarbons given in ppmC to molecular concentrations in ppmV.

total nitrate levels observed during the 30–31 August 1982 period studied here and had the highest measured O_3 concentrations during this 2-day interval (230–260 ppb). As such, these trajectories serve as ideal candidates for model verification tests and can be used to show the effect of emission control strategies on pollutant concentrations. Further model verification was also conducted using the data from the Upland monitoring site, and the results are found in Russell (1985).

4.1. Long Beach forward trajectory

During a previous examination of the data from the 1982 field experiment (Russell and Cass, 1984), an air parcel trajectory was identified that started in the morning at the Long Beach sampling site at the time of the AN peak at that location, passed just north of the Anaheim measurement station in the afternoon, and in the evening terminated close to the Rubidoux site at the time of the AN peak in the Riverside area. This single trajectory provides an ideal opportunity for use in part of the model evaluation effort because the contents of the air parcel are well defined at several locations along its path. Likewise the initial conditions are established using measured pollutant concentrations, minimizing the uncertainty added from interpolating data.

Two distinct calculation schemes were tested against the measurements taken along the Long Beach to Rubidoux trajectory just discussed. In the first calculation, Case 1, AN was assumed to be formed only by the reaction between NH_3 and HNO_3 . In the second test, Case 2, AN formation proceeded by the reaction of HNO_3 with NH_3 , and by the irreversible reaction of HNO_3 with preexisting aerosol (reaction 58, described previously). Use of reaction 58 requires that emissions along the trajectory be specified for the aerosol materials that react readily with HNO_3 . The emission rate of SINK aerosol available to react with HNO_3 was set at a constant rate, such that the total unreacted SINK aerosol plus the cations associated with BAN at the end of the trajectory was approximately equal to the sum of the Na, Ca, K and Mg concentrations measured when the trajectory reached Rubidoux. Actual emission rates of these species as a function of location are unknown.

Results of the Long Beach to Rubidoux forward trajectory calculations are shown in Table 4, along with the measured pollutant concentrations, at 1400 and 1800 PDT, 31 August 1982. The trajectory passed nearest to Anaheim at 1400 PDT, and the measured HNO_3 , NH_3 , AN and TN concentrations at that time are from that station. Measured O_3 and NO_2 values at 1400 are available from a number of monitoring sites in the area, and the O_3 and NO_2 values shown are an average of the values at the three stations nearest to the air parcel's position at that time. As the trajectory passed near Anaheim at 1400, the O_3 prediction very nearly equals the observed average, well within the uncertainty in the observed concentrations. The pre-

dicted NO_2 concentration, corrected to include those species that interfere with the measurement devices (Winer *et al.*, 1974), is slightly lower than the observed. In both Cases 1 and 2, the predicted HNO_3 level is between the values measured for the sampling periods straddling 1400 PDT. The AN predicted for Case 1 is between the measured concentrations, while the amount predicted in Case 2 is slightly greater than the observed values. In both cases the predicted NH_3 matches the two measured values to within the measurement uncertainties.

Farther downwind, at 1800 PDT, the trajectory path calculation showed that the air parcel was 3 km southwest of the Rubidoux sampling site and about 8 km west of the Riverside (UCR) site. Ozone, predicted to be 152 ppb, is equal within the reporting uncertainty of 10 ppb to that measured in Riverside and is slightly greater than that measured at Rubidoux. Again the NO_2 predictions are slightly below the measured values. In this case, the trajectory arrival at Rubidoux again straddles two measurement periods for HNO_3 , NO_3^- and NH_3 , while at the UCR site the 1800 arrival falls within a single sampling interval. In both Cases 1 and 2, the predicted concentrations of HNO_3 , AN and TN fall within the range of the observations at Rubidoux and Riverside. The predicted NH_3 concentration resulting from the Case 2 calculation also lies within the measured range. While the NH_3 concentration prediction for Case 1 may appear slightly lower than that observed at UCR, the circa 5 ppb NH_3 deficit is still within the experimental uncertainty of the NH_3 concentration measured at UCR at that time (Russell and Cass, 1984).

PAN also was measured at the UCR site, and as seen in Table 4, the model closely predicts the observed PAN concentration, which peaked at that time. From the results shown in Table 4, it is concluded that the trajectory model is capable of predicting the downwind concentrations of the secondary pollutants of interest in the Riverside area at the time of arrival of the peak nitrate concentrations, given measured initial conditions at Long Beach.

4.2. Trajectories ending at Rubidoux

While the Long Beach to Rubidoux trajectory calculation adds to confidence in the model's capability, it is unrealistic to expect that high quality data on initial conditions will always be available for arbitrarily selected trajectories. Likewise, the upper level pollutant concentrations needed to initialize the model are seldom, if ever, known. Upper level initial conditions must be estimated from ground level measurements, while pollutants stored aloft may have been affected by chemical processes not evident at the ground. This is especially true in the early morning because of the markedly decreased vertical mixing overnight that traps fresh emissions near the ground and isolates portions of the upper air column from night-time emissions and from deposition. In this case the ground level portion of the air mass may be heavily

Table 4. Predicted and measured concentrations along the trajectory beginning at Long Beach, California, at 1100 (PDT), 31 August 1982

Pollutant	1400 PDT			1800 PDT			
	Measured concentration	Case 1 predicted (NH ₄ NO ₃ only)	Case 2 predicted (reaction 58 included)	Measured at Rubidoux	Measured at UCR	Case 1 predicted (NH ₄ NO ₃ only)	Case 2 predicted (reaction 58 included)
O ₃ (ppb)	173‡	174	174	130	150	152	152
NO ₂ (ppb)	70‡	51*	52*	50	—	35*	38*
HNO ₃ (ppb)	10.1–7.7†	10.0	8.2	5.3–1.8†	2.0	3.3	2.5
AN (μg m ⁻³ NO ₃ ⁻)	8.1–13.4†	11.6	19.9	29.8–14.2†	17.0	14.1	22.7
TN (μg m ⁻³ NO ₃ ⁻)	33.6–32.7†	36.8	40.6	43.1–18.7†	22.1	22.4	29.0
NH ₃ (ppb)	15.3–10.9†	10.8	13.2	59.8–89.0†	32.7	27.3	36.4
PAN (ppb)					22	20.1	20.1
NH ₄ NO ₃ (μg m ⁻³ NO ₃ ⁻)		11.6	6.1			14.1	11.3
BAN § (μg m ⁻³ NO ₃ ⁻)			13.9				11.3

*Predicted NO₂ concentrations are the sum of predicted NO₂, HNO₃, AN and PAN. The instruments used to measure NO₂ possess a quantitative interference due to co-pollutant species (Winer *et al.*, 1974).

† Both at Anaheim and at Rubidoux, the trajectory passed nearby between two sampling periods. Both the measured concentrations from 1200 to 1400 and 1400 to 1600 are shown, respectively, at Anaheim. Likewise at Rubidoux the measured concentrations for 1600–1800 and 1800–2000 are given. The UCR site sampling interval was from 1700 to 1900. Predicted ozone values are 1-h averages, as are the measured concentrations.

‡Ozone and NO₂ concentrations are averaged values from the nearest three stations. Other concentrations are for Anaheim.

§Bound Aerosol Nitrate.

||PAN measured only at UCR.

burdened by NO and NO₂, while in the upper levels of the atmosphere night-time chemical reactions can convert almost all of the NO and NO₂ to HNO₃ (Russell *et al.*, 1985). If this situation is not taken into account, initial conditions based on ground level observations could be specified that are inconsistent with actual pollutant concentrations several hundred meters above the ground.

An alternative method for initializing trajectories was examined. Air parcels arriving at Rubidoux throughout the day of 31 August were followed backward to midnight at the end of 29 August. In that case all the trajectories begin over the ocean upwind of the city and end between 24 and 47 h later at the Rubidoux monitoring site. Use of the longer, 2-day trajectories has three major advantages. First, starting more than 24 h before the arrival of the trajectory allows sufficient time for most of the reactive pollutants present due to initial conditions to be depleted from the system both by ground level deposition and by chemical reactions that form products less crucial to the formation of photochemical oxidants. Secondly, starting the air parcel at a relatively clean background location over the ocean minimizes the effect of initial conditions and the uncertainty in the outcome arising from their specification. Thus, predicted concentrations at the end of the trajectory are primarily a function of the emissions along the trajectory, not of initial conditions, and the mass of each species in the air parcel at the start of 31 August is consistent with the known emissions, meteorology, and chemistry of 30 August. Finally, this procedure enhances the usefulness of subsequent control strategy calculations because predicted concentrations are dominated by emissions along the trajectory that can be attributed to particular air pollution sources rather than being heavily influenced by initial conditions that are not readily assigned to their source. This is a more demanding test of a model and the associated emissions inventory than is the case when using shorter trajectories in which initial conditions play a major, if not dominating, role.

In an effort to determine the importance of uncertainties in the initial conditions, a test was performed in which the initial concentrations established over the ocean were first doubled and then halved for the trajectory arriving at Rubidoux at 1600 PDT. This trajectory displayed the greatest predicted nitrate loading and second highest O₃ concentration among the trajectories terminating at Rubidoux. The predicted TN concentrations at Rubidoux at 1600 PDT for the base case, for the case with the initial conditions doubled, and for the case with initial concentrations cut in half were 18.2, 15.5 and 20.6 ppb, respectively. The O₃ concentrations averaged over the last 1-h of travel along that trajectory were 185, 195 and 176 ppb, respectively. This test shows that initial conditions play a very small role in determining predicted pollutant concentrations for the multi-day trajectories studied here. On the other hand, if the emissions are set to zero

along this same trajectory, the total inorganic nitrate predicted at Rubidoux falls to only 1.6 ppb, and O₃ falls to 38 ppb. Thus, the predicted pollutant levels are almost solely a function of emissions within the urban area when a reasonable set of initial conditions starting over the ocean is used.

Next the air quality model's ability to reproduce the time history of pollutant concentrations at Rubidoux given trajectories that originate over the ocean was examined. Again the model was evaluated in two modes: with and without the addition of aerosol that can irreversibly react with HNO₃ to form AN.

Plots of the pollutant concentrations predicted at Rubidoux for 31 August without the emission of SINK aerosol along the trajectories are compared to measured values in Figs 3–8. Ozone and NO₂ concentrations averaged over the last 1-h of travel are shown in Figs 3 and 4. Trajectories arriving at Rubidoux on the hour were used to estimate 2-h average concentrations when needed for comparison to measured values (2-h average weighted 1/4 start hour, 1/2 midpoint, 1/4 end hour). Predicted 2-h average TN concentrations are shown, with the measured values, in Fig. 5, HNO₃ in Fig. 6, AN in Fig. 7, and NH₃ in Fig. 8.

A plot of the predicted and observed concentrations of O₃ and NO₂ throughout 31 August at Rubidoux

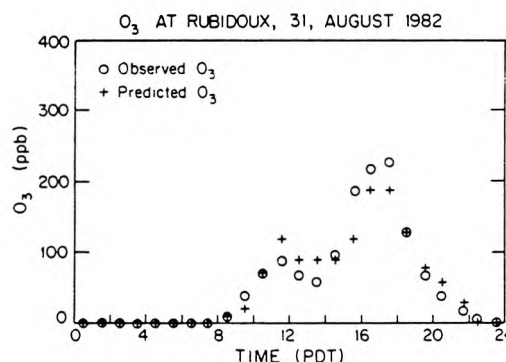


Fig. 3. Observed and predicted O₃ at Rubidoux, CA, 31 August 1982.

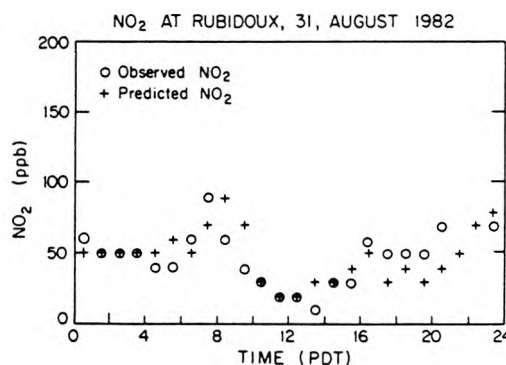


Fig. 4. Observed and predicted NO₂ at Rubidoux, CA, 31 August 1982.

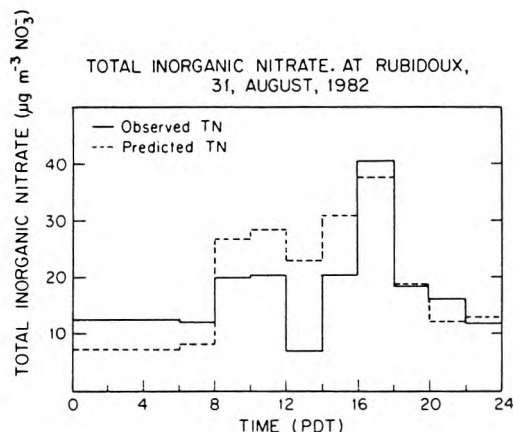


Fig. 5. Observed and predicted total nitrate (TN = AN + HNO₃) at Rubidoux, CA, 31 August 1982.

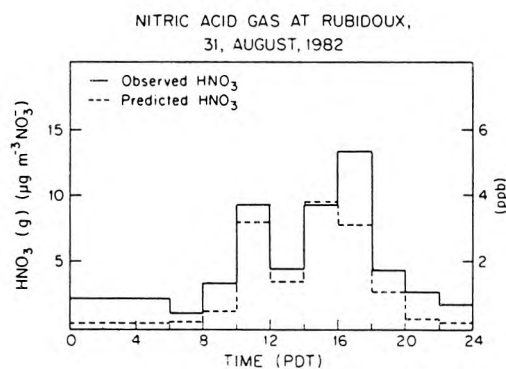


Fig. 6. Observed and predicted HNO₃(g) at Rubidoux, CA, 31 August 1982.

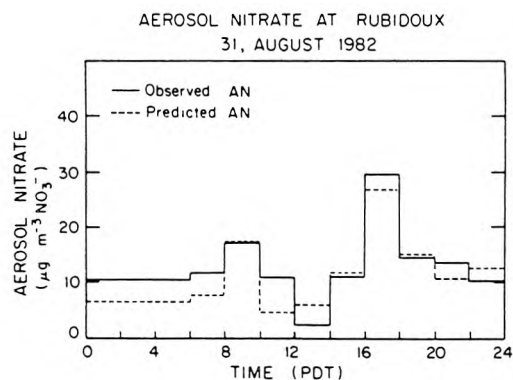


Fig. 7. Observed and predicted NO₃⁻ at Rubidoux, CA, 31 August 1982.

shows that the model predictions are in good agreement with the measured species concentrations. Figure 5 shows the comparison of averaged predicted and observed TN. The model predicts the trends and, approximately, the 2-h average concentrations. The peak predicted TN, $38 \mu\text{g m}^{-3}$ (as NO₃⁻), is only

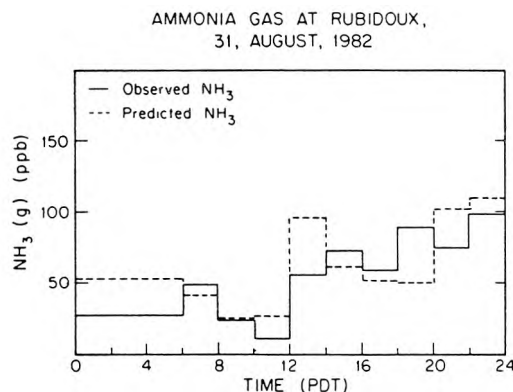


Fig. 8. Observed and predicted NH₃ at Rubidoux, CA, 31 August 1982.

slightly less than the peak measured, $43 \mu\text{g m}^{-3}$, which is considered close given measurement and model input uncertainties. The predicted 24-h average TN is $19 \mu\text{g m}^{-3}$, against a measured $18 \mu\text{g m}^{-3}$.

Having shown that the predicted and measured TN agree well, the question of apportioning the TN between the gas and aerosol phases arises. This is sensitive to the temperature, humidity and NH₃ concentration (Russell *et al.*, 1983), and to the presence of other aerosol constituents (Hildemann *et al.*, 1984). In the first case studied here, pure NH₄NO₃ is assumed to be the only AN species formed. Most of the inorganic nitrate is predicted to be found in the aerosol phase, not the gas phase, and the measurements confirm that prediction (Fig. 6). The measured and predicted 24-h average AN concentrations were 13 and $16 \mu\text{g m}^{-3}$, respectively (Fig. 7). Measured gas phase HNO₃ levels in this case exceed observed values throughout the day (Fig. 6), but the absolute magnitude of this discrepancy is very small. The measured 24-h average HNO₃ was 1.9 ppb compared to the predicted 1.1 ppb. Measurement uncertainties on the HNO₃ values are approximately 0.4 ppb (one standard error).

A plot comparing the NH₃ concentrations (Fig. 8) indicates that throughout much of the day the predictions agree remarkably well with the measurements, considering that the NH₃ emission inventory and model used here represent the first test of a procedure for calculating atmospheric NH₃ levels. The 24-h average NH₃ measured was 51 ppb, compared to the predicted 61 ppb.

In the trajectories terminating at Rubidoux, most of the NH₃ emissions are due to livestock operations, which determine the very tall spike in the NH₃ emission inventory (Fig. 2) located immediately upwind of Rubidoux. The major peak in the NH₃ emission inventory is so sharp that a slight perturbation in the calculated path of an air parcel can create a noticeable difference in the predicted NH₃ concentrations. Also, knowledge of the diurnal emission pattern for livestock waste decomposition and the exact spatial distribution of the animals during the August 1982 experiment could be improved. As a result, NH₃

concentrations cannot be predicted with the same precision as other pollutant concentrations, even though the source of the NH_3 emissions has been identified with reasonable certainty.

In view of the sensitivity of the model's nitrate predictions to NH_3 concentration and temperature and of the uncertainty in the NH_3 emissions from the large sources just upwind of Rubidoux, a second set of calculations was performed in which TN concentrations predicted by the model were apportioned between gas phase HNO_3 and aerosol NH_4NO_3 using the ambient NH_3 concentrations and temperatures measured at Rubidoux. The temperatures at Rubidoux used in the previous modeling calculations were obtained from filtered, interpolated temperature field values calculated for the center of each grid cell and need not equal the measured temperatures at Rubidoux exactly. Using the measured ambient temperature and NH_3 concentration to partition the nitrate at the trajectory endpoint improved the model predictions from those shown in Fig. 7 to those shown in Fig. 9. Thus, given the ability to predict more precisely the NH_3 concentrations and using actual measured temperatures, the model can accurately partition the inorganic nitrate at Rubidoux between the vapor and aerosol phases. This calculation also decreases the predicted 24-h average AN from $16 \mu\text{g m}^{-3}$ to $12 \mu\text{g m}^{-3}$, bracketing the measured value of $13 \mu\text{g m}^{-3}$.

Next the emissions of SINK aerosol were added along each trajectory at a constant rate needed to approximately match the total non-ammonium cationic material seen to arrive at Rubidoux. The entire set of multi-day trajectory calculations beginning over the ocean was repeated with HNO_3 allowed to react with SINK aerosol by reaction 58, and again using the measured ambient temperature and NH_3 concentration at Rubidoux to apportion TN between HNO_3 and the aerosol phase. This change in assumptions tends to increase the AN and TN concentrations predicted, though in this case the effect is small. As seen in Fig. 10,

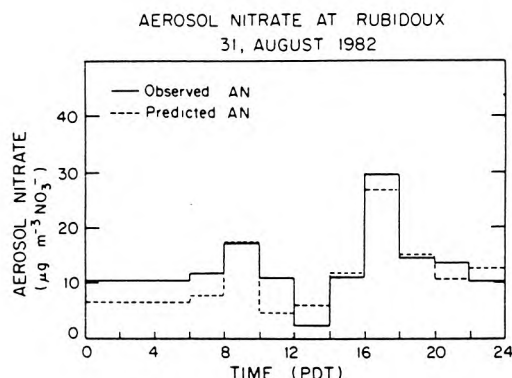


Fig. 9. Observed and predicted NO_3^- at Rubidoux, CA, 31 August 1982 when the partition of computed TN between $\text{HNO}_3(\text{g})$ and aerosol nitrate is based on ambient temperatures and ammonia concentrations measured at the Rubidoux monitoring site.

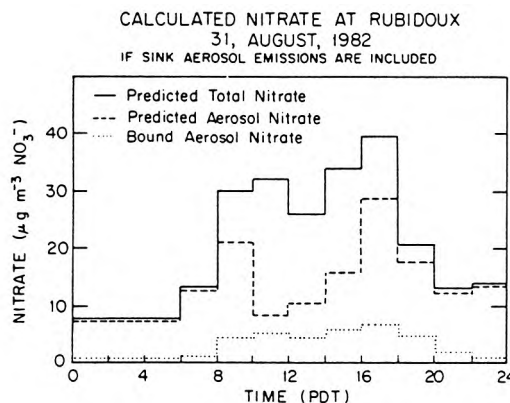


Fig. 10. Predicted total nitrate ($\text{TN} = \text{HNO}_3(\text{g}) + \text{NH}_4\text{NO}_3 + \text{BAN}$), aerosol nitrate ($\text{AN} = \text{NH}_4\text{NO}_3 + \text{BAN}$) and aerosol nitrate formed by reaction 58 (BAN, see text) at Rubidoux, CA, 31 August 1982.

the 24-h average AN increases to $18.4 \mu\text{g m}^{-3}$, of which 84% is ammonium nitrate and the remaining 16% is BAN. The model predicts the coexistence of ammonium nitrate, BAN, HNO_3 , NH_3 and unreacted aerosol SINK, indicating that the consumption of aerosol SINK is kinetically limited. Given more time, or if the collision efficiency for HNO_3 on SINK aerosol is much higher than $\alpha = 0.001$, then the aerosol has the capacity to strip a large fraction, if not all, of the HNO_3 from the atmosphere.

In this study, results from shorter (single day) and longer (multi-day) trajectories have been used to evaluate the model's performance. In both cases the model has performed well. Some uncertainty in the air parcel path is added to the analysis when trajectory paths are calculated over multi-day periods, as discussed in Russell (1985). However, this is the only way to decrease the uncertainties that would otherwise arise from misspecifying initial conditions and to accurately show the effects that changing pollutant emissions would have on the resulting concentrations. If initial conditions dominate or greatly affect the predicted concentrations, a change in emissions within the model may have little effect on model predictions, or in some cases could produce predictions that move in a direction opposite to reality. An example of the latter case could arise if initial conditions placed an excessive amount of NO_x in the air parcel as it starts in the morning. In this case increasing NO_x emissions could further decrease the peak O_3 concentration, while if the correct initial NO_x concentrations were used, then the atmosphere might be sufficiently starved for NO_x that further NO_x emissions would increase predicted O_3 levels.

The use of multi-day trajectories could suffer from the effects of vertical wind shear. On this particular occasion it appears that these effects were small. Upper level wind data were collected at a number of sites. At Point Mugu where the early morning winds were measured at 419 PDT, the winds varied little in direction (less than 10°) with height.

Upper level velocities were also low, less than 2.5 m s^{-1} , to well above the height of the modeling region. In the eastern portion of the basin, the early morning measurement taken at 300 PDT showed that the difference in velocity between the ground and levels up to 188 m was less than 1 m s^{-1} with direction varying no more than 25° ; 188 m is greater than the depth of the early morning mixed layer trapping the pollutants emitted at ground level.

The above discussion, along with the successful model evaluation results, argues that multi-day trajectories can, and should, be used for testing the effects of emission control measures.

5. EVALUATION OF CONTROL STRATEGIES FOR HNO_3 AND AEROSOL NITRATE ABATEMENT

To help guide researchers and public agencies toward an optimal control strategy, the effects of a number of simple candidate control strategies are simulated and the results will now be discussed. The study is directed primarily towards developing strategies that will reduce AN and HNO_3 concentrations in the atmosphere, but the effect on pollutants other than HNO_3 and AN will also be detailed. As discussed above, because of the high nitrate and O_3 concentrations the Rubidoux trajectories were chosen for emission control measure evaluation.

Choice of the first set of control measures examined was motivated by the 1982 Air Quality Management Plan (AQMP) for the SoCAB (SCAQMD and Southern California Association of Governments, 1982). The AQMP outlines control measures that will be used to decrease NO_x emissions by about 23 % and ROG by about 34 % between the years 1979 and 1987, or about a 20 % and 30 % decrease, respectively, below the 1982 estimated emissions inventory used in the present study. For the purpose of this study, these reductions will be applied homogeneously over the air basin and will be applied equally to emissions of each of the lumped organic species. In a more detailed analysis, the original emissions inventory could be modified to reflect the specific reductions in each source category. This would result in a less spatially

regies that will reduce AN and HNO_3 concentrations in the atmosphere, but the effect on pollutants other than HNO_3 and AN will also be detailed. As discussed above, because of the high nitrate and O_3 concentrations the Rubidoux trajectories were chosen for emission control measure evaluation.

Table 5. Effect of emission reductions on nitrate species concentrations, Rubidoux, CA, 31 August 1982

Aerosol nitrate maximum 2-h average ($\mu\text{g m}^{-3}$)							
	Base case THC NO_x emissions reduction					THC emissions reduced 30 % NO_x emissions reduction	
	0 %	20 %	40 %	60 %	80 %	0 %	20 %
Base case NH_3 emissions	27.0	16.3	11.7	8.3	3.4	31.2	19.5
Reduced NH_3 emissions	7.2	6.4	—	—	—	7.0	6.3
Aerosol nitrate 24-h average ($\mu\text{g m}^{-3}$)							
	Base case THC NO_x emissions reduction					THC emissions reduced 30 % NO_x emissions reduction	
	0 %	20 %	40 %	60 %	80 %	0 %	20 %
Base case NH_3 emissions	11.5	8.4	4.8	2.7	1.1	13.3	9.0
Reduced NH_3 emissions	2.8	1.8	—	—	—	2.8	1.8
Total nitrate 24-h average ($\mu\text{g m}^{-3}$)							
	Base case THC NO_x emissions reduction					THC emissions reduced 30 % NO_x emissions reduction	
	0 %	20 %	40 %	60 %	80 %	0 %	20 %
Base case NH_3 emissions	18.6	15.4	10.3	6.8	4.0	21.2	15.9
Reduced NH_3 emissions	16.1	13.1	—	—	—	16.9	13.1
Nitric acid maximum 2-h average (ppb)							
	Base case THC NO_x emissions reduction					THC emissions reduced 30 % NO_x emissions reduction	
	0 %	20 %	40 %	60 %	80 %	0 %	20 %
Base case NH_3 emissions	9.6	7.9	5.9	4.1	2.6	10.1	8.0
Reduced NH_3 emissions	16.9	13.2	—	—	—	18.8	14.2

homogeneous reduction and could change the relative chemical composition of the organic emissions.

Table 5 shows the effects on the inorganic nitrate species of different combinations of emission reductions applied to the multi-day trajectories ending at Rubidoux. Pollutant emissions into these trajectories as they actually occurred on 31 August 1982 will be referred to as the base case emissions, and the observed NH_3 concentration and temperature at Rubidoux are used to apportion total inorganic nitrate between HNO_3 and AN. Results in Table 5 are for the case without the addition of SINK aerosol to react with HNO_3 . The effect of including the addition of SINK via reaction 58 on various control measures will be discussed later. Predicted maximum 2-h average AN, 24-h average AN, 24-h average TN and maximum 2-h HNO_3 are given in each case for comparison.

A 20% decrease in the NO_x emissions alone relative to the base case decreases the predicted maximum AN 40%, and the 24-h average AN value decreases 27%. TN decreases about 18%, or by about the same percentage as the decrease in NO_x emissions. Less change is noted in the predicted HNO_3 . This occurs because HNO_3 concentrations are largely governed by the NH_4NO_3 equilibrium dissociation constant and the ambient NH_3 concentrations. The excess of NH_3 tends to allow only a small amount of HNO_3 in the gas phase while the rest of the inorganic nitrate is transferred into the aerosol phase. Elsewhere in the air basin, NH_3 levels are much lower and a change in TN would be reflected more readily in a change in HNO_3 levels.

Decreasing the organic gas emissions results in an increase in AN, TN and HNO_3 . At first glance this is a slightly discouraging result. Careful examination shows that this increase in inorganic nitrate is primarily due to the oxidized nitrogen being displaced from PAN into inorganic nitrate species. Under some circumstances this trade-off between organic and inorganic nitrate species formation might be deliberately manipulated in order to achieve a desired balance between TN and PAN. Decreasing organic gas emissions also may decrease the formation of other potentially harmful organic and nitrated organic compounds not studied here.

Reducing the NO_x and organic emissions has a beneficial effect on reducing the O_3 levels (Table 6). Note that a 20% decrease in NO_x emissions from the base case decreases the maximum O_3 at Rubidoux by

more than a 30% decrease in organic emissions for the particular event examined here. This finding differs from the results of some previous studies. Possible reasons for these differences are discussed later.

Just before arriving at Rubidoux, the trajectories pass over a number of farming and animal husbandry operations, resulting in the high observed NH_3 concentrations. One possible control strategy for reducing the AN concentrations could be predicated on relocating these large NH_3 sources. The same result may be achieved indirectly as urban sprawl pushes farming operations further away from the center of the SoCAB. To simulate this possibility, NH_3 emissions from farm-oriented operations (due to livestock waste and fertilizer used for agricultural purposes) were removed from the inventory. The same sets of trajectory calculations used in the previous control measure evaluation study were repeated except that the NH_3 emissions were reduced. These results are given in Table 5. The 24-h average NH_3 concentration at Rubidoux decreased from the base case value of 51.0 ppb down to 4.3 ppb when farm-related activities were eliminated. Decreasing the NH_3 has a tremendous effect on the ammonium nitrate and HNO_3 predictions. With farm-related NH_3 emissions removed, only $2.8 \mu\text{g m}^{-3}$ of nitrate is found in the aerosol phase, compared to $13.3 \mu\text{g m}^{-3}$ of HNO_3 gas, a reversal of the base case. Reducing NH_3 to control AN formation results in an increase in HNO_3 and the problems associated with HNO_3 . Thus, the advantages and disadvantages of this avenue of control must be weighed before any action is taken.

If SINK aerosol is present that can react with HNO_3 to produce AN, reducing the NH_3 emissions does not lead to as large a decrease in AN as was predicted above for the case of a pure NH_3 , HNO_3 and NH_4NO_3 system. Increased HNO_3 concentrations that result from NH_3 removal lead to more BAN being formed due to reaction 58. As shown in Table 7, the 24-h average AN drops from $13.8 \mu\text{g m}^{-3}$ with the base case level of NH_3 emissions to $8.3 \mu\text{g m}^{-3}$ for the reduced NH_3 case—not as drastic a reduction as when no SINK is included in the calculations.

Further reduction of NO_x emissions beyond the 20% anticipated by the AQMP was examined. TN concentrations were seen to decline in almost direct proportion to changes in NO_x emissions. Reducing NO_x emissions by 20, 40, 60 and 80% resulted in a decrease in TN of 18, 45, 64 and 78%, respectively, at

Table 6. Predicted peak 1-h ozone concentrations (ppb) at Rubidoux as a function of emission reductions, 31 August 1982

	NO _x emission reduction				
	0%	20%	40%	60%	80%
% THC reduction					
0%*	190	170	144	117	80
30%	181	166	†	†	†

*0% = base case.

†Not examined.

Table 7. Predicted pollutant concentrations at Rubidoux, California when emissions of SINK aerosol are included

	AN Max 2-h avg ($\mu\text{g m}^{-3}$)	AN 24-h avg ($\mu\text{g m}^{-3}$)	TN 24-h avg ($\mu\text{g m}^{-3}$)	HNO ₃ (g) Max 2-h (ppb)
Base case, no SINK	27.0	11.5	18.6	9.6
Base case, SINK included	29.4	13.8	21.4	9.3
SINK included, NH ₃ emissions reduced	14.4	8.3	18.9	12.7

Rubidoux. A similar, almost linear dependence, between HNO₃ formation and NO_x input was found by Spicer (1983) in smog chamber experiments. Returning to the present study, AN decreased at a slightly greater rate than TN: 27, 58, 78 and 90 % for the four levels of decreased NO_x emissions defined above. Maximum O₃ concentrations predicted at Rubidoux also declined as NO_x emissions were decreased. During the present study, a 60 % reduction in NO_x emissions would have been sufficient to meet the federal O₃ standard along the trajectories ending at Rubidoux.

In some previous modeling studies investigators have found that, contrary to the case examined here, lowering NO_x emissions can increase O₃ concentrations. There are obvious reasons that could account for the different findings and some more subtle reasons, too.

First it is well known that depending on the HC to NO_x ratio in an air parcel, NO_x control can either increase or decrease O₃ concentrations. A different mix of organic gas and NO_x emissions resulting from different trajectory paths and the fact that emission inventories for different years have been used could account for part of the difference in the O₃ response to NO_x emission changes. Along the same lines, some investigators have examined the effect of a further decrease in NO_x emissions only after a large decrease in ROG emissions from mobile sources was imposed. This results in a larger reduction in total ROG emissions than studied here and also a different organic gas emission composition. Also, there are inherent differences in the many models that have been used in the past. More subtle causes for the differences in the outcomes of the calculations may well lie in the way that the trajectories are initialized. If shorter trajectories are used, as has been customary in previous studies, then the choice of initial conditions can play a very large role in determining the results. Application of emission controls will affect those initial conditions, but a great deal of uncertainty surrounds the question of estimating the effect of emission controls on initial conditions for short trajectories that start over land within the air basin. If in previous modeling studies the concentrations of NO and NO₂ in the upper levels of a model at the start of the trajectory were based on ground level observations in the morning, then those NO and NO₂ levels may have been estimated to be much higher than reasonably could be expected. Night-time reactions between NO₂ and O₃ could

convert almost all the NO₂ present aloft at night to HNO₃ by sunrise the next morning (Russell *et al.*, 1985). Organic gases, however, can persist aloft at night because little or no photolysis takes place and because OH radical concentrations are greatly reduced at night. As the mixing depth increases the next day, the air entrained downward from aloft is comparatively lean in NO and NO₂, and, as a result, fresh NO_x emissions are required to promote the formation of O₃.

This study concludes that reducing NO_x emissions will result in lower AN, HNO₃, PAN and NO₂ concentrations. Lowering NO_x and ROG emissions also may decrease the formation of other nitrogenous organic compounds, certain of which are mutagenic and carcinogenic (Ohgaki *et al.*, 1982). For the case considered here, NO_x control, independently or combined with ROG control, also assisted in controlling O₃ at Rubidoux, although it is not clear that this result is true in general at other times and locations.

6. CONCLUSIONS

The predictions of a trajectory model describing the photochemical dynamics of O₃, NO₂, HNO₃, PAN and AN were compared to field measurements. Predicted O₃ and NO₂ concentrations closely followed the measured concentrations. Predicted TN concentrations at Rubidoux were very close to those measured at that site, often matching observations to within experimental error. The ability to closely account for the origin of measured O₃, NO₂ and TN concentrations is one of the most severe tests of a gas phase photochemical model. Model predictions of the apportionment of TN between the aerosol and gas phases compare satisfactorily to the observations through much of the day, although on the average the model underpredicts the HNO₃ concentrations by a fraction of a ppb. This could be due to a number of reasons. Among the more likely reasons are inaccuracies in the interpolated temperature fields and uncertainties in the NH₃ emissions inventory. When the observed ambient NH₃ concentrations and temperature are used to apportion the TN between the gas and aerosol phases, the AN predictions match observations very well. In spite of the uncertainties, the predicted NH₃ levels are close to the observed values, averaging slightly greater than observed, indicating

that the inventory does not differ greatly from the actual emissions.

Control strategy tests indicate that reductions in NO_x emissions would result in nearly proportional reductions in TN formation and slightly greater than proportional reductions in AN. For the cases studied, O_3 concentrations also declined as the NO_x emissions were reduced. Decreasing ROG emissions also lowered O_3 concentrations and decreased organic nitrate (PAN) concentrations, though at the expense of increasing inorganic nitrate formation.

AN formation at Rubidoux would be greatly decreased if NH_3 emissions from farm-related operations were suppressed. However, a corresponding increase in HNO_3 concentrations would be expected to accompany this approach to AN control. Combined emission control strategies can be formulated that include a combination of controls on ROG, NO_x and NH_3 emissions that will achieve a greater control of AN and HNO_3 levels than a strategy predicted on control of only a single precursor species.

Acknowledgements—This work was supported by the California Air Resources Board under Agreement A2-150-32.

REFERENCES

- Baldwin A. C. and Golden D. M. (1979) Heterogeneous atmospheric reactions: sulfuric acid aerosols as tropospheric sinks. *Science* **206**, 562–563.
- Cass G. R., Gharib S., Peterson M. and Tilden J. W. (1982) The origin of ammonia emissions to the atmosphere in an urban area. Open File Report 82-6, Environmental Quality Laboratory, California Institute of Technology, Pasadena, CA.
- Chock D. P., Dunker A. M., Kumar S. and Sloane C. S. (1981) Effect of NO_x emission rates on smog formation in the California South Coast Air Basin. *Envir. Sci. Technol.* **15**, 933–939.
- Chock D. P., Dunker A. M., Kumar S. and Sloane C. S. (1983) Reply to comment on Effect of nitrogen oxide emissions in metropolitan regions, Effect of NO_x emission rates on smog formation in the California South Coast Air Basin and Effect of hydrocarbon and NO_x on photochemical smog formation under simulated transport conditions. *Envir. Sci. Technol.* **17**, 58–62.
- Duce R. A. (1969) On the source of gaseous chlorine in the marine atmosphere. *J. geophys. Res.* **70**, 1775–1779.
- Glasson W. A. (1981) Effect of hydrocarbons and NO_x on photochemical smog formation under simulated transport conditions. *J. Air Pollut. Control Ass.* **31**, 1169–1172.
- Glasson W. A. (1983) Reply to comment on Effect of nitrogen oxide emissions in metropolitan regions, Effect of NO_x emission rates on smog formation in the California South Coast Air Basin and Effect of hydrocarbon and NO_x on photochemical smog formation under simulated transport conditions. *Envir. Sci. Technol.* **17**, 62–63.
- Goodin W. R., McRae G. J. and Seinfeld J. H. (1979) A comparison of interpolation methods for sparse data: application to wind and concentration fields. *J. appl. Met.* **18**, 761–771.
- Gray H. A., Cass G. R., Huntzicker J. J., Heyerdahl E. K. and Rau J. A. (1986) Characteristics of atmospheric organic and elemental carbon particles in Los Angeles. *Envir. Sci. Technol.* (in press).
- Grosjean D. and Fung K. (1984) Hydrocarbons and carbonyls in Los Angeles air. *J. Air Pollut. Control Ass.* **34**, 537–543.
- Hildemann L. M., Russell A. G. and Cass G. R. (1984) Ammonia and nitric acid concentrations in equilibrium with atmospheric aerosols: experiment vs theory. *Atmospheric Environment* **18**, 1737–1750.
- Larson S. M., Cass G. R., Hussey K. J. and Luce F. (1984) Visibility model verification by image processing techniques. Final report to the California Air Resources Board under Agreement A2-077-32, Environmental Quality Laboratory, California Institute of Technology, Pasadena, CA.
- Martens C. S., Wesolowski J. J., Harriss R. C. and Kaifer R. (1973) Chlorine loss from Puerto Rican and San Francisco Bay area marine aerosols. *J. geophys. Res.* **78**, 8778–8792.
- Muck R. E. and Steenhuis T. S. (1982) Nitrogen losses from manure storages. *Agricultural Wastes* **4**, 41–54.
- Ohgaki H., Matsukura N., Morino K., Kawachi T., Sugimura T., Morita K., Tokima H. and Hirota T. (1982) Carcinogenicity in rats of the mutagenic compounds 1-nitropyrene and 3-nitrofluoranthene. *Cancer Lett.* **15**, 1–7.
- Pitts J. N., Winer A. M., Atkinson R. and Carter W. P. L. (1983) Comment on Effect of nitrogen oxide emissions in metropolitan regions, Effect of NO_x emission rates on smog formation in the California South Coast Air Basin, and Effect of hydrocarbon and NO_x on photochemical smog formation under simulated transport conditions. *Envir. Sci. Technol.* **17**, 54–57.
- Ranzieri A. (1983) Private communication: forwarded magnetic tape AR3288, 1982-SCAB point and area source emissions. California Air Resources Board, Sacramento.
- Ranzieri A. (1984) Private communication: forwarded magnetic tape AR3292, 1982-SCAB point and area source emissions. California Air Resources Board, Sacramento.
- Russell A. G. (1985) Formation and control of atmospheric aerosol nitrate and nitric acid. Ph.D. thesis, California Institute of Technology, Pasadena.
- Russell A. G. and Cass G. R. (1984) Acquisition of regional air quality model validation data for nitrate, sulfate, ammonium ion and their precursors. *Atmospheric Environment* **18**, 1815–1827.
- Russell A. G., McRae G. J. and Cass G. R. (1983) Mathematical modeling of the formation and transport of ammonium nitrate aerosol. *Atmospheric Environment* **17**, 949–964.
- Russell A. G., McRae G. J. and Cass G. R. (1985) The dynamics of nitric acid production and the fate of nitrogen oxides. *Atmospheric Environment* **19**, 893–903.
- South Coast Air Quality Management District and Southern California Association of Governments (1982) Final Air Quality Management Plan, 1982 Revision.
- Spicer C. W. (1983) Smog chamber studies of NO_x transformation rates and nitrate/precursor relationships. *Envir. Sci. Technol.* **17**, 112–120.
- Steenhuis T. S., Bubbenzer G. D. and Converse J. C. (1982) Ammonia volatilization of winter spread manure. *Trans. Am. Soc. Agric. Engng* **22**, 152–161.
- Winer A. M., Peters J. W., Smith J. P. and Pitts J. N. (1974) Response of commercial chemiluminescent NO – NO_2 analyzers to other nitrogen containing compounds. *Envir. Sci. Technol.* **8**, 1118–1121.

CHAPTER 7

MATHEMATICAL MODELING OF THE FORMATION OF
NITROGEN-CONTAINING AIR POLLUTANTS—I.
EVALUATION OF AN EULERIAN PHOTOCHEMICAL MODEL

**MATHEMATICAL MODELING OF THE FORMATION OF
NITROGEN-CONTAINING AIR POLLUTANTS—I.
EVALUATION OF AN EULERIAN PHOTOCHEMICAL MODEL**

Armistead G. Russell

Department of Mechanical Engineering
Carnegie-Mellon University
Pittsburgh, PA 15213

Kenneth F. McCue and Glen R. Cass

Environmental Quality Laboratory
California Institute of Technology
Pasadena, CA 91125

ABSTRACT

A grid-based, Eulerian airshed model has been used to study the formation and control of gaseous and aerosol phase nitrogen-containing air pollutants. The performance of the model was assessed by comparison against field measurements made for this purpose in the Los Angeles area over the period 30-31 August 1982. Model predictions for O_3 and PAN concentrations are in good agreement with observations. The absolute value of the total inorganic nitrate, NH_3 and HNO_3 predictions on average are within a few ppb of the observations. Lacking an inventory of ionic and alkaline aerosol emissions, accurate apportionment of total inorganic nitrate between the aerosol and gas phases is not possible at coastal locations. At mid-basin sites like Anaheim, where NH_4NO_3 is the dominant nitrate aerosol species present, the aerosol nitrate levels predicted by the model are in good agreement with observed values.

1. Introduction

Nitrogen-containing air pollutants like HNO_3 , aerosol nitrates, and peroxyacetyl nitrate (PAN) are formed as further reaction products of NO_2 in the atmosphere. HNO_3 is implicated as a major contributor to the acid deposition flux in the western U.S., aerosol nitrates contribute to visibility deterioration, and PAN is a well known plant toxicant. Therefore, there is considerable interest in how these pollutants would respond to the imposition of emission controls.

In a previous study, a mathematical model based on the Lagrangian trajectory formulation of the atmospheric diffusion equation was used to test the effects of emissions reductions on the resulting nitric acid, aerosol nitrate, and O_3 concentrations at a receptor site in the Los Angeles basin of California (1). Though a trajectory model is a very valuable tool for determining the probable outcome at a single predetermined location, it may not be the most effective method of determining the basinwide consequences of emission changes, or even the consequences at a large number of sites within a given airshed. In the present paper an Eulerian, grid-based model is used to describe the transport and formation of pollutants, including O_3 , NO_2 , nitric acid, aerosol nitrate, and PAN. Predictions of this model are compared against a set of field experimental data for the 30-31 August 1982 period (2), a data set expressly designed for use in evaluating this type of model. In Part II of this series, the model will be used to test the effects of emission reductions resulting from specific emission control strategies.

2. Model Description

The mathematical model employed by this study is based on numerical solution of the semi-empirical atmospheric diffusion equation for the ensemble mean concentration, $\langle c_i \rangle$, of each pollutant species, i , within the chemical reaction mechanism, R :

$$\frac{\partial \langle c_i \rangle}{\partial t} + \nabla \cdot (\bar{u} \langle c_i \rangle) = \nabla \cdot (K \nabla \langle c_i \rangle) + R_i(\langle c_1 \rangle, \langle c_2 \rangle, \dots, \langle c_n \rangle) \quad (1)$$

where \bar{u} is the wind velocity at the point of interest and K is the atmospheric eddy diffusivity tensor (3). Aside from the improvements detailed below, the methods used for solving equation (1) are as described by McRae et al. (4,5) and Russell et al. (6) and will not be repeated here.

In previous studies, operator splitting techniques were used to decouple the horizontal transport, vertical transport, and chemical reaction components of the atmospheric diffusion equation. In this study, the vertical diffusion remains coupled to the chemical reaction component, so that the resulting sequence is

$$c^{n+1} = A_x A_y [A_{z,c} (2\Delta t)] A_y A_x c^{n-1} \quad (2)$$

where A_x , A_y are the numerical approximations to the horizontal transport operators; $A_{z,c}$ is the approximation to the combined, simultaneous vertical transport and chemical reaction operator; n is the time level and Δt the time step.

A second major difference between this study and the earlier studies is that the chemical reaction mechanism and the associated rate constants have been updated. Because this study concerns itself not only with the formation of O_3 and NO_2 , but also with the production of nitric acid, aerosol nitrate, and PAN, it is necessary to treat the N_xO_y chemistry in much greater detail. The chemical reaction mechanism tracks 28 pollutant species (Table 1) and includes 58 reactions (Table 2). Of particular importance is the expanded treatment of reactions involving the NO_3 radical and N_2O_5 which can be important at night (9). The ability of a Lagrangian trajectory model employing this chemical mechanism to predict the concentrations of O_3 , NO_2 , NO_3 , HNO_3 , and PAN has been verified in previous studies (1,9).

Ammonium nitrate aerosol concentrations (NH_4NO_3 , Table 1) are calculated in the model as being at thermodynamic equilibrium with HNO_3 and NH_3 (10) using the scheme outlined in reference 6. The apportionment of total inorganic nitrate (TN =

Table 1

Definition of Chemical Species Symbols
Used in the Chemical Mechanism of Table 2

ABBREVIATED NAME	FULL NAME
NO	NITRIC OXIDE
NO ₂	NITROGEN DIOXIDE
O ₃	OZONE
HCHO	FORMALDEHYDE
RCHO	LUMPED ALDEHYDE
OLE	LUMPED OLEFIN
ALK	LUMPED ALKANE
ARO	LUMPED AROMATIC
C ₂ H ₄	ETHYLENE
PAN	PEROXYACETYL NITRATE
N ₂ O ₅	DINITROGEN PENTOXIDE
HNO ₂	NITROUS ACID
NO ₃	NITRATE RADICAL
RONO	LUMPED NITRATE
RNO ₄	LUMPED PEROXY NITRATE (RO ₂ NO ₂)
HNO ₄	PEROXY NITROUS ACID (HO ₂ NO ₂)
HO ₂	HYDROPEROXYL RADICAL
RO	ALKOXYL RADICAL
RO ₂	PEROXYALKYL RADICAL
RCO ₃	PEROXYACYL RADICAL
O	ATOMIC OXYGEN
OH	HYDROXYL RADICAL
CO	CARBON MONOXIDE
H ₂ O ₂	HYDROGEN PEROXIDE
CO ₂	CARBON DIOXIDE
HNO ₃	NITRIC ACID
NH ₃	AMMONIA
NH ₄ NO ₃	AMMONIUM NITRATE AEROSOL
RNO ₃	ALKYL NITRATE
RPN	NITROXYPEROXYALKYL NITRATES AND DINITRATES

Table 2

Kinetic Mechanism
(References 4,7,8,9)

reaction #	reaction	notes
1	$\text{NO}_2 + h\nu \rightarrow \text{NO} + \text{O}$	
2	$\text{O} + \text{O}_2 + \text{M} \rightarrow \text{O}_3 + \text{M}$	
3	$\text{O}_3 + \text{NO} \rightarrow \text{NO}_2 + \text{O}_2$	
4	$\text{NO}_2 + \text{O} \rightarrow \text{NO} + \text{O}_2$	
5	$\text{NO} + \text{O} \rightarrow \text{NO}_2$	
6	$\text{NO}_2 + \text{O} \rightarrow \text{NO}_3$	
7	$\text{O}_3 + \text{NO}_2 \rightarrow \text{NO}_3 + \text{O}_2$	
8	$\text{NO}_3 + \text{NO} \rightarrow \text{NO}_2 + \text{NO}_2$	
9	$\text{NO} + \text{OH} \rightarrow \text{HNO}_2$	
10	$\text{HNO}_2 + h\nu \rightarrow \text{OH} + \text{NO}$	
11	$\text{HO}_2 + \text{NO}_2 \rightarrow \text{HNO}_2 + \text{O}_2$	
12	$\text{HNO}_2 + \text{OH} \rightarrow \text{H}_2\text{O} + \text{NO}_2$	
13	$\text{NO}_2 + \text{HO}_2 \rightarrow \text{HNO}_4$	
14	$\text{HNO}_4 \rightarrow \text{HO}_2 + \text{NO}_2$	
15	$\text{HO}_2 + \text{NO} \rightarrow \text{NO}_2 + \text{OH}$	
16	$\text{RO}_2 + \text{NO} \rightarrow \text{NO}_2 + \text{RO}$	
17	$\text{RCO}_3 + \text{NO} \rightarrow \text{NO}_2 + \text{RO}_2 + \text{CO}_2$	
18	$\text{NO}_2 + \text{OH} \rightarrow \text{HNO}_3$	
19	$\text{CO} + \text{OH} \rightarrow \text{HO}_2 + \text{CO}_2$	
20	$\text{O}_3 + h\nu \rightarrow \text{O} + \text{O}_2$	
21	$\text{HCHO} + h\nu \rightarrow \text{HO}_2 + \text{HO}_2 + \text{CO}$	
22	$\text{HCHO} + h\nu \rightarrow \text{H}_2 + \text{CO}$	
23	$\text{HCHO} + \text{OH} \rightarrow \text{HO}_2 + \text{H}_2\text{O} + \text{CO}$	
24	$\text{RCHO} + h\nu \rightarrow \text{RO}_2 + \text{HO}_2 + \text{CO}$	
25	$\text{RCHO} + \text{OH} \rightarrow \text{RCO}_3 + \text{H}_2\text{O}$	
26	$\text{C}_2\text{H}_4 + \text{OH} \rightarrow \text{RO}_2$	
27	$\text{C}_2\text{H}_4 + \text{O} \rightarrow \text{RO}_2 + \text{HO}_2$	
28	$\text{OLE} + \text{OH} \rightarrow \text{RO}_2$	
29	$\text{OLE} + \text{O} \rightarrow \text{RO}_2 + \text{RCO}_3$	
30	$\text{OLE} + \text{O}_3 \rightarrow (\text{A1})\text{RCHO} + (\text{A2})\text{HCHO} + (\text{A3})\text{HO}_2 + (\text{A4})\text{RO}_2 + (\text{A5})\text{OH} + (\text{A6})\text{RO}$	(a)
31	$\text{ALK} + \text{OH} \rightarrow \text{RO}_2$	
32	$\text{ALK} + \text{O} \rightarrow \text{RO}_2 + \text{OH}$	
33	$\text{ARO} + \text{OH} \rightarrow \text{RO}_2 + \text{RCHO}$	
34	$\text{RO} \rightarrow (\text{B1M})\text{RO}_2 + (\text{B1})\text{HO}_2 + (\text{B2})\text{HCHO} + (\text{B3})\text{RCHO}$	(b)
35	$\text{RONO} + h\nu \rightarrow \text{NO} + \text{RO}$	
36	$\text{RO} + \text{NO} \rightarrow \text{RONO}$	
37	$\text{RO} + \text{NO}_2 \rightarrow \text{RNO}_3$	
38	$\text{RO} + \text{NO}_2 \rightarrow \text{RCHO} + \text{HNO}_2$	
39	$\text{NO}_2 + \text{RO}_2 \rightarrow \text{RNO}_4$	
40	$\text{H}_2\text{O}_2 + \text{OH} \rightarrow \text{HO}_2 + \text{H}_2\text{O}$	
41	$\text{RNO}_4 \rightarrow \text{NO}_2 + \text{RO}_2$	
42	$\text{RCO}_3 + \text{NO}_2 \rightarrow \text{PAN}$	
43	$\text{PAN} \rightarrow \text{RCO}_3 + \text{NO}_2$	
44	$\text{NO}_2 + \text{NO}_3 \rightarrow \text{N}_2\text{O}_5$	

Table 2

Kinetic Mechanism
(References 4,7,8,9)

reaction #	reaction	notes
45	$\text{N}_2\text{O}_5 \rightarrow \text{NO}_3 + \text{NO}_2$	
46	$\text{H}_2\text{O} + \text{N}_2\text{O}_5 \rightarrow \text{HNO}_3 + \text{HNO}_3$	
47	$\text{O}_3 + \text{OH} \rightarrow \text{HO}_2 + \text{O}_2$	
48	$\text{O}_3 + \text{HO}_2 \rightarrow \text{OH} + \text{O}_2 + \text{O}_2$	
49	$\text{O}_3 \rightarrow \text{LOSS (not included)}$	
50	$\text{HO}_2 + \text{HO}_2 \rightarrow \text{H}_2\text{O}_2$	
51	$\text{H}_2\text{O}_2 + h\nu \rightarrow \text{OH} + \text{OH}$	
52	$\text{RO}_2 + \text{RO}_2 \rightarrow \text{RO} + \text{RO}$	
53	$\text{NO}_3 + \text{HCHO} \rightarrow \text{HNO}_3 + \text{HO}_2 + \text{CO}$	
54	$\text{NO}_3 + \text{RCHO} \rightarrow \text{HNO}_3 + \text{RCO}_3$	
55	$\text{NO}_3 + h\nu \rightarrow \text{NO}_2 + \text{O}$	
56	$\text{NO}_3 + \text{OLE} \rightarrow \text{RPN}$	
57	$\text{NO}_3 + \text{NO}_2 \rightarrow \text{NO} + \text{NO}_2$	
58	$\text{HNO}_3 + \text{NH}_3 \rightarrow \text{NH}_4\text{NO}_3$ ←	

FOOTNOTES

(a) A1 = 0.50, A2 = 0.50, A3 = 0.30, A4 = 0.31, A5 = 0.14, A6 = 0.03

(b) B1 = 1.00, B2 = 0.50, B3 = 0.50, B1M = 1.0 - B1

HNO_3 + aerosol NO_3^-) and ammonia between the gas and aerosol phases is calculated at every second time step ($2\Delta t$) and is important because of the different depositional rates of aerosol and reactive gases. In the present paper, NH_4NO_3 is the only aerosol nitrate species considered due to the lack of an emission inventory for alkaline aerosol that might be available to act as a "sink" for gaseous HNO_3 (see reference 1).

3. Modeling Region

Figure 1 shows the extent of the modeling region used in this study and the boundaries of the South Coast Air Basin (SoCAB) of California. Meteorological fields, topographical details, and emission inventory data were developed over the $150 \text{ km} \times 400 \text{ km}$ system of $5 \text{ km} \times 5 \text{ km}$ grid cells shown in Figure 1. In the vertical dimension, the model is subdivided into five cells. Starting from ground level, the vertical cell dimensions are 38, 116, 154, 363, and 429 m, reaching an aggregate height of 1100 m above ground level.

4. Meteorological Fields

Meteorological fields required for model evaluation were calculated by interpolating individual measurements available from the South Coast Air Quality Management District (SCAQMD), the California Air Resources Board (CARB), and the National Weather Service (NWS) over the computational grid (12) as described in an earlier trajectory model evaluation study (1). Additional hourly, three-dimensional wind fields were developed using the two-dimensional ground level wind fields and upper level wind measurements gathered from seven locations at a variety of times throughout the day. Solar radiation measurements were obtained at Pasadena, Upland, and Central Los Angeles from the Jet Propulsion Laboratory, the CARB, and the SCAQMD, respectively. These data, along with cloud cover observations, were used to determine the insolation levels within the modeling region.

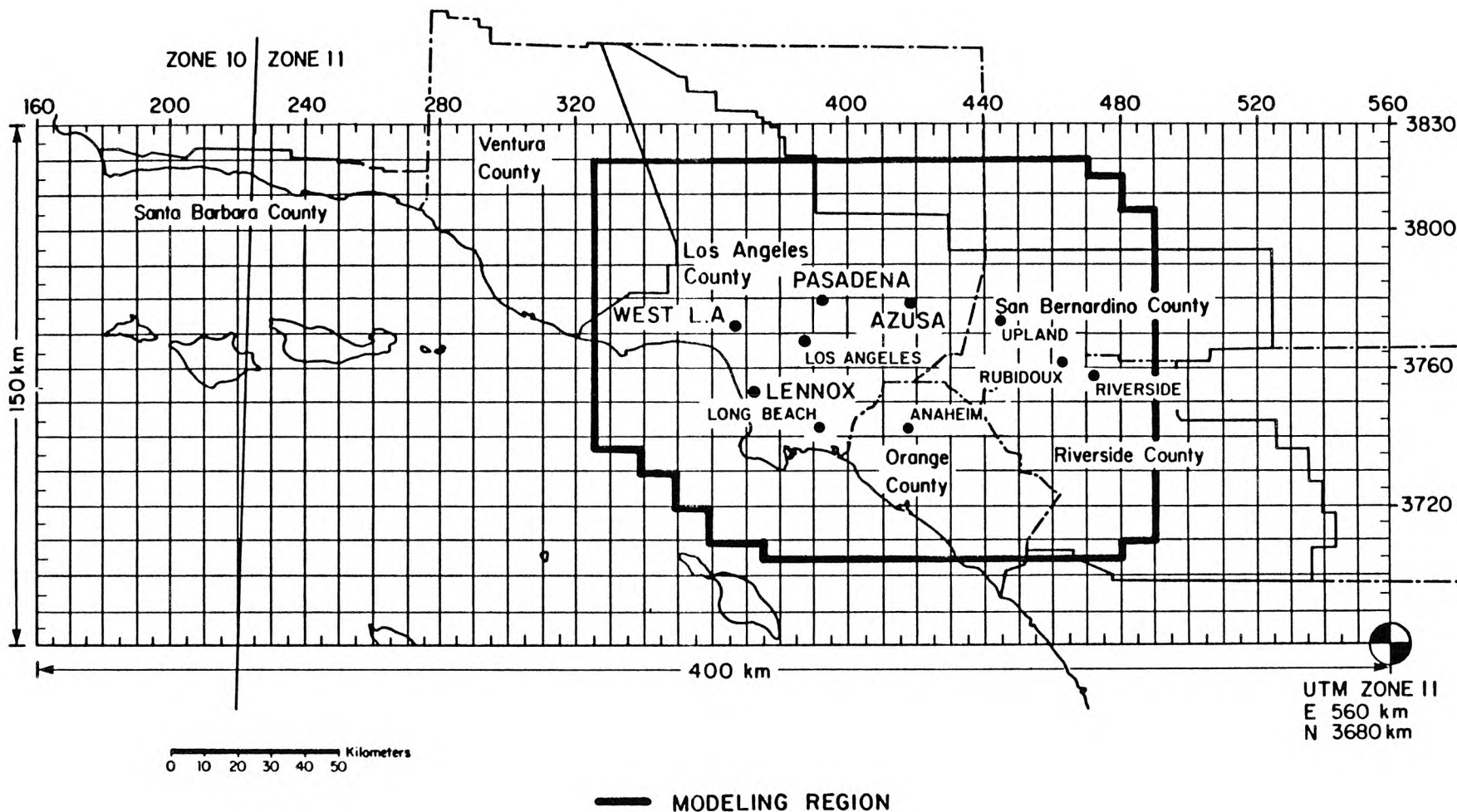


Figure 1. The South Coast Air Basin of California, plus Ventura and Coastal Santa Barbara Counties. Emissions and meteorological data fields are developed over the 150 km \times 400 km gridded area. Air monitoring sites at which HNO_3 , NH_3 , and aerosol nitrate data are available from reference (2) and are shown by (●). Air quality modeling calculations are performed within the region bounded by the heavy solid line in the center of the map.

5. Pollutant Emissions

NO_x , speciated hydrocarbons, and CO emissions were calculated for every hour and grid in the SoCAB from the 1982 forecast emission inventory provided by the CARB (13,14). A 1982 ammonia emissions inventory was developed for use in this study (15). These emission data are presented in detail by Russell and Cass (1) and, therefore, will not be repeated here. Actual NO_x emissions data for each electric utility generating station were obtained for the two days modeled from the SCAQMD along with August 1982 emission data for fuel burning at the petroleum refineries. These data replaced the CARB forecast emissions from electric utility and refinery fuel burning, lowering the total area-wide emissions of NO_x from the 1134 metric tons/day given in reference (1) down to 1120 metric tons/day. The spatial distribution of pollutant emissions is shown in Figure 2.

6. Initial and Boundary Conditions

Concentrations of O_3 , NO_2 , NO, SO_2 , CO, and total hydrocarbons (THC) are measured throughout the basin, and hourly averaged values are recorded by the SCAQMD. The concentrations of $\text{HNO}_3(\text{g})$, $\text{NH}_3(\text{g})$, PAN, aerosol nitrate, and ammonium ion on 30-31 August 1982 were measured as part of a field experiment conducted specifically to acquire model verification data (2). These values then were interpolated to form a two-dimensional ground level initial concentration field over the basin for those pollutants at 0000 hrs Pacific Standard Time (PST), 30 August 1982. The initial concentration of PAN (which was measured at only one location at the beginning of the experiment) was set to one-tenth of the initial O_3 level (on a ppm basis). Upper level O_3 initial conditions were set to the previous 1400 PST ground level O_3 concentrations following the results of Blumenthal et al. (16) and Edinger (17). Trajectory simulations and the experimental results of Sonoma Technology (18) indicated that the NO and NO_2 levels above the mixed

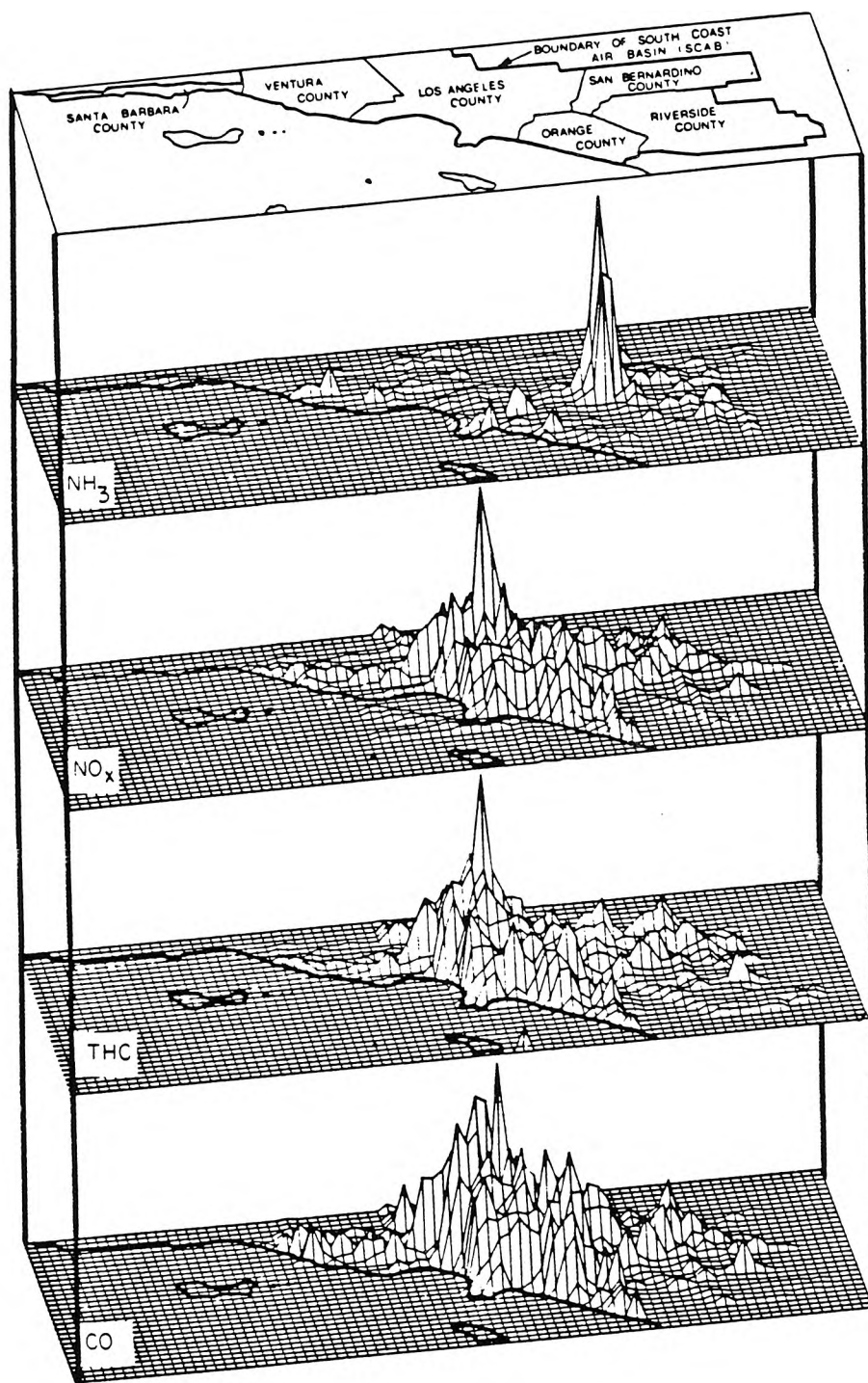


Figure 2. The spatial distribution of NH_3 , NO_x , total hydrocarbons, and CO emissions within the grid system for the summer of 1982.

layer at 0000 hrs PST would be very low, and the initial concentrations of those species aloft were set to zero.

Total hydrocarbon measurements taken by the SCAQMD are not speciated into the different organic compounds actually present. Thus, a set of factors must be developed to split the measured initial hydrocarbon concentrations into the six hydrocarbon classes used by the model. This process is complicated by the need to split the hydrocarbons into the six classes over three distinct regions in which one would expect a very different chemical composition: the urban area, rural surroundings, and over the ocean. Three sets of splitting factors were developed, one for each of the different regions, and are shown in Table 3. Urban area factors were derived from the measurements of Grosjean and Fung (19), and the ocean and rural factors were calculated from measurements (18) and previous modeling analysis (7). The effect of these assumptions about initial conditions on the resulting predictions are minimized by conducting multiday calculations (since subsequent emissions into the model are fully speciated).

Ground level boundary conditions are derived from the interpolated pollutant concentration fields discussed earlier. Those concentration fields start with Pacific Ocean background values (in ppb: O₃, 40; NO₂, 10; NO, 10; CO, 100; HNO₃, 1; NH₃, 1; THC, 1000) at the western edge of the large grid shown in Figure 1 and rise to match the on-land values at near-coastal monitoring sites. The smaller modeling region shown in Figure 1 is superimposed on these concentration fields, and the surface level boundary conditions supplied to the model are defined by the values of the interpolated concentration fields that prevail at the edges of the modeling region. Boundary conditions above the mixed layer at the western, upwind boundary of the modeling region over the ocean were set to a column average of 60 ppb O₃, 250 ppb reactive hydrocarbons, 0.0 ppb NO and NO₂, 1 ppb HNO₃, 4 ppb NH₃, and 3.25 $\mu\text{g m}^{-3}$ aerosol nitrate. The hydrocarbon value was derived from

Table 3
Hydrocarbon Splitting Factors

	URBAN	RURAL	OCEAN
HCHO	0.0037	0.0010	0.0010
RCHO	0.0033	0.0020	0.0050
OLE	0.0042	0.0006	0.0001
ALK	0.0675	0.0226	0.0096
ARO	0.0177	0.0052	0.0017
C ₂ H ₄	0.0061	0.0040	0.0060

For example, the initial HCHO concentration equals 0.0037 x THC measured in ppmC. The splitting factors above incorporate the conversion from total hydrocarbons given in ppmC to molecular concentrations in ppmV.

reports by Sonoma Technology (18) and Killus (20), while the O_3 , NO, and NO_2 values were based on work by Sonoma Technology (18). Upper-level, downwind boundary conditions are set as a function of the predicted pollutant concentrations in air advected out of the basin.

7. Model Application on 30-31 August 1982

Prediction of pollutant concentrations as a function of time began at 0000 hrs PST, 30 August 1982, and was continued for 48 hours. Of the species being modeled, particular attention is paid to NO, NO_2 , O_3 , PAN, HNO_3 , aerosol nitrate, and NH_3 , for which ambient measurements are available for comparison. Previous grid-model evaluation studies have relied on comparison of measurements to predicted concentrations of O_3 and, at times, NO_2 . The present study provides a much more stringent test of the photochemical model as it compares results for HNO_3 , aerosol NO_3^- , NH_3 , and PAN as well as NO_2 and O_3 .

The August 30-31 data set (2) used in this study is the only model evaluation data set in existence with region-wide short-term average observations on all of the unregulated nitrogen-containing pollutants of interest here: HNO_3 , NH_3 , aerosol nitrate and PAN. For that reason, the August 30-31, 1982, time period is the best choice for a model evaluation study of NO_x -derived unregulated pollutants. Ozone concentration predictions are an interesting by-product of this study. While these days were not chosen primarily for their ozone data, it can be noted that the representativeness of the August 31 period as an O_3 modeling event in the Los Angeles area has been examined by Horie (21). August 31, 1982, was found to fall within one of the two most common types of high O_3 event days in the Los Angeles area. That class of events is characterized by a strong temperature inversion, a west to northwest morning wind at Los Angeles International Airport, and an average peak O_3 concentration of 0.235 ppm. If the characteristics of days of this type

are ranked by their deviation from the mean of all similar days, August 31, 1982, would fall within the closest 25% of the days to the group norm.

Results from the model calculation for the two days are presented in two formats. First, a series of concentration isopleths are given for O_3 , NO_2 , HNO_3 , aerosol nitrate, and NH_3 for the second day (31 August) of the simulation in Figure 3. This provides a convenient means for studying the temporal and spatial evolution of the pollutants, making it easier to judge where the highest concentrations of the pollutants can be expected. A second method for presenting the results allows for visual evaluation by plotting the predicted concentrations as a function of time along with the measurements from a monitoring station in the same grid location. This has been done for a number of locations across the Los Angeles basin (Figures 4-7).

Figure 3 shows the predicted spatial distribution of pollutant concentrations at three-hour intervals throughout the day of 31 August. NO_2 levels peak in the early morning in the western and coastal part of the basin, followed by declining values throughout the remainder of the day. HNO_3 concentrations begin at low levels throughout the basin at 0800 hrs PST. By 1100 hrs PST, NO_2 oxidation to form nitric acid accompanied by higher ambient air temperatures leads to the accumulation of $HNO_3(g)$ concentrations above 15 ppb within a zone stretching from central Orange County through the Pomona, San Gabriel and San Fernando Valleys in eastern and northern Los Angeles County. At the same time, very low HNO_3 concentrations (below 3 ppb) occur in adjacent portions of Riverside and San Bernardino Counties. That zone of low HNO_3 levels is centered over the Chino dairy area where high levels of NH_3 (see the NH_3 concentration predictions in Figure 3 and the tall spike in the NH_3 emissions inventory in Figure 2) from decomposition of livestock waste and from farm related fertilizer use act to drive the inorganic nitrate present into the aerosol phase. By 1400 hrs PST the $HNO_3(g)$ concentrations are declining, with the highest remaining levels in north Los Angeles County between Azusa and

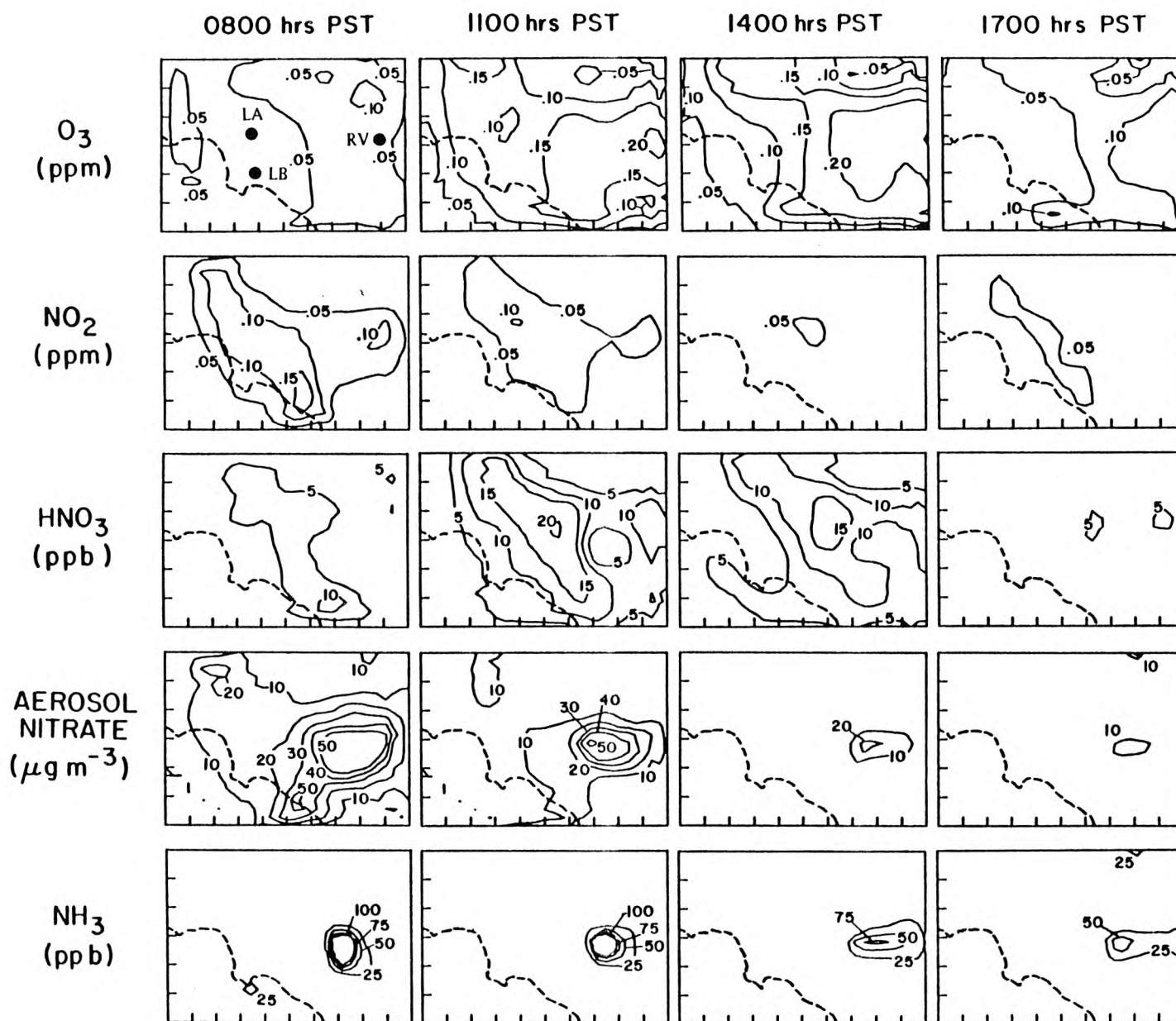


Figure 3. The spatial distribution of predicted concentrations of O_3 , NO_2 , HNO_3 , aerosol nitrate, and NH_3 at 0800, 1100, 1400, and 1700 hrs PST 31 August 1982. (Location code: LB = Long Beach; LA = downtown Los Angeles; RV = Riverside)

Figure 4. Comparison of predicted and observed ozone concentrations in the South Coast Air Basin, 30-31 August 1982.

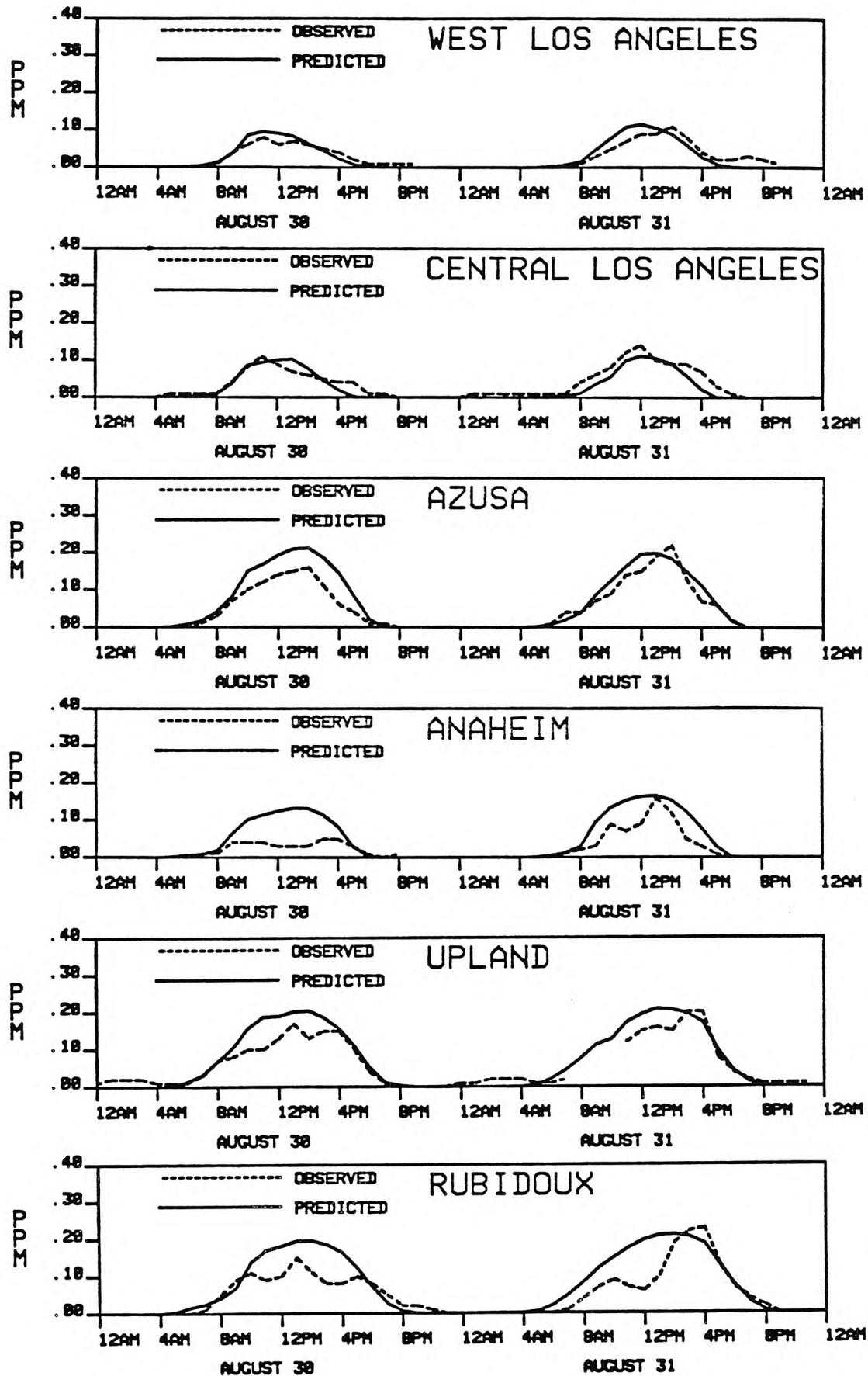


Figure 5. Comparison of predicted and observed concentrations of NO_2 , TN, HNO_3 , aerosol nitrate, and NH_3 at Central Los Angeles on 30-31 August 1982.

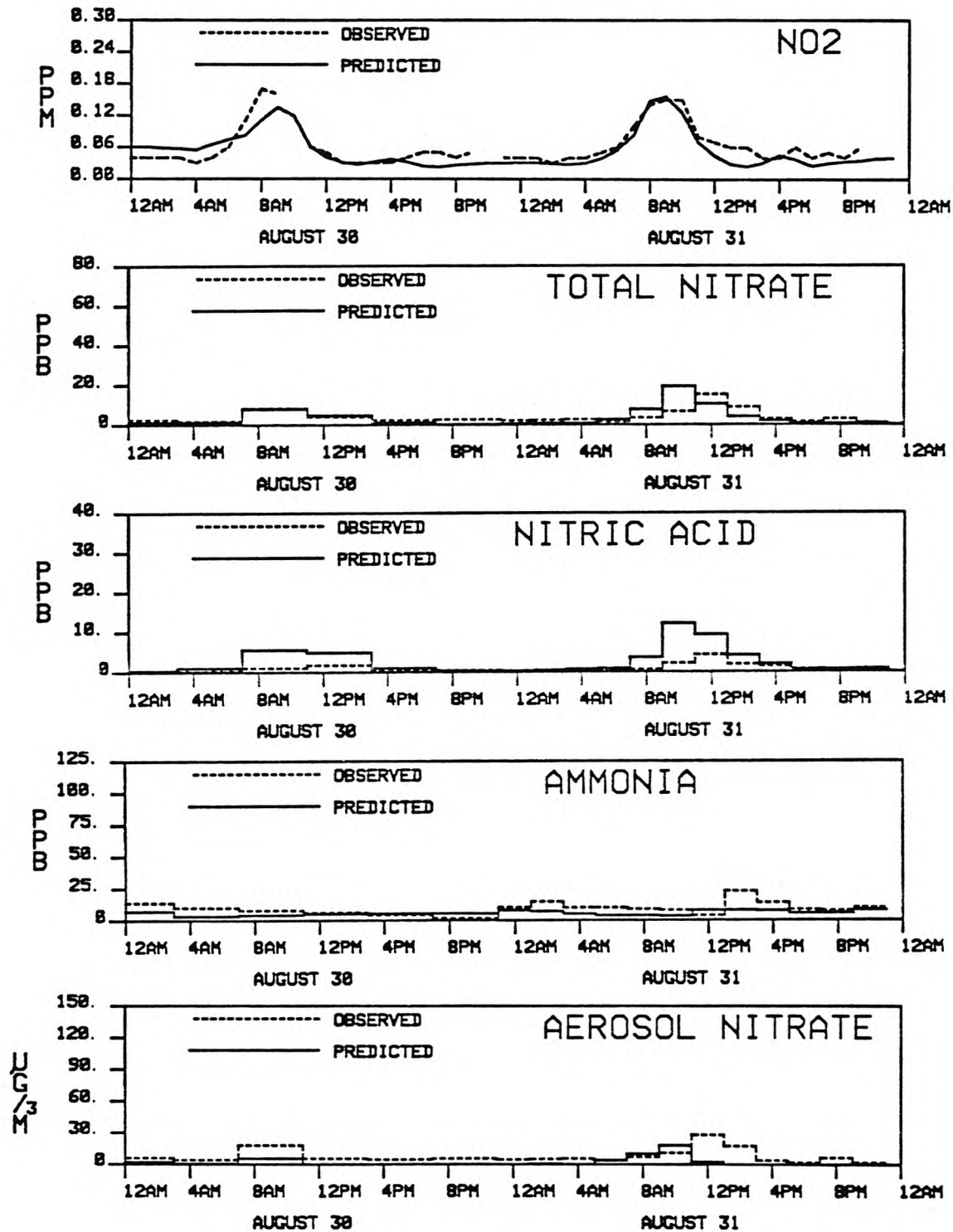


Figure 6. Comparison of predicted and observed concentrations of NO_2 , TN, HNO_3 , aerosol nitrate, and NH_3 at Anaheim on 30-31 August 1982.

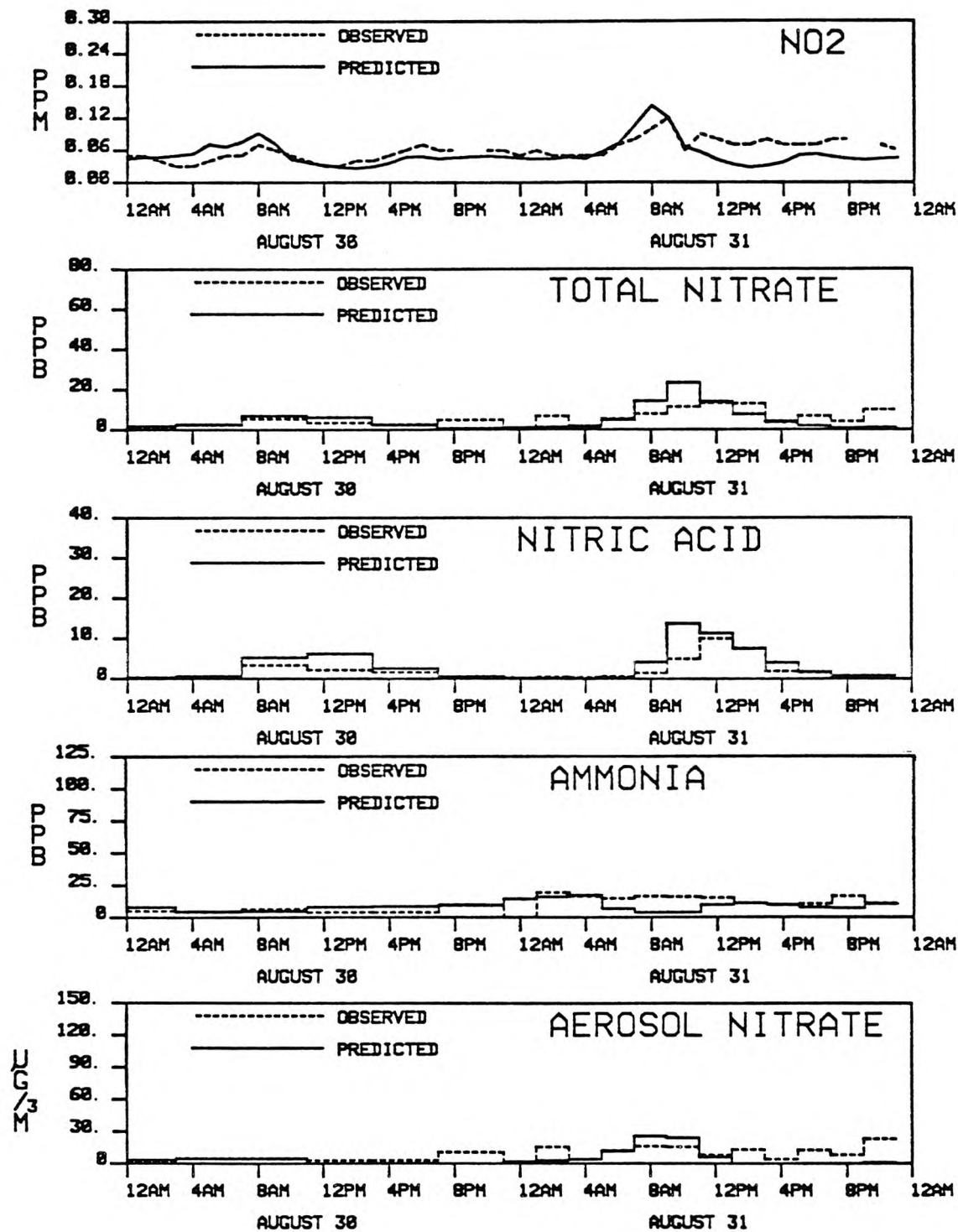
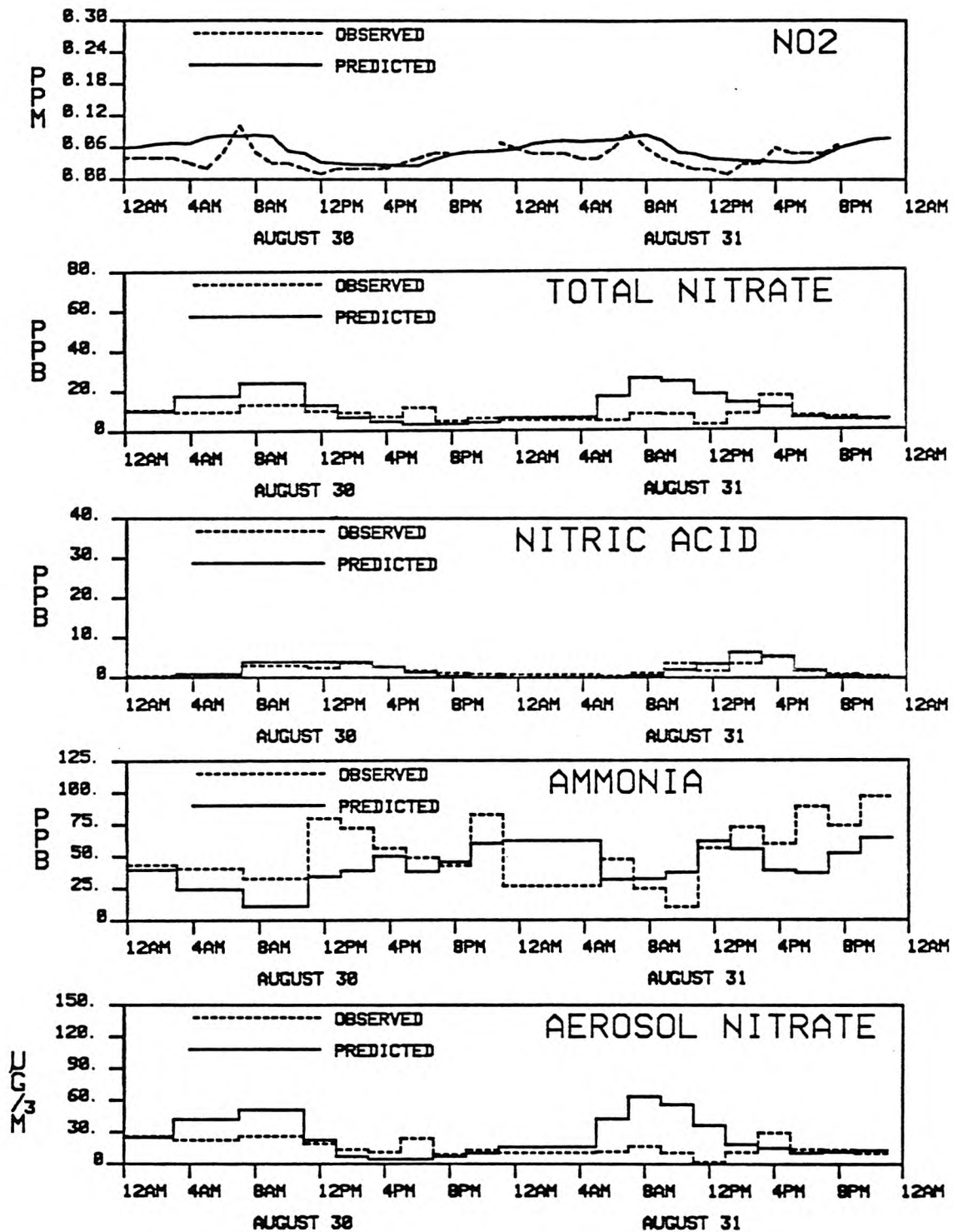


Figure 7. Comparison of predicted and observed concentrations of NO_2 , TN, HNO_3 , aerosol nitrate, and NH_3 at Rubidoux on 30-31 August 1982.



Claremont (near Upland). By 1700 hrs PST in the late afternoon on this particular day, $\text{HNO}_3(\text{g})$ concentrations have returned to low values.

Ozone concentration predictions are compared to observations in time series at six widely spaced monitoring sites in Figure 4. At some near-coastal sites, ozone predictions exceed observations in a manner similar to the results shown for Anaheim in Figure 4. However, at the mid-basin and inland monitoring stations where high ozone concentrations occur, model predictions are generally in excellent agreement with measured ozone values.

Figures 5-7 show the time series of model predictions and experimental observations for nitrogen-containing pollutants at locations moving from west to east across the air basin. At Central Los Angeles, predicted and observed NO_2 and TN values are generally in good agreement except that the timing of the TN peak occurs one interval prior to the time of the observed peak. At Los Angeles and at the coastal sites in the western portion of the air basin, the partition of TN between $\text{HNO}_3(\text{g})$ and aerosol nitrate by the model results in more HNO_3 and less aerosol than is actually observed. This is consistent with previous analysis of the aerosol data at the coastal sites (22) that showed that the nitrate aerosol present near the coast is not pure NH_4NO_3 aerosol. Near the coast, sea salt (or other alkaline aerosol) has stripped the $\text{HNO}_3(\text{g})$ forming non- NH_4NO_3 aerosol nitrate. In a prior analysis of aerosol nitrate formation using a trajectory version of this photochemical model, the heterogeneous reaction between HNO_3 and pre-existing "sink" aerosol (such as NaCl) was simulated (1). In the present study, only the reaction between NH_3 and HNO_3 was included because an accurate description of the chemical composition of aerosol emissions across the entire SoCAB was unavailable. With this heterogeneous reaction step missing, we do not expect to be able to fully account for the partition of total inorganic nitrate between the aerosol and gas phases. This explains why aerosol nitrate is underpredicted at the near-coastal sites (Lennox,

Long Beach, West Los Angeles, and Central Los Angeles) by the present model that incorporates only NH_4NO_3 formation.

Total inorganic nitrate concentrations (TN) measured at ten monitoring stations vary from low values at coastal locations to higher values inland near Rubidoux. The predicted TN concentrations follow the same geographic trends. Since TN accounts for only a very small portion of airborne NO_x -related species, very small absolute differences between the observed and predicted partition of the total oxidized nitrogen in the system between NO_2 , PAN, and TN have the appearance of a large relative difference between observed and predicted TN; in an absolute sense, TN predictions are close to the observations at most sites, as will be discussed in Section 8. At four sites (Anaheim, Los Angeles, Pasadena and Rubidoux), the predicted TN concentration peaks earlier in the morning than does the measured TN concentration. Though the reasons for this result are not certain, this effect could be achieved if the mixing depth as modeled is lower than the actual mixing depths at those times, trapping more nitrate close to the ground. It is difficult to estimate mixing depths precisely during the morning as the inversion base is rising rapidly. The early peak in TN levels also could be produced by faster than actual oxidation of NO_2 by the OH radical to form HNO_3 . OH radical concentration measurements are scarce, and none were available against which to compare model predictions. Predicted midday OH concentrations ranged from 8×10^{-8} ppm to 1.6×10^{-7} ppm, while predicted midday HO_2 levels ranged from 1×10^{-5} ppm to 5×10^{-5} ppm.

Differences between the predicted and observed $\text{HNO}_3(\text{g})$ are governed by the problems inherent in distributing total inorganic nitrate between the aerosol and gas phases. At mid-basin sites like Anaheim, both TN and NH_3 are predicted to be close to the observed values and an ion balance on the composition of the measured aerosol (22) shows that NH_4NO_3 is present. In that case the major assumptions

of the model are satisfied and the observed and predicted HNO_3 and aerosol nitrate also are close to observed values. Far downwind, overpredictions of aerosol nitrate at Rubidoux and Upland occur due to the overprediction of total inorganic nitrate formation just discussed. HNO_3 levels predicted at Rubidoux are still close to observed values in spite of the overprediction of TN because the NH_3 concentration and the temperature modulate the $\text{HNO}_3(\text{g})$ concentrations via the NH_4NO_3 equilibrium dissociation constant and the NH_3 is in great excess at that site.

PAN measurements were taken at two sites during the August 1982 field experiment: the University of California at Riverside (UCR) and the California Institute of Technology (Caltech) in Pasadena. The peak measured PAN concentration was 17 ppb at UCR between 1400-1500 hrs PST 31 August. The predicted PAN peak at UCR was 16 ppb between 1200 and 1300 hrs the same day. The predicted PAN concentration at the time of the measured peak was 15 ppb. At Caltech, the measured maximum PAN concentration was 9 ppb between 1300 and 1500 hrs on 31 August, which compares well to the predicted maximum of 7 ppb occurring during the same time period. The agreement between predicted and measured PAN concentrations for the two days at Pasadena is excellent, as shown in Figure 8.

8. Statistical Evaluation of Model Results

Visual inspection of graphs showing predicted and observed pollutant concentrations provides one method for assessing air quality model performance. However, when the number of monitoring sites to be examined grows large, the amount of information to be absorbed and evaluated by that means can become overwhelming. A number of investigators have addressed the problem of objective evaluation of model performance and have proposed a variety of statistical tests that can be applied to judge the quality of the model's results (23,24,25). In this study, a wide range of performance measures is presented following the format of McRae and Seinfeld (7); for brevity, the significance and relevance of each test is given only for

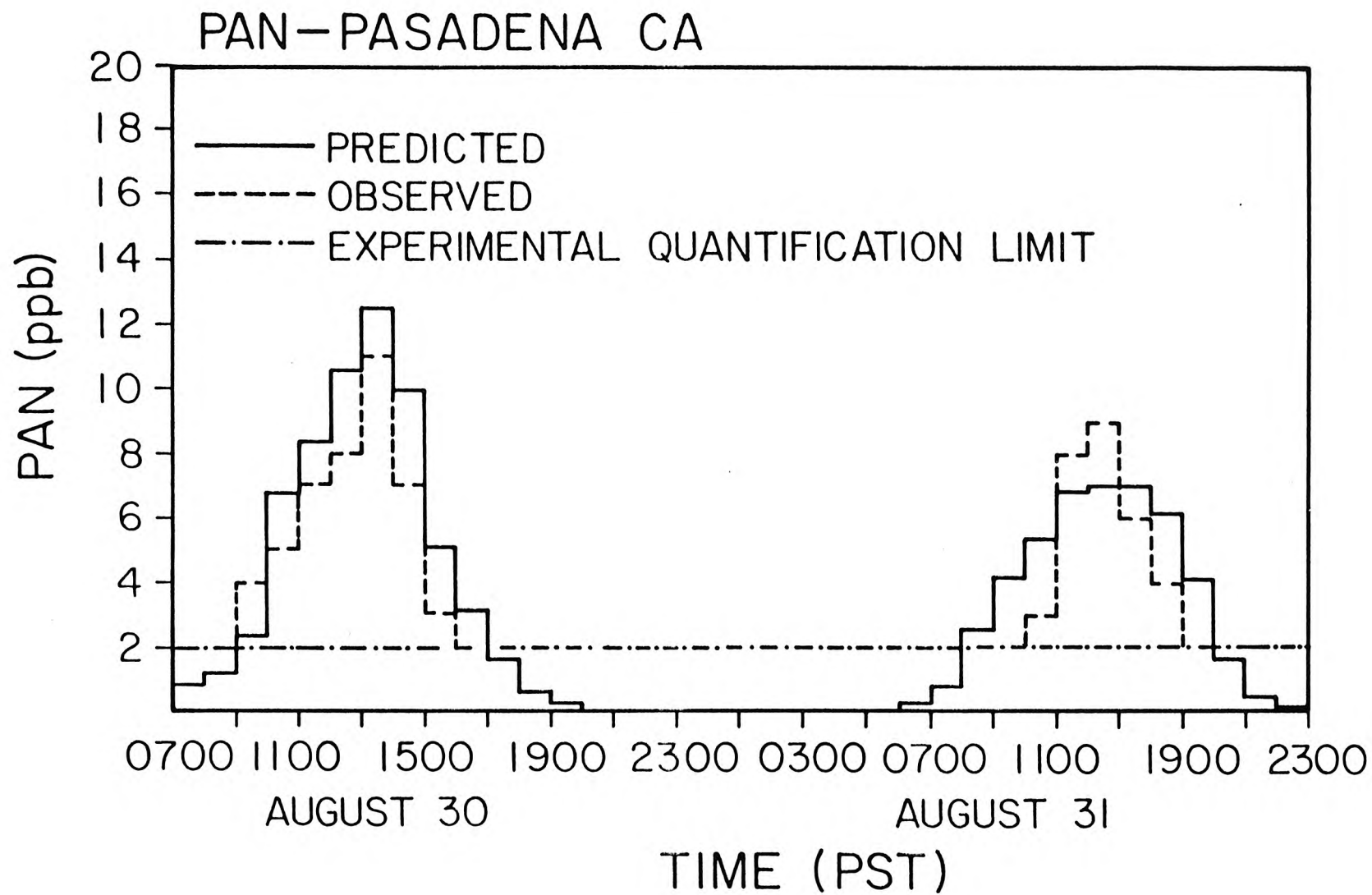


Figure 8. Comparison of predicted and observed PAN concentrations at Pasadena on 30-31 August 1982.

those tests not described in that study. A statistical description of model performance for O_3 and NO_2 is given in Table 4. Corresponding statistics for total inorganic nitrate, NH_3 , HNO_3 , and aerosol nitrate are given separately in Table 5.

As seen in Table 4, the model performance measures for O_3 are excellent. In the case of NO_2 , the predictions are unbiased and the absolute accuracy (RMS error, peak prediction, % residuals within 0.05 ppm) is good, much better than would be expected if one looked only at a correlation analysis. The low correlation coefficient is due to two factors: (1) the predicted NO_2 peaks occur at a slightly different time than the observed peaks (typically the timing of the observed and predicted morning NO_2 peaks differ by one to two hours), and (2) measurements at some locations are anomalous (e.g., NO_2 concentrations reported at the Pasadena SCAQMD station over time do not track the observations at surrounding stations). The correlation coefficient and least squares coefficients are extremely sensitive to any offset between predicted and observed peaks (7,24). Residual frequency plots (Figure 9) show that the residual differences between the predicted and observed concentrations of O_3 and NO_2 center about zero (little or no bias) in approximately a Gaussian form. The RMS error values given in Table 4 provide a measure of the spread of the O_3 and NO_2 residual histograms in Figure 9.

Evaluation of the model's ability to predict nitrate-containing species concentrations can be broken into three steps: (1) the ability to predict correctly the formation of total inorganic nitrate (this is a test of the photochemical, gas phase mechanism); (2) the ability to reproduce correctly the NH_3 concentrations (this evaluates the accuracy of the ammonia emissions inventory and transport calculations); and, given that the first two steps are handled adequately, (3) use of the predicted NH_3 concentrations to apportion the TN between the gas and aerosol phases. Approaching the problem in this order, a statistical comparison of the paired predicted and observed TN concentrations was constructed and is summar-

Table 4^(a)

Statistical Evaluation of Model Performance
for O₃ and NO₂

Performance Measure	Results of Test		Remarks
	O ₃	NO ₂	
Mean of residuals (bias)	0.010 ppm (20%)	-0.002 ppm (-5%)	Predictions and measurements agree closely on the average.
RMS error about the mean (σ of residuals)	0.037 ppm	0.030 ppm	The RMS error about the mean is lower than in previous studies.
Accuracy of peak prediction ^(b)	$\frac{0.262}{0.26} = 1.01$	$\frac{0.157}{0.17} = 0.92$	The magnitudes of the peak predictions are in excellent agreement for both O ₃ and NO ₂ .
Correlation coefficient	0.83	0.43	The predicted and measured O ₃ values agree closely. The low correlation for NO ₂ is due to the prediction that the NO ₂ peaks occur at slightly different times than the measured peaks.
Linear least squares fit			
$C_{OBS} = MC_{PRED} + B$	M = 1.11 B = 0.006	0.47 0.026	Again the O ₃ results are excellent. NO ₂ results suffer from the peak timing problem detailed above.
% of residuals \leq bounds = 0.05 ppm	86%	93%	There are very few outliers.

Notes on Table 4:

- (a) McRae and Seinfeld (7) explain the significance of the performance measures.
- (b) The predicted and observed peak values occur near each other but not necessarily at exactly the same air monitoring site.

Table 5

Statistical Evaluation of Model Performance
for Total Inorganic Nitrate, Ammonia,
Aerosol Nitrate, and Nitric Acid

Performance Measure	TN	NH ₃	AN	HNO ₃
Mean of Observations	12.9 $\mu\text{g m}^{-3}$	13.8 ppb	9.5 $\mu\text{g m}^{-3}$	3.4 $\mu\text{g m}^{-3}$
Mean of Predictions	15.6 $\mu\text{g m}^{-3}$	14.6 ppb	8.0 $\mu\text{g m}^{-3}$	7.6 $\mu\text{g m}^{-3}$
Mean of Residuals	2.7 $\mu\text{g m}^{-3}$	0.7 ppb	-1.5 $\mu\text{g m}^{-3}$	4.2 $\mu\text{g m}^{-3}$
RMS Error about the Mean (σ of Residuals)	14 $\mu\text{g m}^{-3}$	16 ppb	12 $\mu\text{g m}^{-3}$	7.8 $\mu\text{g m}^{-3}$
Correlation Coefficient	0.6	0.6	0.4	0.7
Regression Analysis				
$C_{\text{PRED}} = MC_{\text{OBS}} + B$	M = 1.15 B = 0.7 $\mu\text{g m}^{-3}$	M = 0.54 B = 7.0 ppb	M = 0.74 B = 0.94 $\mu\text{g m}^{-3}$	M = 1.7 B = 1.9 $\mu\text{g m}^{-3}$

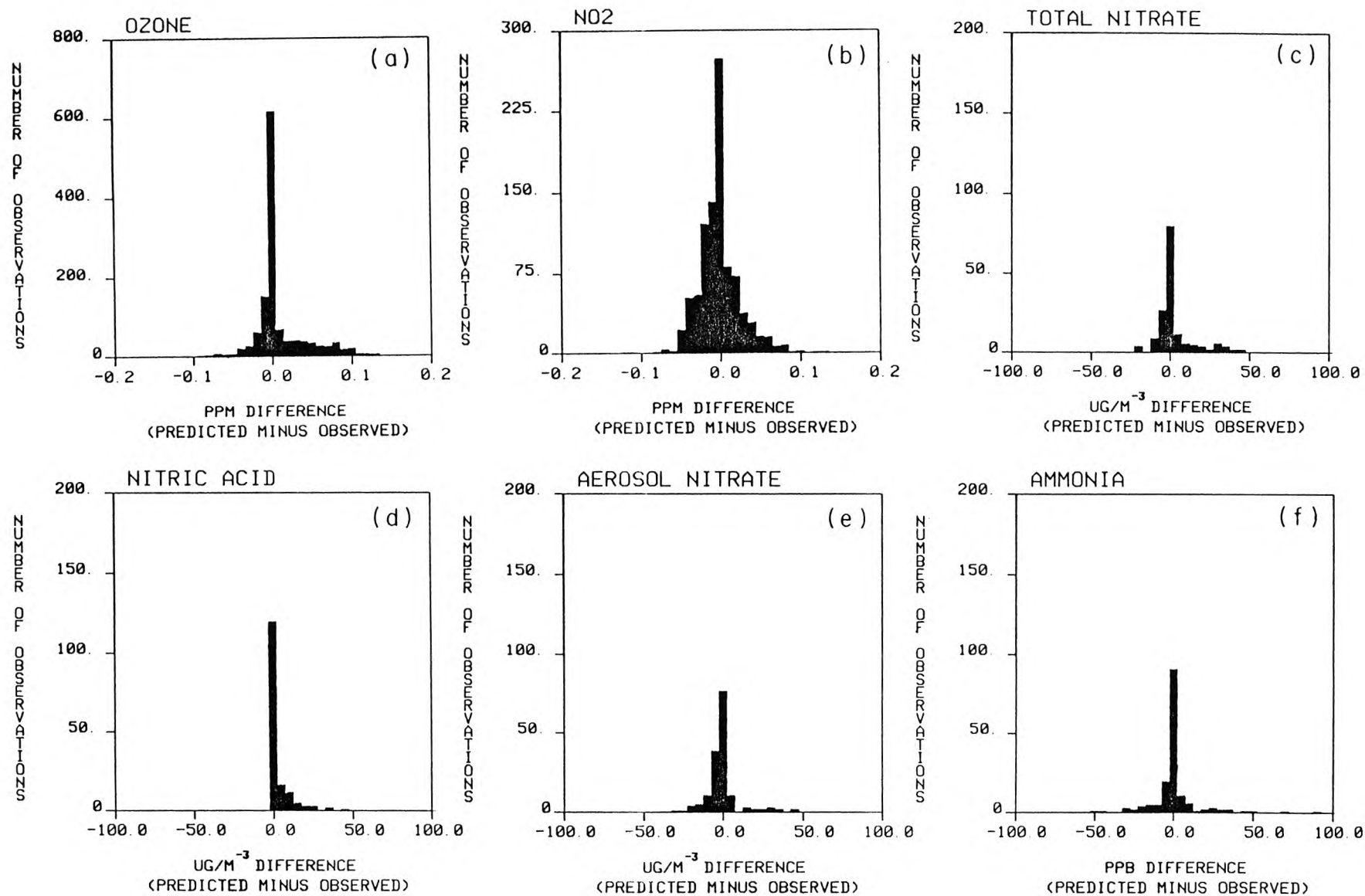


Figure 9. Histogram of concentration residuals (predicted minus observed) determined over all times and locations of the two day period, 30-31 August 1982: (a) O₃, (b) NO₂, (c) total inorganic nitrate, (d) nitric acid, (e) aerosol nitrate, and (f) ammonia.

ized in Table 5. The average of the predicted TN concentrations was $15.6 \mu\text{g m}^{-3}$, and the average of the observations was $12.9 \mu\text{g m}^{-3}$, showing good agreement with little model bias. Regression analysis of TN predictions on observations also showed good agreement (slope 1.15, intercept $0.7 \mu\text{g m}^{-3}$). Residual frequency histograms for TN, AN, HNO_3 and NH_3 are shown in Figure 9. This analysis indicates that the model is adequately predicting the TN concentrations. Improved correlations between predictions and observations over time would be achieved if the morning TN peaks that occur as the mixing depth is increasing rapidly were predicted more accurately. The residual histograms for AN and NH_3 are very similar to that for TN. While most HNO_3 predictions are within a few μgm^{-3} of the observations, Figure 9 shows that HNO_3 is overpredicted more often than it is underpredicted.

Given the spatial distribution of emissions as shown in Figure 2 and the generally westerly winds, one would expect that the greatest NH_3 concentrations would be found in the eastern portion of the air basin. Comparison of measured and predicted NH_3 levels confirms that speculation (e.g., compare NH_3 levels in Figure 5 to those in Figure 7). Statistical analysis of that comparison at all monitoring sites is shown in Table 5. Given the possible uncertainties in the NH_3 inventory (as discussed by 1), the model accurately predicts the NH_3 levels throughout the basin.

Having completed steps (1) and (2) above, the final test is to determine how well the model apportions the inorganic nitrate between the gas and aerosol phases. Since it was impossible to include the heterogeneous reaction between nitric acid and preexisting aerosol within this modeling framework due to the lack of an emissions inventory for alkaline and ionic aerosols, one does not expect that the aerosol nitrate formation calculation will work well at all sites. This expectation is confirmed in Table 5. However, aerosol nitrate concentration predictions do match observations closely at sites like Anaheim where an ion balance on measured aero-

sol composition shows that NH_4NO_3 is present (22) and where TN levels were predicted correctly.

9. Conclusion

An Eulerian grid-based photochemical airshed model has been employed to study the formation of nitrogen-containing air pollutants. Comparison of model predictions to observations in California's South Coast Air Basin over two days in August 1982 shows that the model predictions for O_3 , total inorganic nitrate, and PAN match observations closely. Predicted NO_2 levels showed little bias when compared to the measurements, and predicted peak NO_2 concentrations also matched measurements in magnitude. Apportionment of the inorganic nitrate between the gas and aerosol phases at near-coastal sites is hindered by the absence of an emission inventory for preexisting aerosol that is available to react with $\text{HNO}_3(\text{g})$.

Results from the present grid-based modeling study may be compared to a previous trajectory modeling study (1). The trajectory version employing the same chemical mechanism and the same input data applied to the same days in 1982 produces results at Rubidoux that match observations more closely than the grid-based version of the same model. The reasons for these differences must be due to fundamental differences in the transport calculations, including the better vertical resolution of the trajectory model, the absence of horizontal numerical diffusion in the trajectory model, or the effect of boundary and initial conditions on the grid model. The grid-based version of the photochemical airshed model tested here has the advantage of increased spatial coverage when compared to the trajectory model, and thus can be used to efficiently examine the basinwide consequences of emissions changes. In Part II of this series, the effect of a variety of candidate emission control programs on Los Angeles nitrate air quality will be examined.

References

1. Russell, A.G.; Cass, G.R. Verification of a mathematical model for aerosol nitrate and nitric acid formation and its use for control measure evaluation. *Atmos. Environ.*, **1986**, *20*, 2011-2025.
2. Russell, A.G.; Cass, G.R. Acquisition of regional air quality model validation data for nitrate, sulfate, ammonium ion and their precursors. *Atmos. Environ.* **1984**, *18*, 1815-1827.
3. Seinfeld, J.H. "Air Pollution: Physical and Chemical Fundamentals" McGraw-Hill, New York, 1975.
4. McRae, G.J.; Goodin, W.R.; Seinfeld, J.H. Development of a second generation mathematical model for urban air pollution, I. Model formulation. *Atmos. Environ.* **1982a**, *16*, 679-696.
5. McRae, G.J.; Tilden, J.W.; Seinfeld, J.H. Global sensitivity analysis – A computational implementation of the Fourier Amplitude Sensitivity Test (FAST). *Computers and Chemical Engineering*, **1982b**, *6*, 15-25.
6. Russell, A.G.; McRae, G.J.; Cass, G.R. Mathematical modeling of the formation and transport of ammonium nitrate aerosol. *Atmos. Environ.* **1983**, *17*, 949-964.
7. McRae, G.J.; Seinfeld, J.H. Development of a second generation mathematical model for urban air pollution, II. Model evaluation. *Atmos. Environ.* **1983**, *17*, 501-522.
8. Baulch, D.L. et al. Evaluated kinetic and photochemical data for atmospheric chemistry: Supplement 1. *J. Phys. Chem. Ref. Data* **1982**, *11*, 327-496.
9. Russell, A.G.; McRae, G.J.; Cass, G.R. The dynamics of nitric acid production and the fate of nitrogen oxides. *Atmos. Environ.* **1985**, *19*, 893-903.
10. McRae, G.J. "Mathematical Modeling of Photochemical Air Pollution," Ph.D. Thesis, California Institute of Technology, Pasadena, CA, 1981.
11. Stelson, A.W.; Seinfeld, J.H. Relative humidity and temperature dependence of the ammonium nitrate dissociation constant. *Atmos. Environ.* **1982**, *16*, 983-992.
12. Goodin, W.R.; McRae, G.J.; Seinfeld, J.H. A comparison of interpolation methods for sparse data: Application to wind and concentration fields. *J. Applied Meteorology*, **1979**, *18*, 761-771.
13. Ranzieri, A. Personal Communication: forwarded magnetic tape AR3288, "1982-SCAB Point and Area Source Emissions," California Air Resources Board, Sacramento, CA, 1983.
14. Ranzieri, A. Personal communication: forwarded magnetic tape AR3292, "1982-SCAB Mobile Source Emissions," California Air Resources Board, Sacramento, CA, 1984.

15. Cass, G.R.; Gharib, S. "Ammonia Emissions In The South Coast Air Basin 1982," Open file report 84-2, Environmental Quality Laboratory, California Institute of Technology, Pasadena, CA, 1984.
16. Blumenthal, D.L.; White, W.H.; Smith, T.B. Anatomy of a Los Angeles smog episode: Pollutant transport in the daytime sea breeze regime. *Atmos. Environ.* **1978**, *12*, 893-907.
17. Edinger, J.G. Vertical distribution of photochemical smog in Los Angeles basin. *Environ. Sci. Technol.*, **1973**, *7*, 247-252.
18. Blumenthal, D.L., Sonoma Technology, personal communication, 1984.
19. Grosjean, D.; Fung, K. Hydrocarbons and carbonyls in Los Angeles air. *J. Air. Pollut. Control Assoc.* **1984**, *34*, 537-543
20. Killus J.P., presented at the XV Informal Conference on Photochemistry, Stanford, CA, June 27—July 1, 1984.
21. Horie, Y. "Ozone Episode Representativeness Study for the South Coast Air Basin," Valley Research Corporation, Van Nuys, CA, 1987.
22. Hildemann, L.M.; Russell, A.G.; Cass, G.R. Ammonia and nitric acid concentrations in equilibrium with atmospheric aerosols: Experiment vs. theory. *Atmos. Environ.* **1984**, *18*, 1737-1750.
23. Bencala, K.E.; Seinfeld, J.H. An air quality model performance assessment package. *Atmos. Environ.* **1979**, *13*, 1181-1185.
24. Fox, D. Judging air quality model performance. *Bulletin of the American Meteorological Society*, **1981**, *62*, 599-609.
25. Rao, S.T.; Visalli, J.R. On the comparative assessment of the performance of air quality models. *J. Air Pollut. Control Assoc.* **1981**, *31*, 851-860.

Acknowledgments

This work was supported by the California Air Resources Board under Agreement A2-150-32 and by gifts to the Environmental Quality Laboratory.

CHAPTER 8
MATHEMATICAL MODELING OF THE FORMATION OF
NITROGEN-CONTAINING POLLUTANTS—II.
EVALUATION OF THE EFFECT OF EMISSION CONTROLS



**MATHEMATICAL MODELING OF THE FORMATION OF
NITROGEN-CONTAINING POLLUTANTS—II.
EVALUATION OF THE EFFECT OF EMISSION CONTROLS**

Armistead G. Russell

Department of Mechanical Engineering
Carnegie-Mellon University
Pittsburgh, PA 15213

Kenneth F. McCue and Glen R. Cass

Environmental Engineering Science Department and
Environmental Quality Laboratory
California Institute of Technology
Pasadena, CA 91125

ABSTRACT

A grid-based Eulerian airshed model is used to study the effect of specific emission control measures on ambient NO_2 , total inorganic nitrate (TN), HNO_3 , aerosol nitrate, PAN, NH_3 and ozone concentrations in the Los Angeles area. NO_x and reactive hydrocarbon (RHC) emission reductions of up to 61% and 37%, respectively, are examined. NO_2 and TN concentration reductions in excess of 50% averaged over 20 monitoring sites are achieved at the highest level of emission control studied. The distribution of TN air quality improvements between HNO_3 and aerosol nitrate is affected by the NH_3 emission rate of the NO_x control technologies employed. Peak 1-hr O_3 concentrations at many sites in the eastern portion of the air basin studied decline by more than 25% at the highest NO_x and RHC control levels studied, with the final increment of NO_x control alone capable of producing O_3 concentration improvements at locations with the highest O_3 concentrations.

1. Introduction

In Part I of this series, the performance of a grid-based photochemical airshed model for ozone, NO_2 , total inorganic nitrate (TN), PAN, HNO_3 , NH_3 and aerosol nitrate (AN) formation and transport was evaluated (1). Model predictions were compared against experimental observations made for this purpose in the Los Angeles area over the period August 30-31, 1982 (2). It was found that O_3 and PAN concentration predictions were in excellent agreement with observations, and that NO_2 predictions were in closer agreement with observed values than in many previous studies. On average, TN, NH_3 and HNO_3 concentration predictions differed from observations by very small absolute amounts: $2.7 \mu\text{gm}^{-3}$ (1.1 ppb), 0.7 ppb; and $4.2 \mu\text{gm}^{-3}$ (1.65 ppb), respectively. In the present paper, that model will be used to explore the predicted effect of specific emission control measures on ambient air quality.

2. Emission Control Opportunities

Emission control measures evaluated as part of this study are itemized in Table 1. That table has been divided into 5 groups. Group 1 controls reflect a subset of the reduction possibilities that have been documented as part of the 1982 Air Quality Management Plan (AQMP) for the South Coast Air Basin that surrounds Los Angeles (3). This group of controls approximates the effect of many of the emission reductions that can be expected to be implemented in the Los Angeles area in the years following the 1982 base year, but without extension of vehicular catalyst utilization or ammonia injection technology beyond that used in 1982. Group 2 and Group 3 controls simulate the effect of fleet-wide improvements in emissions from motor vehicles, at target levels that have been discussed by state and federal regulatory agencies (7,9). Group 4 and Group 5 controls would further reduce NO_x emissions from stationary sources through the use of non-catalytic ammonia injection or selective catalytic reduction (SCR) technology.

The 1982 emission inventory employed during the model verification effort of Part I of this study (1, 15) will be referred to as the Base Case. The 1982 Base Case emissions from each source class that will be considered for control are given in Table 1, along with the percentage reduction in those emissions that would result if the control measures had been in effect during 1982 (i.e. 84% reduction implies that $(1-84/100) = 0.16$ times the Base Case emissions from a stated source class would remain if the stated control measure had been implemented). Although several of the control measures cited are cross-referenced to the AQMP planning document, the base year emission inventory of the present study (1982) differs from the 1979, forecast 1987 and forecast year 2000 inventories used in the AQMP. The objective of the present study is to provide information on the air quality effects that would be observed if the controls listed in Table 1 had been applied during the 1982 Base Case model verification days in the amounts specified. No attempt will be made to simulate the effect of emission controls during some hypothetical future year.

The largest number of control measures in Group 1 of Table 1 (those designated B-1 through B-8) are aimed at reducing solvent vapor emissions from painting and surface coating operations, usually through reformulation of the coating material or through reduced overspray during application. Reduction in fugitive hydrocarbon emissions from landfill gas leaks and oil and gas field fixture leaks is anticipated. The remaining hydrocarbon controls would suppress solvent losses from cleaning operations and pesticide application, or capture certain industrial process emissions using incineration, activated carbon adsorption or other vapor recovery methods.

Stationary source oxides of nitrogen controls included in Group 1 involve relatively straightforward modification of combustion system design, but without the use of ammonia injection or selective catalytic reduction technology. The effect of a mandatory vehicle inspection and maintenance program involving a no-load idle

Table 1. Specific Emission Control Measures and Their Effect if Applied to 1982 Emissions in the South Coast Air Basin.

	1982 THC ^(a) Emissions (ton/day)	1982 NO _x Emissions (ton/day)	1982 NH ₃ Emissions (ton/day)	Control Measure	THC Change (%) ^(m)	Effect of Controls NO _x Change (%) ^(m)	NH ₃ Change (%) ^(m)	Notes and References
Group (1)								
1 Wood furniture finishing	16.6	—	—	Use of water-based coatings and reduced overspray. (B-5)	-54.1			3
2 Auto refinishing	6.7	—	—	Use of low solvent or water-based coatings. (B-8)	-21.0			3
3 Wood flatstock coating	1.5	—	—	Afterburners on drying and curing ovens. (B-1)	-75.0			3
4 Industrial maintenance coatings	6.3	—	—	Use of low solvent or water-based coatings. (B-2)	-39.3			3
5 Marine coatings	2.4	—	—	Use of low solvent or more durable coatings. (B-3)	-82.8			3
6 Motor vehicle mfg. (painting)	8.2	—	—	Electrostatic coating and high solids paint. (B-4)	-41.2			3
7 Metal parts mfg. (coatings)	25.8	—	—	Substitute coatings. (B-6)	-28.6			3
8 Aerospace coatings	4.6	—	—	Use of low solvent coatings. (B-7)	-40.5			3
9 Oil and gas well leak reduction	27.3	—	—	Semi-annual inspection and maintenance. (A-3)	-50.0			3
10 Pesticide application	12.9	—	—	Changes in formulation and application methods. (C-3)	-27.3			3
11 Metal and non-metal parts cleaning	40.6	—	—	Covers on circuit board degreasers; fewer exemptions. (C-1)	-12.8			3
12 Paper and fabric coating	10.6	—	—	Afterburners or activated carbon adsorption on curing ovens. (D-2)	-50.0			3
13 Dry cleaning	17.9	—	—	Reduced transfer emissions (wash & dry in a single unit). (G-3)	-35.8			3
14 Landfill gas recovery	778.0 ^(a)	—	—	Methane recovery. (F-1)	-46.1 ^(a)			3
15 Rubber products mfg.	3.6	—	—	Incineration or carbon adsorption on fugitive organics emissions. (D-3)	-10.3			3
16 Synthetic chemical mfg.	2.1	—	—	Chemical absorbers, carbon adsorption, and process changes. (G-1)	-90.9			3
17 Marine fuel transfer	0.4	—	—	Vapor recovery systems. (A-7)	-90.9			3
18 Graphic arts industry	11.9	—	—	High solids or waterborne ink; incineration or adsorption. (G-2)	-85.0			3
19 Refinery boilers and heaters	—	40.3	—	Combustion modification.		-8.0		4
20 Residential water heaters	—	10.3	—	Intermittent ignition devices and stack vent valves. (N-18)		(-25.0)		3
21 Non-refinery industrial boilers	—	35.0	—	Combustion modification. (G-11)		-25.0		3
22 Cement kilns	—	9.7	—	Combustion modification. (G-7)		-40.0		3
23 Glass furnaces	—	3.2	—	Process modification.		-45.3		5
24 Light-duty highway vehicle exhaust	439.0	427.0	—	Inspection and maintenance (no-load idle test & repair).	-11.3	-9.4		6
Group (2) Additional Mobile Source Control								
25 Light-duty highway vehicle exhaust	439.0	427.0	2.8	Entire fleet meets 0.7 g/mi NO _x and 0.41 g/mi THC objective; NH ₃ emissions reach 0.035 g/km; inspection and maintenance program continued.	-84.8	-73.3	+222	(b) 7.8
26 Heavy-duty diesel highway vehicle exhaust	25.8	157.0	0.02	Entire fleet meets objective of 10.7 g NO _x /BHP-hr and 2.65 g/mi THC.	-30.0	-25.9	—	(c) 9
27 Heavy-duty gasoline highway vehicle exhaust	18.6	35.7	(0.1)	Entire fleet meets objective of 10.7 g NO _x /BHP-hr and 2.65 g/mi THC.	-49.2	-34.8	0	(d) 9
28 Medium-duty highway vehicle exhaust (gasoline and diesel)	32.6	38.7	(0.3)	Entire fleet meets 1.5 g/mi NO _x and 0.6 g/mi THC objective (NH ₃ emissions reach 0.035 g/km).	-82.0	-62.1	(+83)	(e) 8.9

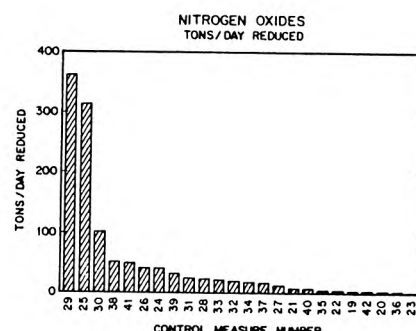
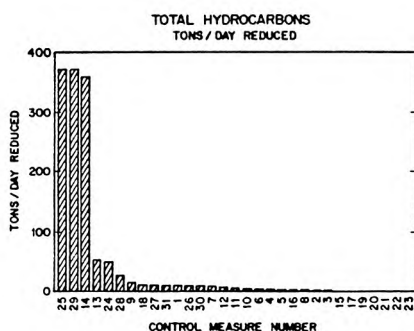
Table 1. Continued

		1982 THC ^(a) Emissions (ton/day)	1982 NO _x Emissions (ton/day)	1982 NH ₃ Emissions (ton/day)	Control Measure	THC Change (%) ^(m)	Effect of Controls NO _x Change (%) ^(m)	NH ₃ Change (%) ^(m)	Notes and References
Group (3) Stringent Mobile Source Control									
29	Light-duty highway vehicle exhaust	439.0	427.0	2.8	Entire fleet meets objective of 0.40 g/mi NO _x and 0.41 g/mi THC (NH ₃ emissions held at 0.035 g/km).	-84.8	-84.8	+222	(f) 7,8
30	Heavy-duty diesel highway vehicle exhaust	25.8	157.0	0.02	Entire fleet meets objective of 5.1 g NO _x /BHP-hr and 2.65 g/mi THC.	-30.0	-65	0	(f) 9
31	Heavy-duty gasoline highway vehicle exhaust	18.6	35.7	(0.1)	Entire fleet meets objective of 5.1 g NO _x /BHP-hr and 2.65 g/mi THC.	-49.2	-69	0	(f) 9
Group (4) Stationary Source NO_x Control-Non-Catalytic NH₃ Injection									
32	Refinery boilers and heaters	—	40.3	(0.5)	Direct NH ₃ injection.		-50	+869	(g) 4
33	Utility boilers	—	57.6	(1.6)	Direct NH ₃ injection.		-40	+344	(h), 10
34	Non-refinery industrial boilers	—	35.0	(0.65)	Direct NH ₃ injection + combustion modification.		-55	+392	(i) 10
35	Cement kilns	—	9.7	—	Direct NH ₃ injection.		-50	+	11
36	Glass melting furnaces	—	3.2	—	Direct NH ₃ injection.		-50	+	5
Group (5) Stationary Source NO_x Control-Selective Catalytic Reduction									
37	Refinery boilers and heaters	—	40.3	(0.5)	Selective catalytic reduction.		-44	+ small	(j), 12
38	Utility boilers	—	57.6	(1.6)	Selective catalytic reduction.		-90	+ small	(k), 13
39	Non-refinery industrial boilers	—	35.0	(0.65)	SCR plus combustion modification.		-92	+ small	(l), 13
40	Cement kilns	—	9.7	—	Selective catalytic reduction.		-90	+ small	11
41	Stationary industrial IC engines	—	74.2	—	Use of catalytic converters.		-66.7	+ small	14
42	Glass melting furnaces	—	3.2	—	Selective catalytic reduction.		-90.0	+ small	5

Notes

- (a) THC equals Total Hydrocarbon emissions; in all cases except landfill gas leak reduction and oil and gas well leak reduction, THC \approx RHC (Reactive Hydrocarbon emissions). Landfill emissions are mostly methane, with only 1.4% non-methane hydrocarbons. Only the non-methane hydrocarbon (NMHC) data are used by the air quality model, and the % control shown applies to the NMHC content of the emissions only.
- (b) Computed by multiplying vehicle miles traveled (VMT) per day times 0.7 g/mi NO_x and 0.41 g/mi THC. NH₃ emissions become 9.14 metric tons/day.
- (c) Computed by taking emissions from a new (undeteriorated) 1984 heavy diesel truck as representing 6.5 g/BHP-hr NO_x and also as equaling 10.31 g/mi NO_x. Ratio gives scale factor of 1.59 g mi⁻¹/(g/BHP-hr) NO_x. If entire fleet achieves 10.7 g/BHP-hr NO_x (representing a fleet average of 1984 trucks with deterioration) then emissions factor for entire fleet would be 17.0 g/mi. Emissions computed by multiplying VMT for heavy diesel vehicles times 17.0 g/mi. Hydrocarbon emissions obtained by multiplying 2.65 g/mi times heavy diesel vehicle VMT.
- (d) A new 1984 heavy gasoline truck emits 4.25 g/mile NO_x corresponding to 6.94 g/BHP-hr. Calculation proceeds as in note (c) above.
- (e) Computed by multiplying medium truck VMT per day times 1.5 g/mi NO_x and 0.6 g/mi THC. NH₃ emissions become 0.55 metric tons/day.
- (f) Emission reductions computed by procedure analogous to that for Group (2) Mobile Source Controls (see notes (b), (c), or (d)).

- (g) NH₃ breakthrough is assumed to be 50 ppm NH₃ for reduction of 75 ppm NO_x (50%). Final NH₃ emission is 5.04 metric tons/day.
- (h) NH₃ breakthrough is 50 ppm NH₃ giving total NH₃ emissions of 7.1 metric tons/day.
- (i) Estimated based on utility boiler performance, see note (h) and reference 10.
- (j) SCR achieves 90% NO_x control but is applied only to the largest units, yielding 44% reduction relative to the entire source class.
- (k) Ammonia bleed-through is 12 ppm.
- (l) 25% control by combustion modification plus 90% control via SCR, see note (k) and also control measure 21 in Table 1 above. Rule-making process would probably choose to exclude smaller boilers, but no indication is yet given of where the line would be drawn. NH₃ break-through assumed to be 12 ppm.
- (m) Percent change in emissions is defined as follows: -84% implies that $(1 - 84/100) = 0.16$ times original 1982 emission rate remains after control; +222% implies that $(1 + 222/100) = 3.22$ times original 1982 emission rate remains after control.



test, followed by repairs to the vehicle designed to correct defects observed also is included among the relatively simple control measures in Group 1.

Two further levels of mobile source NO_x control were considered. At the Group 2 level in Table 1, the entire light duty vehicle fleet was assumed to have achieved a NO_x emission rate of 0.7 g mi^{-1} , while the NO_x emissions from medium duty trucks were assumed to be reduced to 1.5 g mi^{-1} , and the NO_x emissions from heavy duty trucks were assumed to be reduced to 10.7 g/BHP-hr . There are two ways that one could view this case with 0.7 g mi^{-1} NO_x emitted from the light duty vehicle fleet. Since new cars sold in California must presently meet a 0.7 g mi^{-1} NO_x standard, this level of control could be used to approximate a successful completion of conversion of the entire vehicle fleet to meet current regulatory objectives for new cars, in combination with a high level of catalyst system durability and maintenance. In the absence of high durability and maintenance, catalyst system deterioration can be expected to increase actual on-road emissions to levels above legal objectives. The 0.7 g/mile NO_x fleet-wide emission rate employed here closely approximates the introduction of a fleet of cars initially set to achieve 0.4 g/mi NO_x when new, followed by a typical degree of control system deterioration in the hands of the final consumer. The 10.7 g/BHP-hr NO_x objective for heavy duty trucks reflects an intermediate level of control proposed by the U.S. Environmental Protection Agency (9).

Mobile source controls shown in Group 3 reflect the emissions pattern that would result if the 0.4 g/mi NO_x and 0.41 g/mi total hydrocarbon (THC) emission rate for light duty vehicles called for under the Clean Air Act in fact were achieved and maintained by the vehicle fleet. Increased control system durability or maintenance would be needed for this event to occur. Further NO_x reductions from heavy duty vehicles have been added to Group 3, at the most stringent level discussed by the federal government (9).

NO_x emission reductions from stationary combustion sources can be achieved by non-catalytic ammonia injection into the stack exhaust within a narrow exhaust temperature range. This direct NH_3 injection technology has been demonstrated on a utility boiler in the Los Angeles area (10). NO_x emission reductions in the vicinity of 50% are observed, accompanied by significant bleed-through of NH_3 into the atmosphere. Group 4 controls in Table 1 simulate the installation of such controls on all of the largest stationary combustion sources in the South Coast Air Basin. A major objective of our analysis of this group of controls is to determine if aerosol nitrate formation would be suppressed or enhanced by this NO_x emission reduction combined with NH_3 emission increase.

Selective catalytic reduction (SCR) technology involves NO_x abatement by injection of NH_3 into stationary source exhaust in the presence of a catalyst. Control efficiencies are generally higher than in the case of the direct non-catalytic NH_3 injection systems cited in control Group 4, and NH_3 bleed-through into the atmosphere is reduced. The effect of SCR technology applied to a variety of stationary sources in the Los Angeles area is indicated in Group 5 of Table 1.

By applying the controls in Table 1 in various combinations, a matrix of control opportunities can be constructed that represents the trade-off between increasingly stringent stationary source control vs. increasingly stringent mobile source control, as shown in Table 2. Ten cases will be defined. Beginning near the upper left corner of Table 2, the Base Case 1982 emission inventory first will be perturbed by applying the Group 1 controls from Table 1 to the emission sources. Moving from left to right across the top of the table, increasingly stringent mobile source controls are added to the Group 1 stationary source controls. Moving from top to bottom along the left edge of the table, increasingly demanding stationary source NO_x controls are added to a minimal motor vehicle control program. At the lower right corner of that table, the intersection of all of the most stringent mobile and station-

Table 2. Combinations of mobile and stationary source controls that will be examined for their effect on air quality in the South Coast Air Basin. Control measures refer to the control measures numbered in Table 1. Labels on columns and rows of this table are indicative of the maximum degree of NO_x control required.

		MOBILE SOURCE CONTROLS		
BASE CASE		VEHICLE INSPECTION AND MAINTENANCE	LIGHT DUTY FLEET 0.41 g/mi THC; 0.7g/mi NO _x HEAVY DUTY FLEET 2.65g/mi THC 10.7g/bhp-hr NO _x	LIGHT DUTY FLEET 0.41g/mi THC; 0.4g/mi NO _x HEAVY DUTY FLEET 2.65g/mi THC 5.1 g/bhp-hr NO _x
1982 Emissions (tons/day) THC = 2416 RHC = 1224 NO = 1120 NH ₃ ^x = 164				
STATIONARY SOURCE CONTROLS	AQMP EVAPORATIVE CONTROLS & COMBUSTION MODIFICATION	Control Measures: 1-24 Effect on Emissions: RHC -9.3% NO -5.4% NH ₃ ^x No change	Control Measures: 1-28 Effect on Emissions: RHC -37.2% NO -36.6% NH ₃ ^x +3.9%	Control Measures: 1-24, 28-31 Effect on Emissions: RHC -37.2% NO -47.6% NH ₃ ^x +3.9%
	AQMP + NON-CATALYTIC AMMONIA INJECTION	Control Measures: 1-18, 20, 24, 32-36 Effect on Emissions: RHC -9.3% NO -10.0% NH ₃ ^x +8.7%	Control Measures: 1-18, 20, 24-28, 32-36 Effect on Emissions: RHC -37.2% NO -41.2% NH ₃ ^x +12.7%	Control Measures: 1-18, 20, 24, 28-36 Effect on Emissions: RHC -37.2% NO -52.2% NH ₃ ^x +12.7%
	AQMP + SELECTIVE CATALYTIC REDUCTION	Control Measures: 1-18, 20, 24, 37-42 Effect on Emissions: RHC -9.3% NO -18.4% NH ₃ ^x +0.7%	Control Measures: 1-18, 20, 24-28, 37-42 Effect on Emissions: RHC -37.2% NO -49.6% NH ₃ ^x +4.7%	Control Measures: 1-18, 20, 24, 28-31, 37-42 Effect on Emissions: RHC -37.2% NO -60.6% NH ₃ ^x +4.7%

ary source controls is applied. The headings aligned with the columns and rows of Table 2 are suggestive of the maximum cumulative degree of NO_x control achieved in each case; the hydrocarbon controls shown in Table 1 also are included.

The tenth perturbed case examined here explores the effect of NH_3 emission reduction alone. The Base Case 1982 emission inventory for NO_x and hydrocarbons remains untouched, but all of the NH_3 emissions from livestock waste decomposition and farming activities in the air basin are removed. This perturbation completely eliminates the large spike in the NH_3 inventory centered over the Chino dairy area in western Riverside and San Bernardino Counties (see Figure 2 of reference 1). That emission reduction may occur in the near future without the action of governmental air pollution control agencies. Rapid urban development in that area of both counties could displace the dairy industry within a few years.

3. The Effect of Emission Controls

The grid-based air quality model evaluated in Part I of this study (1) was used to determine the effects on air quality that could be expected if each of the combinations of emission control measures defined in Table 2 were applied in the South Coast Air Basin (SoCAB). For each set of control measures considered, the Base Case 1982 emission inventory for the SoCAB discussed in references (1) and (15) was modified to reflect the addition of that particular group of control measures. Then the air quality modeling calculations were executed over two days of simulation using the modified emission inventory along with the meteorological conditions observed during the Base Case model verification days (August 30-31, 1982).

The initial conditions and boundary conditions supplied to the air quality model in each case were identical to those observed during August 30-31, 1982, as described in reference (1). The purpose of the first day of each two-day simulation was to establish initial conditions for the second day of calculations that reflect the altered emissions into the air basin. The effect of emission controls on air quality

then was determined by comparison between Base Case and post-control air quality predictions for the second day of each two-day simulation. As changes in emission controls might affect the boundary conditions supplied to the model, a perturbation analysis of the effect of altered boundary conditions was conducted. Reducing the inflow O_3 boundary conditions from those observed on August 30-31, 1982, to 0.04 ppm all around the border of the modeling region reduced Base Case peak O_3 concentrations by only 0.01 ppm. Inflow NO_x boundary conditions on August 30-31, 1982, were examined and found to be very low except along a small stretch of the southeast corner of the grid system. In summary, predicted changes in air quality on the second day of simulation are determined predominantly by changes in emissions into the model and not by altered initial or boundary conditions.

The results of this comparison of alternative emission control strategies are presented in several formats. First, an account of the changes in basin-wide peak 1-hr average pollutant concentrations is given in Table 3. Base Case peak pollutant levels as they were calculated for August 31, 1982 in the absence of further emission controls are stated in the upper left hand corner of that table. Then for each combination of emission controls as defined in Table 2, the predicted basin-wide peak values are given, both in absolute concentration units and as a percent deviation from the pre-control Base Case. Since the effect of some control measures is to change the location or timing of the basin-wide peaks, the values shown in Table 3 may not be typical of the effects seen at most air monitoring sites. Therefore in Table 4, the average change in the peak 1-hr pollutant concentrations at the 20 sites shown in Figure 1 is given, along with the range of the changes observed between the least affected and most affected air monitoring stations.

As seen in the upper left corner of the matrix of control opportunities in Table 2, completion of the stationary source evaporative hydrocarbon controls that are a part of the 1982 AQMP for the Los Angeles area, plus stationary source combustion

Table 3. Effect of emission controls on basin-wide peak 1-hr average pollutant concentrations in the South Coast Air Basin, August 31, 1982. The combinations of emission control technologies considered in each cell of this matrix are defined in Tables 1 and 2. Values shown are the peak 1-hr average concentrations in the presence of the emission controls, followed by the % change relative to the Base Case (in parentheses).

BASE CASE		MOBILE SOURCE CONTROLS					
NO ₂	0.156 ppm	VEHICLE INSPECTION AND MAINTENANCE	LIGHT DUTY FLEET 0.41 g/mi THC; 0.7g/mi NO _x		LIGHT DUTY FLEET 0.41g/mi THC; 0.4g/mi NO _x		
TN	0.036 ppm		HEAVY DUTY FLEET 2.65g/mi THC 10.7g/bhp-hr NO _x		HEAVY DUTY FLEET 2.65g/mi THC 5.1 g/bhp-hr NO _x		
HNO ₃	0.024 ppm						
AN	91 µg m ⁻³						
PAN	0.021 ppm						
O ₃	0.26 ppm						
STATIONARY SOURCE CONTROLS	AQMP EVAPORATIVE CONTROLS & COMBUSTION MODIFICATION	NO ₂	0.150 ppm (-4.0%)	NO ₂	0.123 ppm (-21%)	NO ₂	0.089 ppm (-43%)
		TN	0.033 ppm (-6.8%)	TN	0.021 ppm (-41%)	TN	0.018 ppm (-48%)
		HNO ₃	0.022 ppm (-9.2%)	HNO ₃	0.013 ppm (-44%)	HNO ₃	0.011 ppm (-55%)
	AN	85 µg m ⁻³ (-5.5%)	AN	55 µg m ⁻³ (-39%)	AN	49 µg m ⁻³ (-47%)	
	PAN	0.020 ppm (-2.2%)	PAN	0.018 ppm (-14%)	PAN	0.017 ppm (-19%)	
	O ₃	0.255 ppm (-1.6%)	O ₃	0.230 ppm (-11%)	O ₃	0.221 ppm (-15%)	
	AQMP + NON-CATALYTIC AMMONIA INJECTION	NO ₂	0.152 ppm (-2.6%)	NO ₂	0.118 ppm (-24%)	NO ₂	0.090 ppm (-42%)
		TN	0.033 ppm (-6.1%)	TN	0.020 ppm (-42%)	TN	0.017 ppm (-52%)
		HNO ₃	0.021 ppm (-13%)	HNO ₃	0.013 ppm (-45%)	HNO ₃	0.010 ppm (-57%)
AN	81 µg m ⁻³ (-8.8%)	AN	52 µg m ⁻³ (-41%)	AN	46 µg m ⁻³ (-48%)		
PAN	0.020 ppm (-2.9%)	PAN	0.018 ppm (-15%)	PAN	0.016 ppm (-20%)		
O ₃	0.254 ppm (-1.8%)	O ₃	0.230 ppm (-11%)	O ₃	0.219 ppm (-15%)		
AQMP + SELECTIVE CATALYTIC REDUCTION	NO ₂	0.155 ppm (-0.5%)	NO ₂	0.117 ppm (-25%)	NO ₂	0.073 ppm (-53%)	
	TN	0.032 ppm (-9.2%)	TN	0.019 ppm (-47%)	TN	0.014 ppm (-59%)	
	HNO ₃	0.020 ppm (-13%)	HNO ₃	0.012 ppm (-50%)	HNO ₃	0.009 ppm (-59%)	
AN	78 µg m ⁻³ (-14%)	AN	48 µg m ⁻³ (-47%)	AN	39 µg m ⁻³ (-57%)		
PAN	0.020 ppm (-4.6%)	PAN	0.017 ppm (-18%)	PAN	0.016 ppm (-22%)		
O ₃	0.251 ppm (-3.1%)	O ₃	0.224 ppm (-13%)	O ₃	0.215 ppm (-17%)		

Table 4. Effect of emission controls on peak 1-hr average pollutant concentrations observed at the 20 sites shown in Figure 1. Values shown are averages over the 20 sites, followed by the range of the values observed among the 20 sites (in parentheses). Aerosol nitrate concentrations shown are computed as if the aerosol is pure NH_4NO_3 .

MOBILE SOURCE CONTROLS							
BASE CASE		VEHICLE INSPECTION AND MAINTENANCE	LIGHT DUTY FLEET	LIGHT DUTY FLEET			
			0.41 g/mi THC;	0.41g/mi THC;			
			0.7g/mi NO _x	0.4g/mi NO _x			
			HEAVY DUTY FLEET	HEAVY DUTY FLEET			
			2.65g/mi THC	2.65g/mi THC			
			10.7g/bhp-hr NO _x	5.1 g/bhp-hr NO _x			
STATIONARY SOURCE CONTROLS	AQMP EVAPORATIVE CONTROLS & COMBUSTION MODIFICATION	NO ₂	-5.1% (-8.3% to -1.4%)	NO ₂	-37.4% (-49.7% to -19.1%)	NO ₂	-45.6% (-59.5% to -26.1%)
		TN	-4.8% (-7.4% to -3.0%)	TN	-35.7% (-41.2% to -22.1%)	TN	-45.6% (-52.8% to -26.8%)
		HNO ₃	-4.1% (-7.0% to -0.9%)	HNO ₃	-31.8% (-46.5% to -14.8%)	HNO ₃	-40.0% (-53.7% to -18.6%)
		NH ₃	+1.0% (-3.5% to +10.1%)	NH ₃	+10.6% (-4.1% to +29.8%)	NH ₃	+9.0% (-5.9% to +27.4%)
	AN	-3.4% (-6.7% to -1.1%)	AN	-22.7% (-40.1% to -4.4%)	AN	-34.0% (-52.8% to -17.1%)	
	PAN	-2.7% (-4.3% to -0.6%)	PAN	-15.6% (-25.7% to -1.3%)	PAN	-14.3% (-28.8% to +2.1%)	
	O ₃	-1.8% (-2.9% to -0.7%)	O ₃	-11.7% (-18.9% to -4.1%)	O ₃	-12.8% (-23.6% to -1.1%)	
	AQMP + NON-CATALYTIC AMMONIA INJECTION	NO ₂	-5.9% (-9.1% to -0.04%)	NO ₂	-38.4% (-50.9% to -19.0%)	NO ₂	-46.9% (-59.8% to -27.2%)
		TN	-5.5% (-8.4% to -3.2%)	TN	-36.7% (-41.8% to -22.4%)	TN	-46.8% (-54.5% to -28.2%)
		HNO ₃	-9.3% (-25.0% to -3.6%)	HNO ₃	-34.4% (-49.0% to -21.0%)	HNO ₃	-42.5% (-55.7% to -24.9%)
		NH ₃	+17.3% (-15.8% to +60.5%)	NH ₃	+27.9% (-7.3% to +68.0%)	NH ₃	+28.0% (-8.5% to +67.4%)
	AN	+3.7% (-7.7% to +20.7%)	AN	-19.0% (-39.0% to +3.3%)	AN	-31.2% (-54.1% to -9.0%)	
PAN	-2.0% (-4.2% to +2.2%)	PAN	-15.3% (-25.1% to -0.1%)	PAN	-14.3% (-30.0% to +3.1%)		
O ₃	-1.7% (-3.1% to +0.6%)	O ₃	-11.7% (-19.0% to -1.6%)	O ₃	-13.4% (-24.4% to -1.2%)		
AQMP + SELECTIVE CATALYTIC REDUCTION	NO ₂	-8.5% (-14.9% to -1.8%)	NO ₂	-42.4% (-55.3% to -21.4%)	NO ₂	-51.9% (-67.4% to -27.8%)	
	TN	-8.9% (-14.3% to -5.0%)	TN	-41.3% (-46.9% to -25.5%)	TN	-52.3% (-60.0% to -33.1%)	
	HNO ₃	-9.9% (-13.3% to -6.0%)	HNO ₃	-37.7% (-51.0% to -21.2%)	HNO ₃	-47.3% (-60.7% to -27.1%)	
	NH ₃	+4.0% (-13.4% to +25.0%)	NH ₃	+12.6% (-8.2% to +36.0%)	NH ₃	+13.7% (-6.6% to +38.5%)	
AN	-4.8% (-13.8% to +3.2%)	AN	-27.6% (-46.8% to -8.6%)	AN	-39.6% (-59.8% to -24.2%)		
PAN	+0.4% (-7.1% to +7.7%)	PAN	-14.3% (-27.6% to +1.0%)	PAN	-14.8% (-36.0% to +7.2%)		
O ₃	-1.4% (-4.9% to +3.0%)	O ₃	-12.6% (-22.2% to -2.8%)	O ₃	-15.0% (-28.2% to -0.7%)		

modifications and a vehicle maintenance program would result in a 5.4% reduction in basin-wide NO_x emissions and a 9.3% reduction in reactive hydrocarbon (RHC) emissions. Comparison to Table 4 shows that the 1-hr peak levels of NO_2 and TN typically drop by an amount that is roughly proportional to the change in NO_x emissions. The greatest percentage decreases in total inorganic nitrate (TN) levels occur in the eastern portion of the air basin (from Pomona: TN = -5.5% to Rubidoux: TN = -7.4%), while TN levels decline by only 3% to 5% in the western part of the air basin. The effect on HNO_3 and AN levels likewise is highest in the eastern portion of the air basin. O_3 and PAN levels in this case decline by only 1.6% and 2.2% at the location of the basin-wide 1-hr peak, a reduction that is less than proportional to the degree of emission control achieved for either RHC or NO_x .

The effect of progressively more stringent NO_x controls on stationary sources alone is observed by moving down the left edge of Tables 2, 3 and 4. Addition of non-catalytic ammonia injection technology at major stationary NO_x sources combined with AQMP hydrocarbon controls produces a net 10% reduction in basin-wide NO_x emissions along with a +8.7% increase in basin-wide NH_3 emissions, as seen in Table 2. Most of these emissions changes occur in the heavily industrialized western portion of the air basin, which has very low ambient NH_3 levels at present (see Figures 2, 3 and 5 of reference 1). As a result of the NH_3 emissions from the ammonia injection systems, peak 1-hr average ambient NH_3 levels near industrial areas at the coast (Long Beach and Lennox) rise by nearly 60%, while ambient NH_3 levels at central Los Angeles, La Habra, Anaheim and Pico Rivera rise by 25% or more. HNO_3 levels drop by as much as 25% at Lennox, and by more than 13% at central Los Angeles, Anaheim, La Habra and Pico Rivera, but this is largely due to the formation of additional aerosol nitrates by reaction of HNO_3 with the increased NH_3 . Peak 1-hr average aerosol nitrate levels rise by 14% to 21% at central Los Angeles, Long Beach and Lennox in the presence of this NH_3 emission increase.

Farther downwind, in the vicinity of the Chino dairy area where the air is already loaded with very high NH_3 levels even in the Base Case (e.g., 0.67 ppm 1-hr peak at Chino, see Table 4), the reduction in NO_x emissions achieved through this combination of controls that includes non-catalytic NH_3 injection at upwind sources does act to reduce TN and aerosol nitrate levels by 7% to 8%. In summary, use of non-catalytic ammonia injection technology for NO_x emission reduction has the potential to degrade NH_3 and aerosol nitrate air quality in the industrialized western portion of the South Coast Air Basin, accompanied by aerosol nitrate concentration reductions in already NH_3 -enriched agricultural areas downwind.

Through addition of selective catalytic reduction (SCR) technology on stationary sources, combined with AQMP hydrocarbon controls, an 18% reduction in basin-wide NO_x emissions is achieved relative to Base Case 1982 emissions accompanied by only a 0.7% increase in NH_3 emissions (lower left corner, Tables 2, 3 and 4). These stationary source NO_x reductions are concentrated at a few major point source locations (e.g. power plants and petroleum refineries). As a result, the effect of these controls varies greatly between monitoring sites. When SCR is added to major point sources, NO_2 concentration reductions of 12% to 15% occur at Burbank, Long Beach, Azusa and Anaheim. Typically, NO_2 levels in that case decline by 8.5% averaged over the 20 locations cited in Figure 1 and Table 4. At the location of the basin-wide NO_2 concentration peak, and at Upland and Fontana, NO_2 concentration reductions are small (2.6% or less). Total inorganic nitrate concentration improvements show less variability between monitoring sites: TN levels decline by 11% to 14% in the eastern portion of the air basin (from Pomona to Rubidoux), and by 5% to 10% in the western area of the basin. Reductions in basin-wide 1-hr peak HNO_3 and AN levels of 13% and 14% respectively also are achieved. The basin-wide peak O_3 and PAN concentrations decline slightly as stationary source NO_x controls are applied. At 5 of the sites shown in Figure 1 in the area from central Los Angeles

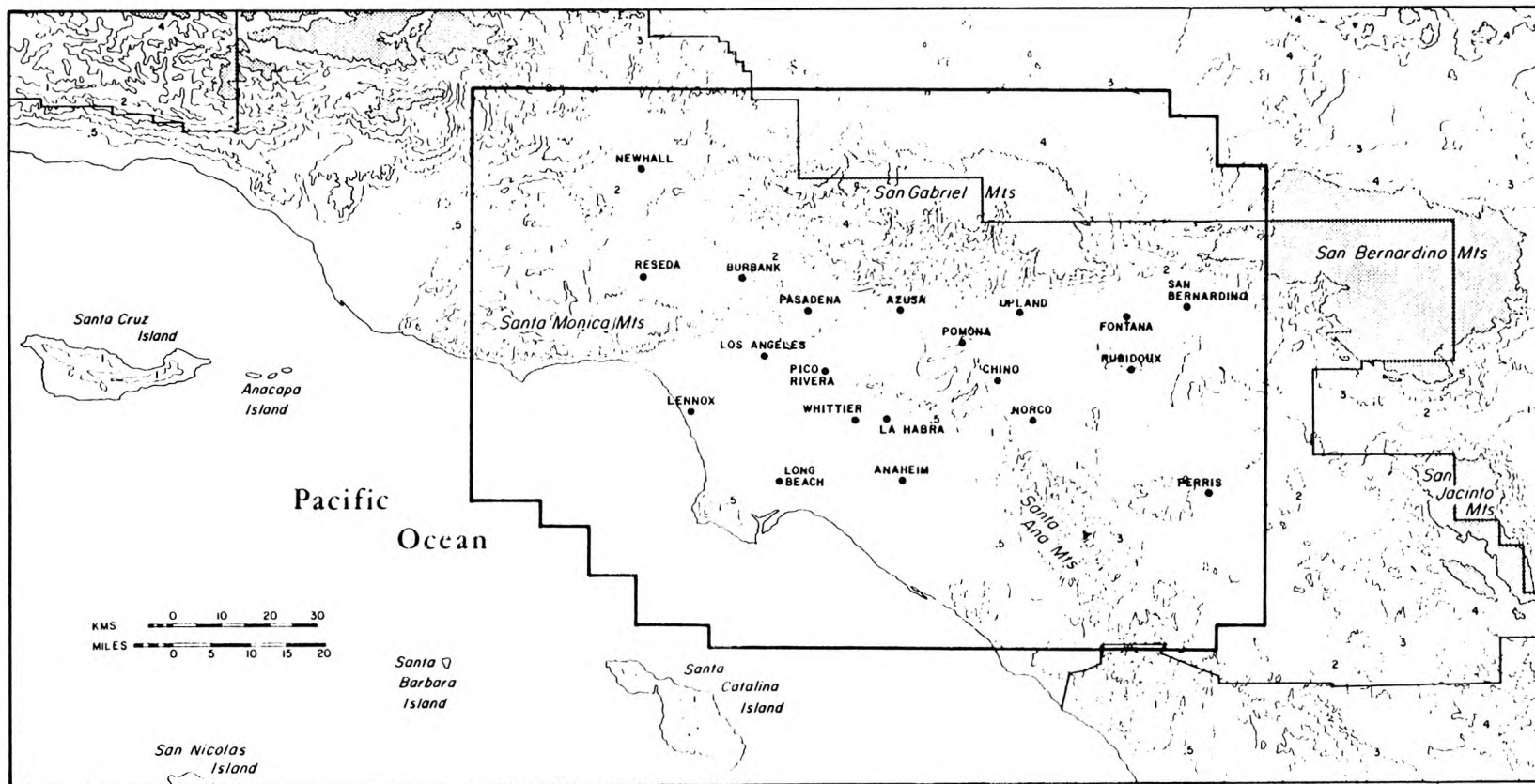


Figure 1. The South Coast Air Basin, showing 20 sites at which the effect of emission controls will be evaluated. Air quality modeling calculations are performed within the region bounded by the heavy solid line in the center of the map.

and Pasadena to La Habra, addition of SCR on stationary sources alone causes peak 1-hr O_3 levels to increase relative to the Base Case, but that increase is +3% or less. PAN air quality changes by amounts that are less than proportional to the NO_x reduction achieved, with 7 of the 20 sites studied experiencing a PAN increase. In short, with addition of SCR technology on stationary sources alone, improvements in many NO_x -related species concentrations are achieved. Those improvements are less than proportional to the NO_x emissions change, and are accompanied by slight increases in O_3 and PAN at a few locations.

The effect of progressively more stringent mobile source controls alone can be examined by moving from left to right across the upper row of Tables 2, 3 and 4. As seen in Table 2, complete conversion of the vehicle fleet to an intermediate level of mobile source control (light-duty fleet meets 0.41 g/mi THC; 0.7 g/mi NO_x along with additional heavy-duty vehicle controls plus AQMP stationary source controls) would result in a 37% reduction in basin-wide NO_x emissions and a 37% reduction in RHC emissions relative to the Base Case. Tables 3 and 4 show that major improvements in TN, HNO_3 and AN levels would result, with improvements almost directly proportional to the NO_x emission reduction achieved. Basin-wide peak O_3 and PAN concentrations both decline by 11% and 14% respectively.

Further reduction in NO_x emissions from motor vehicles alone is examined in the upper right hand corner of Tables 2, 3 and 4. If a 0.4 g/mi NO_x emission rate from the light-duty fleet had been achieved in 1982 along with strict heavy truck NO_x controls, NO_x emissions would have been reduced by 48% relative to the base case, with similar major improvements in ambient NO_2 , TN, HNO_3 and AN concentrations. O_3 and PAN concentrations both decline as additional NO_x controls are added to the vehicle fleet without further hydrocarbon controls beyond the 0.41 g/mi THC light-duty vehicle standard examined in the preceding square on the top row of Table 2.

As seen in the lower right hand corner of Table 2, the simultaneous use of all mobile and stationary source control measures considered here would reduce NO_x emissions relative to the base case by 61% in the presence of a 37% decline in RHC emissions. This combination of controls is more effective than controls on either the mobile or stationary sources alone. Basin-wide peak total inorganic nitrate, HNO_3 and aerosol nitrate concentrations are reduced by nearly 60%. Basin-wide peak NO_2 concentrations are reduced by 53%. A 17% reduction in the basin-wide peak O_3 concentration is achieved. The 1-hr O_3 concentration peak is reduced relative to the Base Case at every site shown in Figure 1.

As is quickly seen from Tables 3 and 4, the simultaneous use of all of the mobile and stationary source control measures considered produces major improvements in many air quality parameters at the time of the daily pollutant concentration peaks. The performance of that combination of control measures is explored in detail in Figures 2-7. Figure 2 gives the spatial distribution of pollutant concentrations in the presence of the maximum degree of NO_x control studied. By subtracting these pollutant levels from the spatial distribution of concentrations predicted by the Base Case simulation (see Figure 3 of reference 1) it is possible to define the spatial distribution of pollutant concentration changes experienced due to the emission controls, as seen in Figure 3. Figures 4, 5 and 6 permit rapid visualization of changes in the diurnal pattern of pollutant levels at key monitoring sites characteristic of the western and eastern portions of the air basin. In Figure 7, the effect of this set of emissions controls on 24-hour average pollutant levels is explored.

One effect of the maximum degree of mobile and stationary source control considered in this study (case in lower right corner of Table 2) is to preferentially reduce the NO_2 concentrations during the early morning peak hours of the day at sites in the western portion of the air basin, like Los Angeles, and Anaheim, as seen

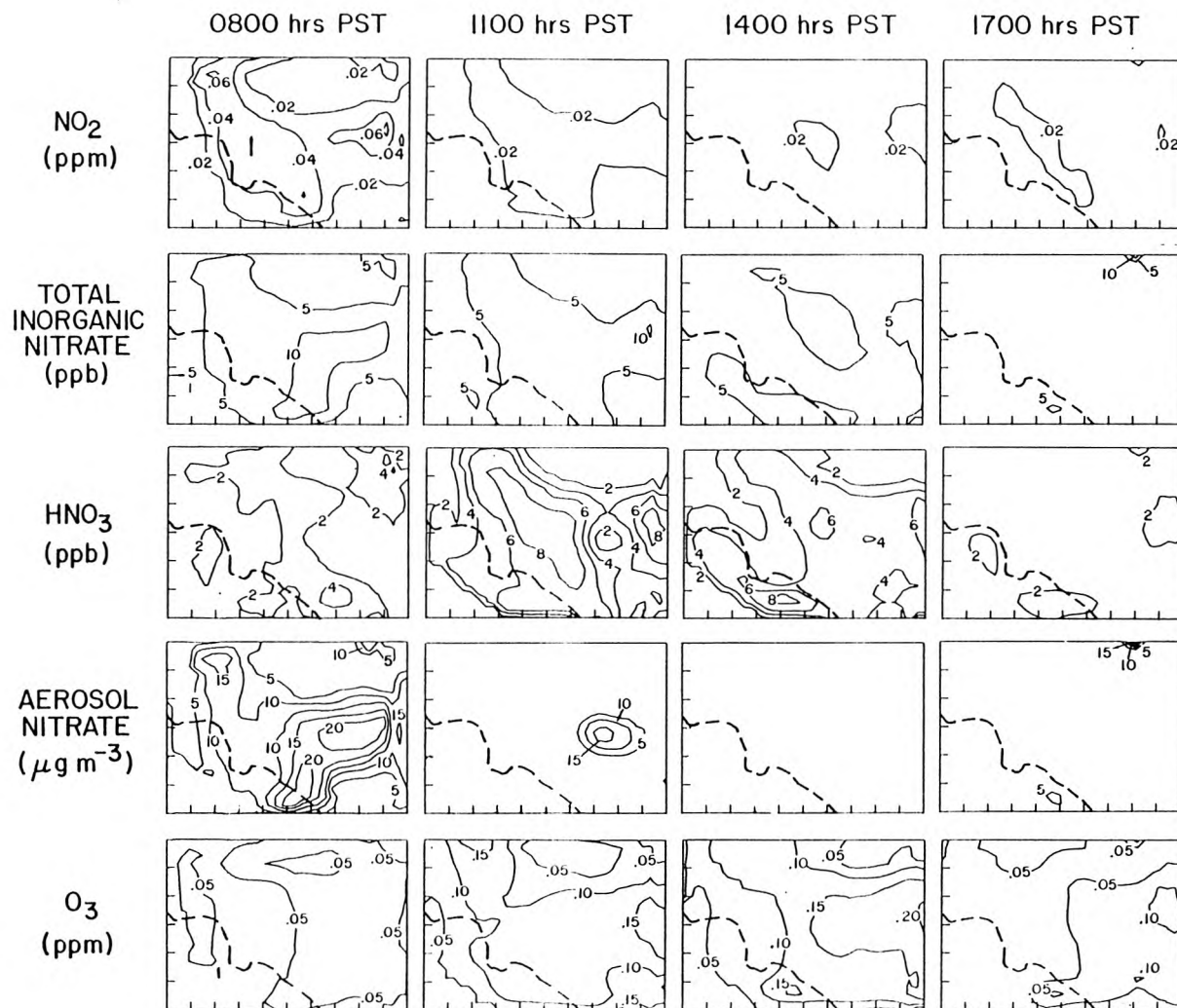


Figure 2. The spatial distribution of pollutant concentrations predicted in the presence of the maximum degree of NO_x and RHC control studied (case in lower right corner of Table 2).

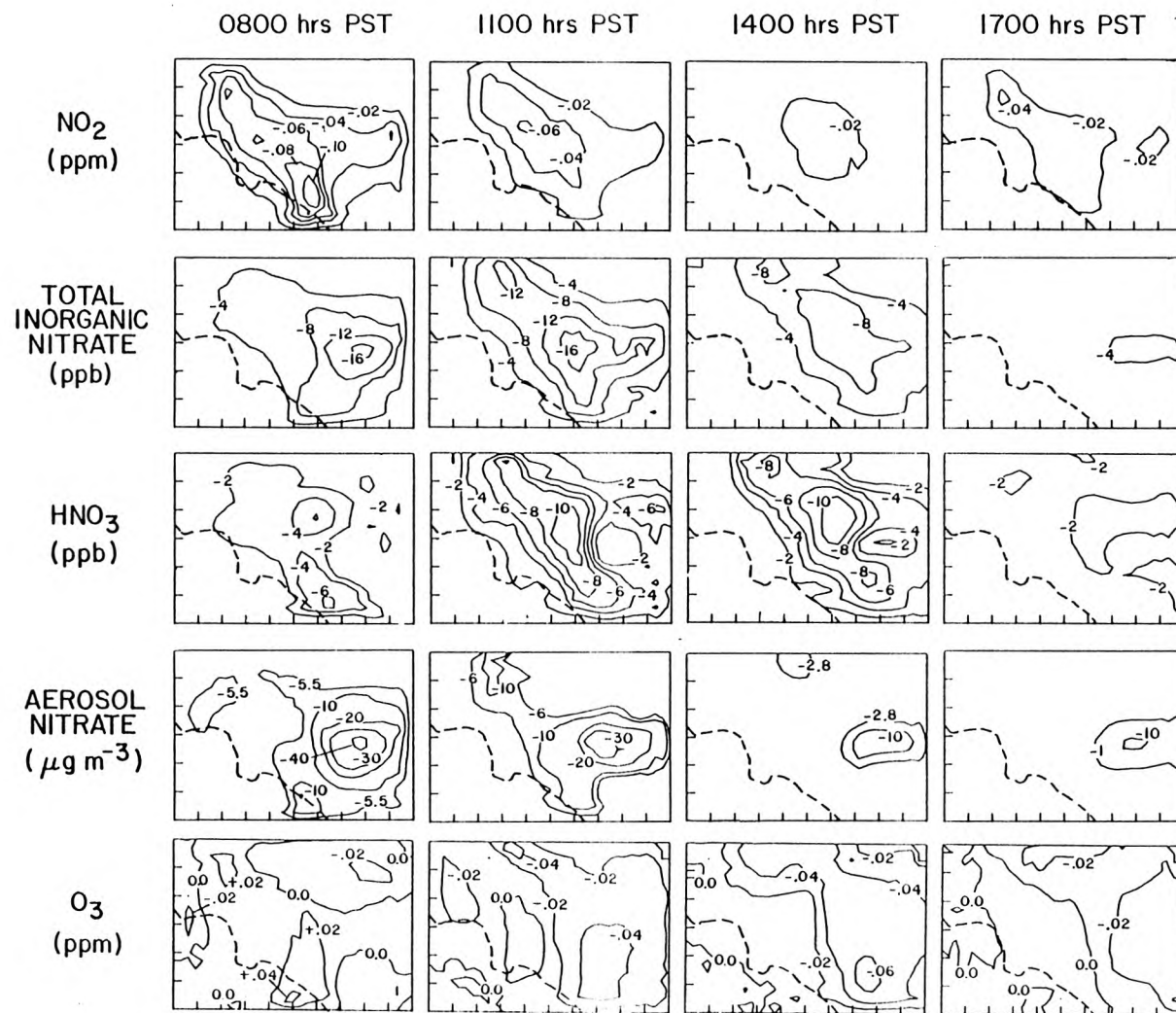


Figure 3. The spatial distribution of pollutant concentration changes predicted in the presence of the maximum degree of NO_x and RHC control studied (difference between the case in lower right corner of Table 2 vs. the Base Case).

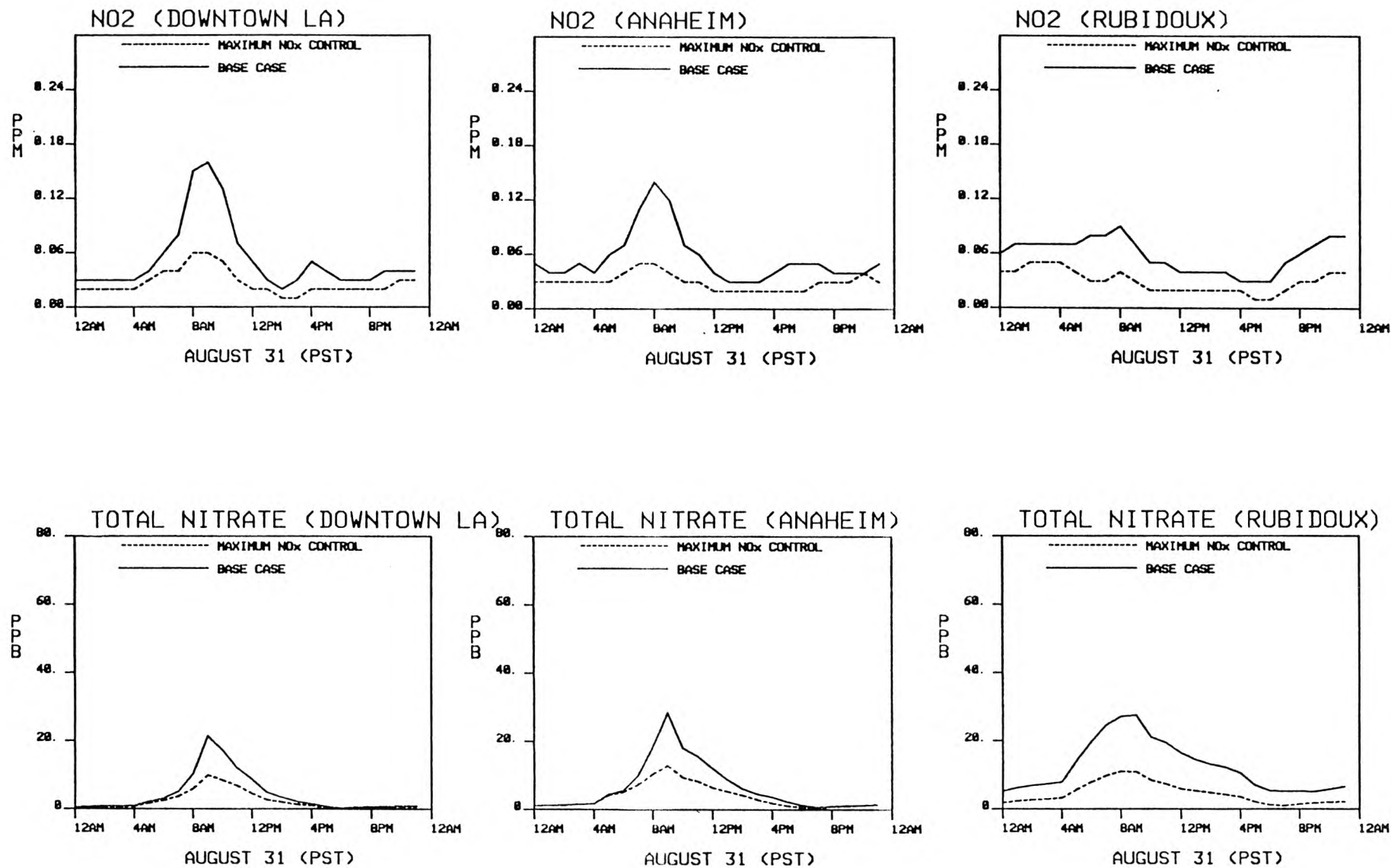


Figure 4. NO₂ and total inorganic nitrate (TN) concentrations at Los Angeles, Anaheim and Rubidoux under Base Case conditions and in the presence of the maximum degree of NO_x and RHC control studied.

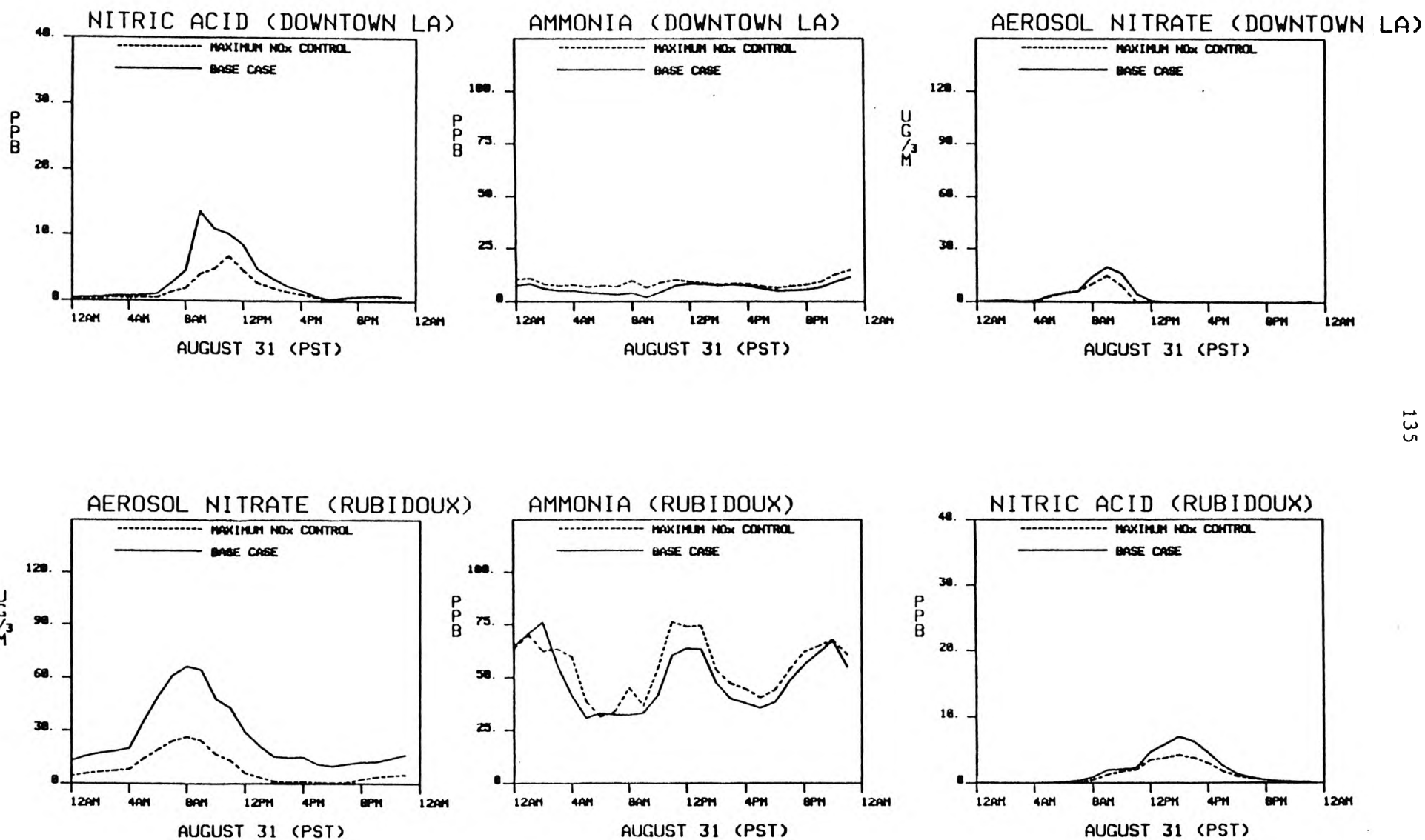


Figure 5. Nitric acid, ammonia and aerosol nitrate concentrations at Los Angeles and at Rubidoux under Base Case conditions and in the presence of the maximum degree of NO_x and RHC control studied.

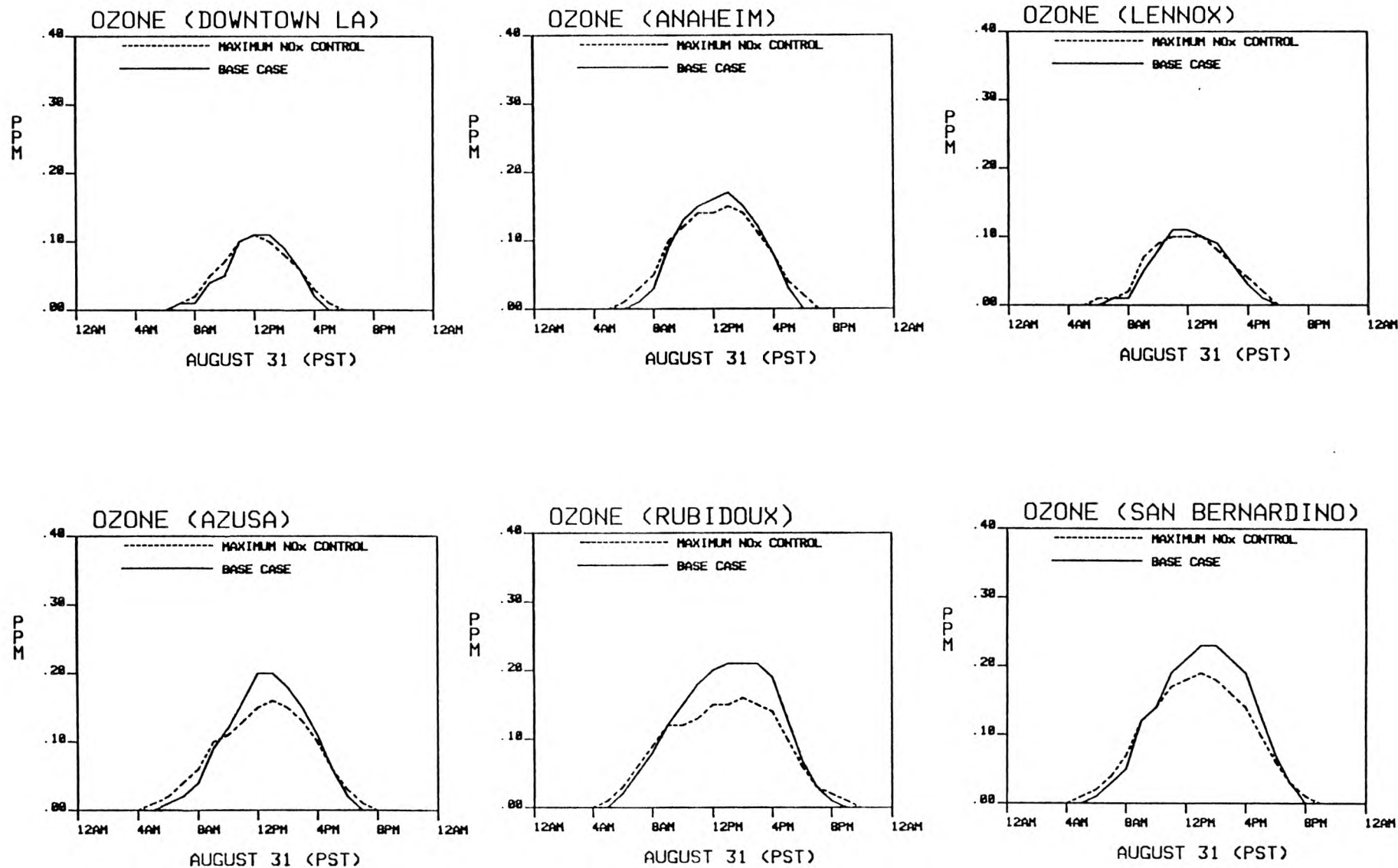
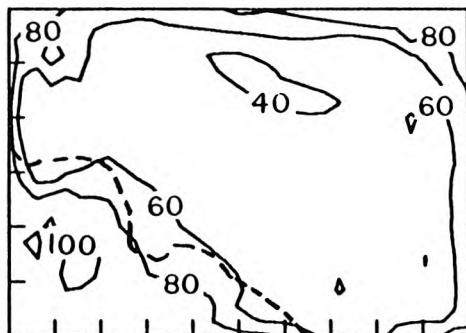
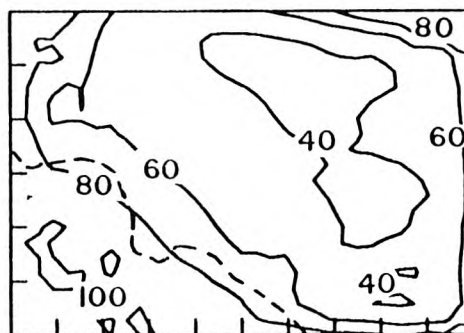


Figure 6. Ozone concentrations under Base Case conditions and in the presence of the maximum degree of NO_x and RHC control studied.

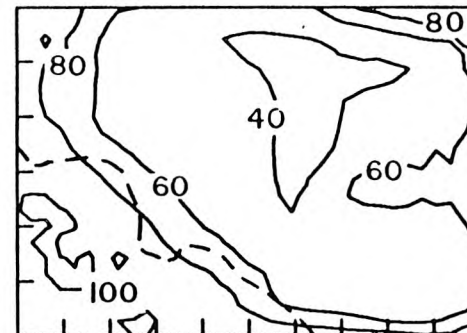
NO_2



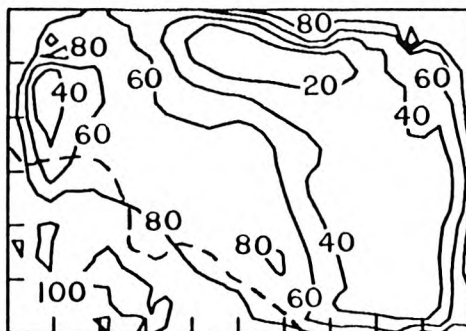
TOTAL INORGANIC NITRATE



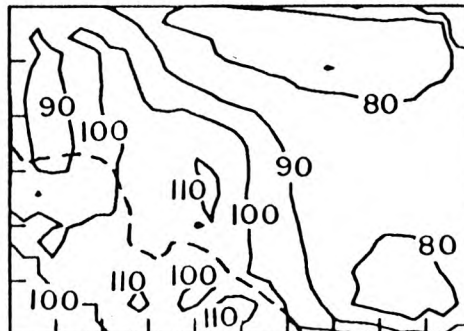
HNO_3



AEROSOL NITRATE



O_3



PAN

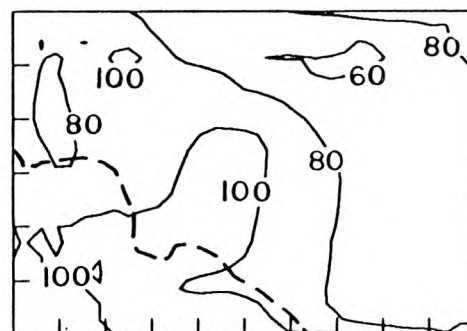


Figure 7. 24-hour average NO_2 , inorganic nitrate, nitric acid, aerosol nitrate, O_3 and PAN concentrations in the presence of the maximum degree of NO_x and RHC control studied, expressed as a percentage of Base Case concentrations.

in Figures 3 and 4. NO_2 concentrations which exceeded 0.15 ppm during early morning hours under Base Case conditions have been reduced by more than 0.06 ppm at 0800 hours PST throughout much of the western area of the basin, and by as much as 0.10 ppm in portions of coastal Orange County, as seen in Figure 3. At sites in the eastern area of the basin, at Upland, Rubidoux and San Bernardino, NO_2 levels are reduced by large percentage amounts throughout the entire 24-hour period studied (Figure 4). As a result, 24-hour average NO_2 levels decline by between 40% and 60% throughout nearly the entire on-land portion of the air basin as seen in Figure 7.

The effect of NO_x emission controls on total inorganic nitrate levels is felt to the greatest extent in the central and eastern portions of the air basin. As seen in Figure 3, TN concentration reductions in excess of 16 ppb occur in the inland areas throughout the morning hours in response to the maximum degree of NO_x control studied here.

The partition of this inorganic nitrate air quality improvement between reductions in gas phase HNO_3 versus reductions in aerosol nitrate is determined by co-occurring NH_3 concentrations. In the western portion of the air basin, HNO_3 reductions, especially in the morning hours, are proportionally greater than aerosol nitrate reductions, as shown at Los Angeles in Figure 5. The use of selective catalytic reduction technology plus more effective reducing catalysts on mobile sources leads to a small increase in NH_3 emissions. While that NH_3 increase is very minor compared to basin-wide NH_3 emissions, the NH_3 emissions increase by a significant *percentage* in the NH_3 -starved western urban area of the air basin (see the spatial distribution of Base Case NH_3 emissions in Figure 2 of reference (1)). NH_3 concentrations at sites like downtown Los Angeles that are located in the immediate vicinity of stationary combustion sources and heavy traffic density experience a rough doubling of base case NH_3 levels during the morning traffic peak hours. The pro-

duct of the NH_3 and HNO_3 concentrations is limited by the equilibrium dissociation constant for the $\text{NH}_4\text{NO}_3\text{--NH}_3\text{--HNO}_3$ system (16). The NH_3 concentration increase shifts the equilibrium HNO_3 concentration downward, while favoring aerosol nitrate formation. However, the same emission controls that produce the NH_3 emission increase also reduce NO_2 and TN concentrations by enough that a net increase in aerosol nitrate concentrations is not observed. Instead, both HNO_3 and AN decline in the western part of the air basin, but the HNO_3 reduction is more pronounced and begins in the morning as NH_3 levels rise, while the aerosol nitrate reduction relative to the base case occurs later in the day. In the central portion of the air basin, the combination of a major decrease in TN formation along with a small increase in NH_3 emissions is manifested by greater than a 10 ppb reduction in HNO_3 concentrations in the late morning and early afternoon (Figure 3).

In the eastern area of the air basin, Base Case NH_3 concentrations due to dairy farming and other agricultural sources are so high that a small change in upwind NH_3 emissions does not affect ambient NH_3 levels by more than a few percent. Again, the amount of gas phase HNO_3 is limited by the co-occurring ammonia levels. In this case the post-control NH_3 levels are nearly unchanged as a percentage of the pre-control NH_3 levels and as a result, HNO_3 concentrations do not change greatly. The large drop in TN levels at Rubidoux and San Bernardino that occurs when all available RHC and NO_x emission controls are applied thus is reflected in a major reduction in aerosol nitrate levels, and to a lesser degree by reduced HNO_3 concentrations as seen in Figure 5. At eastern basin sites, aerosol nitrate levels are reduced throughout the day, not just during peak hours.

The effect of RHC and NO_x controls on O_3 air quality has been a matter of considerable debate (15-22). Most recent studies (15, 22) agree that large NO_x reductions (above 19%) in the Los Angeles area combined with moderate RHC controls will produce lower O_3 levels in the downwind and eastern areas of the SoCAB near

Rubidoux and San Bernardino where the highest O_3 levels often are observed. Concern has been voiced, however, that if NO_x emissions are controlled to the maximum extent possible, then O_3 levels will rise in the western portion of the air basin (22).

The results of the present study indicate that the maximum degree of NO_x and RHC control studied here produces significant O_3 reductions in the eastern area of the South Coast Air Basin. The peak measured and predicted O_3 levels on August 31, 1982 that occurred at Rubidoux and at San Bernardino would be reduced substantially as seen in Figure 6. Peak 1-hour average O_3 levels in this case decline relative to the Base Case by 25% or more at Pomona, Chino, Norco, Upland, Fontana and Rubidoux, and by 21% at Azusa. The additional NO_x emission reductions achieved when moving from the group of control measures specified in the center column of Table 2 to the right hand column of Table 2 leads to reduced O_3 levels in the high- O_3 concentration zone at the eastern end of the air basin without addition of further hydrocarbon emission controls.

At all western urban sites, O_3 concentrations respond to this package of emission controls in a manner like that shown for central Los Angeles and Anaheim in Figure 6. In the presence of stringent NO_x controls, O_3 levels begin to rise at a slightly earlier hour in the morning due to less effective scavenging of O_3 by fresh NO emissions during the early morning traffic peak. Peak O_3 levels are decreased at all sites at midday, as mentioned previously. Then O_3 levels at western basin sites exceed 1982 Base Case concentrations for a short period in the afternoon in the presence of stringent NO_x controls, again due to less effective O_3 scavenging processes in the presence of the NO_x controls. If viewed on a 24-hour average basis, O_3 concentrations do rise slightly in the western area of the air basin in response to this control program, as seen in Figure 7. But since O_3 concentration standards are written to control peak 1-hour averages and since peak O_3 values

decline at all stations, it is unclear that this change in 24-hour average O_3 concentrations is of any regulatory consequence. In summary, the change in total O_3 dose received by western basin residents due to the NO_x control program studied is very small: the areas under the pre-control and post-control O_3 concentration time series graphs are practically the same. The high O_3 dose received by residents in the Azusa, Pomona, Riverside and San Bernardino areas, however, is significantly reduced by the combination of emission controls given in the lower right corner of Table 2.

The final alteration in emissions studied involves removal of all agriculture-related NH_3 emissions from the Base Case 1982 emission inventory given in reference (15). NH_3 emissions from livestock waste decomposition in the Chino dairy area and elsewhere are suppressed, as are NH_3 emissions from chemical fertilizer application at farms. This type of change in emissions could occur as increasing urbanization displaces agricultural activities in the air basin. This alteration in NH_3 levels alone does not affect atmospheric NO_2 , O_3 and PAN concentrations. Ammonia concentrations decline by 87% to 91% at Chino and Upland in the immediate vicinity of the dairy farms, and by about 70% at Rubidoux and San Bernardino downwind. Aerosol nitrate concentrations at San Bernardino, Fontana, Upland and Pomona decline by more than 50% as the agricultural NH_3 emissions are suppressed. In response, HNO_3 levels increase at eastern basin locations by 43% to 45% at San Bernardino and Upland, and by 89% to 100% at Fontana and Rubidoux. Suppression of aerosol nitrate formation without a corresponding decrease in NO_x emissions acts to shift inorganic nitrate from the aerosol phase to gas phase HNO_3 . Total inorganic nitrate levels decline at Upland, Fontana and Rubidoux by 7% to 13% as this shift from AN to HNO_3 formation occurs, probably because the deposition velocity for HNO_3 is higher than for fine aerosols.

4. Summary and Conclusions

Emission control measures that would reduce reactive hydrocarbon and NO_x emissions in the Los Angeles area by up to 37% and 61%, respectively, have been examined for their effects on air quality. In most cases studied, NO_2 and total inorganic nitrate concentrations decline by amounts only slightly less than proportional to the degree of precursor NO_x emission reduction. Peak 1-hr average NO_2 and TN levels averaged over 20 monitoring sites would decline by more than 50% relative to 1982 Base Case conditions if the light-duty vehicle fleet in practice met the originally proposed federal exhaust emission standards (0.4 g/mi NO_x and 0.41 g/mi THC) in conjunction with heavy-duty vehicle control, evaporative hydrocarbon controls, plus installation of selective catalytic NO_x reduction systems on major stationary sources. This reduction in inorganic nitrate levels would be reflected in major improvements in HNO_3 and aerosol nitrate air quality.

The partition of inorganic nitrate air quality improvements between aerosol nitrate and HNO_3 can be affected by the choice of NO_x emission controls. In particular, widespread use of non-catalytic NH_3 injection technology for NO_x emission control at stationary sources alone has the potential to increase aerosol nitrate formation in near-source areas if significant co-occurring bleed-through of NH_3 to the atmosphere occurs. Selective catalytic reduction technology at stationary sources and advanced catalyst systems on vehicles also have the potential to increase NH_3 emissions, but in those cases the NH_3 increase is so slight that the NO_x emission decrease achieved through use of these devices will drive aerosol nitrate levels downward in spite of the added NH_3 emissions.

Installation of the most stringent set of NO_x and RHC emission controls studied here causes peak 1-hr average O_3 concentrations to decline by 25% or more in the high O_3 concentration areas of eastern Los Angeles, Riverside and San Bernardino counties. The final increment of NO_x control alone produces O_3 concentration

improvements at the margin in the eastern portion of the air basin. In the western area of the air basin, near downtown Los Angeles, the most stringent package of NO_x and RHC controls studied leaves Base Case 1982 peak 1-hr average O_3 concentrations practically unchanged.

Acknowledgments

This work was supported by the California Air Resources Board under Agreement A2-150-32 and by gifts to the Environmental Quality Laboratory.

References

1. Russell, A.G.; McCue, K.F.; Cass, G.R. Mathematical Modeling of the Formation of Nitrogen-Containing Pollutants-I. Evaluation of an Eulerian Photochemical Model, submitted to *Environmental Science and Technology*, **1987**.
2. Russell, A.G.; Cass, G.R. Acquisition of regional air quality model validation data for nitrate, sulfate, ammonium ion and their precursors. *Atmos. Environ.*, **1984**, 18, 1815-1827.
3. South Coast Air Quality Management District. "Final Air Quality Management Plan 1982 Revision--Final Appendix No. VII-A-- Short Range Tactics for the South Coast Air Basin," South Coast Air Quality Management District: El Monte, CA, 1982.
4. California Air Resources Board. "Public Meeting to Consider a Suggested Measure for the Control of Nitrogen from Boilers and Process Heaters in Refineries;" California Air Resources Board: Sacramento, CA, 1981; Agenda Item 81-23-2, Appendix L, page L-1.
5. California Air Resources Board. "Suggested Control Measure for the Control of Oxides of Nitrogen Emissions from Glass Melting Furnaces;" California Air Resources Board: Sacramento, CA, 1980.
6. California Air Resources Board. "Public Hearing to Consider Amendments to Section 2176, Title 13, California Administrative Code, to Implement and Adopt Standards for Loaded Mode Testing and Make Other Changes in Regard to Motor Vehicle Inspection Standards;" California Air Resources Board: Sacramento, CA, 1981; Table 5, page 16, option 3.
7. California Air Resources Board. "Report to the Legislature on the Feasibility of a 0.4 Gram per Mile Oxide of Nitrogen Exhaust Emission Standard for Passenger Cars and Light Trucks;" California Air Resources Board: Sacramento, CA.
8. Cass, G.R.; Gharib, S. "Ammonia Emissions in the South Coast Air Basin 1982," Open file report 84-2, Environmental Quality Laboratory, California Institute of Technology: Pasadena, CA, 1984.
9. Environmental Protection Agency. "Control of Air Pollution from New Motor Vehicles and New Motor Vehicle Engines; Gaseous Emission Regulations for 1987 and Later Model Year Light-Duty Vehicles, and for 1988 and Later Model Year Light-Duty Trucks and Heavy-Duty Engines; Particulate Emission Regulations for 1988 and Later Model Year Heavy-Duty Diesel Engines;" U.S. Environmental Protection Agency: Washington, D.C., 1984; *Federal Register* 40 CFR, Parts 86 and 600.

10. Dziegiel, H.T.; Aure, T.B.; Anderson, D.W. "The Thermal DeNO_x Demonstration Project." Los Angeles Department of Water and Power: Los Angeles, CA, 1982. Presented at the Joint Symposium on Stationary Combustion NO_x Control, Dallas, TX, Nov. 1-4, 1982, Figures 11, 12 and 13.
11. California Air Resources Board. "Suggested Control Measure for the Control of Emissions of Oxides of Nitrogen From Cement Kilns;" California Air Resources Board: Sacramento, CA, 1981; page 2.
12. South Coast Air Quality Management District. "Staff Report - Proposed Rule 1109 - Petroleum Refinery Boilers and Process Heaters - Oxides of Nitrogen;" South Coast Air Quality Management District: El Monte, CA, 1982.
13. Kerry, H.A.; Weir, A. Jr. "Operating Experiences on Southern California Edison's 107.5 MW Selective Catalytic Reduction DeNO_x System;" Southern California Edison Co.: Rosemead, CA, 1985. Presented at the Joint Symposium on Stationary Combustion NO_x Control, Boston, MA, May 6-9, 1985; page 2.
14. South Coast Air Quality Management District. "Staff Report - Proposed Rule 1110.1 - Emissions from Internal Stationary Combustion Engines;" South Coast Air Quality Management District: El Monte, CA, 1984; page 1.
15. Russell, A.G., and Cass, G.R. Verification of a mathematical model for aerosol nitrate and nitric acid formation and its use for control measure evaluation. *Atmos. Environ.* **1986**, 20, 2011-25.
16. Russell, A.G.; McRae, G.J.; Cass, G.R. Mathematical modeling of the formation and transport of ammonium nitrate aerosol. *Atmos. Environ.* **1983**, 17, 949-964.
17. Pitts, J.N.; Winer, A.M.; Atkinson, R; Carter, W.P.L. Comment on "Effect of nitrogen oxide emissions on ozone levels in metropolitan regions, etc." *Environ. Sci. Technol.* **1983**, 17, 54-57.
18. Chock, D.P.; Dunker, A.M.; Kumar, S.; Sloane, C.S. Effect of NO_x emission rates on smog formation in the California South Coast Air Basin. *Environ. Sci. Technol.* **1981**, 15, 933-939.
19. Chock, D.P.; Dunker, A.M.; Kumar, S.; Sloane, C.S. Comment on "Effect of nitrogen oxide emissions on ozone levels in metropolitan regions, etc." *Environ. Sci. Technol.* **1983**, 17, 58-62.
20. Glasston, W.A. Effect of hydrocarbon and NO_x on photochemical smog formation under simulated transport conditions. *J. Air Pollut. Control Assoc.* **1981**, 31, 1169-1172.
21. Glasston, W.A. Comment on "Effect of nitrogen oxide emissions on ozone levels in metropolitan regions, etc." *Environ. Sci. Technol.* **1983**, 17, 62-63.

22. Tesche, T.W.; Seigneur, C.; Oliver, W.R.; Haney, J.L. Modeling ozone control strategies in Los Angeles. *J. Environ. Eng.* **1984**, *110*, 208-225.

APPENDIX A
AMMONIA EMISSIONS IN THE
SOUTH COAST AIR BASIN 1982
(Environmental Quality Laboratory
Open File Report 84-2)

AMMONIA EMISSIONS IN THE
SOUTH COAST AIR BASIN 1982

by

S. Gharib and G. R. Cass

Open File Report 84-2

Environmental Quality Laboratory
California Institute of Technology
Pasadena, California 91125

December 1984

References

- Addis, D., Cooperative Extension Service, University of California at Riverside. Personal communication, 15 April 1981.
- Adriano, D.C., A.C. Chang, and R. Sharpless. 1974. Nitrogen loss from manure as influenced by moisture and temperature. J. Environmental Quality 3:258-261.
- Adriano, D.C., P.F. Pratt, and S.E. Bishop. 1971. Fate of inorganic forms of N and salt from land-disposed manures from dairies. Livestock waste management and pollution abatement--proceedings--International Symposium of Livestock Wastes, 243-246. American Society of Agricultural Engineers. St. Joseph, MI.
- Alber, E., Marine Exchange. Personal communication, 1984: provided data on direction of ship arrivals and departures.
- Altman, P.L., and D.S. Dittmer. 1968. Metabolism. Federation of American Societies for Experimental Biology. Bethesda, MD.
- Anderson, E.E. Letter, 19 September 1979: forwarded 1971 inventory of horse population by county from vaccination records.
- Bartz, D.R., K.W. Arledge, J.E. Gabrielson, L.G. Hays, and S.C. Hunter. 1974. Control of oxides of nitrogen from stationary sources in the South Coast Air Basin. KVB, Inc., Report No. 5800-179. Tustin, CA.
- Bishop, S., Cooperative Extension Service, University of California at Riverside. Personal communication, 9 April 1981.
- Braddock, J.N. 1981. Impact of low ambient temperature on three-way catalyst car emissions. SAE Technical Paper Series, no. 810280.
- Bradow, R.L., and F.D. Stump. 1977. Unregulated emissions from three-way catalyst cars. SAE Technical Paper Series, no. 770369.
- Cadle, S.H., General Motors Research Laboratories, Warren, MI. Letter, 21 September 1983.
- Cadle, S.H., and P.A. Mulawa. 1980. Low molecular weight aliphatic amines in exhaust from catalyst-equipped cars. Environmental Science and Technology 14:718-723.
- Cadle, S.H., G.J. Nebel, and R.L. Williams. 1979. Measurements of unregulated emissions from General Motors' light-duty vehicles. SAE Technical Paper Series, no. 790694.

- California Department of Finance. 1982. California statistical abstract. Sacramento.
- California Department of Food and Agriculture and U.S. Department of Agriculture. California Crop and Livestock Reporting Service. 1983. California livestock--annual report 1983--cattle county estimates (also sheep). Sacramento.
- California Department of Food and Agriculture. 1982. Fertilizing materials--tonnage report, July-August-September 1982. Sacramento.
- Carter, P., and N. Trembley. 1981. FAA air traffic activity, FY 81. Federal Aviation Administration Report FAA-AMS-220. Washington, D.C. Available from NTIS as PB82-200361.
- Cass, G.R. 1978. Methods for sulfate air quality management with applications to Los Angeles. Ph.D. thesis, California Institute of Technology. Pasadena.
- Cass, G.R., S. Gharib, M. Peterson, and J.W. Tilden. 1982. The origin of ammonia emissions to the atmosphere in an urban area. California Institute of Technology, Environmental Quality Laboratory Open File Report no. 82-6. Pasadena.
- Cecotti, P., Los Angeles Glendale Reclamation Plant. Telephone conversation, 29 February 1984.
- City of Long Beach. Letter, 24 January 1983: forwarded natural gas sales data.
- Coe, D., Chino Basin Regional Plants, San Bernardino County. Telephone conversation, 5 March 1984.
- County Supervisors Association of California. 1981. California county fact book, 1980-81. Sacramento.
- Dale, A.C. 1971. Status of dairy cattle waste treatment and management research. Animal waste management--proceedings of national symposium on animal waste management. 85-95. Council of State Governments. Washington, D.C.
- Denmead, O.T., J.R. Freney, and J.R. Simpson. 1976. A closed ammonia cycle within a plant canopy. Soil Biol. Biochem. 8:161-164.
- Denmead, O.T., R. Nulsen, and G.W. Thurtell. 1978. Ammonia exchange over a corn crop. Soil Science Soc. Amer. J. 42:840-842.
- Diesel Impacts Study Committee. 1982. Diesel cars--benefits, risks, and public policy. Washington, D.C.: National Academy Press.

- Elliot, L.F., G.E. Schuman, and F.G. Viets, Jr. 1971. Volatilization of nitrogen-containing compounds from beef cattle areas. Soil Sci. Soc. Amer. Proc. 35:752-755.
- Ethyl Corporation. 1982. Yearly report of gasoline sales by state.
- Fogg, C.E. 1971. Livestock waste management and the conservation plan. Livestock waste management and pollution abatement--proceedings--International Symposium on Livestock Wastes, 34-35. American Society of Agricultural Engineers. St. Joseph, MI.
- Fretz, R. 1980. Jet Propulsion Laboratory, California Institute of Technology, Pasadena. Provided photographs.
- Gentel, J.E., O.J. Manary, and J.C. Valenta. 1973. Characterization of particulates and other non-regulated emissions from mobile sources and the effects of exhaust emissions control devices on these emissions. Dow Chemical Company and U.S. Environmental Protection Agency Document APTD-1567. Midland, MI.
- Giddens, J., and A.M. Rao. 1975. Effect of incubation and contact with soil on microbial and nitrogen changes in poultry manure. J. Environmental Quality 4:275-278.
- Harkins, J.H., and S.W. Nicksic. 1967. Ammonia in auto exhaust. Environmental Science and Technology 1:751-752.
- Hartling, E.C., County Sanitation Districts of Los Angeles County. Letter, 2 March 1984.
- Harvey, C.A., R.J. Garbe, T.M. Baines, J.H. Somers, R.H. Hellan, and P.M. Carey. 1983. A study of the potential impact of some unregulated motor vehicle emissions. SAE Technical Paper Series, no. 830987.
- Healy, T.V., H.A.C. McKay, A. Plibeam, and D. Scargill. 1970. Ammonia and ammonium sulfate in the troposphere over the United Kingdom. J. Geophysical Research 75:2317-21.
- Henein, N. 1975. The diesel as an alternative automobile engine. SAE Technical Paper Series, no. 750931.
- Holman, T., and W. Lauderdale. 1983. Diesel emissions: Their formation, impacts, and recommendations for control. Air Pollution Control Division, Colorado Department of Public Health. Denver.
- Hovey, H.H., A. Risman, and J.F. Cunnann. 1966. The development of air contaminant emission tables for nonprocess emissions. J. Air Pollution Control Association 16:362-366.

- Hudson, R., Orange County Animal Control. Telephone communication, 7 April 1981.
- Hunter, J.E., Jr. 1971. Effect of catalytic converters on automotive ammonia emissions. General Motors Research Laboratories, Research Publication GMR-1061. Warren, MI.
- Kirk-Othmer Encyclopedia. 1963. Kirk-Othmer encyclopedia of chemical technology. 2d ed. Vol. 2. New York: John Wiley & Sons.
- Kupprat, I., R.E. Johnson, and B.A. Hertig. 1976. Ammonia: A normal constituent of expired air during rest and exercise (abstract). In Proceedings of Federation of American Societies for Experimental Biology 35:1499. 60th Annual Meeting, 11-16 April, at Anaheim, CA.
- Livingstone, J., Joint Water Pollution Control Plant, County Sanitation Districts of Los Angeles County. Telephone conversation, 29 March 1984.
- Luebs, R.E., K.R. Davis, and A.E. Lagg. 1973a. Enrichment of the atmosphere with nitrogen compounds volatilized from a large dairy area. J. Environmental Quality 2, 137-141.
- Luebs, R.E., A.E. Lagg, and K.R. Davis. 1973b. Ammonia and related gases emanating from a large dairy area. California Agriculture. February 1973 edition, 10-12.
- Magill, P.L., and R.W. Benoliel. 1952. Air pollution in Los Angeles County. Industrial and Engineering Chemistry 44:1347-1351.
- Meyer, J.L., Cooperative Extension Service, University of California at Riverside. Personal communication, 1981: provided data on fertilization practices in the Los Angeles area and estimates of the fractional loss of NH_3 from fertilizers as used locally.
- Miner, J. R. 1976. Production and transport of gaseous NH_3 and H_2S associated with livestock production. U.S. Environmental Protection Agency document EPA-600/2-76-239. Ada, OK.
- Miner, S. 1969. Air pollution aspects of ammonia. Litton Systems Inc., National Air Pollution Control Administration document APTD 69-25. Bethesda, MD.
- Motor Vehicle Manufacturer's Association (1983) MVMA motor vehicle facts and figures '83. Motor Vehicle Manufacturer's Association, Detroit, MI.

- Muehling, A.J. 1971. Swine waste management. Animal waste management--Proceedings of National Symposium on Animal Waste Management, Council of State Governments, 111-120. Washington, D.C.
- Muzio, L.J., and J.K. Arand. 1976. Homogeneous gas phase decomposition of oxides of nitrogen. KVB Incorporated, Electric Power Research Institute report FP-253, project 461-1. Tustin, CA.
- Pampson, G., Orange County Sanitation District, Fountain Valley. Telephone conversation, 12 January 1984.
- Perez, J.M. 1980. Measurement of unregulated emissions--some heavy duty diesel engine results. In Health effects of diesel engine emissions, ed. W.E. Peapelko, R.M. Danner and N.A. Clarke. U.S. Environmental Protection Agency document EPA-600/9-80-057a, 128-174. Cincinnati, OH.
- Peters, J.A., and T.R. Blackwood. 1977. Source assessment: Beef cattle feedlots. U.S. Environmental Protection Agency document EPA-600/2-77-107. Washington, D.C.
- Pierson, W.R., and W.W. Brachaczek. 1983. Emissions of ammonia and amines from vehicles on the road. Environ. Sci. Technol. 17:757-760.
- Porter, L.K. et al. 1975. Pollution abatement from cattle feedlots in northeastern Colorado and Nebraska. U.S. Environmental Protection Agency document EPA-660/2-75-015. Corvallis, OR.
- Richards, B., Los Angeles County Animal Control. Telephone communication, 7 April 1981.
- San Bernardino Animal Licenses Office. Telephone communication, 7 April 1981.
- Scholz, H.G. 1971. Systems for the dehydration of livestock wastes--A technical and economical review. Livestock waste management and pollution abatement--proceedings--International Symposium on Livestock Wastes, 27-29. American Society of Agricultural Engineers. St. Joseph, MI.
- Smith, L.R., and F.M. Black. 1980. Characterization of exhaust emissions from passenger cars equipped with three-way catalyst control systems. SAE Technical Paper Series, no. 800822.
- Smith, L.R., and P.M. Carey. 1982. Characterization of exhaust emissions from high mileage catalyst equipped automobiles. SAE Technical Paper Series, no. 820783.

- Sonderlund, R. 1977. NO_x pollutants and ammonia emissions--A mass balance for the atmosphere over NW Europe. Ambio 6:118-122.
- South Coast Air Quality Management District. 1983a. Forwarded electric utility fuel use data reports.
- South Coast Air Quality Management District. 1983b. Forwarded refinery fuel use data reports.
- Southern California Association of Governments. 1982. SCAG 82 Growth forecast policy. Los Angeles, CA.
- Southern California Gas Company. 1983. Gas sales volume by air basin, South Coast and portions of South Central Air Basin. Computer printout, dated 14 January.
- Stanford Research Institute. 1973. Meeting California's energy requirements, 1975-2000. SRI project ECC-2355. Menlo Park, CA.
- Taigonides, E.P., and T.E. Hazen. 1966. Properties of farm animal excreta. Trans. Am. Soc. Agri. Engrs. 9:374-376.
- U.S. Army Corps of Engineers. 1980. Waterborne Commerce of the United States. Part 4, Waterways and harbors, Pacific Coast, Alaska and Hawaii. Department of the Army, Corps of Engineers.
- U.S. Bureau of the Census. 1972. 1970 Census of population and housing, census tracts--Santa Barbara, California. Standard metropolitan statistical area. U.S. Department of Commerce. Washington, D.C.
- U.S. Bureau of the Census. 1977. 1974 census of agriculture. Vol. 1, part 5, California state and county data. U.S. Department of Commerce. Washington, D.C.
- U.S. Bureau of the Census. 1981a. United States foreign trade--Bunker fuels. U.S. Department of Commerce. Washington, D.C.
- U.S. Bureau of the Census. 1981b. 1978 census of agriculture. Vol. 1, part 5, California state and county data. U.S. Department of Commerce. Washington, D.C.
- U.S. Bureau of the Census. 1981c. Statistical abstract of the United States, 1981. U.S. Department of Commerce. Washington, D.C.
- U.S. Bureau of the Census. 1982. 1980 census of population--Characteristics of the population--Number of inhabitants--California. U.S. Department of Commerce. Washington, D.C.

- U.S. Bureau of the Census. 1984. 1982 census of agriculture. Vol. 1, Geographic area series. Part 5, California state and county data. U.S. Department of Commerce. Washington, D.C.
- U.S. Department of Energy. 1983. Petroleum supply annual--1982. U.S. Department of Energy, Energy Information Administration report DOE/EIA-0340(82)/1. Washington, D.C.
- U.S. Environmental Protection Agency. 1976. Compilation of air pollutant emission factors, 2d ed., including supplements 1-8. U.S. Environmental Protection Agency document AP-42. Research Triangle Park, N.C.
- U.S. Environmental Protection Agency. 1980. Compilation of air pollutant emission factors, 3d ed. U.S. Environmental Protection Agency, report AP-42, supplement 10. Research Triangle Park, N.C.
- U.S. Environmental Protection Agency. 1981. Procedures for emission inventory preparation. Vol. 4, Mobile sources. U.S. Environmental Protection Agency report no. EPA-450/4-81-026d. Research Triangle Park, N.C.
- U.S. Geological Survey. 1976. Land use and land cover 1972-1975, Santa Ana, CA (1971-1974), San Bernardino, CA; 1971-1974, Santa Maria, CA; 1972-1975, Long Beach, CA; 1973-1975, Los Angeles, CA). U.S. Department of the Interior, Geological Survey, Open File Maps no. 76-114-1 76-115-1; 76-117-1; 76-118-1; 76-119-1, Land Use Series.
- Urban, C.M., and R.J. Garbe. 1979. Regulated and unregulated exhaust emissions from malfunctioning automobiles. SAE Technical Paper Series, no. 790696.
- Urban, C.M., and R.J. Garbe. 1980. Exhaust emissions from malfunctioning three-way catalyst-equipped automobiles. SAE Technical Paper Series, no. 800511.
- Ventura County, Air Pollution Control District. 1983. Forwarded electric utility fuel use data reports.
- Viets, F.G., Jr. 1971. Cattle feedlot pollution. Animal waste management--Proceedings of National Symposium on Animal Waste Management, Council of State Governments, 97-106. Washington, D.C. (Also published in Agricultural Science Review 9:1-8.)
- Walkup, H.G., and J.L. Nevins. 1966. The cost of doing business in agricultural ammonia for direct application. Agricultural Ammonia News 16:96-100.

Walters, J., Irvine Ranch Water District, Orange County. Telephone conversation, 29 February 1984.

Warner, S.B., Los Alisos Water District, Orange County. Telephone conversation, 26 March 1984.

Williams, J., Aliso Water Management Agency, Orange County. Telephone conversation, 28 March 1984.

Williams, R.L., and D.P. Chock. 1980. Characterization of diesel particulate exposure. In Health effects of diesel engine emissions, ed. W.E. Pepelko, R.M. Danner, and N.A. Clarke, 3-33. U.S. Environmental Protection Agency document EPA-600/9-80-057a. Cincinnati, OH.

Wohlers, H.C., and G.B. Bell. 1956. Literature review of metropolitan air pollutant concentrations--Preparation, sampling, and assay of synthetic atmospheres. Stanford Research Institute final report on project no. S-1816. Menlo Park, CA.

APPENDIX

**Tabulation of Emission Factors, Activity Levels,
and Ammonia Emission Rates**

TABLE A.1
Emission Factors for Ammonia from Combustion Sources

	VALUE REPORTED	REFERENCE	EMISSION FACTOR (Kg NH ₃ /10 ⁹ Btu)	VALUE ADOPTED FOR EMISSION INVENTORY USE (Kg NH ₃ /10 ⁹ Btu)
STATIONARY SOURCES				
Fuel Combustion				
Natural Gas				
Average of Los Angeles Source Tests	0.4 mg/m ³ NH ₃ in exhaust	(a)	0.119	
New York Emission Inventory Emission Factor	0.5 lb NH ₃ /10 ⁶ ft ³ gas burned	(b)	0.214	
Literature Survey (1969)	0.3 to 0.56 lb NH ₃ /10 ⁶ ft ³ gas	(c)	0.128-0.240	
Literature Review (1956)	0.010 tons NH ₃ /10 ⁶ ft ³ gas	(d)	8.56	
Recent Source Test: 200,000 Btu/hr combustor				
(1) at 2% excess O ₂ ; 17 test avg	14.44 ppm NH ₃ in exhaust	(e)	3.25	3.25
(2) at 4% excess O ₂ ; 23 test avg	6.00 ppm NH ₃ in exhaust	(e)	1.351	1.35
(3) at 6% excess O ₂ ; 15 test avg	1.00 ppm NH ₃ in exhaust	(e)	0.225	0.22
Residual Fuel Oil				
Average of Los Angeles Source Tests	0.4 mg/m ³ NH ₃ in exhaust	(a)	0.125	
New York Emission Inventory Emission Factor	1 lb/1000 gal oil	(f)	3.03	
Literature Survey (1956)	0.001 tons NH ₃ /ton oil	(g)	23.1	
Recent Source Test: 200,000 Btu/hr combustor at 2% excess air; avg of 2 tests	11.3 ppm in exhaust	(h)	2.8	2.8
Distillate Oil				
New York Emission Inventory Emission Factor	1 lb/1000 gal oil	(i)	3.29	3.3
Coal				
Literature Review (1956)	2 lb NH ₃ /ton coal	(j)	37.8	38
Mass Balance over N.W. Europe	1.21 g NH ₃ /920 g coal	(k)	50	
Recent Source Test: 200,000 Btu/hr combustor at 4% excess air, 1 test	85 ppm NH ₃ in exhaust	(l)	~20	
Wood				
Literature Review (1956)	2.4 lb NH ₃ /ton wood	(m)		

Notes:

- (a) Magill and Benoliel (1952)
- (b) Hovey, Risman and Cunnann (1966), Range reported 0.3 to 20 lb NH_3 /10⁶ ft³ natural gas
- (c) Miner (1969); literature survey
- (d) Wohlers and Bell (1956)
- (e) Muzio and Arand (1976)
- (f) Hovey, Risman and Cunnann (1966); Range reported 0.06 lb/1000 gal to 8 lb/1000 gal; converted at 0.011 scf prod/btu; 6.11 x 10⁶ btu/bbl
- (g) Wohlers and Bell (1956); value appears high but note that data may be rounded up to 0.001 tons NH_3 /ton oil
- (h) Muzio and Arand (1976); 2 tests range 20 ppm - 2.54 ppm
- (i) Hovey, Risman and Cunnann (1966); converted at 0.011 scf prod/btu; 5.8 x 10⁶ btu/bbl
- (j) Wohlers and Bell (1956)
- (k) Soderlund (1977)
- (l) Muzio and Arand (1976); combustion product data unavailable, converted from ppm to Kg/10⁹ btu in proportion to oil and natural gas data
- (m) Wohlers and Bell (1956)

TABLE A.2
Fuel Economy Calculation for 1982 Automobile Fleet

Age (years)	Model Year	Percentage of Total Vehicles in Use (a)	Percent Sold with Diesel Engines (b) (US)	Percentage of Vehicles in Use (gasoline engine)	Percentage of Vehicles in Use (diesel engine)	Annual Average Mileage Driven (c)	Fraction of Light Duty Fleet Miles Traveled by Gasoline Engines	Fraction of Light Duty Fleet Miles Traveled by Diesel Engines	Fuel Economy for Gasoline Cars MPG (d)	Weighted Average Fuel Economy for Gasoline Cars MPG	Weighted Average Fuel Economy for Diesel Cars MPG
1	1982	7.77	4.6	7.41	0.36	15,900	0.111	0.0054	26.2		
2	1981	7.77	5.9	7.31	0.46	15,000	0.104	0.0065	25.1		
3	1980	8.76	4.6	8.36	0.40	14,000	0.111	0.0053	23.5	21.10	24.69
4	1979	9.20	2.2	9.0	0.20	13,100	0.111	0.0025	20.3		
5	1978	8.50	0.4	8.47	0.03	12,200	0.098	0.0004	19.9	fleet avg. for cat. autos	fleet avg. for diesel autos
6	1977	6.73	0.1	6.72	0.01	11,300	0.072	0.00011	18.3		
7	1976	5.51	0.1	5.5	0.01	10,300	0.054	0.00010	17.5		
8	1975	5.37	0.1	5.36	0.01	9,400	0.048	0.00009	15.8		
9	1974	6.45	0.1	6.44	0.01	8,500	0.052	0.00008	14.2		
10	1973	5.78	-	5.78		7,600	0.042		13.6		
11	1972	4.90	-	4.9		6,700	0.031		13.6	13.65	
12	1971	3.88	-	3.88		6,700	0.025		13.6	fleet avg. for non-cat. autos	
13	1970(-)	19.38	-	19.38		6,700	0.123		13.6		

NOTES:

- (a) Derived from California Department of Finance (1982), Table J-5, p. 170.
- (b) Values for 1980 and previous years are from Diesel Impacts Study Committee (1982), pp. 1 and 90. Values for 1981 and 1982 are Automotive News, 7/5/82, as cited by Holman and Lauderdale (1983), p. 7. Data shown are based on nationwide sales statistics.
- (c) U.S. Environmental Protection Agency, 1976.
- (d) Motor Vehicle Manufacturers' Association (1983).
- (e) A fuel economy value of 27 MPG is given by Cadle (1983) for General Motors light duty diesel vehicles. Since fuel economy for all automobiles has been improving in recent years, we estimate a fleet average fuel economy weighted over new and older diesel cars to be about 25 MPG.

TABLE A.3

Emission Factors for Ammonia from Highway Vehicles

	VALUE FOR VEHICLES IN PROPER OPERATING CONDITION (mg/km)	REFERENCE	VALUE ADOPTED FOR EMISSION INVENTORY	
			(mg/km)	(kg NH ₃ /10 ⁹ Btu)
HIGHWAY VEHICLES				
Autos and Lt. Trucks (gasoline engines)				
Catalyst Equipped Engines				
Oxidation Catalyst Only				
1. 1977 and 1978 production vehicles, 1975 FTP cycle	2.5	(a)		
2. California emission controls, 1975 FTP cycle	3.06	(b)		
3. 1978 Buick, Ford, Volvo, Oldsmobile, Chevrolet, Chrysler, 1979 FTP cycle, unleaded fuel	5.7	(c)	10 (x)	2.7
4. 1978 Chevrolet Malibu, 1978 Ford Granada, 1977 FTP cycle, unleaded fuel, with air pump	3.6	(d)		
5. 1978 Chevrolet Malibu, 1978 Ford Mustang II, 1977 FTP cycle, unleaded fuel, without air pump	3.1	(d)		
3-way Catalyst				
1. General Motors vehicles; 1975 FTP cycle	5.0	(e)		
2. 1978 Pontiac Sunbird; 1978 Saab 99; 1978 FTP cycle	3.6	(f)		
3. 1979 Mercury (2); 1978 Volvo; 1979 FTP cycle	10.7	(g)		
4. 1977 Volvo (California model); 1975 FTP cycle	4.7	(h)	35 (x)	
5. 1980 Lincoln Continental, 1975 FTP cycle	16.7	(i)		
6. 1978 Pontiac Sunbird; 1978 FTP cycle	11.1	(j)		
7. 1978 Saab; 1978 FTP cycle	60.8	(j)		
3-way Catalyst Plus Oxidation Catalyst				
1. 1978 Ford Pinto; 1979 Mercury Marquis; 1978 FTP cycle	2.6	(k)		
2. 1978 Ford Pinto; 1980 Chevrolet Caprice; 1975 FTP cycle	20.1	(l)	10 (x)	
3. 1978 Ford Pinto; 1979 Mercury Marquis; 1978 FTP cycle	5.6	(m)		
Non-Catalyst Pre-1975 Cars				
1. General Motors vehicles; 1975 FTP cycle; unleaded fuel	2.5	(n)		
2. 1977 AMC Pacer; 1977 FTP cycle; unleaded fuel	3.1	(o)	5 (x)	0.87
3. 1956 Oldsmobile engine on driving cycle	2.5	(p)		
4. 1972 HFW driving cycle	5	(q)		
Catalyst Medium Trucks				2.7 (y)
Non-Catalyst Medium and Heavy Gasoline Trucks				0.87 (z)
Diesel Vehicles				
Diesel Automobiles				
1. Diesel automobile	0.62	(r)	0.6	0.19
2. Experimental diesel auto, FTP cycle	0.6	(s)		
3. Peugeot, driving cycle	10.92	(t)		
4. 1972 Mercedes Benz, 60 mph	0.35	(u)		
5. Lt. duty diesel vehicles	0-8	(v)		
Diesel Trucks				
1. Three 8-cylinder diesel engines	2.3	(w)	2	0.14
2. Heavy duty diesel	0-33	(v)		
LPG for Carburetion				0.87 (z)

NOTES:

- (a) Cadle (1983); NH_3 emission rate from properly running oxidation catalyst car is about 4 mg/mi.
- (b) Cadle and Mulawa (1980), Table V; Average of 5 tests (runs 9 through 13), range 0.6 to 14.8 mg/mi (avg. equals 4.9 mg NH_3 /mi or 3.06 mg/km).
- (c) Smith and Carey (1982), Tables C-1 to C-6; average values of oxidation-catalyst-equipped cars 1, 4, 6, 7, 8, 9, 10. All values are measured before tune-up in "as received" condition.
- (d) Urban and Garbe (1979); Avg. values from Table 8.
- (e) Cadle et al. (1979), Table 8; avg. value for dual and 3-way catalysts under normal operation. Note that NH_3 emissions from malfunctioning cars of this type can be very high, about 114 mg/km.
- (f) Smith and Black (1980); value of 3.43 (mg/km) used for Sunbird as given in Table B-16; value of 3.83 mg/km used for Saab as discussed in text on page 2465. Value shown in table is average of these two results. Saab emissions are much higher (21.68 mg/km) if car is tested with initial malfunction.
- (g) Smith and Carey (1982), Tables C-2 and C-4; avg. values for cars 2, 3, and 5 in "as received" condition.
- (h) Bradow and Stump (1977), Table 5; average of two tests with sensor active.
- (i) Braddock (1981); value from Figure 8 at 78°F. Value from test on Buick Century is not used because value is high (212.36 mg/mi) due to vehicle malfunction.
- (j) Urban and Garbe (1980); Table 4.
- (k) Smith and Black (1980), Table B-16; average of results for the two cars indicated.
- (l) Braddock (1981), Figure 8; average of values for two cars indicated at 78°F.
- (m) Urban and Garbe (1980), Table 4; average of values for two cars indicated.
- (n) Cadle et al. (1979), Table 8; non-catalyst cars.
- (o) Urban and Garbe (1979), Table C-1; unmodified condition.
- (p) Harkins and Nickle (1967); value reported is 2.2 ppm; converted to mg/km at fuel consumption rate of 13.6 mpg.
- (q) Hunter (1971), Figure 2; standard carburetion.
- (r) Cadle et al. (1979); text gives value of 1 mg/mile.
- (s) Williams and Chock (1980), Table XIII.
- (t) Hensein (1975), Table 3; original value equal to 11.1 ppm NH_3 in exhaust; converted to mg/km assuming stoichiometric combustion of the fuel and fuel economy of 24.69 mpg.
- (u) Gentel et al. (1973), Table 38; original value equal to 0.36 ppm NH_3 in exhaust; converted to mg/km assuming stoichiometric combustion of the fuel and fuel economy of 24.69 mpg.
- (v) Harvey et al. (1983), Table 1.
- (w) Perez (1980); maximum value reported is 0.4 mg NH_3/m^3 exhaust; converted to mg/km assuming stoichiometric combustion of the fuel and fuel economy of 5.5 mpg.
- (x) Based on recommended values given by Pierson and Brachaczek (1983), text page 759. Values adopted for use with emission inventory are higher than for average of properly operated cars. These higher figures are needed to reflect actual vehicle fleet that includes cars with malfunctions that lead to high NH_3 emission rates. See notes above.
- (y) Assumed similar to catalyst automobiles.
- (z) Assumed similar to non-catalyst automobiles.

TABLE A.4

Ammonia Emission Estimates for Stationary Combustion Sources

Six-County South Coast Air Basin--1982

	ESTIMATED 1982 FUEL USE (10 ⁹ Btu/day)		EMISSION FACTOR (Kg NH ₃ /10 ⁹ Btu)	AMMONIA EMISSIONS (metric tons/day)
STATIONARY SOURCES				
FUEL COMBUSTION				
Electric Utilities				
Natural Gas	802.	(a)	1.47 (k)	1.18
Residual Oil	134.	(a)	2.8 (l)	0.38
Digester Gas	0.6	(a)	1.47 (m)	0.0009
Refinery Fuel				
Natural Gas	101.	(b)	1.17 (n)	0.118
Residual Oil	5.3	(b)	2.8 (o)	0.015
Refinery Gas	334.	(b)	1.17 (p)	0.39
Industrial and Low Priority Commercial				
Natural Gas	324.	(c)	1.45 (q)	0.47
LPG	5.52	(d)	1.45 (r)	0.008
Residual Oil	8.	(e)	2.8 (s)	0.022
Distillate Oil	37.23	(e)	3.3 (t)	0.123
Digester Gas	18.04	(f)	1.45 (r)	0.026
Coke Oven Gas	37.53	(g)	0.40 (u)	0.015
Residential and High Priority Commercial				
Natural Gas	918.	(h)	0.225(v)	0.207
LPG	16.85	(i)	0.225(w)	0.004
Residual Oil	30.4	(i)	2.8 (x)	0.085
Distillate Oil	23.86	(i)	3.3 (x)	0.079
Coal	0.6	(j)	38. (x)	0.023
TOTAL				3.15

NOTES:

- (a) 1982 average daily use, from South Coast Air Quality Management District (1983a) and Ventura County (1983).
- (b) 1982 average daily use, from South Coast Air Quality Management District (1983b).
- (c) 1982 average daily use, by all industries from Southern California Gas Company (1983) and City of Long Beach (1983), less electric utility and refinery natural gas usage cited above.
- (d) U.S. Department of Energy (1963) gives the ratio of industrial to chemical LPG sales in the U.S. as 0.22. This ratio was used for data from the state of California to break LPG sales into sales to chemical and industrial plants. This value includes sales for refinery fuel use which cannot be separated from the total.
- (e) State of California total residual and distillate fuel oil use by industries other than oil companies and electric utilities was taken from U.S. Department of Energy (1983). Seventy-five percent of the non-refinery industrial heating demand in Southern California is within the six-county 1974 boundaries of the South Coast Air Basin (Cass, 1978), and 64% of state industrial fuel use is in Southern California (Stanford Research Institute, 1973). Therefore, air basin fuel oil use by industry is estimated as 0.48% of total state use by industry. Kerosene use has been added to the distillate fuel use number shown.
- (f) From survey of eight large sewage treatment plants in the inventory area.
- (g) Based on 1973 fuel use data at Kaiser Steel, from Cass (1978).
- (h) 1982 average daily use by residential and commercial users taken from Southern California Gas Company (1983) and City of Long Beach (1983). Fuel use in south coastal strip of Santa Barbara County estimated as 78% of county total on the basis of fraction of 1970 population living in southern portion of that county (U.S. Bureau of the Census, 1972).
- (i) State total LPG, residual fuel oil and distillate oil use by residential and commercial customers is given by U.S. Department of Energy (1983). Forty percent of residential/commercial oil use in the state is in Southern California (Stanford Research Institute, 1973) and 77% of Southern California population is within the six-county boundaries of the South Coast Air Basin (Southern California Association of Governments, 1982). SCAB LPG use thus is estimated as 31% of state total (i.e., $0.40 \times 0.77 = 0.31$).
- (j) 1973 data from Cass (1978).
- (k) Weighted average: 33% emission factor at 2% O₂ in stack, 22% factor at 4% O₂, 45% factor at 6% O₂ based on frequency of occurrence of O₂ levels given by Bartz et al. (1974; tests 279-289, 298-301).
- (l) From Table A.1.
- (m) Assumed similar to utility boiler burning natural gas.
- (n) Weighted average: 19% emission factor at 2% O₂ in stack, 33% factor at 4% O₂, 48% factor at 6% O₂ based on frequency of occurrence of O₂ levels given by Bartz et al (1974; tests 12-73, 95-103).
- (o) From Table A.1.
- (p) Assumed similar to refinery equipment burning natural gas.
- (q) Weighted average: 35% emission factor at 2% O₂ in stack, 15% factor at 4% O₂, 50% factor at 6% O₂ based on frequency of occurrence of O₂ levels for industrial fuel-burning equipment given by Bartz et al. (1974).
- (r) Assumed similar to industrial equipment burning natural gas.
- (s) From Table A.1.
- (t) From Table A.1.
- (u) Weighted average: 2% emission factor at 2% O₂ in stack, 10% factor at 4% O₂, 88% factor at 6% O₂ based on frequency of occurrence of O₂ levels for steel mill equipment given by Bartz et al. (1974; tests 104-157).
- (v) Source tests by Bartz et al. (1974) show that home heaters have high levels of excess O₂ in their exhaust.
- (w) Assumed similar to home heaters burning natural gas.
- (x) From Table A.1.

TABLE A.5

Ammonia Emission Estimates for Stationary Combustion Sources

Six-County South Coast Air Basin--1982

	ESTIMATED 1982 FUEL USE		EMISSION FACTOR		NH ₃ EMISSIONS
	(10 ⁹ Btu/day)		(Kg NH ₃ /10 ⁹ Btu)		(metric tons/day)
MOBILE SOURCES					
Highway Vehicles					
Catalyst Autos and Lt. Trucks	870.4	(a)	2.7	(1)	2.35
Non-Catalyst Autos and Lt. Trucks	557.3	(a)	0.87	(1)	0.485
Diesel Autos and Lt. Trucks	18.3	(b)	0.19	(1)	0.0035
Catalyst Medium Vehicles	85.1	(a)	2.7	(1)	0.23
Non-Catalyst Medium and Heavy Trucks	159.8	(a)	0.87	(1)	0.14
Diesel Trucks	162.4	(b)	0.14	(1)	0.023
LPG for Carburetion	8.2	(c)	0.87	(1)	0.0071
Civil Aviation					
Jet Aircraft	49.5	(d)	0.14	(m)	0.0069
Aviation Gasoline	2.4	(d)	0.87	(n)	0.0021
Commercial Shipping					
Residual Oil-Fired Ships' Boilers	24.3	(e)	2.8	(o)	0.068
Diesel Ships	11.2	(e)	0.14	(m)	0.0016
Railroad					
Diesel Oil	24.8	(f)	0.14	(m)	0.0035
Military					
Gasoline	5.65	(g)	0.87	(n)	0.0049
Diesel Oil	16.7	(h)	0.14	(m)	0.0023
Jet Fuel	16.71	(i)	0.14	(m)	0.0023
Residual Oil (Bunker Fuel)	0.28	(j)	2.8	(o)	0.0008
Miscellaneous					
Off-Highway Vehicles and Miscellaneous Sources	46.26	(k)	0.14	(m)	0.0065
TOTAL					3.34

NOTES:

- (a) State of California total sales of leaded and unleaded gasoline taken from Ethyl Corporation (1982). Fuels apportioned to six-county air basin based on ratio of that region's population to entire state's population. Fuels apportioned among vehicle types based on fraction of VMT and fuel economy for each vehicle class.
- (b) State of California total sales of distillate oil for on-highway use taken from U.S. Department of Energy (1983), apportioned to six-county air basin in proportion to percentage of state truck registrations in that region from County Supervisors Association of California (1981). Fuel apportioned among light trucks, autos, and heavy vehicles on basis of the fraction of VMT by each vehicle type.
- (c) State of California total taken from U.S. Department of Energy (1983), value of LPG for internal combustion use. Apportioned to study region on basis of fraction of state population in that region.
- (d) Aircraft operations taken from Carter and Trembley (1981). Fuel use computed from operations by the procedure outlined by U.S. Environmental Protection Agency (1980).
- (e) Computed by procedure described by Cass (1978). Ship traffic in local harbors is given by U.S. Army Corps of Engineers (1980). Fraction of ships sailing northward and southward along the coast determined from data given by Alber (1984). Residual-to-distillate fuel use ratio taken from dockside fuel sales data of the U.S. Bureau of Census (1981a). Ship fuel economy given by U.S. Environmental Protection Agency (1981).
- (f) Fuel sales to railroads in California taken from U.S. Department of Energy (1983). Fuel use apportioned to six-county study region in proportion to fraction of railroad track in the region versus in the entire state.
- (g) Scaled from 1973 value given by Cass (1978). Scale factor is ratio of 1982 to 1973 diesel fuel sales to military in California from U.S. Department of Energy (1983) and the 1973 issue of that report series.
- (h) 20% of statewide sales of distillate oil to the military as given by U.S. Department of Energy (1983). See Cass (1978) for justification of procedure.
- (i) 1973 data from Cass (1978).
- (j) 2% of total California sales of residual fuel oil to the military as given by U.S. Department of Energy (1983). See Cass (1978) for justification of procedure.
- (k) California sales of distillate oil to off-highway vehicles plus "other" sources given by U.S. Department of Energy (1983). Fuel use apportioned to six-county study area on the basis of population. Kerosene use has been added to the distillate fuel use numbers shown.
- (l) From Table A.3.
- (m) Assumed to emit NH_3 at the same rate as a diesel truck from Table A.3.
- (n) Assumed to emit NH_3 at the same rate as the non-catalyst gasoline engine automobile given in Table A.3.
- (o) Assumed to emit NH_3 at the same rate as the industrial boiler given in Table A.1.

TABLE A.6

Emissions from Industrial Process Sources

	NH ₃ Emissions (metric tons/day)	
Ammonia Storage	0.06	(a)
Refinery FCC Units	0.67	(a)
Refinery Waste Water Treatment	0.35	(a)
Steel Industry	0.23	(a)
Chemical Plants	0.76	(a)
Refrigerant Loss	0.38	(b)

NOTES:

- (a) From survey of Cass et al. (1982).
 (b) See Table A.28.

Table A.7 Estimated NH_3 Emissions from Municipal Waste Water Treatment - 1982 (excluding sludge processing)

Plant	Treatment Stage	Flow Rate (mgd)	Flow Rate (10 ⁶ l/day)	Influent NH ₃ -N (mg/l)	Effluent			NH ₃ -N Loss from water		Nitrogen-Containing Gases to Atmosphere (metric tons -N/day)	NH ₃ Emission to Atmosphere (metric tons/day as NH ₃)
					NH ₃ -N (mg/l)	NO ₂ ⁻ -N (mg/l)	NO ₃ ⁻ -N (mg/l)	To Bacterial Cells ^(a) (mg/l)	To Atmosphere as NH ₃ or as N ₂ ^(b) (mg/l)		
COUNTY SANITATION DISTRICTS OF L.A. COUNTY											
1. San Jose Creek	Secondary	36.84	139.4	19.9	15.6	0.603	2.0	0.8	0.9	0.125	0.15
2. Whittier Narrows	Secondary	13.41	50.8	20.4	16.4	0.967	1.5	0.82	0.71	0.036	0.044
3. Pomona	Secondary	9.26	35.0	18.8	11.8	0.845	2.0	0.75	3.4	0.119	0.144
4. Los Coyotes (Has 3 separate secondary units.)											
Unit 1	Secondary	11.36	43.0	23.3	10.5	1.326	2.6	0.93	7.94	0.342	0.414
Unit 2	Secondary	11.44	43.3	23.3	11.5	0.04	3.0	0.93	7.83	0.339	0.410
Unit 3	Secondary	11.37	43.0	23.3	7.6	0.719	4.8	0.93	9.25	0.398	0.482
5. Long Beach	Secondary	9.95	37.7	21.7	11.1	0.922	2.3	0.87	6.51	0.245	0.296
6. Joint Plant	Primary	360	1362.6	36	36					0	
CITY OF LOS ANGELES											
7. Hyperion Plant	Primary	379	1434.5	18.8	18.5	0	0	0	0.3	0.43	0.52
	Secondary	100	378.5	18.5	2.5	0.2	5.2	0.74	9.86	3.73	4.51
8. Terminal Island	Secondary	17.8	67.4	39.1	12.6	0.79	5.3	1.56	18.85	1.27	1.54
9. L.A. Glendale Reclamation Plant	Secondary	10	37.9	19.5	6.5	(11.70)(c)		0.78	0.52	0.020	0.024

Table A.7 Estimated NH₃ Emissions from Municipal Waste Water Treatment - 1982 (excluding sludge processing) (Continued)

Plant	Treatment Stage	Flow Rate (mgd)	Flow Rate (10 ⁶ l/day)	Influent NH ₃ -N (mg/l)	Effluent			NH ₃ -N Loss from water		Nitrogen-Containing Gases to Atmosphere (metric tons -N/day)	NH ₃ Emission to Atmosphere (metric tons/day as NH ₃)
					NH ₃ -N (mg/l)	NO ₂ ⁻ -N (mg/l)	NO ₃ ⁻ -N (mg/l)	To Bacterial Cells ^(a) (mg/l)	To Atmosphere as NH ₃ or as N ₂ ^(b) (mg/l)		
ORANGE COUNTY SANI-TATION DISTRICT											
10. Fountain Valley	Secondary	60	227.1	23	12	(9.20)(d)	0.92	0.88	0.2	0.242	
11. Huntington Beach	Secondary	160	605.6	23	12	(9.20)(d)	0.92	0.88	0.533	0.645	
OTHER AGENCIES											
12. Water Factory 21	NH ₃ Strip-ping Tower	8	30.3	24.22	19.59			4.63	0.14	0.17	
13. Irvine Ranch Water District	Secondary	8.5	32.2	20	2	(17)(e)	0.8	0.2	0.0064	0.008	
14. Los Alisos Water District	Secondary	2.5	9.5	50	12	(30)(f)	2.0	6	0.057	0.069	
15. Aliso Water Man-agement Agency	Secondary	3	11.4	35	20	(5.25)(g)	1.4	8.35	0.095	0.115	
16. Laguna Hills Sani-tation District	Secondary	4.5	17.0	(21)(h)	5	(3.15)(i)	0.84	12.01	0.204	0.247	
17. South East Regional Reclamation Authority	Secondary	8.5	32.2	(21)(h)	2	(3.15)(i)	0.84	15.01	0.483	0.584	

Table A.7 Estimated NH₃ Emissions from Municipal Waste Water Treatment - 1982 (excluding sludge processing) (continued)

Plant	Treatment Stage	Flow Rate (mgd)	Flow Rate (10 ⁶ l/day)	Influent NH ₃ -N (mg/l)	Effluent			NH ₃ -N Loss from water		Nitrogen-Containing Gases to Atmosphere (metric tons -N/day)	NH ₃ Emission to Atmosphere (metric tons/day as NH ₃)
					NH ₃ -N (mg/l)	NO ₂ ⁻ -N (mg/l)	NO ₃ ⁻ -N (mg/l)	To Bacterial Cells (a) (mg/l)	To Atmosphere as NH ₃ or as N ₂ (b) (mg/l)		
OTHER AGENCIES (Cont)											
18. Moulton-Niguel Water District	Secondary	0.4	1.5	(21)(h)	(12)(j)	(3.15)(i)		0.84	5.01	0.0075	0.0069
19. South Coast County Water District	Primary	3.5	13.2	28	23	0		0	5	0.066	0.080
	Secondary	3.5	13.2	23	6	(3.45)(i)		0.92	12.63	0.167	0.202
20. City of San Clemente	Secondary	3.2	12.1	(21)(h)	0.5	(3.15)(i)		0.84	16.51	0.200	0.242
21. Capistrano Beach Sanitary District	Secondary	0.85x10 ⁻³	3.2x10 ⁻³	(21)(h)	(12)(j)	(3.15)(i)		0.84	5.01	0.016x10 ⁻³	0.019x10 ⁻³
22. City of Riverside	Secondary	23.5	88.9	24.5	12.5	(3.68)(i)		0.98	7.34	0.653	0.790
23. Hemet Treatment Plant	Secondary	5.1	19.3	22.5	15	(3.38)(i)		0.9	3.22	0.062	0.075
24. Sun City Treatment Plant	Secondary	0.7	2.6	(21)(h)	4.6	(3.15)(i)		0.84	12.41	0.032	0.039
25. Sunnymead Treatment Plant	Secondary	3	11.4	(21)(h)	(12)(j)	(3.15)(i)		0.84	5.01	0.057	0.069
26. City of San Bernardino	Secondary	21	79.5	19	16	(0)(k)		0.76	2.24	0.178	0.215

Table A.7 Estimated NH₃ Emissions from Municipal Waste Water Treatment - 1982 (excluding sludge processing) (Continued)

Plant	Treatment Stage	Flow Rate (mgd)	Flow Rate (10 ⁶ l/day)	Influent NH ₃ -N (mg/l)	Effluent			NH ₃ -N Loss from water		Nitrogen-Containing Gases to Atmosphere (metric tons -N/day)	NH ₃ Emission to Atmosphere (metric tons/day as NH ₃)
					NH ₃ -N (mg/l)	NO ₂ ⁻ -N (mg/l)	NO ₃ ⁻ -N (mg/l)	To Bacterial Cells ^(a) (mg/l)	To Atmosphere as NH ₃ or as N ₂ ^(b) (mg/l)		
OTHER AGENCIES (cont)											
27. Chino Basin Regional Plant #1	Secondary	19	71.9	20	6.4	(12)(1)		0.8	0.8	0.058	0.070
28. Chino Basin Regional Plant #2	Secondary	3.5	13.2	19.8	2.2	(11.88)(1)		.79	4.93	0.065	0.079
29. Chino Basin Regional Plant #3	Primary	3.2	12.1	25	25					0	
30. City of Colton	Secondary	3.4	12.9	(21)(h)	6	(3.15)(1)		0.84	11.01	0.142	0.172
31. City of Redlands	Secondary	4	15.1	(21)(h)	(12)(j)	(3.15)(1)		0.84	5.01	0.076	0.092
32. City of Rialto	Secondary	3.5	13.2	(21)(h)	(12)(j)	(3.15)(i)		0.84	5.01	0.066	0.080
33. City of Santa Barbara	Secondary	8.5	32.2	28	20	(4.20)(1)		1.12	2.68	0.086	0.104
34. Montecito Sanitation District	Secondary	1.0	3.8	21(h)	<1	(3.15)(i)		0.84	16.01	0.061	0.074
35. Goleta Sanitation District	Primary	6.2	23.5	(22.5)(m)	22.5					(0)	
36. Carpinteria Sanitation District	Secondary	1.3	4.9	(21)(h)	0.01	(3.15)(1)		0.84	17	0.083	0.1

Table A.7 Estimated NH_3 Emissions from Municipal Waste Water Treatment - 1982 (excluding sludge processing) (Continued)

Plant	Treatment Stage	Flow Rate (mgd)	Flow Rate (10 ⁶ l/day)	Influent NH ₃ -N (mg/l)	Effluent			NH ₃ -N Loss from water		Nitrogen-Containing Gases to Atmosphere (metric tons -N/day)	NH ₃ Emission to Atmosphere (metric tons/day as NH ₃)
					NH ₃ -N (mg/l)	NO ₂ ⁻ -N (mg/l)	NO ₃ ⁻ -N (mg/l)	To	To		
								Bacterial Cells ^(a) (mg/l)	Atmosphere as NH ₃ or as N ₂ ^(b) (mg/l)		
OTHER AGENCIES (cont)											
37. Summerland Sanitation District	SECONDARY	0.15	0.57	(21)(h)	(12)(j)	(3.15(i)	0.84	5.01	<u>0.0028</u>	<u>0.0034</u>	
									10.77	13.03	

NOTES

- (a) Estimated to be 4% of influent $\text{NH}_3\text{-N}$ for secondary treatment processes (Hartling, 1984)
- (b) By difference between influent, effluent and bacterial nitrogen fluxes, stated as mg/l relative to influent flow.
- (c) Most of the ammonia in the influent to this plant is oxidized during the secondary treatment process (Cecotti, 1984). A value equal to 60% of secondary influent $\text{NH}_3\text{-N}$ is assumed to be nitrified.
- (d) This agency tries to remove 40-50% of NH_3 during the secondary treatment stage (Pampson, 1984). A value equal to 40% of secondary influent $\text{NH}_3\text{-N}$ is assumed to be nitrified.
- (e) Nitrification removes almost all of the $\text{NH}_3\text{-N}$ (Walters, 1984). A value equal to 85% of secondary influent $\text{NH}_3\text{-N}$ concentration is assumed to be nitrified.
- (f) Most of the $\text{NH}_3\text{-N}$ at this plant is nitrified (Warner, 1984). A value equal to 60% of secondary influent $\text{NH}_3\text{-N}$ concentration is assumed to be nitrified.
- (g) Operators of this plant try not to nitrify the $\text{NH}_3\text{-N}$ (Williams, 1984). The average percentage of nitrification during secondary treatment at L.A. County Sanitation District facilities is 15% and that degree of nitrification is assumed here.

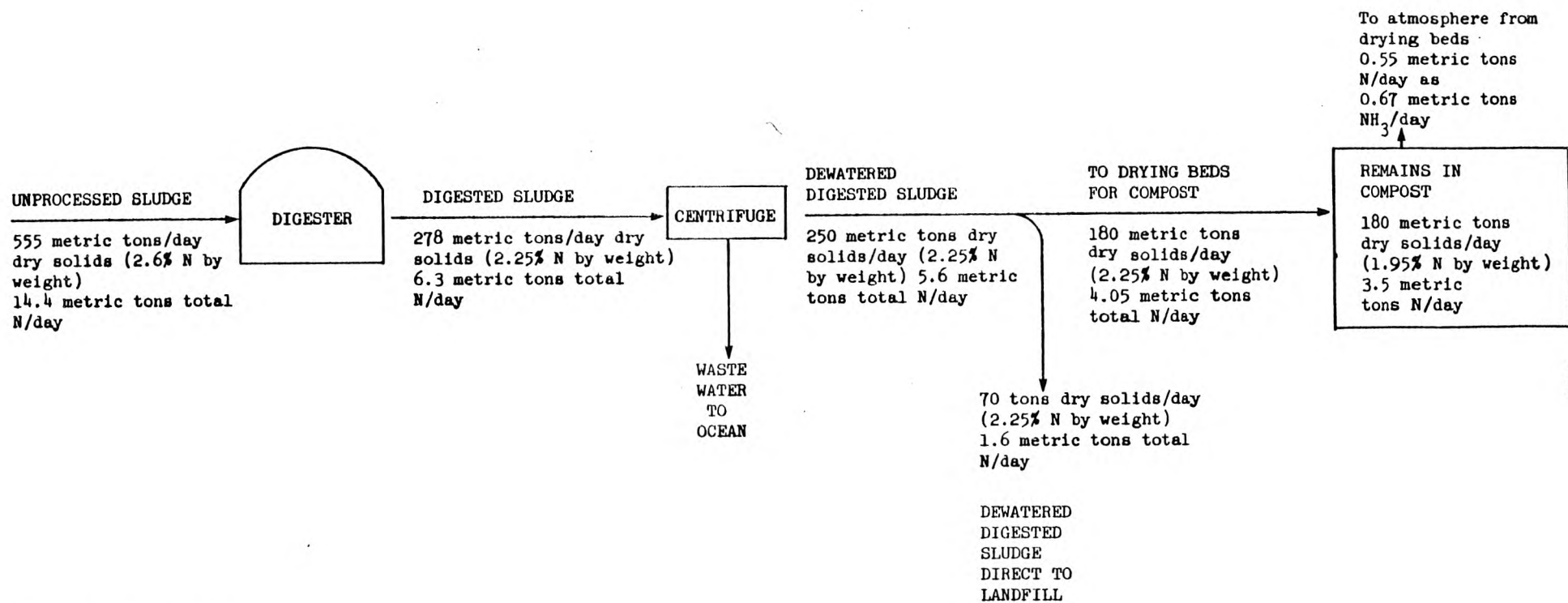
Table A.7 Estimated NH_3 Emissions from Municipal Waste Water Treatment - 1982 (excluding sludge processing) (Continued)

Plant	Treatment Stage	Flow Rate (mgd)	Flow Rate (10^6 l/day)	Influent $\text{NH}_3\text{-N}$ (mg/l)	Effluent			NH ₃ -N Loss from water		Nitrogen-Containing Gases to Atmosphere (metric tons -N/day)	NH ₃ Emission to Atmosphere (metric tons/day as NH_3)
					$\text{NH}_3\text{-N}$ (mg/l)	$\text{NO}_2^-\text{-N}$ (mg/l)	$\text{NO}_3^-\text{-N}$ (mg/l)	To Bacterial Cells (a) (mg/l)	To Atmosphere as NH_3 or as N_2 (b) (mg/l)		

NOTES (Continued)

- (h) Estimated based on average secondary influent $\text{NH}_3\text{-N}$ concentration for Plants #1-5, 7, 9-11, 18, 20, 21, 24-26, 31.
- (i) The average percentage nitrification of $\text{NH}_3\text{-N}$ at plants operated by the County Sanitation District of Los Angeles County is equal to 15% of secondary influent ammonia concentration. That degree of nitrification is assumed here.
- (j) Estimate based on average secondary effluent $\text{NH}_3\text{-N}$ concentration for plants #1-5, 7, 9-11, 18, 20, 21, 24-26, 31.
- (k) Since there is little difference between influent and effluent ammonia concentrations, it is assumed that very little nitrification occurred.
- (l) Operators at this plant try to keep the $\text{NH}_3\text{-N}$ concentrations low by encouraging nitrification (Coe, 1984). It is assumed that 60% of incoming $\text{NH}_3\text{-N}$ is nitrified.
- (m) For primary treatment only, influent $\text{NH}_3\text{-N}$ will be very close to effluent $\text{NH}_3\text{-N}$.

Figure A.1 Emission Factors for NH_3 Loss from Sludge Processing at the Joint Water Pollution Control Plant Operated by the County Sanitation Districts of Los Angeles County (Reference: Livingston, 1984)



Possible Emission Factors

NH_3 to atmosphere/ton of unprocessed sludge (corrected for sludge sent to landfill) = 1.36 kg NH_3 -N/metric ton unprocessed sludge
 NH_3 to atmosphere/ton of dry digested sludge sent to drying beds = 3.03 kg NH_3 -N/metric ton digested sludge
 NH_3 -N loss as % of total N in unprocessed sludge (corrected for sludge sent to landfill) = 5.2%
 NH_3 -N loss as % of total N in digested sludge sent to drying beds = 13.5%

Table A.8 Ammonia Emissions from Sludge Processing at Wastewater Treatment Plants

Plant	Undigested Sludge metric tons/day (dry solids)(a)	Digested Sludge metric tons/day (dry solids)(a)	NH ₃ -N Content of digested sludge (a)	Emission Factor Used (c)	Ammonia lost to the atmosphere (metric tons/day)
1. Joint Water Pollution Control Plant	400 ^(b)	180 ^(b)	2.25% by weight	13.5% of NH ₃ -N in digested sludge	0.66
2. Terminal Island	27	11 ~ (120x10 ³ gal/day) 2.5% solids	700 mg/lit	13.5% of NH ₃ -N in digested sludge	0.052
3. Orange County Sanitation District	202.5	133	3200 mg NH ₃ -N/ kg of dry sludge	13.5% of NH ₃ -N in digested sludge	0.695
4. Irvine Ranch Water District		10	50 mg/lit	3.03 kg NH ₃ -N/metric tons of digested sludge	0.037
5. South East Regional Reclamation Authority		65x10 ³ gal/day (before drying) 12.12x10 ³ gal/day (after drying)	(50 mg/lit)(d)	13.5% of NH ₃ -N in digested sludge	0.037x10 ⁻²
6. Aliso Water Manage- ment Agency	9	4.8	1000 mg/lit	3.03 kg NH ₃ -N/metric tons of digested sludge	0.018
7. City of Riverside Plant		9.5		3.03 kg NH ₃ -N/metric tons of digested sludge	0.035
8. Hemet Treatment Plant	4.5	1.93	0.2% by weight(e)	13.5% of NH ₃ -N in digested sludge	0.0006

Table A.8 Ammonia Emissions from Sludge Processing at Wastewater Treatment Plants (Continued)

Plant	Undigested Sludge metric tons/day (dry solids)(a)	Digested Sludge metric tons/day (dry solids)(a)	NH ₃ -N Content of digested sludge (a)	Emission Factor Used (c)	Ammonia lost to the atmosphere (metric tons/day)
9. Sun City Treatment Plant	0.52			1.36 kg of NH ₃ -N/metric tons of unprocessed sludge	0.0009
10. Sunnymead Treatment Plant	0.32	0.013		3.03 kg NH ₃ -N/metric tons of digested sludge	0.0476x10 ⁻³
11. City of San Bernardino	19			1.36 kg NH ₃ -N/metric tons of unprocessed sludge	0.0313
12. Chino Basin Regional Plant #1	14.5	9.1		3.03 kg NH ₃ -N/metric tons of digested sludge	0.0334
13. Chino Basin Regional Plant #2	3.6	2.3		3.03 kg NH ₃ -N/metric tons of digested sludge	0.0083
14. City of Colton		1.25		3.03 kg NH ₃ -N/metric tons of digested sludge	0.0046
15. City of Santa Barbara		5.5	0.8% by weight	13.5% of NH ₃ -N in digested sludge	0.0072
16. Summerland Sanitation District	0.34	0.11		3.03 kg NH ₃ -N/metric tons of digested sludge	<u>0.0004</u> 1.584

(a) Sludge quantities and NH₃-N content are from mail survey form completed by each plant.

(b) Based on only that portion of sludge that will contribute to compacting operations (72% of total unprocessed sludge output of plant).

(c) Emission factor based on percentage of NH₃-N in sludge lost at Joint Water Pollution Control Plant. See Figure A.1 for nitrogen balance.

(d) Assume same value as Irvine Ranch Water District

(e) 1977 data are the latest available

TABLE A.9
Emission Factors for Ammonia Release from Soil Surface

LAND SURFACE TYPE	VALUE REPORTED	REFERENCE	EMISSION FACTOR ADOPTED (kg NH ₃ /km ² -day)
Cropland	11 kg N/ha-yr	(a)	3.65
Lawn Surface (campus sidewalk)	0.5 to 1.5 mg NH ₃ /m ² -day	(b)	1
Bare Soil	1 to 2 mg NH ₃ /m ² -day	(c)	1 (f)
Ungrazed Grass-Clover Pasture	2 g N/ha-hr	(d)	5.81
Forest Land (estimate)		(e)	(1)
Pasture (near animals - no manure)			
Pasture Grass (>30 m from manure source)	1 to 2 mg NH ₃ /m ² -day	(b)	1.5
Grassland Near Swine Barn with no manure	2 to 3 mg NH ₃ /m ² -day	(b)	2.5
Pasture (with manure)			
Pasture with dried manure	2 to 5 mg NH ₃ /m ² -day	(b)	(g)
Pasture with recent liquid dairy manure	5 to 20 mg NH ₃ /m ² -day	(b)	(g)
Grazed Pasture			
	15 kg N/ha-yr	(a)	(g)
	13 g N/ha-hr	(d)	(g)

NOTES

- (a) Porter et al. (1975) and Elliot et al. (1971). Note that Denmead et al. (1978) give much higher values over short periods of time.
- (b) Miner (1976)
- (c) Miner (1976; bare soil located more than 30 m from university dairy farm)
- (d) Denmead et al. (1976)
- (e) Release from decomposition of organic matter in forests estimated as being low
- (f) Taken at low end of range given in order not to exceed estimate for lawns
- (g) Not used; emissions of NH₃ due to presence of animal wastes will be estimated separately

TABLE A.10
Ammonia Estimates for Release from Soil Surfaces

	LAND AREA DEVOTED TO THIS USE (km ²) (a)	FRACTION OF LAND NOT MASKED BY BUILDINGS AND PAVEMENT	EMISSION FACTOR (Kg NH ₃ /Km ² -day)	NH ₃ EMISSIONS METRIC TONS PER DAY
SOIL SURFACE RELEASE (Excluding Chemical Fertilizers & Manures)				
Urban or Built-up Land				
11 Residential (single and multiple)	2884.41	44% (b)	1 (e)	1.27
12 Commercial and Services	826.21	34% (b)	1 (e)	0.28
13 Industrial	429.16	47% (b)	1 (e)	0.2
14 Transportation, Communication & Utilities	218.91	55% (b)	1 (e)	0.12
15 Industrial and Commercial Complexes	20.83	40% (c)	1 (e)	0.01
16 Mixed Urban or Built-Up Land	43.95	43% (d)	1 (e)	0.02
17 Other Urban or Built-Up Land	348.23	43% (d)	1 (e)	0.15
Agricultural Land				
21 Cropland and Pasture	1770.72		3.4 (f)	6.02
22 Orchards, Groves, Vineyards, Nurseries, and Ornamental	857.65		(3.6) (g)	3.09
23 Confined Animal Feeding Operations	47.26		estimated separately (h)	
24 Other Agricultural Land	25.32		(3.4) (i)	0.09
Rangeland				
31 Herbaceous Rangeland	686.48		(1) (j)	0.69
32 Shrub and Brush Rangeland	8053.08		(1) (j)	8.05
33 Mixed Rangeland	1165.01		(1) (j)	1.17
Forest Land				
41 Deciduous Forest Land	12.53		(1) (k)	<0.01
42 Evergreen Forest Land	2291.58		(1) (k)	<2.29
43 Mixed Forest Land	40.08		(1) (k)	<0.04
Wetland				
61 Forested Wetland	33.10			neglected
62 Non-Forested Wetland	53.89			neglected
Barren Land				
72 Beaches	16.21		< (1) (l)	<0.02
73 Sandy Areas (other than beaches)	107.35		< (1) (l)	<0.11
76 Transitional Areas	149.76		1 (m)	0.15
77 Mixed Barren Land	10.62		1 (n)	0.01
				<u><23.79</u>

NOTES:

- (a) Obtained by counting areas in each category as shown on land use maps prepared by U.S. Geological Survey (1976a-e).
- (b) Obtained by examination of aerial photographs (Fretz, 1980). Twenty-four zone photos distributed widely over Los Angeles County were overlayed with land use categories and examined to estimate the fraction of land in each category which had been paved or built upon. Values shown are averages of the 24 photographs examined.
- (c) Estimated by average of commercial and industrial categories shown above.
- (d) Estimated by weighted average of land use categories 11 through 14.
- (e) Emission factor of lawn and bare soil from Table A.9.
- (f) Average of cropland, ungrazed clover, and two types of grassland without animals present on land.
- (g) Assumed same as cropland from Table A.9.
- (h) Emissions from livestock operations estimated separately based on animal head count and wastes produced.
- (i) Assumed similar to crop and pasture combination.
- (j) Assumed similar to bare soil/grass combination.
- (k) Estimate.
- (l) Less than or equal to bare soil data from Table A.9.
- (m) Bare soil data from Table A.9.

TABLE A.11

Nitrogen in Dry and Liquid Fertilizers for Farm Plus
Non-Farm Use (3rd quarter 1982 from California Department
of Food and Agriculture, 1982)

COUNTY	FERTILIZER TOTAL NITROGEN (metric tons/day)	PARTITION	
		DRY ^(a)	LIQUID ^(a)
Los Angeles	18	0.8	0.2
Orange	6.1	0.85	0.15
Riverside	49.6	0.21	0.79
San Bernardino	1.7	0.92	0.08
Santa Barbara	36.8	0.35	0.65
Ventura	17.3	0.47	0.53

(a) Fraction of total N applied in liquid and dry form
estimated by summing N content of those liquid and dry
fertilizers for which nitrogen content data were given.

TABLE A.12

Percentage of N Applied, Apportioned Between Farm and
Non-Farm Use (California Department of Agriculture, 1982)

COUNTY	FARM		NON-FARM	
	DRY	LIQUID	DRY	LIQUID
Los Angeles	43	11	37	9
Orange	49	9	36	6
Riverside	20.7	77.7	0.3	1.3
San Bernardino	37	3	55	5
Santa Barbara	34.7	64.5	0.3	0.5
Ventura	45	50.5	2	2.5

(a) Example: $\text{Fraction (farm N/total N)} \times \text{fraction dry from Table A.11.}$

TABLE A.13

Fertilizer Nitrogen Applied
(Tons N/day)

COUNTY	DRY		LIQUID	
	FARM	NON-FARM	FARM	NON-FARM
Los Angeles	7.7	6.7	2	1.6
Orange	3	2.2	0.5	0.4
Riverside	10.3	0.15	38.5	0.65
San Bernardino	0.63	0.94	0.05	0.09
Santa Barbara	12.8	0.11	23.7	0.18
Ventura	7.8	0.35	8.7	0.43

Estimated by combining data of Tables A.11 and A.12

TABLE A.14

Percentage of Farm Fertilizer Applied on Crops

(From U.S. Bureau of the Census, 1977)^(a)

COUNTY	% of Farm Fertilizer Applied on Crops(a)	
	% DRY	% LIQUID
Los Angeles	63	80
Orange	57	34
Riverside	63	84
San Bernardino	31	42
Santa Barbara	79	95
Ventura	60	39

(a) Data taken from U.S. Bureau of the Census (1977) as shown in Table A.11 of Cass et al. (1982). 1982 Census of Agriculture does not contain this information.

TABLE A. 15

Nitrogen Applied on Crops, Orchards, and Non-Farm Areas
(County Totals in Metric Tons/day)

COUNTY	DRY			LIQUID		
	CROP ^(a)	ORCHARDS AND ORNAMENTALS	NON-FARM	CROP ^(a)	ORCHARDS AND ORNAMENTALS	NON-FARM
Los Angeles	4.85	2.85	6.7	1.6	0.4	1.6
Orange	1.7	1.3	2.2	0.17	0.33	0.4
Riverside	6.5	3.8	0.15	32.3	6.2	0.65
San Bernardino	0.2	0.43	0.94	0.02	0.03	0.09
Santa Barbara	10	2.7	0.11	22.5	1.2	0.18
Ventura	4.7	3.1	0.35	3.4	5.3	0.43

(a) Farm use split between crops vs. orchards and ornamentals using crop percentages of Table A.14 applied to total farm use given in Table A.13.

TABLE A.16

Percentage of Land Use in Each County Located within the Gridded
Inventory Map Area and within the South Coast Air Basin

County	Cropland	Orchards	Non-Farm Fertilized Land (a)
Los Angeles	34	84	99
Orange	100	100	100
Riverside	53	43	77
San Bernardino	69	100	82
Santa Barbara	7	100	78
Ventura	95	100	100

(a) Estimated from percentage of county population living within the
air basin in 1980.

TABLE A.17

Fertilizer Nitrogen Applied Inside the South Coast Air Basin
(metric tons/day)^(a)

COUNTY	DRY			LIQUID		
	CROP	ORCHARDS AND ORNAMENTALS	NON FARM	CROP	ORCHARDS AND ORNAMENTALS	NON FARM
Los Angeles	1.65	2.4	6.6	0.54	0.34	1.58
Orange	1.7	1.3	2.2	0.17	0.33	0.4
Riverside	3.45	1.6	0.12	17.1	2.67	0.5
San Bernardino	0.14	0.43	0.77	0.01	0.03	0.07
Santa Barbara	0.7	2.7	0.09	1.58	1.2	0.14
Ventura	4.5	3	0.35	3.23	5.3	0.43
TOTAL	12.14	11.4	10.1	22.63	9.87	3.12

(a) Data of Tables A.15 and A.16 combined.

TABLE A.18
Ammonia Loss Due to Fertilizer Application by County--3rd Quarter-- 1982
(handling loss given separately)

COUNTY	DRY						LIQUID						TOTAL NH ₃ LOSS KG/DAY
	CROPLAND		ORCHARDS AND ORNAMENTALS		NON-FARM		CROPLAND		ORCHARDS AND ORNAMENTALS		NON-FARM		
	FERTILIZER N		FERTILIZER N		FERTILIZER N		FERTILIZER N		FERTILIZER N		FERTILIZER N		
	APPLIED METRIC TONS/DAY	NH ₃ LOSS KG/DAY ^(a)	APPLIED METRIC TONS/DAY	NH ₃ LOSS KG/DAY ^(a)	APPLIED METRIC TONS/DAY	NH ₃ LOSS KG/DAY ^(b)	APPLIED METRIC TONS/DAY	NH ₃ LOSS KG/DAY ^(c)	APPLIED METRIC TONS/DAY	NH ₃ LOSS KG/DAY ^(c)	APPLIED METRIC TONS/DAY	NH ₃ LOSS KG/DAY ^(b)	
Los Angeles	1.65	200	2.4	290	6.6	2396	0.54	13	0.34	8	1.58	573.5	3480.5
Orange	1.7	206	1.3	157	2.2	799	0.17	4	0.33	8	0.4	145	1319
Riverside	3.45	417	1.6	194	0.12	44	17.1	414	2.67	65	0.50	182	1316
San Bernardino	0.14	17	0.43	52	0.77	280	0.01	0.24	0.03	0.73	0.074	27	377
Santa Barbara	0.7	85	2.7	327	0.09	33	1.58	38	1.2	29	0.14	51	563
Ventura	4.5	544	3	363	0.35	127	3.23	78	5.3	128	0.43	156	1396
TOTAL	12.14	1469	11.43	1383	10.15	3679	22.6	547	9.9	239	3.12	1135	8452

Total NH₃ Loss = 8452 kg/day (for the 3rd quarter)
= 8.45 metric tons/day

(a) Assuming 10% of N applied is lost to atmosphere as NH₃ (Meyer, 1981)

(b) Assuming 30% of N applied is lost to atmosphere as NH₃ (Meyer, 1981)

(c) Assuming 2% of N applied is lost to atmosphere as NH₃ (Meyer, 1981)

TABLE A.19
Loss of Anhydrous Ammonia Due to Handling and Field Application
(3rd Quarter, 1982)

COUNTY	ANHYDROUS AMMONIA (metric tons N/day) (County Total) ^(a)	% OF LIQUID FERTILIZER APPLIED ON CROPS	% OF CROPLAND IN BASIN	% OF ORCHARDS IN BASIN	ANHYDROUS AMMONIA IN BASIN ^(b) (metric tons N/day)	1% LOSS DUE TO HANDLING ^(c) (metric tons N/day)	3% LOSS DURING APPLICATION ON FIELD ^(c) (metric tons N/day)
Los Angeles	1.28	80	34	84	0.56	0.006	0.017
Orange	-	34	100	100	-	-	-
Riverside	15	84	53	43	7.71	0.08	0.23
San Bernardino	-	42	69	100	-	-	-
Santa Barbara	1.53	95	7	100	0.18	0.002	0.005
Ventura	-	39	95	100	-	-	-
TOTAL	17.8				8.45	0.088	0.25

Total loss = 0.34 metric tons N/day

= 0.41 metric tons NH₃/day

(a) From liquid fertilizer sales classed as 82-00-00 by the California Department of Food and Agriculture (1982)

(b) County total multiplied by [% of liquid fertilizer applied to crops (Table A.14) x % cropland in basin (Table A.16) + % of liquid fertilizer applied to orchards x % orchards in basin.]

(c) Walkup and Nevins (1966)

TABLE A.20

Summary of NH_3 Emissions from Fertilizer Application and Handling

COUNTY	LOSS FROM FARM APPLICATION OF FERTILIZER(metric tons/day)		LOSS FROM NON-FARM APPLICATION (metric tons/day)	LOSS DUE TO HANDLING (metric tons/day)	TOTAL NH_3 LOSS (metric tons/day)
	CROPS	ORCHARDS			
Los Angeles	0.21	0.3	2.97	0.03	3.51
Orange	0.21	0.17	0.94	-	1.32
Riverside	0.83	0.26	0.23	0.38	1.7
San Bernardino	0.02	0.05	0.31	-	0.38
Santa Barbara	0.12	0.36	0.08	0.01	0.57
Ventura	0.62	0.49	0.28	-	<u>1.39</u>
				TOTAL	8.87

TABLE A.21

Summary of Animal Waste Data

ANIMAL	SOURCE	ANIMAL WEIGHT (kg)	MANURE (TOTAL WASTE) kg/head-day	TOTAL NITROGEN EXCRETED kg/head-day
Dairy Cattle	Dale (1971)	680	49	
	Fogg (1971)	600	45	0.17
	Luebs et al. (1973b)			0.18
	Adriano et al. (1974)			0.19
Value Used		640	47	0.18
Beef Cattle	Fogg (1971)	400	34	0.24
	Peters & Blackwood (1977)	500	27	
	Taiganides & Hazen (1966)	450	29	0.17
	Scholz (1971)	500	45	
Value Used		450	32	0.21
Horses	Fogg (1971)	450	25	0.22
Hogs	Fogg (1971)	70	3.9	0.03
	Muehling (1971)	70	5.5	0.038
	Scholz (1971)	70	3.6	
	Taiganides & Hazen (1966)	45	3.2	0.023
Value Used		70	3.9	0.03
Sheep	Fogg (1971)	45	1.8	0.018
Chickens	Fogg (1971)	2	0.11	0.0014
	Scholz (1971)		0.185	
	Taiganides & Hazen (1966)	2	0.11	0.0019
Value Used		2	0.14	0.0016
Turkey	taken in proportion to chickens on body weight basis	5.5	0.39	0.0044

TABLE A.22
DISTRIBUTION OF CATTLE BETWEEN DAIRY, FEEDLOT AND RANGE

COUNTY	CATTLE & CALVES (a)	BEEF COWS(a)	MILK COWS(a)	Heifers and Heifer Calves ^(a)		STEERS(a)	DAIRY CATTLE	FEEDLOT CATTLE ^(c)	RANGE CATTLE (c)
				BEEF HEIFERS(b)	MILK HEIFERS(b)				
Los Angeles	33,604	4,907	6,019	5,116	4,536	13,026	10,555	12,677	10,372
Orange	12,889	4,000(d)	300(d)	2,226	592	4,226	892	48	11,949
Riverside	178,703	7,563	87,126	14,956	44,870	24,186	131,996	33,629	13,078
San Bernardino	283,742	6,707	167,120	80,167	10,932	18,816	178,052	42,276	63,414
Santa Barbara	94,605	30,425	4,628	18,210	3,997	37,345	8,625	43,850	42,130
Ventura	18,835	8,000(d)	2,500(d)	2,701	4,801	3,123	7,301	10,150	1,384

(a) U.S. Bureau of the Census (1984)

(b) Heifers and heifer calves apportioned between beef heifers and milk heifers in same ratio as given by U.S. Bureau of the Census (1977).

(c) Beef cattle apportioned between feedlot and range in same ratio as given by U.S. Bureau of the Census (1977).

(d) From California Crop and Livestock Reporting Service (1983).

TABLE A.23

Fraction of Animals Located Inside South Coast Air Basin Portion of Each County

ANIMAL TYPE	LOS ANGELES	ORANGE	RIVERSIDE	SAN BERNARDINO	SANTA BARBARA	VENTURA
Dairy Cattle	90 ^(b)	100 ^(a)	100 ^(a)	97 ^(b)	0 ^(d)	100
Feedlot Cattle	(60) ^(c)	100	20	100	0 ^(d)	100
Range Cattle	100	100	100	100	16 ^(e)	100
Horses	98	100	98	98	16 ^(e)	100
Sheep	10	100	(50)	100	16 ^(e)	100
Hogs	10	100	90	90	16 ^(e)	100
Chickens	100	100	100	100	16 ^(e)	100
Turkeys	100	100	100	100	16 ^(e)	100

Estimates are by Addis (1981) unless noted otherwise:

- (a) Bishop (1981)
- (b) 2000 dairy cows in desert area of Los Angeles County and 3835 dairy cows located in desert portion of San Bernardino County (Bishop, 1981).
- (c) Most Los Angeles County feedlot cattle are located within the South Coast Air Basin; Addis (1981) estimates more than 10,000 within the air basin (i.e. 54% or greater are in the air basin). We will estimated that 60% of the total are in the air basin.
- (d) U.S. Geological Survey (1976) maps show negligible land area devoted to confined animal feeding in the South Coast Air Basin portion of Santa Barbara Count.
- (e) Estimated in rough proportion to the fraction of the county land area within the air basin boundary.

Table A.24a

Livestock Inventory

COUNTY	COUNTY TOTALS ^(a)			LOCATED IN SOUTH COAST AIR BASIN ^(b)		
	DAIRY	FEEDLOT	RANGE	DAIRY	FEEDLOT	RANGE
Los Angeles	10,555	12,677	10,372	9,500	7,606	10,372
Orange	892	48	11,949	892	48	11,949
Riverside	131,996	33,629	13,078	131,996	6,726	13,078
San Bernardino	178,052	42,276	63,414	172,710	42,276	63,414
Santa Barbara	8,625	43,850	42,130	-	-	6,741
Ventura	7,301	10,150	1,384	7,301	10,150	1,384
				322,399	66,806	106,938

(a) See Table A.22

(b) See Table A.23

TABLE 24b

Livestock Inventory (continued)

COUNTY	HORSES		SHEEP		HOGS	
	COUNTY TOTAL ^(a)	IN SOUTH COAST AIR BASIN ^(b)	COUNTY TOTAL ^(c)	IN SOUTH COAST AIR BASIN ^(b)	COUNTY TOTAL ^(c)	IN SOUTH COAST AIR BASIN ^(b)
Los Angeles	54,700	53,606	32,330	3,233	5,706	571
Orange	10,500	10,500	166	166	699	699
Riverside	30,300	29,694	58,228	29,114	5,289	4,760
San Bernardino	19,900	19,502	34,915	34,915	6,875	6,188
Santa Barbara	8,300	1,328	19,131	3,061	1,226	196
Ventura	7,200	7,200	8,290(d)	8,290	1,904	1,904
				78,779		14,318

(a) Anderson (1979)

(b) See Table A.23

(c) U.S. Bureau of the Census (1984)

(d) U.S. Bureau of the Census (1981b)

TABLE A.24c

Livestock Inventory - Continued

COUNTY	CHICKENS		TURKEYS	
	COUNTY TOTAL ^(a)	IN SOUTH COAST AIR BASIN ^(b)	COUNTY TOTAL ^(a)	IN SOUTH COAST AIR BASIN ^(b)
Los Angeles	711,793	711,793	133,196	133,196
Orange	260,089	260,089	20	20
Riverside	8,411,609	8,411,609	26,875	26,875
San Bernardino	6,039,468	6,039,468	24,709	24,709
Santa Barbara	797,009	127,521	16(e)	3
Ventura	(1,438,861)(c)	1,438,861	38	38
		16,989,341		184,841

(a) U.S. Bureau of the Census (1984)

(b) 1974 data from U.S. Bureau of the Census (1977); more recent years data all withheld by the government.

(c) Estimated as 1.19 times the sales data given for chickens based on ratio of inventory to sales in Los Angeles, Riverside, San Bernardino and Orange Counties. Inventory data in Ventura County withheld by the government.

(d) See Table A.23

(e) 1978 data from U.S. Bureau of the Census (1981b); 1982 data withheld by the government

TABLE A.25

Total NH₃ Emissions from Livestock in the
Modeling Region of the South Coast Air Basin - 1982

ANIMAL	INVENTORY IN SOUTH COAST AIR BASIN (HEAD)	TOTAL ANIMAL WASTE kg/head-day	NITROGEN EXCRETED kg/head-day	NH ₃ EMISSIONS AT 50% RATE OF NITROGEN EXCRETED IN TOTAL WASTE ^(a) metric tons/day
Dairy Cattle	322,399	47	0.18	29.84(b)
Feedlot Cattle	66,806	32	0.21	7.21(b)
Range Cattle	106,938		0.21	13.59
Horses	121,830	25	0.22	16.22
Sheep	78,779	1.8	0.018	0.86
Hogs	14,318	3.9	0.03	0.26
Chickens	16,989,341	0.14	0.0016	16.45
Turkeys	184,841	0.39	0.0044	<u>0.49</u>
				84.92

(a) Adriano et al. (1974); Adriano et al. (1971); Giddens and Rao (1975); Viets (1971); Leubs et al. (1973ab)

(b) Since only 85% of manure from these animals is spread on soil, totals have been multiplied by 0.85 (see Adriano et al. (1974)).

TABLE A.26
Emission Factors for Ammonia Loss Due to Non-Farm Animals

NON-FARM ANIMALS	ANIMAL WEIGHT (kg) ^(a)	TOTAL N EXCRETED IN URINE ^(a) (mg/kg body wt-day)	NITROGEN EXCRETED IN URINE DAILY ^(b) (kg/head-day)	EMISSION FACTOR ^(c) (kg NH ₃ /head-day)
Cats	2.5	500 - 1100	2×10^{-3}	2.2×10^{-3}
Dogs	12	250 - 800	6.3×10^{-3}	6.9×10^{-3}
Goats	50	120 - 400	1.3×10^{-2}	1.4×10^{-2}
Monkey	12	140 - 400	3.2×10^{-3}	3.5×10^{-3}
Rabbits	2	120 - 300	4.2×10^{-4}	4.6×10^{-4}
Rats	0.33	200 - 1000	2.0×10^{-4}	2.2×10^{-4}

(a) From Altman and Dittmer (1968) p. 528.

(b) Based on body weight and mid-point of range of nitrogen excretion rates given in adjacent columns.

(c) Cattle data show that about half of the nitrogen excreted in manure is in urine and half is in feces, and that when manure is applied to dry alkaline soil half of the total nitrogen is lost to the atmosphere as NH₃ (i.e. total N lost as NH₃ is approximately equal to nitrogen content of urine). We will estimate that loss rate is similar for other animals and that in the absence of data on total animal waste a value equal to 90% of urine N will reasonably estimate loss of N from total animal wastes.

TABLE A.27

NH₃-Emissions from Human and Domestic Animal Populations

COUNTY	COUNTY POPULATION (1980)(a)	RATIO: PEOPLE TO DOGS	RATIO: PEOPLE TO CATS	SOUTH COAST AIR BASIN POPULATION(a)	SOUTH COAST AIR BASIN EMISSIONS			
					ANIMAL WASTE(i)		HUMANS	
					(metric tons NH ₃ /day) DOGS	(metric tons NH ₃ /day) CATS	(metric tons NH ₃ /day) RESPIR.(j)	(metric tons NH ₃ /day) PERSPIR.(k)
Los Angeles	7,462,000	7.8(b)	7.0(g)	7,357,300	6.51	2.31	0.03	5.0
Orange	1,920,700	5.8(c)	(7.0)(h)	1,921,000	2.29	0.60	0.008	1.3
Riverside	655,900	(4.5)(d)	(7.0)(h)	505,900	0.78	0.16	0.002	0.34
San Bernardino	882,500	4.5(e)	(7.0)(h)	724,000	1.11	0.23	0.003	0.49
Santa Barbara	298,674	5.8(f)	(7.0)(h)	232,981	0.28	0.07	0.001	0.16
Ventura	524,800	5.8(f)	(7.0)(h)	523,700	0.62	0.16	0.002	0.36
					11.59	3.53	0.046	7.65

- (a) County population figures from Southern California Association of Governments (1982) except for Santa Barbara County, which is 1980 data from U.S. Bureau of the Census (1982). The portion of Santa Barbara County located within the study area is estimated on the basis of 1974 data, at which time 0.78 of the total county population lived on the south coastal side of the county.
- (b) Richards, B. (1981)
- (c) Hudson, R. (1981)
- (d) Estimated from San Bernardino data
- (e) San Bernardino (1981)
- (f) Estimated from Orange County data
- (g) Richards, B. (1981)
- (h) Estimated from Los Angeles County response
- (i) Computed using emission factors from Table A.26; (dogs, 6.9×10^{-3} kg NH₃/head day; cats 2.2×10^{-3} kg/head-day)
- (j) Respiration loss estimated at 4 μ l NH₃ per min per person (Kupprat et al., 1976) This implies 4.4×10^{-6} kg NH₃ respired/person-day
- (k) 24.5 g urea produced in human body/day (Altman and Dittmer, 1968); 5% released in perspiration (Healy et al., 1970; all of that assumed lost as NH₃. This implies 0.68 g NH₃/person-day.

TABLE A.28

Ammonia Emission Estimates for Refrigerants and Household Cleaning Chemicals--1982

COUNTY	SOUTH COAST AIR BASIN POPULATION ^(a)	NH ₃ EMISSIONS ^(d) metric tons/day	
		CLEANING AGENTS(b)	REFRIGERATION(c)
Los Angeles	7,357,300	0.37	0.25
Orange	1,921,000	0.098	0.065
Riverside	505,900	0.026	0.017
San Bernardino	724,000	0.037	0.025
Santa Barbara	232,981	0.012	0.008
Ventura	523,700	0.027	0.018
		<u>0.57</u>	<u>0.38</u>

(a) See Table A.27

(b) U.S. Ammonia Production for 1980: 30.99×10^9 lb = 15.5×10^6 short tons/yr (Chem. & Eng. News, 1983-May 2): 0.03% of total synthetic ammonia is used in the manufacture of household ammonia from Kirk-Othmer Encyclopedia (1963)

(c) 0.02% of total synthetic ammonia is used for refrigeration (Kirk-Othmer Encyclopedia, 1963)

(d) Emissions were calculated based on ratio of air basin population in 1980 to U.S. population. 100% NH₃ loss to the atmosphere was assumed. The population of the United States in July 1981 was 227.6×10^6 persons from U.S. Bureau of Census (1981c).

Summary of Ammonia Emissions by Source Category
in the South Coast Air Basin

1982

SOURCE CATEGORY	TOTAL EMISSIONS (kg/day)	
Stationary Fuel Combustion		
Electric Utility		
Natural Gas	1180.0	
Residual Oil	380.0	
Digester Gas	0.9	
Refinery Fuel Burning		
Natural Gas	118.0	
Residual Oil	15.0	
Refinery Gas	390.0	
Industrial Fuel Burning		
Natural Gas	470.0	
Liquified Petroleum gas (LPG)	8.0	
Residual Oil	22.0	
Distillate Oil	123.0	
Digester Gas	26.0	
Coke Oven Gas	15.0	
Residential/Commercial Fuel Burning		
Natural Gas	207.0	
Liquid Propane Gas (LPG)	4.0	
Residual Oil	85.0	
Distillate Oil	79.0	
Coal	23.0	
Subtotals	3145.9	(1.91%)
Mobile Source Fuel Combustion		
Automobiles		
Catalyst Autos and Light Trucks	2350.0	
Non-catalyst Autos and Light Trucks	485.0	
Diesel Autos and Light Trucks	3.5	
Catalyst Medium Vehicles	230.0	
Non-catalyst Medium and Heavy Trucks	140.0	
Diesel Trucks	23.0	
LPG for Carburetion	7.1	
Civilian Aircraft		
Jet	6.9	
Piston	2.1	
Shipping		
Residual Oil Boilers	68.0	
Diesel Ships	1.6	
Railroad—Diesel Oil	3.5	
Military		
Gasoline	4.9	
Diesel	2.3	
Jet Fuel	2.3	
Residual Oil	0.8	
Off-Highway Vehicles	6.5	
Subtotals	3337.5	(2.03%)
Industrial Point Sources	2450.0	(1.49%)
Sewage Treatment Plants	14,614.0	(8.88%)
Soil Surface	23,790.0	(14.5%)
Fertilizer		
Farm Crop	2010.0	
Orchards	1630.0	
Handling	420.0	
Non-farm	4810.0	
Subtotals	8870.0	(5.39%)
Livestock		
Cattle		
Dairy	29,840.0	
Feedlot	7210.0	
Range	13,590.0	
Horses	16,220.0	
Sheep	860.0	
Hogs	260.0	
Chickens	16,450.0	
Turkeys	490.0	
Subtotals	84,920.0	(51.6%)
Domestic		
Dogs	11,590.0	
Cats	3530.0	
Human Respiration	46.0	
Human Perspiration	7650.0	
Household Ammonia Use	570.0	
Subtotals	23,386.0	(14.2%)
*** Total ***	164,512.4	(100.0%)

APPENDIX B
ON SOME ASPECTS OF NIGHTTIME
ATMOSPHERIC CHEMISTRY

(Reprinted from
Environmental Science and Technology, 20,
1167-1172)

On Some Aspects of Nighttime Atmospheric Chemistry

Armistead G. Russell,[†] Glen R. Cass, and John H. Seinfeld*

Environmental Quality Laboratory, California Institute of Technology, Pasadena, California 91125

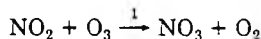
■ Nighttime atmospheric chemistry is simulated in two different situations: an offshore oceanic environment, the Santa Barbara Channel region of the south central coast of California, and a dry environment, the Mojave Desert of California. In the marine case, conversion of NO_x to peroxyacetyl nitrate (PAN) and HNO_3 is rapid; HNO_3 is formed by homogeneous hydrolysis of N_2O_5 and by nitrate radical reactions with organic gases, and the rate of HNO_3 production is limited by the abundance of O_3 . Even in the desert case, predictions indicate that homogeneous hydrolysis of N_2O_5 dominates HNO_3 formation at night. The implications of recent studies concerning the unimolecular decomposition of NO_3 are discussed.

Introduction

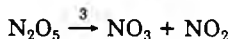
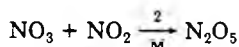
The central species in nighttime atmospheric chemistry is the nitrate free radical NO_3 . With utilization of its absorption spectrum, there have been a number of recent ambient measurements of NO_3 (1-6), as well as attempts to understand observed NO_3 behavior on a theoretical basis (7-11). Questions of continuing interest are (1) can the ambient nighttime measurements of NO_3 be explained on the basis of our current understanding of its chemistry and (2) how does nighttime chemistry vary in different environments? This paper addresses each of these questions by simulating nighttime chemistry in two distinctly different environments: an offshore regime, based on ambient hydrocarbon and NO_x data from the Santa Barbara Channel, in the Pacific Ocean off the coast of California, and a dry environment, the Mojave Desert of California. In the latter case, NO_3 measurements are available against which to evaluate the simulations.

Nighttime NO_x Chemistry

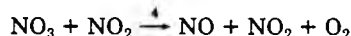
The nitrate radical, NO_3 , is generated in the troposphere largely through the reaction of O_3 and NO_2 :



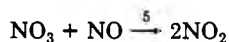
This is the principal reaction driving the nighttime chemistry of the N_2O_5 system. During the daytime hours, NO_3 concentrations are maintained at very low levels by photolysis (12). At night, however, NO_3 may accumulate due to reaction 1. NO_3 reacts with NO_2 to form N_2O_5 , which itself may decompose to return NO_3 and NO_2 :



A second route exists for the NO_3 - NO_2 reaction:

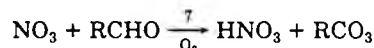
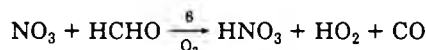


Also, NO_3 reacts with NO to form NO_2 :



The bimolecular reaction $2\text{NO}_3 \rightarrow 2\text{NO}_2 + \text{O}_2$ also occurs but can be neglected under atmospheric conditions. NO_3

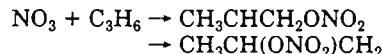
reacts with a number of organic species. The aldehyde- NO_3 reaction proceeds according to



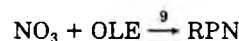
where RCO_3 denotes an acylperoxy radical. The reaction of NO_3 with alkanes can be represented in general by the H-atom abstraction step:



The olefin- NO_3 reaction is generally thought to proceed by addition, where, for propylene, for example

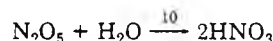


At low olefin concentrations, it is sufficient to represent the olefin- NO_3 reaction as



where RPN denotes a nitrogen-containing product whose further participation in the chemistry can be neglected.

Finally, the N_2O_5 formed in reaction 2 may react with water vapor to form nitric acid:



And the acetylperoxy radical from reaction 7 can react with NO_2 to form peroxyacetyl nitrate (PAN):

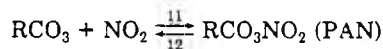
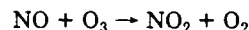


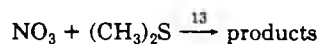
Table I summarizes reactions 1-12 with their rate constants.

At night, due to the absence of NO_2 photolysis, the NO - O_3 reaction



proceeds unimpeded to convert NO to NO_2 as long as both NO and O_3 are available. Generally, one expects, as a result, that nighttime NO levels will be very low if a reasonable quantity of O_3 is present from daytime photochemistry. Nighttime NO levels might be expected to increase once the O_3 has been consumed if there are continued fresh emissions of NO from sources.

At the concentration levels to be considered in this study, reactions 8 and 9 will not be important NO_3 consumption reactions. The NO_3 -dimethyl sulfide reaction (8)



might be an appreciable sink for NO_3 in the absence of other competing species.

Winer et al. (8) also studied the reaction of monoterpenes with NO_3 :



[†] Present address: Department of Mechanical Engineering, Carnegie-Mellon University, Pittsburgh, PA 15213.

Table I. Chemical Reactions of Nighttime Atmosphere^a

reaction	rate constant, cm ³ molecule ⁻¹ s ⁻¹	rate constant, 298 K, ppm ⁻¹ min ⁻¹	ref
(1) NO ₃ + O ₃ → NO ₂ + O ₂	1.2 × 10 ⁻¹³ e ^{-2450/T}	0.05	21
(2) NO ₃ + NO ₂ → N ₂ O ₅	1.7 × 10 ⁻¹²	2.51 × 10 ³	19
(3) N ₂ O ₅ \xrightarrow{M} NO ₃ + NO ₂	6.0 × 10 ⁻¹⁴ e ^{-11080/T}	2.9	21
(4) NO ₃ + NO ₂ → NO + NO ₂ + O ₂	2.5 × 10 ⁻¹⁴ e ^{-1230/T}	0.59	22
(5) NO ₃ + NO → 2NO ₂	2 × 10 ⁻¹¹	2.956 × 10 ⁴	21
(6) NO ₃ + HCHO $\xrightarrow{O_2}$ HNO ₃ + HO ₂ + CO	5.8 × 10 ⁻¹⁶	0.86	10
(7) NO ₃ + RCHO $\xrightarrow{O_2}$ HNO ₃ + RCO ₂	2.4 × 10 ⁻¹⁵	3.6 (R = CH ₃)	10
(8) NO ₃ + ALK $\xrightarrow{O_2}$ HNO ₃ + RO ₂	3.6 × 10 ⁻¹⁷	0.05 (R = C ₄ H ₉)	24
(9) NO ₃ + OLE $\xrightarrow{O_2}$ RPN	7.6 × 10 ⁻¹⁶	12.4	23
(10) N ₂ O ₅ + H ₂ O → 2HNO ₃	≤ 1.3 × 10 ⁻²¹ b	≤ 1.9 × 10 ⁻⁶	11, 22
(11) RCO ₂ + NO ₂ → RCO ₂ NO ₂ (PAN)	4.7 × 10 ⁻¹²	6.9 × 10 ³ (R = CH ₃)	22
(12) PAN → RCO ₂ + NO ₂	1.9 × 10 ⁻¹⁶ e ^{-13643/T}	0.022	22
(13) NO ₃ + (CH ₃) ₂ S → products	9.7 × 10 ⁻¹³	1.4 × 10 ³	8
(14) NO ₃ + monoterpene → products	3.0 × 10 ⁻¹²	4.4 × 10 ³	8
(15) NO ₃ + M → NO + O ₂ ^c		k ₁₅ [M] ≈ 0.13 min ⁻¹	16

^a The reactions above are the major nighttime reactions of the N₂O₅ species. Forty-four other reactions in McRae et al. (25) are included in the mechanism for completeness. ^b The rate constant given for this reaction is an upper bound. The text discusses the ramifications of decreasing this value. For a comprehensive evaluation of this reaction, see Atkinson et al. (11) and Russell et al. (9). ^c The NO₃ decomposition reaction was not included except as noted in the text.

And they indicated that this reaction could be of possible importance in clean environments.

At sufficiently high NO levels, like those found in urban areas, the RCO₂ may react with NO to generate NO₂. However, in the presence of greatly reduced nighttime NO concentrations, most of the RCO₂ produced instead will react with NO₂ to form PAN. For the same reason, the PAN produced by photochemical reactions the previous day will not decay substantially by the reverse reaction 12. Note, however, that for each PAN molecule formed by reaction 11 one HNO₃ molecule is formed from the preceding reaction 7 and two net NO₂ molecules are consumed, forming products PAN and HNO₃. Likewise, reaction 10 converts two reactive oxidized nitrogen species to two molecules of a stable product (HNO₃). However, the reaction between NO₃ and HCHO consumes only a single odd nitrogen molecule before reaching the final products (presumably the HO₂ produced will oxidize the NO or react to form H₂O₂).

While the rate equations for the system of nighttime reactions involving NO_x (Table I) plus those other reactions involving organic and inorganic species that might be important (see footnote to Table I) can be integrated numerically in order to compute atmospheric NO₃ and N₂O₅ levels, it is useful to investigate the formation of those species with steady-state analysis of the major nighttime reactions alone. On the basis of the first 12 reactions in Table I, the rate of change of the NO₃ concentration is given by

$$\frac{d[\text{NO}_3]}{dt} = k_1[\text{NO}_2][\text{O}_3] - k_5[\text{NO}_3][\text{NO}] - (k_2 + k_4)[\text{NO}_3][\text{NO}_2] + k_3[\text{N}_2\text{O}_5] - k_{\text{org}}[\text{ORG}][\text{NO}_3] \quad (1)$$

where $k_{\text{org}}[\text{ORG}] = k_6[\text{HCHO}] + k_7[\text{RCHO}] + k_8[\text{ALK}] + k_9[\text{OLE}]$. The characteristic reaction times for NO₃ and N₂O₅ are both sufficiently short that their concentrations can be assumed to be in a pseudo steady state:

$$[\text{NO}_3] = \frac{k_1[\text{NO}_2][\text{O}_3](k_3 + k_{10}[\text{H}_2\text{O}])}{(k_5[\text{NO}] + k_{\text{org}}[\text{ORG}] + k_4[\text{NO}_2])(k_3 + k_{10}[\text{H}_2\text{O}]) + k_2k_{10}[\text{NO}_2][\text{H}_2\text{O}]} \quad (2)$$

$$[\text{N}_2\text{O}_5] = \frac{k_2[\text{NO}_2][\text{NO}_3]}{k_3 + k_{10}[\text{H}_2\text{O}]} \quad (3)$$

Since it generally will be the case that $k_3 \gg k_{10}[\text{H}_2\text{O}]$, the

NO₂-NO₃-N₂O₅ cycle of reactions 2 and 3 can be assumed to be near equilibrium at any instant of time:

$$[\text{N}_2\text{O}_5] = \frac{k_2[\text{NO}_2][\text{NO}_3]}{k_3} \quad (4)$$

And, as a result

$$[\text{NO}_3] = \frac{k_1k_3[\text{NO}_2][\text{O}_3]}{k_3(k_5[\text{NO}] + k_{\text{org}}[\text{ORG}] + k_4[\text{NO}_2]) + k_2k_{10}[\text{NO}_2][\text{H}_2\text{O}]} \quad (5)$$

The denominator comprises the four NO₃ sinks: NO₃ scavenging by NO, NO₃ reaction with organics, NO₃ reaction with NO₂ to form NO, and nitric acid formation by the N₂O₅-H₂O reaction. Equation 5 can be evaluated to give NO₃ concentration estimates with only the necessary rate constants plus the concentrations of basic precursors often available from ambient measurements.

Nitric acid is produced by N₂O₅ hydrolysis (reaction 10) and by the organic-NO₃ reactions 6-8. The rate of nitric acid production is

$$\frac{d[\text{HNO}_3]}{dt} = 2k_{10}[\text{N}_2\text{O}_5][\text{H}_2\text{O}] + (k_6[\text{HCHO}] + k_7[\text{RCHO}] + k_8[\text{ALK}])([\text{NO}_3]) \quad (6)$$

The pseudo-steady-state expressions for NO₃ and N₂O₅ can be used in this equation to obtain the rate of HNO₃ production in terms of the concentrations of routinely measured pollutants. As will be seen in the next section, this steady-state analysis can be used to estimate the product distribution that arises from the numerical integration of the complete nighttime chemical mechanism.

Nighttime Chemistry in an Offshore Oceanic Environment

The first situation considered is an offshore oceanic environment, the Santa Barbara Channel off the south central coast of California. This region is of interest from the standpoint of atmospheric chemistry because of projected increases in emissions associated with offshore petroleum production (13). Although NO₃ data are not available in this area, other ambient concentration measurements have been carried out over the past 2 years (14). These measurements can serve to specify initial conditions for a simulation of the nighttime chemistry in the region

Table II. Initial Conditions for Simulation of Nighttime Chemistry in an Offshore Oceanic Environment^a

species	less polluted, ppb	base case, ppb	more polluted, ppb
O ₃	40	70	100
NO	0.1	1	1
NO ₂	1.0	10	10
HCHO	0.5 ^b	7 ^b	7 ^b
RCHO	0.5 ^b	6 ^b	6 ^b
ALK	10 (40 ppbc) ^c	15 ^c	37
ARO	2 (14 ppbc) ^c	3 ^c	7
PAN	3	3	3

^aConcentration ranges from South Central Coast Cooperative Aerometric Monitoring Program, the Santa Barbara Oxidant Study, and the 1983 Ozone Transport Study (13, 14). ^bPersonal communication with Alan Lloyd. ^cPersonal communication with Rei Rasmussen.

as predicted by the reactions in Table I. Of particular interest are the dynamics of NO₃ and the paths of conversion of NO_x into nitrate species. The photochemical trajectory model of Russell et al. (9) will be used to track the evolution of the NO_x species in an air column from sunset until 12 h thereafter.

Table II presents the range of initial concentrations that we will employ for simulating a nighttime air parcel in the Santa Barbara Channel. In the more polluted case, the air mass is expected to have originated from source-enriched areas such as the Los Angeles basin, while in the less polluted case the air is of "background" oceanic origin. The base case is in between. Four simulations were carried out, in the fourth of which the base case concentrations have been used and the rate constant for reaction 10 is decreased by a factor of 10. We include this case because of the uncertainty in the magnitude of k_{10} .

Each simulation begins at sunset and proceeds 12 h, with no fresh emissions. In the vertical diffusion calculation, surface roughness was taken as 10⁻⁴ m, corresponding to water. As will be seen, due to the presumably stable stratification at night and low surface roughness, turbulent transport of species to the surface is limited, and hence, removal by deposition at the ocean surface is relatively minor.

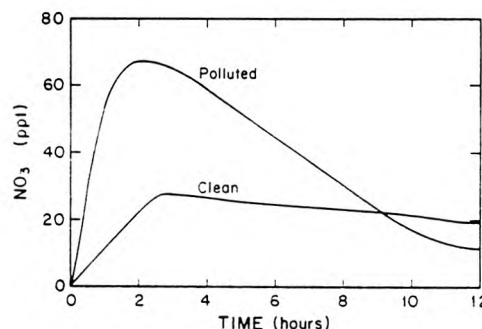
Results of the four simulations are given in Table III. Shown are the hourly NO₂ depletion rate, τ^{-1} , the HNO₃ formation rate (as % h⁻¹ relative to the NO₂ present), net PAN formation rate (as % h⁻¹ relative to the NO₂ present), maximum NO₃ and N₂O₅ concentrations, HNO₃ formation as percent of initial NO_x, total deposited HNO₃, and the maximum PAN produced.

Nitric acid formation rates, expressed relative to the NO₂ concentration, vary between 16% and 36% h⁻¹. Formation of PAN is responsible for the bulk of the remaining NO₂ consumed. Again, on the basis of the chemistry involved, the HNO₃ formation rate must be at least as great as that for PAN. The absolute increase in PAN concentration due to nighttime reactions varies between about 1 and 3 ppb, or between 2% and 23% of the initial NO₂. As can be seen from the last column in Table III, reducing the value used for k_{10} has little effect on the NO₂ loss rate, but it does affect the split between the predicted HNO₃ and PAN formation. Significant quantities of HNO₃ still are formed. Note that in the absence of fresh emissions initially NO₂ is transformed to HNO₃ very rapidly, faster, in fact, than would be predicted during the day by reaction with OH. Likewise, PAN formation is rapid. The rate of NO₃ (and, hence, PAN and HNO₃) formation is limited by the O₃ and NO₂ concentrations and the extent of formation by the initial NO₂ concentration. In all cases studied, there is an

Table III. Results of Simulations of Nighttime Chemistry in an Offshore Oceanic Environment

	case ^a			
	1	2	3	4
NO ₂ depletion rate (τ^{-1}), % h ⁻¹ ^b	17	27	37	25
HNO ₃ formation rate, % h ⁻¹ of NO ₂ ^b	16	26	36	17
PAN formation rate, % h ⁻¹ of NO ₂ ^b	1	1	1	5
max NO ₃ , ppt	25	45	70	260
max N ₂ O ₅ , ppt	30	540	700	1700
max PAN increase, ppb (% of [NO ₂] ₀)	0.02 (2)	0.6 (5)	0.6 (5)	2.6 (23)
HNO ₃ produced, % of [NO _x] ₀ ^c	84	92	92	71
HNO ₃ produced, % of [NO _x] ₀ ^c by				
NO ₂ + OH	~0	~0	~0	~0
N ₂ O ₅ + H ₂ O	80	86	84	43
NO ₃ + HCHO	0.5	1	1	5
NO ₃ + RCHO	3	5	6	23
HNO ₃ deposited, % of [NO _x] ₀ ^c	1.4	1.7	1.9	1.1

^aThese four cases correspond to the initial conditions in Table II as follows: (1) less polluted; (2) base case; (3) more polluted; (4) base case, k_{10} reduced by a factor of 10. ^bAverage over first 6 h. After 6 h, very little NO₂ remains. ^cPercent at the end of a 12-h simulation.

**Figure 1.** Time evolution profiles of NO₃ for a relatively clean and a more polluted oceanic environment.

abundance of aldehydes to form PAN.

For the more polluted marine situation, about 49% of the NO₂ is oxidized to form NO₃; 5% reacts with the RCO₃ radical to form PAN, and 43% reacts with NO₃ to form N₂O₅ (and then HNO₃). Less than 2% of the initial NO₂ deposits out in any form.

Figure 1 shows a comparison of the predicted NO₃ concentration for the more and the less polluted cases. Note that the peak in the NO₃ concentration for the polluted case is much sharper, rising much higher and then dropping below the less polluted profile. Because of the lower ozone concentrations in the less polluted case, the NO_x is not converted to HNO₃ and PAN as quickly, allowing noticeable NO₃ concentrations to be sustained. The more polluted case more closely reproduces the spiked profile found just after sunset in urban environments (9).

Mechanistic explanation of the rate of NO₂ conversion and the product split between HNO₃ and PAN can be obtained by inserting the pollutant concentration data of Table II into the equations derived on the basis of the previous steady-state analysis. From the base-case concentrations in Table II, it is seen that the HCHO and ALK reactions together are about 3 times less important than

the RCHO-NO₃ reaction as a sink for NO₃. The only sinks from the NO₂-NO₃-N₂O₅ cycle back to NO and NO₂ are reactions 4 and 5, with reaction 4 being the only route to produce NO in the absence of fresh emissions. Note that at both the polluted and the unpolluted concentration levels reaction 4 is dominated by reaction 7. Thus, once an NO₃ molecule has been formed, it is highly probable that that molecule will end up as HNO₃ and that an associated NO₂ molecule will react to form either HNO₃ or PAN, in accordance with the results of the full-model simulation. Thus, the rate of NO₂ depletion at night should be about twice the rate of NO₃ formation by reaction 1:

$$\frac{d[\text{NO}_2]}{dt} \approx -2k_1[\text{NO}_2][\text{O}_3] \quad (7)$$

which can be expressed as

$$\frac{d[\text{NO}_2]}{dt} = -\tau^{-1}[\text{NO}_2] \quad (8)$$

where $\tau = (2k_1[\text{O}_3])^{-1}$ is the characteristic decay time for NO₂ by reaction 1, followed by reaction 10 or 11.

Next, the formation rates of PAN and HNO₃ can be considered. An expression for the rate of nitric acid formation was given in eq 6. Using the pseudo-steady-state expressions for [NO₃] and [N₂O₅] gives

$$\frac{d[\text{HNO}_3]}{dt} = [2k_2k_{10}[\text{H}_2\text{O}][\text{NO}_2]/k_3 + k_6[\text{HCHO}] + k_7[\text{RCHO}] + k_8[\text{ALK}]]/[k_3k_1[\text{O}_3][\text{NO}_2]/(k_3(k_5[\text{NO}] + k_{\text{org}}[\text{ORG}] + k_4[\text{NO}_2]) + k_2k_{10}[\text{NO}_2][\text{H}_2\text{O}])] \quad (9)$$

Since NO₂ is converted almost quantitatively to HNO₃ and PAN, both nitric acid and PAN formation rates can be expressed with the NO₂ decay rate as

$$\frac{d[\text{HNO}_3]}{dt} = \frac{1}{2}\tau^{-1}[\text{NO}_2](2 - f) \quad (10)$$

Similarly for PAN

$$\frac{d[\text{PAN}]}{dt} = \frac{1}{2}\tau^{-1}[\text{NO}_2]f \quad (11)$$

where f is the fraction of NO₃ formed by reaction 1 that reacts with RCHO. Comparing (9) and (10), it is seen that f will be a function of the pollutant concentrations. Once f has been computed by equating (9) and (10), the formation rate of PAN is apparent from (11). Given the conditions for the base case in Table II, the rates of nitric acid and PAN formation are approximately 4 and 0.2 ppb h⁻¹, respectively. The dominant route for nitric acid production is reaction 10.

Analysis of the reaction rate equations for the mechanism in Table I shows that the depletion rate of NO₂ should be approximately equal to twice the rate of reaction 1. Comparison of the decay rate obtained by the full computer simulation to that based on twice the initial rate of reaction 1, which should represent an upper limit to the NO₂ loss rate, gives close agreement in all simulations. The small deviations between the approximate calculation and the full model are due to reactions of NO₃ with HCHO and with NO₂ to form NO and NO₂ and to the continued decrease of the O₃ level.

Simulation of Nighttime Atmospheric Chemistry in a Desert Environment

We now turn our attention to a desert environment, typically very dry (relative humidities of about 20%) with low pollutant loadings. In this case, one could expect that the important chemical reactions dominating the nighttime

Table IV. Initial Conditions for Desert Simulations

	Edwards AFB ^a	Death Valley ^b
O ₃ , ppb	35	35
NO ₂ , ppb	0.95	0.15–0.075
NO, ppb	0.1	0.01
NO ₃ , ppb	0	0
RCHO, ppb	0.5	0.5
monoterpene, ppb	0.005 ^c	0.005 ^c
CO, ppm	0.1	0.1
RH, %	29	31
temp, °C	31	29

^aData for 23 May 1982 at Edwards Air Force Base. ^bData for 3 May 1982 at Death Valley. ^cFrom Winer et al. (8).

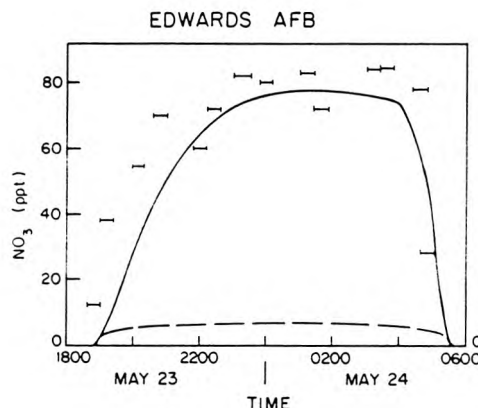


Figure 2. Predicted (solid line) and measured (data bars) NO₃ concentrations (3) at Edwards Air Force Base, CA, 23–24 May 1982. The dashed line near the bottom is the predicted concentration if the unimolecular decomposition of NO₃ is included in the simulation.

chemistry of N₂O₅ might differ from those over the ocean, particularly because of the lower water vapor concentrations. In this section, the trajectory model is used to investigate the fate of nitrogen oxides in the desert at night.

The chemical mechanism used is identical with that described for the ocean cases, except that the reaction of NO₃ with monoterpenes (MNT, see Table I) is included. A very small NO emission rate was included in the calculations, corresponding to arid, bare soil conditions (15). The initial conditions used for the simulations are from measurements taken by Platt et al. (3) in the Mojave Desert of California and are shown in Table IV. In this case, the predictions are compared against NO₃ measurements at Edwards Air Force Base and at Death Valley, CA (3). Results of this evaluation are shown in Figures 2, 3, and 4 for the Edwards and Death Valley locations. As seen, model predictions at Edwards closely track observations for both NO₃ (Figure 2) and NO₂ (Figure 3).

At Death Valley, the measured NO₂ concentrations were below the detection limit (0.3 ppb) of Platt et al. (3). For the simulations, the initial concentration of NO₂ was set equal to one-half and one-fourth of that value. At this site, two calculations were performed with the 0.15 ppb initial condition: with and without emissions of NO. As seen (Figure 4), the predicted NO₃ concentrations over time with and without NO emissions are different, though the peak NO₃ concentrations are about equal (~35 ppt). Emissions of NO slightly retard the rise in NO₃ concentrations due to scavenging by NO. The peak measured concentration of 19 ppt is about 40% less than that predicted and is attributable, in part, to the uncertainty in the initial NO₂ concentration. NO₃ scales approximately with the NO₂ concentration, so a lower initial NO₂ concentration would provide closer agreement and still be

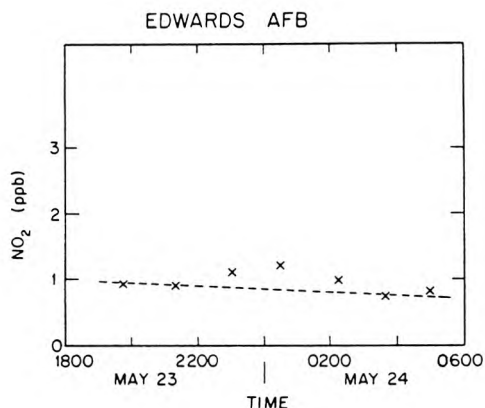


Figure 3. Predicted (dashed line) and measured (data points) NO_2 concentrations (3) at Edwards Air Force Base, CA, 23–24 May 1982.

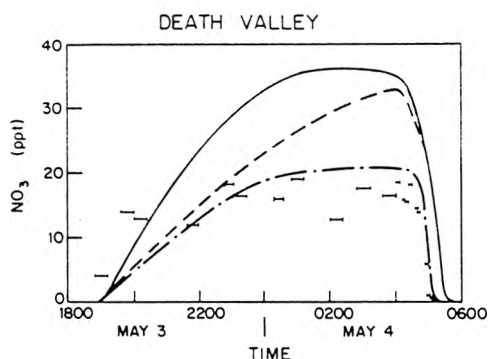


Figure 4. Predicted and measured (data bars) NO_3 concentrations (3) at Death Valley, CA, 3–4 May 1982. The solid line shows the predicted concentration given an initial NO_2 concentration of 0.15 ppb if no emissions of NO are included in the calculations, and the dashed line includes a very small emission rate (15). The alternating dashed line shows the predicted concentration of NO_3 given an NO_2 initial concentration of 0.075 ppb (one-fourth the detection limit of NO_2).

consistent with measurements. Using $[\text{NO}_2]_0 = 0.075$ ppb proves this to be the case.

Integrating the reaction fluxes indicates that the homogeneous hydrolysis of N_2O_5 is the dominant reaction producing nitric acid, even in a dry environment. In the Edwards case, approximately 77% of the nitric acid is produced by reaction 10, constituting 22% of the oxidized nitrogen originally in the air column plus that emitted during the night. Seven percent of the oxidized nitrogen is converted to PAN by the following morning. Due to the atmospheric stability and low nitric acid concentrations, less than 1% of the total NO_x deposits out during the night. The peak N_2O_5 concentration is predicted to be about 25 ppt.

Unimolecular Decomposition of NO_3

Recently Johnston et al. (16) reported that a number of experiments (17–20) contain evidence for the unimolecular decomposition of the NO_3 radical. Though the experiments varied widely in nature and reaction volume, reinterpretation of the results from the three room temperature experiments led to approximately the same first-order rate constant of about $(3 \pm 2) \times 10^{-3} \text{ s}^{-1}$. Using results from the high-temperature experiment, they derived the temperature-dependent expression of

$$k_{15}[\text{M}] = 2.5 \times 10^6 \exp(-6.1 \times 10^3/T) \text{ s}^{-1}$$

at 1 atm and T in K, (reaction 15, Table I). They cited

further evidence for this reaction rate from field experiments in which NO_3 and NO_2 were measured in relatively clean atmospheres at an altitude of 3 km (4, 5). These measurements indicated the loss rate of NO_3 by scavenging is about $1 \times 10^{-3} \text{ s}^{-1}$, that the scavenger is not depleted, and that the products of the NO_3 scavenging are neither NO nor NO_2 . Reaction 15 satisfies the first two conditions, and Johnston et al. (16) give reasoning that the final criterion can be explained by other phenomena.

In this section, the unimolecular decomposition of NO_3 is discussed in light of the recent review (16) and the field measurements of Platt et al. (2, 3). In very clean atmospheres, such as the desert cases considered in this study, the proposed NO_3 unimolecular decomposition would be the major loss reaction from the NO_3 - N_2O_5 system. An upper bound on the NO_3 concentration then can be found by steady-state analysis, as done previously, and by assuming that reaction 15 is the only loss mechanism. Inclusion of any other reactions of NO_3 or N_2O_5 would only lower the calculated NO_3 concentration. In this case

$$[\text{NO}_3]_{\text{MAX}} = \frac{k_1[\text{NO}_2][\text{O}_3]}{k_{15}[\text{M}]} \quad (12)$$

By rearranging this equation, the measured concentrations can be used to estimate an upper bound for $k_{15}[\text{M}]$. For the two desert cases previously discussed, use of the proposed rate constant for NO_3 decomposition and the observed NO_2 and O_3 concentrations gives $[\text{NO}_3]_{\text{MAX}}$ of about 9 and <1.5 ppt for Edwards and for Death Valley, respectively. This is in substantial disagreement with the measured NO_3 concentrations of 81 and 19 ppt. In fact, using the data for other sites and times (2, 3) in the same calculation gives the same results: the measured NO_3 concentration is much greater than the maximum calculated with steady-state analysis and the proposed decomposition rate (16), except at higher relative humidities. [This indicates that the loss of NO_3 (or N_2O_5) is due to hydrolysis, either homogeneous or on deliquesced aerosols.] Likewise, many of the data from the field studies in Germany (2) are at variance with $k_{15}[\text{M}] \approx 3 \times 10^{-3} \text{ s}^{-1}$. The magnitude of the effect of including this reaction in the mechanism is seen in Figure 2. As shown, the peak predicted concentration drops substantially, from 78 to 7 ppt. Inclusion of the decomposition reaction in the simulations of the offshore environment would decrease the formation of HNO_3 and PAN. This reaction would have little effect on simulations of urban environments because of the much heavier loadings of hydrocarbon pollutants, plus the effect of continued fresh emissions.

It is difficult to explain the reason for the discrepancy between the experiments of Platt et al. (2, 3) and the study of Johnston et al. (16), though a number of hypotheses can be proposed: (1) the proposed rate of NO_3 decomposition is too high, (2) the rate of formation of NO_3 (or N_2O_5) is much greater than is implied by our general knowledge of N_2O_5 chemistry, or (3) there is a systematic bias in the measurements. The actual rate of reaction 15 could lie between that implied by the field measurements (2, 3) and those derived from laboratory measurements (16). A small uncertainty in the comparison is introduced by the possibility that the air parcels were not uniform over the path of the measurement beam. However, the consistency of the O_3 measurements would indicate that the error introduced from the nonuniformities would be small compared to the apparent discrepancy. Inhomogeneities induced by nocturnal emissions would tend to increase the apparent discrepancy, whereas air parcels enriched in both NO_2 and O_3 would tend to decrease the discrepancy.

Conclusions

A series of calculations were performed to elucidate the important chemical reactions of N_2O_5 species at night in two quite different environments and under different pollutant loadings. Calculations performed for conditions found over the ocean near the California coast showed a rapid conversion of NO_2 to nitric acid and PAN, predominantly by hydrolysis of N_2O_5 and by production of peroxyacetyl radicals from the NO_3 -aldehyde reaction. The same reactions dominated the desert calculations, even though the ambient conditions and pollutant levels were quite different. However, the time evolutions of pollutant species in the two cases were quite different, and a much lower conversion rate of NO_2 to HNO_3 and PAN was found for the desert case. In the desert case, predicted NO_3 concentrations compare well with experimental measurements.

The predicted NO_3 concentration-time profile for the polluted, ocean environment case shows a sharp peak just after sunset, much like that found in earlier calculations for urban environments, though for different reasons. In the urban environment, the sharp peak is due to ozone loss by scavenging by NO emissions and deposition, whereas over the ocean the NO emissions are small and the sharp drop in NO_3 concentration is due to NO_2 depletion. In the desert solution, low ambient ozone levels and small NO emissions lead to a very small change in NO_2 concentration and a smooth, sustained NO_3 profile that plateaus instead of peaks. Calculations for marine, urban, and desert environments indicate that nighttime reactions of N_2O_5 can be important in forming nitric acid and PAN in all three situations.

Steady-state analysis and simulation indicate that there is a discrepancy between field measurements and a recently proposed rate for the unimolecular decomposition of NO_3 . Given our current knowledge of atmospheric chemistry, the proposed value for the rate of decomposition of NO_3 is too high, some other aspect of the NO_3 - N_2O_5 system is not well understood, or a systematic bias in the measurements exists.

Acknowledgments

We thank J. G. Calvert and H. Johnston for providing a preprint of their article and for a number of helpful comments on a draft of the manuscript.

Registry No. PAN, 2278-22-0; NO_2 , 11104-93-1; HNO_3 , 7697-37-2; N_2O_5 , 10102-03-1; NO_3 , 12033-49-7; O_3 , 10028-15-6.

Literature Cited

- (1) Platt, U.; Perner, D.; Winer, A. M.; Harris, G. W.; Pitts, J. N. *Geophys. Res. Lett.* 1980, 7, 89.
- (2) Platt, U.; Perner, D.; Schroeder, J.; Kessler, C.; Toennissen, A. *J. Geophys. Res., C: Oceans Atmos.* 1981, 86(11), 965.
- (3) Platt, U. F.; Winer, A. M.; Biermann, H. W.; Atkinson, R.; Pitts, J. N. *Environ. Sci. Technol.* 1984, 18, 365.
- (4) Noxon, J. F. *J. Geophys. Res., C: Oceans Atmos.* 1983, 88, 11017.
- (5) Noxon, J. F.; Norton, R. B.; Marovich, E. *Geophys. Res. Lett.* 1980, 7, 125.
- (6) Atkinson, R.; Aschmann, S. M.; Winer, A. M.; Pitts, J. N. *Environ. Sci. Technol.* 1984, 18, 370.
- (7) Calvert, J. G.; Stockwell, W. R. *Environ. Sci. Technol.* 1983, 17, 428a.
- (8) Winer, A. M.; Atkinson, R.; Pitts, J. N. *Science (Washington, D.C.)* 1984, 224, 156.
- (9) Russell, A. G.; McRae, G. J.; Cass, G. R. *Atmos. Environ.* 1985, 19, 893.
- (10) Cantrell, C. A.; Stockwell, W. R.; Anderson, L. G.; Busarow, K. L.; Perner, D.; Schmeltekopf, A.; Calvert, J. G.; Johnston, H. S. *J. Phys. Chem.* 1985, 89, 139.
- (11) Atkinson, R.; Winer, A. M.; Pitts, J. N. *Atmos. Environ.* 1986, 20, 331.
- (12) Magnotta, F.; Johnston, H. S. *Geophys. Res. Lett.* 1980, 7, 769.
- (13) Ziman, S. D.; Roth, P. M. "South Central Coast Cooperative Aerometric Monitoring Program—An Integrated Atmospheric Pollutant Monitoring Program for the California Outer Continental Shelf"; 15th International Technical Meeting on Air Pollution Modelling and Its Application, St. Louis, MO, 1985; NATO: 1985.
- (14) Blumenthal, D., Sonoma Technology Incorporated, private communication, 1984 and 1986.
- (15) Slemr, F.; Seiler, W. *J. Atmos. Chem.* 1984, 2, 1.
- (16) Johnston, H. S.; Cantrell, C. A.; Calvert, J. G. *J. Geophys. Res., D: Atmos.*, in press.
- (17) Graham, R. A. Ph.D. Thesis, University of California, Berkeley, 1975.
- (18) Cantrell, C. A.; Calvert, J. G., National Center for Atmospheric Research, unpublished results, 1984.
- (19) Tuazon, E. C.; Sanhueza, E.; Atkinson, R.; Carter, W. P. L.; Winer, A. M.; Pitts, J. N. *J. Phys. Chem.* 1984, 88, 3095.
- (20) Schott, G.; Davidson, N. *J. Am. Chem. Soc.* 1958, 80, 1841.
- (21) Baulch, D. L.; Cox, R. A.; Crutzen, P. J.; Hampson, R. F.; Kerr, J. A.; Troe, J.; Watson, R. T. *J. Phys. Chem. Ref. Data* 1982, 11, 327.
- (22) Atkinson, R.; Lloyd, A. *J. Phys. Chem. Ref. Data* 1984, 13, 315.
- (23) Atkinson, R.; Plum, C. N.; Carter, W. P. L.; Winer, A. M.; Pitts, J. N. *J. Phys. Chem.* 1984, 88, 1210.
- (24) Atkinson, R.; Plum, C. N.; Carter, W. P. L.; Winer, A. M.; Pitts, J. N. *J. Phys. Chem.* 1984, 88, 2361.
- (25) McRae, J. G.; Goodin, W. R.; Seinfeld, J. H. *Atmos. Environ.* 1982, 16, 679.

Received for review September 20, 1985. Revised manuscript received April 18, 1986. Accepted July 21, 1986. This project was funded, in part, by the California Air Resources Board under Agreement A2-150-32.

